NUREG/CR-6769

Technical Basis for Revision of Regulatory Guidance on Design Ground Motions: Development of Hazard- and Risk-consistent Seismic Spectra for Two Sites

Risk Engineering, Inc.

U.S. Nuclear Regulatory Commission
Office of Nuclear Regulatory Research
Washington, DC 20555-0001

AVAILABILITY OF REFERENCE MATERIALS IN NRC PUBLICATIONS

NRC Reference Material

As of November 1999, you may electronically access NUREG-series publications and other NRC records at NRC's Public Electronic Reading Room at www.nrc.gov/NRC/ADAMS/index.html. Publicly released records include, to name a few, NUREG-series publications; *Federal Register* notices; applicant, licensee, and vendor documents and correspondence; NRC correspondence and internal memoranda; bulletins and information notices; inspection and investigative reports; licensee event reports; and Commission papers and their attachments.

NRC publications in the NUREG series, NRC regulations, and *Title 10, Energy*, in the Code of *Federal Regulations* may also be purchased from one of these two sources.

1. The Superintendent of Documents
   U.S. Government Printing Office
   Mail Stop SSOP
   Washington, DC 20402–0001
   Internet: bookstore.gpo.gov
   Telephone: 202-512-1800
   Fax: 202-512-2250
2. The National Technical Information Service
   Springfield, VA 22161–0002
   www.ntis.gov
   1–800–553–6847 or, locally, 703–605–6000

A single copy of each NRC draft report for comment is available free, to the extent of supply, upon written request as follows:

Address: Office of the Chief Information Officer,
Reproduction and Distribution
Services Section
U.S. Nuclear Regulatory Commission
Washington, DC 20555-0001
E-mail: DISTRIBUTION@nrc.gov
Facsimile: 301–415–2289

Some publications in the NUREG series that are posted at NRC's Web site address www.nrc.gov/NRC/NUREGS/indexnum.html are updated periodically and may differ from the last printed version. Although references to material found on a Web site bear the date the material was accessed, the material available on the date cited may subsequently be removed from the site.

Non-NRC Reference Material

Documents available from public and special technical libraries include all open literature items, such as books, journal articles, and transactions, *Federal Register* notices, Federal and State legislation, and congressional reports. Such documents as theses, dissertations, foreign reports and translations, and non-NRC conference proceedings may be purchased from their sponsoring organization.

Copies of industry codes and standards used in a substantive manner in the NRC regulatory process are maintained at—

The NRC Technical Library
Two White Flint North
11545 Rockville Pike
Rockville, MD 20852–2738

These standards are available in the library for reference use by the public. Codes and standards are usually copyrighted and may be purchased from the originating organization or, if they are American National Standards, from—

American National Standards Institute
11 West 42nd Street
New York, NY 10036–8002
www.ansi.org
212–642–4900

Legally binding regulatory requirements are stated only in laws; NRC regulations; licenses, including technical specifications; or orders, not in NUREG-series publications. The views expressed in contractor-prepared publications in this series are not necessarily those of the NRC.

The NUREG series comprises (1) technical and administrative reports and books prepared by the staff (NUREG–XXXX) or agency contractors (NUREG/CR–XXXX), (2) proceedings of conferences (NUREG/CP–XXXX), (3) reports resulting from international agreements (NUREG/IA–XXXX), (4) brochures (NUREG/BR–XXXX), and (5) compilations of legal decisions and orders of the Commission and Atomic and Safety Licensing Boards and of Directors' decisions under Section 2.206 of NRC's regulations (NUREG–0750).

NUREG/CR-6769

Technical Basis for Revision of Regulatory Guidance on Design Ground Motions: Development of Hazard- and Risk-consistent Seismic Spectra for Two Sites

Manuscript Completed: March 2002
Date Published: April 2002

Prepared by
R. K. McGuire[1]
W. J. Silva[2]
C. J. Costantino[3]

[1]Risk Engineering, Inc., Principal Contractor
4155 Darley Avenue, Suite A
Boulder, CO 80305

Subcontractor:
[2]Pacific Engineering & Analysis
311 Pomona Avenue
El Cerrito, CA 94530

[3]Carl J. Costantino, Consultant
4 Rockingham Road
Spring Valley, NY 10977

R. M. Kenneally, NRC Project Manager

Prepared for
Division of Engineering Technology
Office of Nuclear Regulatory Research
U.S. Nuclear Regulatory Commission
Washington, DC 20555-0001
NRC Job Code W6248

Abstract

We develop recommendations for design spectra at two sites, one in the Mojave desert, California, and the second at Columbia, South Carolina. These sites were chosen because local, small earthquakes dominate the high frequencies ($f \geq 10$ Hz), but large distant events dominate the low frequencies ($f \leq 1$ Hz). Both rock and soil conditions are examined at each site.

For rock conditions, the uniform hazard spectrum (UHS) is determined at each site with a probabilistic seismic hazard analysis (PSHA). The hazard at 10 Hz and 1 Hz is deaggregated to determine the dominant magnitude **M** and distance R, and these values are used to generate two sets of spectral shapes. The first set comes from the recommended functions documented in McGuire et al. (2001); the second set comes from the attenuation equations used in the PSHA. In the CEUS there are separate shapes for the 1- and 2-corner seismic source model, and these are weighted using weights justified in the PSHA. The two sets of spectral shapes are scaled to the UHS amplitudes at 10 Hz and 1 Hz, as a consistency check on the shape of the UHS.

We calculate a scale factor to derive a rock uniform reliability spectrum (URS) based on the slopes of the hazard curves across the frequency range of interest at each site. The URS achieves an approximately consistent annual frequency of plant component seismic failures for all sites and across all structural frequencies. For these examples the 10^{-4} URS is illustrated by scaling the 10^{-4} UHS. The attenuation equation spectral shapes derived from the UHS are scaled to the 10 Hz and 1 Hz URS amplitudes. If the scaled spectra match the URS within a designated criterion, the scaled spectra may be used as separate design motions. This will be more accurate and realistic for sites where a broad-banded earthquake motion is not likely.

The database of strong motion records provides a source of rock motions with the correct magnitudes and distances. To develop design motions, these records are used as the starting point to develop artificial records fit to the individual scaled spectra. Matching criteria are applied to ensure compatibility between the target spectra and the artificial motions.

For soil sites, we illustrate the development of design spectra using a profile of the Meloland station in California assumed to lie at the Mojave site, and a generalized profile of the Savannah River site in South Carolina assumed to lie at the Columbia site. Soil amplification is calculated for these two sites using an equivalent-linear formulation of dynamic soil response, and using as input the rock motions calculated from the PSHA. For the Mojave site it is necessary to remove the effects of the shallow soft-rock velocity gradient to a depth corresponding to a shear-wave velocity of 4000 ft/sec, in order to provide an accurate input to the base of the soil column. We calculate soil amplification factors for rock motions corresponding to the 10^{-4} and 10^{-5} hazard, accounting for uncertainties in soil properties and documenting the uncertainty in soil response. From these calculations we can determine with sufficient accuracy the 10^{-4} and 10^{-5} UHS on soil. This accuracy is illustrated with a separate calculation of the soil hazard, using soil-specific attenuation equations developed specifically for the two profiles studied here. From the UHS on soil we derive the 10^{-4} URS on soil.

We scale soil spectra to the 10 Hz and 1 Hz UHS and URS, using the soil-specific amplification studies, because generic shapes for soil sites are not appropriate. The soil-specific shapes are scaled to the UHS to check consistency, and are scaled to the URS as optional design spectra. If these scaled shapes are to be used for design, they must match the URS within a stated criterion.

Artificial motions for soil sites are created in a manner similar to that for rock sites. The database of records includes soil motions for the WUS and the CEUS, and records with the appropriate magnitudes and distances are adjusted to match the target spectra (either a broad-banded spectrum or individual scaled spectra).

Overall, the procedures recommended in McGuire et al. (2001) work well in developing design spectra for the rock and soil sites examined here. Care must be taken in calculating the URS from the UHS, and in determining soil response given a rock PSHA, but sufficient consistency checks are illustrated so that one can make a determination of the validity of the final recommended spectra.

Reference

McGuire, R.K., W.J. Silva, and C. Costantino (2001). *Tech. Basis for Rev. of Reg. Guidance on Dsgn. Grnd. Motions: Hazard and Risk-consistent Grnd. Motion Spectra Guidelines*, US Nuc. Reg. Comm., Rept. NUREG/CR-6728, Oct.

Contents

List of Figures

List of Tables

List of Terms

a,b	parameters of geometric attenuation
a_{rp}	rock amplitude for return period rp
AF	amplification factor, soil amplitude/rock amplitude
$\overline{AF}_{rp}$	mean amplification factor for rock motion with return period rp
A_R	ratio of 10^{-5} spectral amplitude to 10^{-4} spectral amplitude
A^S	ground motion amplitude on soil
b	Richter b-value, a parameter of the exponential magnitude distribution
c_1, c_2, c_4, c_6, c_7, c_{10}	coefficients used to define ground motion attenuation for the WUS and the CEUS (eq. 2-1)
CDMG	California Division of Mines and Geology
CEUS	central and eastern United States
d_1, d_2, d_3	parameters of soil amplification
D	source depth
f	frequency in Hz
f_c	intersection frequency
F_{SM}	minimum seismic margin factor
G/G_{max}	shear modulus behavior of non-linear soils
H	horizontal component of motion
H_D	annual hazard exceedence frequency
$H(a)$	hazard associated with amplitude *a*
H1	one horizontal component of motion
H2	second horizontal component of motion
HCLPF	high confidence of low probability of failure point on fragility curve
k, K_H	slope parameter of hazard curve
m'	mean magnitude from deaggregation
M, m	earthquake magnitude (moment magnitude scale)
m_L, m_M, m_H	low, medium, and high magnitudes used to discretize a magnitude distribution
$\mathbf{M}_{min}$	minimum magnitude
$\mathbf{M}_X$	maximum magnitude
P[ ]	probability of event [ ]
P_F	annual frequency of component failure
PGA	peak ground acceleration
PGD	peak ground displacement

List of Terms (continued)

PGV	peak ground velocity
PSD	power spectral density
PSHA	probabilistic seismic hazard analysis
Q_O	frequency-independent component of Q model
Q(f)	deep crustal damping quality factor
R, r	source-to-site distance
rp	return period
R_P	probability ratio of hazard frequency to failure frequency
RS	response spectrum of artificial record
RVT	random vibration theory
SA	spectral acceleration
SF	scale factor for converting UHS to URS
TH	time history of motion
UHS	uniform hazard spectrum
URS	uniform reliability spectrum
USGS	United States Geological Survey
V	vertical component of motion
V_s	shear-wave velocity
WUS	western United States
z	soil amplitude
z_{rp}	soil amplitude for return period rp
Δt	time step for strong motion records
$\Delta\sigma$	earthquake stress drop
δ	logarithmic variation of soil amplification
ε	logarithmic deviation of rock motion for predicted value
η	frequency exponent of Q model
σ	standard deviation
υ_o	frequency (rate) of earthquake occurrence on a fault or in a source

1.0 INTRODUCTION

1.1 Background

This report documents the application of recommended procedures to derive seismic design ground motions at two sites. A companion report (McGuire et al., 2001) describes the recommended procedures in detail and documents the earthquake ground motion database that is recommended for development of ground motion time histories. These procedures are implemented in this report as a demonstration of how they work at two sites, one in the western US (WUS) and the other in the central and eastern US (CEUS).

The overall objectives of the project (McGuire et al., 2001) are to (1) update the standardized design spectra used in the evaluation of nuclear facilities to accommodate the effects of magnitude, site condition, distance, and tectonic environment, (2) assemble a database of strong motion records appropriate for use in design analyses, (3) recommend procedures and requirements for the scaling of ground motion records to be consistent with design spectra, (4) develop recommendations for conducting site response analyses to produce soil motions consistent with rock outcrop hazard results (hazard consistency), and (5) develop recommendations on how to derive seismic design spectra that provide risk consistency (uniform conservatism) across structural frequency. These objectives support the goal of developing uniform hazard spectra and design spectra that take into account the seismic threat at a site and the response of surficial rock and soil to that threat.

1.2 Summary of procedures for rock and soil sites

Figures 1-1 and 1-2 present flowcharts of the recommended procedures for developing design ground motions on rock and soil, respectively.

The procedure for rock sites (Figure 1-1) starts with a probabilistic seismic hazard analysis (PSHA) at a site using rock conditions. The hazard results at 10 and 1 Hz are then deaggregated at 10 Hz and 1 Hz, to define two deaggregation events (defined by **M** and *R*). We define two sets of spectra from these **M** and *R* values: one from PSHA, and a second from the spectra defined in this project. These spectra are used for a consistency check on the shape of the UHS.

We then derive a Uniform Reliability Spectrum (URS) from the UHS, and scale the spectra from attenuation equations to the URS at 10 and 1 Hz. For these scaled spectra, time histories are selected from the appropriate **M**-*R* bin. The time history spectra are compared to the scaled spectra, and are adjusted to match the target. For rock sites these adjusted time histories are used to conduct building dynamic analysis.

For soil sites (Figure 1-2) the first five steps are the same as for rock sites, except that the UHS is not scaled to a URS but is used as calculated to define the target spectra. The reason is that the scaling of UHS to URS depends on the slope of the hazard curve, and for soil sites, the slope must be determined by several soil analyses at different amplitudes. Following the adjustment of time histories to match the target spectra, dynamic soil analysis is performed with parameter uncertainty, using the scaled rock time histories as input. The relevant soil response is calculated as the average spectrum (or spectra) over earthquake and soil uncertainties. The soil response calculations lead to a soil URS that accounts for the slope of the soil hazard curves. Next, time histories from soil sites are chosen based on the dominant **M** and *R* values (in a similar manner to rock time histories). The soil time histories are then adjusted to target soil spectra and are used as input to building dynamic analysis.

1.3 Purpose of current report

It is often observed in developing new procedures that "the devil is in the details," and that is certainly true with the recommended methods for design ground motions. With that in mind, the current report's purpose is to apply the recommended procedures at two sites and to confront and resolve any problems in application of the procedures. In this way, recommendations on how to handle the details can be made in a manner consistent with how the procedures were developed.

1.4 Organization of report

Section 2 of this report describes the two sites chosen for this implementation study, one in the WUS and one in the CEUS. For each site, design ground motions for both rock and soil conditions are developed. Soil properties for the WUS site are assumed to be those from Meloland, a deep soil site in the Imperial Valley of California. Soil properties for the CEUS site represent a generic Savannah River profile, a deep soil site typical of the CEUS. Section 2 also documents the attenuation equations developed for rock and soil conditions and used in the calculation of seismic hazard. Section 3 describes the seismic hazard at the two sites, including the UHS, and Section 4 documents the Uniform Reliability Spectra for rock conditions at each site, including the estimation of vertical motions. Artificial time histories for rock conditions are derived and explained in Section 5, which completes the derivation of design ground motions for rock conditions.

Results for soil conditions are addressed beginning in Section 6. This section illustrates the estimation of the Uniform Hazard Spectra (UHS) on soil for the two test sites, including the estimation of vertical motions. The UHS is modified into a URS for soil conditions in Section 7 for the two sites. Finally, Section 8 illustrates the generation of artificial time histories of motion for the soil sites, given the URS documented in Section 7. In addition, Section 9 summarizes all recommendations for deriving design spectra for both rock and soil sites.

Overall, the report illustrates the derivation of seismic ground motions for two sites, starting with a description of the seismic threat and proceeding to the estimation of UHS, URS, and artificial motions. For comparison purposes at soil sites, the direct approach is used, in which we derive an attenuation equation for site-specific soil conditions and calculate the seismic hazard directly using this attenuation equation. This allows demonstration of the accuracy of approximate procedures based on rock UHS. The methods based on rock UHS are less cumbersome and are more applicable to a site with multiple soil depths and profiles.

The implementation at soil sites illustrates that simplistic methods of estimating soil UHS are not accurate. Specifically, one cannot use a broad-banded rock UHS as input to a soil analysis that disregards uncertainties in soil properties, to estimate a soil UHS. Additionally, the slope of the soil hazard curve must be determined, to estimate a soil URS from which design motions can be obtained.

REFERENCE

McGuire, R.K., W.J. Silva, C.J. Costantino (2001). "Technical Basis for Revision of Regulatory Guidance on Design Ground Motions: Hazard and Risk-consistent Ground Motion Spectra Guidelines," U.S. Nuclear Reg. Comm., Rept NUREG/CR-6728, October.

Overview of Design Ground Motion Procedure and Application to Rock Sites

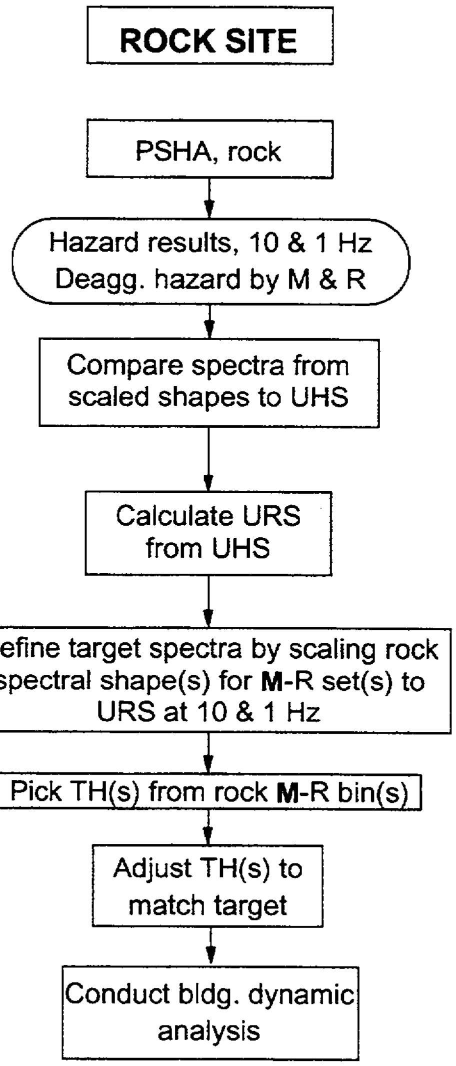

Figure 1-1. Flowchart of design ground motion procedure and application to rock sites.
TH = time history

Overview of Design Ground Motion Procedure and Application to Soil Sites

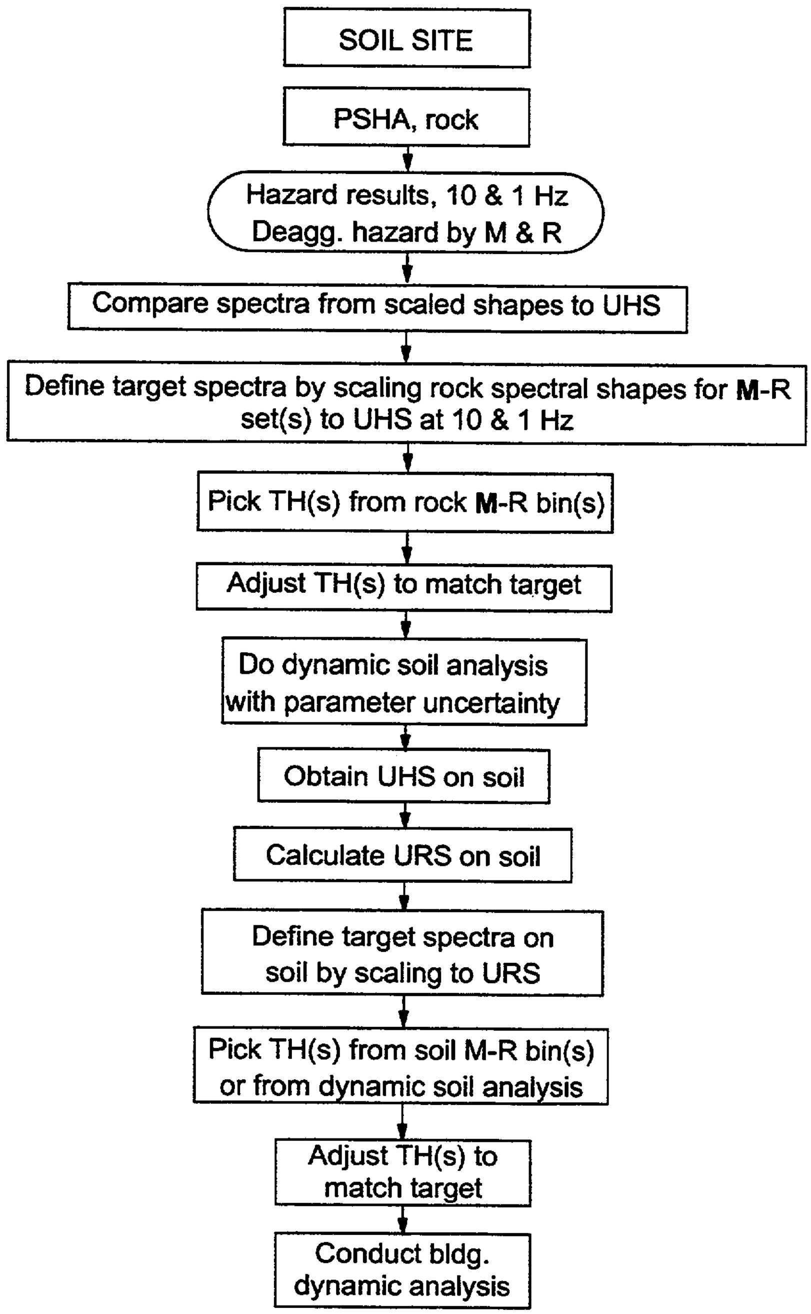

Figure 1-2. Flowchart of design ground motion procedure and application to soil sites. TH = time history

2.0 TWO SITES CHOSEN FOR IMPLEMENTATION STUDY

2.1 Mojave site seismic environment

A site in the Mojave Desert in California was chosen as the example site for the WUS. This site, the nearby faults, and background seismicity points are illustrated in Figure 2-1. The site is located at 117.5° W, 34.6° N.

Seismicity parameters for the faults and background points were selected following the USGS/ CDMG interpretation for California. In this interpretation, major earthquakes (**M**>6.5) are ascribed to faults, and lower-level seismicity is ascribed to background points. The rate of activity of these background points, spaced at 0.1° longitude and latitude, is calculated based on a smoothed interpretation of historical seismicity. An exponential magnitude distribution with a b=0.9 is assigned to these points.

The seismicity model for the faults was taken to be that used by the USGS/CDMG in deriving seismic hazard maps for California. That is, each fault is assumed to produce a single characteristic magnitude with a specified annual frequency of occurrence. The characteristic magnitudes and associated frequencies were taken from the USGS/CDMG work.

Important sources that contribute to the hazard at the Mojave site are the San Andreas Fault and the background seismicity. All faults with a closest approach within 50 km of the site were modeled, for completeness.

2.2 Columbia site seismic environment

Columbia, South Carolina was the site chosen as the example site in the CEUS. Its seismic hazard is affected by a local source and by the Charleston earthquake zone, represented here by a fictitious fault (see Figure 2-2).

Seismicity parameters of the two earthquake sources affecting Columbia were as follows. The local source consisted of a box surrounding Columbia, 220 km on a side, with a minimum magnitude $\mathbf{M}_{min}$ of 4.5 (corresponding to $m_{Lg} = 5$, which is standard for CEUS seismic hazard assessments) and a maximum magnitude $\mathbf{M}_x$ of 6.5. The seismicity in the local source was taken to be exponentially distributed and spatially homogeneous, with an annual rate of occurrence (υ_0) of 1.13E-2 and a Richter b-value of 0.9. Both values came from the US Geological Survey assessment of seismicity for the national hazard maps, the rate being calculated as an average over the spatially-varying rate for the southeastern US derived by the USGS.

For the fictitious Charleston fault, earthquakes between **M**=6.5 and 7.8 were considered equally likely, that is a characteristic magnitude model was used between these two magnitudes with a rate of occurrence υ_0=1.54E-3, meaning a mean recurrence period of 650 years. This is the rate used by the USGS for the Charleston fault, although they used a single characteristic magnitude of 7.3. We assumed a range of magnitudes for this test example to make the task of choosing a single (or a few) analysis earthquakes more challenging.

Both sources contribute to the hazard at Columbia as demonstrated in the next section. The background seismicity dominates the high-frequency motion, and the Charleston fault dominates the low-frequency motion.

2.3 Development of WUS and CEUS attenuation relations for generic rock and site specific soil sites

Regional- and site-(soil column) specific attenuation relations are required to evaluate the suitability of various approaches in developing soil spectra with hazard levels that are consistent with the control motions (rock outcrop UHS spectra). Soil-column-specific attenuation relations (median spectra and uncertainties) are used to generate uniform hazard spectra at the soil surface while regional-specific rock profiles are used to develop attenuation relations for outcropping rock. The soil uniform hazard spectra are then compared to soil motions generated by applying traditional equivalent-linear site response analyses using the rock UHS or scaled spectra as control motions. This process is applied to the California strong motion recording site Meloland assumed to be located in the WUS, and to a generic Savannah River profile assumed to be located in the CEUS (Sections 2.1 and 2.2). We developed appropriate attenuation relations for ground motions on these profiles, including parameter uncertainties and reflecting the appropriate crustal environments.

The process of developing site- and region-specific attenuation relations involves exercising the stochastic point source model (McGuire et al., 2001) for a suite of magnitudes and distances, and then regressing on the predicted ground motions. Site- and region-specific elements are introduced through the selection of appropriate model parameters and their uncertainties. Parametric uncertainty about the median ground motion regression (which includes regression uncertainty) is estimated through multiple ground motion estimates at each magnitude and distance based on random model parameters. This process results in a regression equation for median ground motions (5% damped response spectra) as a function of magnitude and distance, and in estimates of the uncertainty, both of which are required by probabilistic seismic hazard analyses. This process has been applied to a number of Department of Energy sites and to many other commercial projects and forms the basis for a number of CEUS attenuation relations. As a result, the process is both mature and stable, having undergone the scrutiny of widespread applications to engineered structures.

2.3.1 Point source model parameters

Dependent parameters for the point-source model include source depth (D), stress drop ($\Delta\sigma$), Q (f) model (deep crustal damping), kappa (shallow crustal damping), a crustal model, and a shallow profile along with nonlinear dynamic material properties parameterized through G/G_{max} and hysteretic damping curves. Independent parameters are magnitude and distance, which were selected to cover the appropriate range in **M** and *R* in the hazard analyses. Three magnitudes were run for the WUS (**M** 5.5, 6.5, and 7.5) and four magnitudes were run for the CEUS (**M** 4.5, 5.5, 6.5 and 7.5) over the distance range of 1 to 400 km (Tables 2-1 and 2-2).

For the dependent parameters, base case (mean or median) values and their uncertainties are listed in Table 2-1 for the WUS and Table 2-2 for the CEUS. Source depth distributions are based on region specific seismicity while Q(f) [$Q(f) = Q_o f^\eta$] models are based on inversions using the point-source model (Silva et al., 1997). WUS stress drops are based on inversions of the Abrahamson and Silva (1997) empirical attenuation relation and show a magnitude dependency (EPRI, 1993; Atkinson and Silva, 1997). CEUS stress drops (Table 2-2) are assumed to follow the same magnitude scaling as WUS. The **M** 5.5 stress drop was set to 160 bars to correspond to Atkinson's (1993) value, which is based on high frequency spectral levels from CEUS earthquakes. In her database of CEUS earthquakes the mean magnitude is about 5.5. Interestingly, these stress drop values result in an average (over magnitude) difference of about a factor of two between CEUS (122 bars, Table 2-2) and WUS (65 bars, Table 2-1), in agreement with Hanks and Johnston's (1992) analyses of intensity data.

Kappa values are based on ground motion observations at hard rock sites in the CEUS (EPRI, 1993; Silva and Darragh, 1995) and soft rock sites in the WUS. The WUS kappa value of 0.025 sec (Table 2-1) applied to the shallow portions of the Wald and Heaton (1994) crust (Table 2-3) and this value was adjusted to give a total kappa value of about 0.04 sec for WUS rock (EPRI, 1993; Silva and Darragh, 1995; Silva et al., 1997; Boore and Joyner, 1997). The remaining kappa, 0.015 sec, is contributed by the shallow geotechnical portion of the profile, which has a shear-wave velocity of about 250 m/sec at the surface and increases roughly linearly to 1 km/sec at a depth of 30m, where it merges with the Wald and Heaton (1994) crustal model (Figure 2-3). The shallow geotechnical profile was based on shear-wave velocity measurements at strong motion sites classified as rock (Silva et al., 1997). The profile is considered nonlinear to a depth of 30m (shear-wave velocity of 1 km/sec, Table 2-3) and the damping for the shallow kappa contribution is taken from the rock damping curve (Figure 2-5). The crustal model is shown in Figure 2-3 along with the generic CEUS hard rock crustal model (Table 2-4).

The kappa value for the CEUS rock site is 0.006 sec (Table 2-2), which is significantly lower than the 0.04 sec value for the WUS rock site and is based on analyses of recordings at hard rock CEUS sites (EPRI, 1993). The variability in kappa, $\sigma_{\ln k} = 0.30$, is assumed to be the same in WUS and CEUS and is the observed variability in kappa values at rock sites in northern California that recorded the **M** 6.9 1989 Loma Prieta earthquake (EPRI, 1993). While this uncertainty of 0.3 for kappa may seem low to characterize both epistemic (uncertainty in the median value) and aleatory (uncertainty about the median value) variability in a site specific kappa value, the point-source modeling uncertainty (Silva et al., 1997) already accommodates the effects of kappa variability. This is the case because a fixed kappa value of 0.03 sec was used to characterize the linear rock damping at all rock sites in the validation exercises. As a result, site specific departures of kappa from the assumed constant value of 0.03 sec increases model deviations from recorded motions, and this results in larger estimates of model uncertainty. This also applies to shallow rock profiles and soil profiles (to a depth of 300m [1,000 ft]), both of which were randomized in developing the attenuation relations. While it is possible that the total variability in the attenuation relations is overestimated due to this probable double counting, validations are sparse for the CEUS (and are nonexistent for deep soil sites), and are sparse for **M** larger than about 7.0 in the WUS. Thus the assessment and partitioning of appropriate variability is not an unambiguous issue, particularly in the CEUS, and the approach taken here is to follow prudent design practice and not underestimate uncertainty.

To illustrate the profile variability (which was assessed over the top 300m, to be consistent with the deepest soil profile also described in the next section), Figure 2-4 shows median and $\pm$ 1σ shear-wave velocity profiles for the WUS and CEUS rock sites (Figure 2-3). The profile randomization scheme was developed by Toro (1997) based on an analysis of variance of over 500 measured profiles. The analysis is appropriate for WUS rock (both hard and soft) and soil conditions (EPRI, 1993; Silva et al., 1997). For WUS rock the soft rock model was used. For the CEUS profile, the WUS hard rock model was used, since there are few, if any, shallow CEUS rock geotechnical profiles with which to develop statistics on variability.

The profile variability models for rock are based on an analysis of variance of all rock profiles in the database and therefore are appropriate for generic applications. Site-specific applications would likely result in a lower variability that reflects random (aleatory) variations over the dimensions of a foundation (or to a foundation dimension extending outside the footprint) as well as uncertainty in the mean or base case profile (epistemic). To develop these non-generic or small area models, multiple closely spaced holes are necessary. Such an analysis was undertaken at a deep soil site in the CEUS, and a footprint correlation model was developed by Silva et al., 1997. However, similar data are not currently available for rock sites. The use of a generic statistical model for both WUS and CEUS rock sites therefore may also contribute to an overestimate of the variability in the rock outcrop attenuation relations.

To accommodate potential nonlinear response in the shallow portion (top 30m) of the soft rock profile (Table 2-3, Figures 2-3 and 2-4), the modulus reduction and hysteretic damping curves shown in Figure 2-5 were used. These curves were developed by modeling the rock site motions produced by a recently developed empirical attenuation relation (Abrahamson and Silva, 1997). The generic WUS rock profile (Figure 2-3) was used in developing the G/G_{max} and hysteretic damping curves and were validated by modeling the motions recorded from 17 earthquakes at about 150 soft rock sites (Silva et al., 1997).

As with the soil material strain dependencies (Section 2.3.2), the rock G/G_{max} and hysteretic damping curves were randomized based on an analysis of variance of recent laboratory dynamic test results. To develop probabilistic models, multiple test results were analyzed and yielded standard errors (natural log) of 0.1 and 0.3 for G/G_{max} and hysteretic damping respectively, these values calculated at cyclic shear strains of 0.03%. These variabilities are appropriate for within-class (cohesionless or cohesive soil) uncertainties and were used to generate suites of random curves that follow the shapes of the base case G/G_{max} and hysteretic damping curves (EPRI, 1993). In the randomization process, upper and lower bounds of about $\pm$ 2 σ were used to prohibit physically implausible excursions (EPRI, 1993).

To model nonlinear response at the WUS rock site and at the soil sites, RVT equivalent-linear analyses were performed (EPRI, 1993). This process, the use of the simple point-source model coupled to RVT equivalent-linear site response, has been validated at about 500 sites for 17 earthquakes (Silva et al., 1997). This validation showed that the process results in an acceptably accurate characterization of strong ground motions for engineering design.

2.3.2 Soil profiles and nonlinear properties

The Meloland measured shear-wave velocity profile was analyzed at the WUS site and the generic Savannah profile was analyzed at the CEUS site, for the application of soil-site procedures. The soil profile was either merged (WUS) or placed on top (CEUS) of the rock crustal models (the Wald and Heaton, 1994 model for the WUS site, see Table 2-3; the hard rock profile developed here for the CEUS, see Table 2-4). The Meloland profile in the Imperial Valley is actually located at a strong motion site that recorded the 1979 **M** 6.5 Imperial Valley earthquake. The site recorded a maximum horizontal peak acceleration of about 0.4g with about 0.6g reflecting the highest peak acceleration at similar sites in the region.

The base case shear-wave velocity profile for the Meloland site is shown in Figure 2-6a. Meloland is a "bottomless" soft profile (i.e. it has no sharp shear-wave contrast at the soil-bedrock interface) consisting mainly of silty clays and silty sands with clay zones having a plasticity index (PI) less than about 20 but with some medium hard (MH) clays (PI ≈ 40). The soil profile was truncated at a depth of 300m. For the CEUS site, the generic Savannah River profile is shown in Figure 2-6b. The profile reaches a shear-wave velocity of 1 km/sec at a depth of about 220m, which was extended to 300m. It is placed on top of the CEUS crustal model (Table 2-4).

As with the shallow rock profile, the soil profiles (top 300m) were randomized using the same approach but with a soil statistical model appropriate for a footprint areal extent. The resulting median and $\pm 1\ \sigma$ profiles are show in Figures 2-7a and 2-7b for the Meloland and generic Savannah River profiles, respectively. Compared to the rock site generic variability shown in Figure 2-4, the footprint soil site variability is significantly smaller. Part of the difference is caused by deep soil sites showing significantly smaller absolute variability than rock sites (EPRI, 1993; Silva et al., 1997). The remaining difference is attributed to variability over a limited area or similar depositional environment vs. generic conditions.

In addition to velocity and layer thickness variability, depth to underlying bedrock material (1 km/sec for the WUS, Table 2-3; 2.83 km/sec for the CEUS, Table 2-4) was also varied $\pm 10\%$ (uniform distribution) to accommodate changes that may occur over a site.

For the Meloland soil site, a regional set of G/G_{max} and hysteretic damping curves were used. Validation exercises using the stochastic point-source model at Meloland for the Imperial Valley earthquake showed that the Vucetic and Dobry (1991) (depth-independent) curves for cohesive soils resulted in too much nonlinearity (overdamping). Additional validation exercises for the Los Angeles area (Peninsular Range) soils showed too much nonlinearity using the recently developed EPRI curves for cohesionless soils. As a result, revised sets of curves were developed for Imperial Valley and Peninsular Range soils by modeling exercises at a number of soil sites (Silva et al., 1997). The Peninsular Range curves were assumed for the relatively stiff cohesionless soils of the Savannah River generic profile (Figure 2-8b). The revised sets of region-specific curves are shown in Figure 2-8a for Imperial Valley soils. For reference, G/G_{max} and hysteretic damping curve recommendations from SHAKE (1991) and Vucetic and Dobry (1991) are shown in Figures 2-9 and 2-10. The revised curves generally reflect more linear response, particularly at depth. This may result from the maximum depth over which the profiles are considered nonlinear, which was taken to be 150m based on extensive validation exercises. The SHAKE (1991) and Vucetic and Dobry (1991) curves are independent of depth and may not have been intended to be implemented over such large depth ranges.

For the soil profiles, material damping was fixed at the low-strain value from the corresponding damping curves and linear analyses assumed for depths exceeding 150m (500 ft). The kappa value for the rock material was kept at 0.006 sec for CEUS sites and 0.03 sec for the WUS sites. For the WUS soil sites, the total kappa values were about 0.04 sec, similar to WUS rock and consistent with observations at low strains (Silva et al., 1997). For the CEUS soil sites, this process resulted in total kappa values for the soil sites between about 0.01 and 0.02 sec, as the low strain kappa values for the soil columns was about 0.01 sec. This suggests the possibility of different spectral shapes for the same soil profile located in the WUS and CEUS, particularly at low loading levels and with similar limited depth to base rock material.

In general the evaluation of appropriate nonlinear properties (e.g. G/G_{max} and hysteretic damping curves) for a particular site requires considerable judgment.

The curves used in this study (and in McGuire et al., 2001) are generic. They are based on both high quality laboratory testing as well as validation and refinement through analyses of recorded motions at moderate-to-high loading conditions. Recently these soil models have become increasingly linear; that is, less modulus degradation and lower hysteretic damping occurs with induced cyclic shear strain. These characteristics have been required to better reproduce recorded motions through convolution studies.

In addition, detailed review of some proposed soil models developed from laboratory studies have indicated potential problems. These problems have tended to arise from disturbance effects induced in the sample from both sampling and sample preparation processes. Such disturbance effects can lead to soil models which are too nonlinear which can tend to seriously erode the proper characterization of soil site response and will tend to lead to underestimates of ground response at the soil surface.

As a result, site specific or alternate generic nonlinear dynamic material properties could depart significantly from the curves presented here (and in McGuire et al., 2001). It is therefore critical for these cases to ensure that where nonlinear dynamic material properties are deduced from laboratory studies, the sampling and testing programs are critically peer reviewed to ensure that the generated soil models are appropriate to properly characterize site response. If possible, the selected nonlinear properties should be validated at sites with appropriate soil conditions and with recordings reflecting moderate-to-high levels of loading conditions.

2.3.3 Form of attenuation relations

The functional form used in the regression analyses accommodates magnitude saturation, from a magnitude-dependent stress drop and potential nonlinear response, and accommodates a magnitude-dependent, far-field attenuation (Tables 2-1 and 2-2):

$$\ln(y) = c_1 + c_2 M + (c_6 + c_7 M) \cdot \ln (R + e^{c_4}) + c_{10} (M - 6)^2 \qquad (2\text{-}1)$$

where R is taken as the closest distance to the surface projection of the rupture (Boore et al., 1997). In arriving at this functional form, about 15 variations were used in regression analyses. This particular form resulted in the best combination of low sigma, accommodation of significant trends with **M** and R, stability over oscillator frequency (smoothness in spectral shape), and simplicity. The fictitious depth term c_4 in equation (2-1) appears to be related to nonlinear site response, being nearly constant for CEUS rock (with a value near 3) and increasing strongly with frequency for WUS rock and for soil profiles (Tables 2-5 to 2-8). For the CEUS both single- and double-corner source models (McGuire et al., 2001) were run to replicate epistemic uncertainties in CEUS ground motion models and to show how this uncertainty should be treated.

To illustrate the nature of the fits to the simulations and the distribution about the regression lines, Figures 2-11 and 2-12 show peak accelerations for **M** 7.5, for WUS and CEUS (single- corner source model) rock conditions, respectively. The model captures the trends in the simulations for both rock site conditions. Variability about the regression for the CEUS (Figure 2-12) is larger than for the WUS (Figure 2-11) reflecting the larger variability in stress drop and source depth (Tables 2-1 and 2-2) and in the shallow profile (Figure 2-4). The increase in variability at large distance for both WUS and CEUS results from the effects of variability in Q(f). The large variability at close distance for the CEUS results from the large range in source depth. The difference in the variability between WUS and CEUS rock site conditions for peak acceleration is significant, being about 0.65 for CEUS and 0.57 for WUS (this is presented below in connection with Figure 2-19).

2.3.4 Attenuation relations for WUS and CEUS rock site conditions

Attenuation curves of peak acceleration for **M** 5.5, 6.5, and 7.5 for WUS and CEUS rock site conditions predicted by the regression equations are shown in Figures 2-13 and 2-14 respectively. Figure 2-14a plots results for the single-corner source model, and Figure 2-14b plots results for the double-corner source model (Atkinson, 1993). Magnitude saturation at close distances is apparent in the decreasing jumps in peak acceleration as **M** increases. This results primarily from the magnitude dependent stress drops (Tables 2-1 and 2-2). CEUS peak accelerations for the single-corner source model exceed WUS by about 30% to 50% at large distance and are comparable at close distances, because of the greater CEUS source depths (Tables 2-1 and 2-2). For the double-corner CEUS relation, the implied stress drop associated with high frequency ($f \geq 1$ Hz) ground motion is independent of magnitude with a value of about 150 bars (for the CEUS crustal model, see Figure 2-3 and Table 2-4). This results in significantly higher large magnitude high frequency motions (McGuire et al., 2001) and no magnitude saturation (Figure 2-14b). The WUS relation is generally consistent with empirical relations for comparable site conditions. The CEUS single-corner relation shows lower peak accelerations than the Toro et al., 1997 and EPRI, 1993 relations, particularly at large magnitude. This difference results from the assumption of decreasing stress drop with increasing magnitude in the CEUS (Table 2-2). Toro et al. (1997) used a constant stress drop of 120 bars, resulting in motions that may be too high at large magnitudes and somewhat low at small magnitudes. Tables 2-5 and 2-6 list the regression coefficients for rock sites, and includes the uncertainty due to parametric variability and regression fit. For the CEUS double-corner source model, variabilities were not available for the low and high frequency stress drops (corner frequencies), so the single-corner parametric variability was assumed to be appropriate for the double-corner model (for both the rock and soil attenuation relations).

To illustrate the resulting spectra for typical conditions, Figure 2-15 shows spectral accelerations (5% of critical damping) at a distance of 10 km for magnitudes 5.5, 6.5, and 7.5 for WUS rock site conditions. Since the regression coefficients (equation (2-1)) were not smoothed, some of the crustal resonances are present in the spectra. Shallow profile resonances (top 30m) were smoothed in the profile randomization, and the bump in the spectra near 0.5 Hz results from a deeper crustal velocity discontinuity (Figure 2-3). For **M** 6.5, Figure 2-16 shows median and $\pm 1\sigma$ estimates of the WUS rock site spectra. Interestingly, the logarithmic standard deviation displayed in Figure 2-16 decreases at low frequency, which is opposite the trend in most empirical regressions (Abrahamson and Shedlock, 1997). The modeling uncertainty, however, increases with decreasing frequency (Silva et al., 1997) and, when combined with the parametric uncertainty, reverses the trend exhibited in Figure 2-16. Apparently neither the model nor regressions on recorded motions capture deterministic elements in the WUS strong ground motions at low frequency. Interesting, the empirical relation of Campbell (1997), which includes depth to basement material ($V_S \approx 3$ km/sec), results in a largely frequency-independent sigma. Since sigma is computed over all site conditions, the depth dependency suggests that the effects of deep sedimentary basins may not be fully captured in other empirical relations that neglect the depth-to-basement term.

For the CEUS rock site conditions, Figures 2-17 and 2-18 show corresponding plots prepared using equation (2-1) and the coefficients of Table 2-6. The CEUS spectra show the expected shift in peak to higher frequencies (near 30 Hz) and the larger uncertainty in CEUS predictions (Figure 2-18). Figures 2-17a and 2-18a plot the single-corner source model and Figures 2-17b and 2-18b plot the double-corner source model. The difference in motions between the two source models depends on magnitude and frequency. The single-corner source model generally shows larger low-frequency motions and smaller high-frequency motions than the double-corner source model (McGuire et al., 2001), with the difference being greatest at large magnitude (**M** $\geq$ 6.5). The large difference in ground motion variabilities between the single- and double-corner source models (Figures 2-18a and 2-18b) reflects the large contribution of stress drop variability. This variability is not included in the double-corner estimates of variability shown in Figure 2-18b, as explained previously.

Logarithmic uncertainties for WUS and CEUS rock site conditions are plotted in Figure 2-19. This sigma reflects variation about the median regression over the magnitude and distances listed in Tables 2-1 and 2-2. It includes only the variability in motions due to parametric variability and goodness-of-fit using the functional form shown in equation (2-1). The difference between CEUS and WUS sigmas ranges up to about 30% at high frequency (above 10 Hz), but the two uncertainties are comparable moderate and low frequency (less than 10 Hz). As previously mentioned, the uncertainty for CEUS rock site conditions exceeds that for WUS because of the larger variability in stress drop and source depth (see Tables 2-1 and 2-2) and in the shallow (300m) part of the crustal models.

These rock outcrop attenuation relations are not intended for use exclusively of others. They are used in this study to provide consistency between the rock and site specific soil attenuation relations. For applications to WUS crustal conditions, if appropriate empirical relations are available their use is preferred. For the CEUS and regions of the WUS where ground motion data are sparse, provided the relations presented here reflect appropriate parameter values and produce motions consistent with available recordings, they may be used in hazard evaluations.

2.3.5 Attenuation relations for WUS and CEUS soil site conditions

This section illustrates the attenuation of peak acceleration and the magnitude dependence of response spectra at a distance of 10 km for the soil profiles Meloland (WUS) and Savannah River generic (CEUS). Results are presented for WUS and CEUS source and path conditions, as appropriate.

Figures 2-20 through 2-23 show the attenuation of peak acceleration and the magnitude dependence of spectra at 10 km for the two profiles and, in the case of the CEUS, for the single- and double-corner source models. Tables 2-7 and 2-8 list the coefficients.

For both the Meloland and Savannah River generic profiles, the magnitude saturation effect is very strong near 10 Hz (Figures 2-21 and 2-23). This trend indicates that the soils saturate in the levels of motion they can transmit as strains increase to high levels. This observation is not new, since soils are known to fail (lose shear strength) at very high loading levels and simply will not propagate waves with wave lengths shorter than about four times the width of the failed zone. However, early predictions on saturation of peak acceleration have routinely been exceeded, suggesting an incorrect assumption in the dynamic nonlinear properties of soils, particularly soft soils. The revised sets of G/G_{max} and hysteretic damping curves, based on modeling high levels of motions (Figure 2-8), are believed to capture nonlinear properties reasonably well, meaning that the saturation displayed in spectral plots for the Meloland and Savannah River generic profiles are appropriate for these sites. These results should be confirmed with nonlinear (effective stress) analyses with properties adjusted so that the nonlinear soil models produce the same G/G_{max} and hysteretic damping curves used in the equivalent-linear analyses. This is an important issue and may have significant impacts on probabilistic seismic hazard analyses since the uncertainties typically used in attenuation relations assume a lognormal distribution, symmetric about the median in log spectral ordinates. Saturation, on the other hand, suggests a negatively skewed distribution (in log space) with a lower probability of motions above the median $+1\sigma$ level than below the median -1σ level, with the difference increasing with increasing cyclic shear-strains. To partially accommodate this effect, a magnitude- and distant-dependent uncertainty was used in the hazard analyses (Section 4).

The uncertainties about the regression equations over all magnitudes and distances (Tables 2-7 and 2-8) are shown in Figure 2-24 for WUS and CEUS (single-corner source model) conditions. These uncertainties result from the regression analyses and reflect parametric variability as well as goodness-of-fit provided by the regression functional form (equation (2-1)). They average about 0.5

to 0.6 (natural log units), lower than the corresponding sigmas for rock site conditions (Figure 2-19). This reduction is likely due to the reduced profile variability, (compare Figures 2-4 and 2-7), and the effect of nonlinear response, which dampens variability in the input motions (EPRI, 1993). Modeling (or model) uncertainty has not been added to the parametric plus regression uncertainty for the hazard study because it would mask the differences in approaches to soil hazard being examined here (see Section 6). Total uncertainty, which includes the addition of modeling uncertainty, would be the appropriate uncertainty to use in applications to assess probabilistic hazard at a site for actual design purposes (EPRI, 1993).

REFERENCES

Abrahamson, N.A and K.M. Shedlock (1997). "Overview." *Seis. Res. Let.,* 68(1), 9-23.

Abrahamson, N.A. and W.J. Silva (1997). "Empirical response spectral attenuation relations for shallow crustal earthquakes." *Bull. Seism. Soc. Am.*, 68(1), 94-127.

Atkinson, G.M and W.J. Silva (1997). "An empirical study of earthquake source spectra for California earthquakes." *Bull. Seism. Soc. Am.* 87(1), 97-113.

Atkinson, G.M. (1993). "Source spectra for earthquakes in eastern North America." *Bull. Seism. Soc. Am.*, 83(6), 1778-1798.

Boore, D.M, and W.B. Joyner (1997). "Site amplifications for generic rock sites." *Bull. Seism. Soc. Am.*, 87(2), 327-341.

Boore, D.M., W.B. Joyner and T.E. Fumal (1997). "Equations for estimating horizontal response spectra and peak acceleration from Western North American earthquakes: A summary of recent work." *Seism. Res. Let.,* 68(1), 128-153.

Campbell, K W. (1997). "Empirical near-source attenuation relationships for horizontal and vertical components of peak ground acceleration, peak ground velocity, and pseudo-absolute acceleration response spectra." *Bull. Seism. Soc. Am.,* 68(1), 154-176.

Electric Power Research Institute (1993). "Guidelines for determining design basis ground motions." Electric Power Research Institute, Palo Alto, CA, EPRI TR-102293, vol. 1-5:
vol. 1: Methodology & guidelines for estimating earthquake ground motion in eastern NA
vol. 2: Appendices for ground motion estimation.
vol. 3: Appendices for field investigations.
vol. 4: Appendices for laboratory investigations.
vol. 5: Quantification of seismic source effects.

Hanks, T.C. and A.C. Johnston (1992). "Common features of the excitation and propagation of strong ground motion for north American earthquakes." *Bull. Seism. Soc. Am.*, 82(1), 1-23.

McGuire, R.K., W.J. Silva, C.J. Costantino (2001). "Technical Basis for Revision of Regulatory Guidance on Design Ground Motions: Hazard and Risk-consistent Ground Motion Spectra Guidelines," U.S. Nuclear Reg. Comm., Rept NUREG/CR-6728, October.

SHAKE (1991). "*A computer program for conducting equivalent linear seismic response analyses of horizontally layered soil deposits*." Sponsored by Structures Building and Fire Research Lab., Nat'l Institute of Standards and Technology, Gaithersburg, Maryland. Modifications by I. Idriss and J. Sun.

Silva, W.J. and R. Darragh (1995). "Engineering characterization of earthquake strong ground motion recorded at rock sites." Electric Power Res. Inst., Palo Alto, CA, Rept TR-102261.

Silva, W.J., N. Abrahamson, G. Toro, C. Costantino (1997). "Description and validation of the stochastic ground motion model." Report to Brookhaven National Laboratory, Associated Universities, Inc. Upton, New York, Contract 770573.

Toro, G.R. (1997). "Probabilistic Models of Site Velocity Profiles for Generic and Site-Specific Ground Motion Amplification Studies." Published as an appendix in Silva et al (1997).

Toro, G.R., N.A. Abrahamson, and J.F. Schneider (1997). "Model of strong ground motions from earthquakes in Central and Eastern North America: Best estimates and uncertainties." *Seism. Res. Let.,* 68(1), 41-57.

Vucetic, M. and R. Dobry (1991). "Effects of Soil Plasticity on Cyclic Response," *Journal of Geotechnical Engineering, ASCE,* 117(1), 89-107.

Wald, D.J. and T.H. Heaton (1994). "A dislocation model of the 1994 Northridge, California, earthquake determined from strong ground motions." *USGS,* Open-File Rpt. 94-278.

Table 2-1
Parameters for WUS Rock Outcrop Simulations

M 5.5, 6.5, 7.5

R(km) 1, 5, 10, 20, 50, 75, 100, 200, 400

30 simulations for each **M**, *R* pair = 810 runs

Randomly vary source depth, $\Delta\sigma$, kappa, Q_o, profile

Depth, $\sigma_{\ln D} = 0.6$, $\bar{R}$ (**M** > 5) = 8 km; Source, California Seismicity

M	Lower Bound (km)	$\bar{R}$ (km)	Upper Bound (km)
5.5	2	6	25
6.5	4	8	20
7.5	5	8	15

$\Delta\sigma$, $\sigma_{\ln\Delta\sigma} = 0.5$, Based on California earthquake inversions (Silva et al., 1997)

M	$\Delta\sigma$ (bars)	AVG. $\Delta\sigma$ (bars) = 65
5.5	85	Based on inversions of the Abrahamson and Silva (1997) relation.
6.5	64	
7.5	50	

Q(f), $\bar{Q}_o$ = 275, *Southern California inversions*; σ_{lnQ_o} = 0.4, (Silva et al., 1997)

η = 0.60, *Southern California inversions*; σ_η = 0, (Silva et al., 1997)

Varying Q_o only is sufficient, since $\pm 1\ \sigma$ covers range of Southern California inversions from 1 to 20 Hz

Kappa, $\bar{\kappa}$ = 0.025 sec, $\sigma_{\ln\kappa}$ = 0.3 (EPRI, 1997): linear zone ($V_S \geq 1$ km/sec)

Profile, California soft rock: GEOMATRIX A + B over Wald and Heaton (1994) Los Angeles Crust, randomize to 30m.

Geometrical attenuation $R^{-(a+bM)}$, a = 1.0296, b = -0.0422
$R^{-(a+bM)/2}$, R > 65 km

Based on inversions of the Abrahamson and Silva (1997) relation

Table 2-2
Parameters for CEUS Rock Outcrop Simulations

M 5.5, 6.5, 7.5

D(km) 1, 5, 10, 20, 50, 75, 100, 200, 400

30 simulations for each **M**, *R* pair = 810 runs

Randomly vary source depth, $\Delta\sigma$, kappa, Q_o, η, profile

Depth, $\sigma_{lnD} = 0.6$, $\bar{R}$ (**M** > 5) = 10 km; Intraplate Seismicity (EPRI, 1993)

M	Lower Bound (km)	$\bar{R}$ (km)	Upper Bound (km)
5.5	3	8	30
6.5	4	10	30
7.5	5	12	30

$\Delta\sigma$, $\sigma_{ln\Delta\sigma} = 0.7$ (EPRI, 1993)

M	$\Delta\sigma$ (bars)	AVG. $\Delta\sigma$ (bars) = 122; Assumes **M** 5.5 = 160 bars (Atkinson, 1993) with magnitude scaling taken from WUS (Table 2-1)
5.5	160	
6.5	120	
7.5	95	

Q(f), $\overline{Q_o}$ = 351, *Saguenay earthquake inversions*; σ_{lnQ_o} = 0.4, (Silva et al., 1997)

η = 0.84, *Saguenay earthquake inversions*; σ_η = 0, (Silva et al., 1997)

Varying Q_o only is sufficient, since $\pm$ 1 σ covers range of CEUS inversions from 1 to 20 Hz

Kappa, $\bar{\kappa}$ = 0.006 sec $\sigma_{ln\kappa}$ = 0.3, (EPRI, 1993)

Profile, Midcontinent Crust (EPRI, 1993), randomize to 300m

Geometrical attenuation $R^{-(a + bM)}$, a = 1.0296, b = -0.0422
$R^{-(a + bM)/2}$, R > 100 km

Based on inversions of the Abrahamson and Silva (1997) relation

Table 2-3
Southern California Crustal Model*

Thickness (km)	V_s (km/sec)	Density (cgs)
0.0015239	0.24383	2.0
0.0024383	0.30478	2.0
0.0030479	0.42670	2.0
0.0042670	0.53337	2.0
0.0033526	0.63091	2.0
0.0042670	0.71624	2.0
0.0057909	0.83016	2.0
0.0067503	0.96617	2.0
0.5	1.0	2.1
1.5	2.0	2.3
2.5	3.2	2.5
23.0	3.6	2.6
5.0	3.9	2.9
	4.5	3.0

Table 2-4
CEUS Crustal Model (EPRI, 1993 Midcontinent)

Thickness (km)	V_s (km/sec)	Density (cgs)
1.0	2.830	2.52
11.0	3.520	2.71
28.0	3.750	2.78
	4.620	3.35

*Wald and Heaton (1994) begins at $V_s = 1$ km/sec

Table 2-5
WNA Rock Attenuation Coefficients

Freq. (Hz)	c_1	c_2	c_4	c_6	c_7	c_{10}	$\sigma_{\ln y}$
0.2	-15.07355	2.28803	2.0	-1.42561	.05553	-.49468	.4089
0.4	-8.68981	1.56496	2.3	-1.76499	.08297	-.39232	.4721
0.5	-6.47823	1.30499	2.4	-1.91086	.09548	-.33494	.4886
0.6	-5.24277	1.14930	2.4	-1.98227	.10227	-.29832	.4712
1.	-1.33267	.70799	2.6	-2.30588	.12753	-.18914	.5187
1.3	.67113	.48815	2.7	-2.53819	.14943	-.14236	.5515
2.	3.95381	.15441	2.9	-2.98310	.19125	-.08925	.5724
2.5	5.55431	.00724	3.0	-3.20781	.21165	-.07728	.6010
3.	6.94024	-.12170	3.1	-3.42954	.23215	-.07278	.6221
4.	8.66812	-.28522	3.2	-3.71372	.25897	-.06717	.6291
5.	10.06003	-.40764	3.3	-3.95717	.27975	-.06039	.6370
6.	11.31119	-.51492	3.4	-4.18633	.29881	-.05821	.6367
7.	11.71011	-.56219	3.4	-4.27015	.30773	-.05541	.6388
8.	12.92842	-.66660	3.5	-4.49380	.32645	-.05512	.6390
10.	13.35592	-.72377	3.5	-4.59214	.33758	.05646	.6397
12.	13.54154	-.75771	3.5	-4.64435	.34432	-.05630	.6392
14.	13.65565	-.78728	3.5	-4.68724	.35100	-.05612	.6385
16.	12.75687	-.73975	3.4	-4.55259	.34412	-.05604	.6356
18.	12.65100	-.74165	3.4	-4.54515	.34469	-.05561	.6304
20.	12.47129	-.73133	3.4	-4.52315	.34314	-.05542	.6258
25.	11.24288	-.64422	3.3	-4.33387	.32974	-.05790	.6144
31.	10.09850	-.55919	3.2	-4.14941	.31588	-.05892	.5997
40.	9.69120	-.52302	3.2	-4.08971	.31031	-.06071	.5830
50.	8.72729	-.44775	3.1	-3.92599	.29736	-.06070	.5720
100.	8.49206	-.42582	3.1	-3.88996	.29388	-.06198	.5647
PGA	8.51069	-.42805	3.1	-3.88703	.29324	-.06028	.5655
PGV	5.27143	.39517	2.5	-3.04853	.24741	-.17693	.4586

Table 2-6a
ENA Rock Attenuation Coefficients
Single-corner Model

Freq. (Hz)*	c_1	c_2	c_4	c_6	c_7	c_{10}	$\sigma_{\ln y}$
0.2	-16.20991	2.49652	2.7	-1.58692	.05635	-.59273	.4167
0.4	-10.16041	1.83310	2.8	-1.87976	.08425	-.57716	.5078
0.5	-7.71149	1.54904	2.9	-2.03483	.09820	-.51778	.5194
0.6	-6.08736	1.33854	2.9	-2.11588	.10738	-.46899	.5220
1.	-1.84398	.81332	3.0	-2.44002	.14132	-.35788	.5276
1.3	.00430	.57674	3.0	-2.57387	.15757	-.29458	.5581
2.	2.43166	.27522	3.0	-2.75419	.17904	-.19872	.5634
2.5	3.39155	.16089	3.0	-2.83133	.18792	-.18914	.5783
3.	4.07443	.07375	3.0	-2.89207	.19480	-.13571	.5751
4.	5.29015	-.02768	3.1	-3.05076	.20786	-.13790	.5827
5.	5.81926	-.07821	3.1	-3.09271	.21166	-.13063	.5888
6.	6.14411	-.10668	3.1	-3.12637	.21465	-.11957	.5922
7.	6.45032	-.13433	3.1	-3.15042	.21655	-.11286	.5961
8.	6.64633	-.14804	3.1	-3.17080	.21812	-.10990	.6050
10.	7.63608	-.22487	3.2	-3.30190	.22694	-.09675	.6225
12.	7.85878	-.23912	3.2	-3.32890	.22891	-.09573	.6381
14.	8.02846	-.25176	3.2	-3.35244	.23069	-.09286	.6482
16.	8.18918	-.26865	3.2	-3.37280	.23226	-.08486	.6519
18.	8.34875	-.28887	3.2	-3.39042	.23362	-.07596	.6540
20.	8.49056	-.30814	3.2	-3.40586	.23484	-.06867	.6573
25.	8.79761	-.35210	3.2	-3.43792	.23746	-.05063	.6725
31.	9.67978	-.42541	3.3	-3.58327	.24787	-.04007	.6929
40.	10.04410	-.46691	3.3	-3.62090	.25119	-.05504	.7326
50.	10.15048	-.49206	3.3	-3.63049	.25133	-.01202	.7451
100.	8.32910	-.39607	3.2	-3.49089	.24863	-.05120	.6534
PGA	8.01521	-.36903	3.2	-3.47207	.24770	-.06451	.6387
PGV	5.60957	.38668	2.9	-3.12813	.24391	-.23165	.5251

*SA and PGA in g, PGV in cm/sec

Table 2-6b
ENA Rock Attenuation Coefficients
Double-corner Model

Freq. (Hz)	c_1	c_2	c_4	c_6	c_7	c_{10}	$\sigma_{\ln y}$
0.2	-13.34719	1.91021	2.7	-1.54032	.04731	-.38333	.4167
0.4	-8.16519	1.39932	2.9	-1.90878	.08018	-.23634	.5078
0.5	-6.80414	1.26025	2.9	-2.02956	.09463	-.19126	.5194
0.6	-5.79540	1.15773	2.9	-2.13792	.10789	-.16775	.5220
1.	-3.11160	.92878	3.0	-2.52258	.15109	-.18150	.5276
1.3	-1.84321	.81242	3.0	-2.64729	.16641	-.18533	.5581
2.	.27394	.60149	3.0	-2.80138	.18464	-.16462	.5634
2.5	1.30196	.49268	3.0	-2.86111	.19122	-.17390	.5783
3.	2.09397	.39888	3.0	-2.90936	.19644	-.12758	.5751
4.	3.53297	.27523	3.1	-3.05421	.20762	-.13367	.5827
5.	4.22534	.20596	3.1	-3.08968	.21056	-.12575	.5888
6.	4.66605	.16347	3.1	-3.12045	.21318	-.11309	.5922
7.	5.05561	.12547	3.1	-3.14287	.21486	-.10489	.5961
8.	5.31133	.10435	3.1	-3.16283	.21639	-.10100	.6050
10.	6.37944	.01780	3.2	-3.29300	.22504	-.08614	.6225
12.	6.65330	-.00290	3.2	-3.32066	.22708	-.08411	.6381
14.	6.85694	-.01977	3.2	-3.34480	.22891	-.08055	.6482
16.	7.04234	-.03969	3.2	-3.36590	.23053	-.07201	.6519
18.	7.21940	-.06199	3.2	-3.38405	.23190	-.06274	.6540
20.	7.37512	-.08287	3.2	-3.40016	.23315	-.05512	.6573
25.	8.34631	-.17182	3.3	-3.54380	.24297	-.03648	.6725
31.	8.60903	-.20481	3.3	-3.57998	.24612	-.02542	.6929
40.	8.99110	-.24821	3.3	-3.61832	.24933	-.03957	.7326
50.	9.12345	-.27688	3.3	-3.63110	.24966	.00639	.7451
100.	7.30879	-.18410	3.2	-3.49724	.24682	-.02587	.6534
PGA	6.98479	-.15610	3.2	-3.47944	.24601	-.03936	.6387
PGV	6.51003	.23997	3.0	-3.18672	.23808	-.12459	.5251

Table 2-7
WNA Soil Attenuation Coefficients
Meloland Profile

Freq. (Hz)	c_1	c_2	c_4	c_6	c_7	c_{10}	$\sigma_{\ln y}$
0.2	-14.79366	2.34611	2.0	-1.30310	.03351	-.44903	.4236
0.4	-7.57877	1.53337	2.2	-1.77620	.08364	-.34626	.4590
0.5	-4.57983	1.14690	2.4	-2.09712	.12540	-.29611	.4363
0.6	-2.32052	.85779	2.6	-2.33181	.15398	-.25486	.4444
1.	2.97459	.22254	2.9	-2.91186	.22047	-.16493	.4599
1.3	4.26798	.08493	3.0	-3.06475	.22888	-.13884	.4820
2.	9.49210	-.53398	3.3	-3.87960	.32441	-.10106	.5015
2.5	12.71682	-.90851	3.5	-4.39494	.38377	-.08527	.5036
3.	14.75347	-1.15533	3.6	-4.71940	.42266	-.07488	.5118
4.	17.48099	-1.50130	3.7	-5.21022	.48190	-.06209	.5294
5.	21.00123	-1.89390	3.9	-5.79498	.54618	-.05371	.5312
6.	21.29599	-1.94596	3.9	-5.86151	.55512	-.05182	.5290
7.	21.28144	-1.95033	3.9	-5.86701	.55507	-.04711	.5283
8.	21.20482	-1.94677	3.9	-5.86410	.55400	-.04046	.5264
10.	20.91175	-1.91782	3.9	-5.82368	.54829	-.03502	.5262
12.	18.99363	-1.71934	3.8	-5.51762	.51534	-.03331	.5188
14.	18.37632	-1.63593	3.8	-5.42634	.50172	-.03389	.5134
16.	16.62846	-1.45166	3.7	-5.14314	.47122	-.03515	.5074
18.	15.09565	-1.29202	3.6	-4.89674	.44538	-.03854	.5016
20.	14.74662	-1.24279	3.6	-4.84672	.43782	-.04137	.4971
25.	13.20808	-1.07739	3.5	-4.60376	.41156	-.04580	.4887
31.	11.97449	-.95102	3.4	-4.40563	.39138	-.04922	.4837
40.	11.76486	-.92102	3.4	-4.37960	.38739	-.05189	.4800
50.	11.67101	-.90757	3.4	-4.36871	.38572	-.05332	.4782
100.	11.58735	-.89572	3.4	-4.35865	.38419	-.05448	.4769
PGA	10.79847	-.82842	3.3	-4.21658	.37161	-.05187	.4774
PGV	5.52514	.47014	2.6	-2.84291	.21580	-.15289	.4340

Table 2-8a
ENA Soil Attenuation Coefficients
Single-corner Model

Freq. (Hz)	c_1	c_2	c_4	c_6	c_7	c_{10}	$\sigma_{\ln y}$
0.20	-13.46820	2.17130	2.7	-1.67419	.05839	-.33475	.4575
0.40	-9.89286	1.95352	2.7	-1.68767	.04480	-.45054	.5365
0.50	-8.04432	1.77492	2.7	-1.80349	.05968	-.46856	.5399
0.60	-5.32191	1.43172	2.8	-2.11656	.10825	-.47163	.5168
1.00	-2.80428	1.11337	2.9	-2.29798	.12009	-.40219	.5625
1.30	00.19768	.74467	3.0	-2.60912	.16359	-.35786	.5643
2.00	2.142000	.46727	3.0	-2.78470	.18589	-.28980	.5789
2.50	5.108680	.06749	3.2	-3.17610	.24345	-.25946	.5536
3.00	5.730590	.00237	3.2	-3.27162	.24991	-.23697	.5941
4.00	7.202390	-.23007	3.2	-3.45317	.28163	-.20367	.5918
5.00	9.068490	-.49378	3.3	-3.73124	.32256	-.18881	.5735
6.00	10.51087	-.68183	3.4	-3.96146	.35227	-.17356	.5743
7.00	11.02282	-.77051	3.4	-4.02002	.36418	-.16911	.5702
8.00	12.30466	-.92417	3.5	-4.22802	.38865	-.16348	.5801
10.00	13.04199	-1.06225	3.5	-4.33863	.41066	-.15138	.5809
12.00	14.36650	-1.22462	3.6	-4.55542	.43635	-.14297	.5730
14.00	14.60592	-1.27242	3.6	-4.59270	.44329	-.13784	.5720
16.00	15.81457	-1.40855	3.7	-4.79204	.46486	-.13234	.5723
18.00	15.83779	-1.41944	3.7	-4.79439	.46539	-.12877	.5766
20.00	15.79335	-1.41821	3.7	-4.79295	.46497	-.12554	.5776
25.00	15.60403	-1.39813	3.7	-4.76756	.46027	-.11831	.5866
31.00	15.20687	-1.33830	3.7	-4.72216	.45059	-.11664	.5904
40.00	13.62076	-1.15201	3.6	-4.48030	.41966	-.11532	.5877
50.00	13.03486	-1.05485	3.6	-4.41445	.40545	-.11948	.5836
100.0	10.12073	-.69989	3.4	-4.00714	.35364	-.13737	.5696
PGA	10.00517	-.67940	3.4	-3.99504	.35058	-.13799	.5706
PGV	5.970300	.48921	2.9	-2.99431	.22119	-.24318	.5551

Table 2-8b
ENA Soil Attenuation Coefficients
Double-corner Model

Freq. (Hz)	c_1	c_2	c_4	c_6	c_7	c_{10}	$\sigma_{\ln y}$
0.2	-11.68753	1.75687	2.7	-1.67563	.05803	-.31947	.4575
0.4	-8.53757	1.61478	2.8	-1.76645	.05208	-.28536	.5365
0.5	-7.44955	1.56539	2.8	-1.81054	.05412	-.25663	.5399
0.6	-5.32462	1.33981	2.9	-2.07425	.09220	-.24186	.5168
1.	-3.44962	1.12158	2.9	-2.27562	.11334	-.18710	.5625
1.3	-1.00704	.88393	3.0	-2.53903	.14750	-.18048	.5643
2.	0.888050	.65634	3.0	-2.72212	.17064	-.17311	.5789
2.5	3.370070	.31278	3.1	-3.02331	.22163	-.18018	.5536
3.	3.837880	.29120	3.1	-3.06863	.21864	-.17275	.5941
4.	6.102460	-.00163	3.2	-3.36031	.25959	-.16476	.5918
5.	8.148440	-.28331	3.3	-3.64975	.30241	-.16424	.5735
6.	9.054380	-.43569	3.3	-3.77384	.32498	-.15811	.5743
7.	10.38986	-.59729	3.4	-3.96016	.34793	-.15892	.5702
8.	11.01992	-.70282	3.4	-4.05205	.36406	-.15818	.5801
10.	12.82658	-.95201	3.5	-4.33487	.40417	-.15305	.5809
12.	14.43801	-1.16336	3.6	-4.59703	.43820	-.14936	.5730
14.	14.90221	-1.25136	3.6	-4.67086	.45208	-.14746	.5720
16.	16.30052	-1.42129	3.7	-4.90004	.47925	-.14443	.5723
18.	16.43841	-1.45524	3.7	-4.92024	.48350	-.14092	.5766
20.	16.47880	-1.47228	3.7	-4.93247	.48607	-.13676	.5776
25.	17.54555	-1.58996	3.8	-5.11309	.50360	-.12705	.5866
31.	17.17517	-1.54047	3.8	-5.06993	.49480	-.12083	.5904
40.	16.49071	-1.43517	3.8	-4.97584	.47601	-.11247	.5877
50.	14.67235	-1.21557	3.7	-4.70503	.44066	-.11021	.5836
100.	11.31446	-.79933	3.5	-4.23331	.37818	-.11554	.5696
PGA	10.34848	-.70192	3.4	-4.07802	.36229	-.11577	.5706
PGV	7.184400	.25885	3.0	-3.17174	.24092	-.12760	.5551

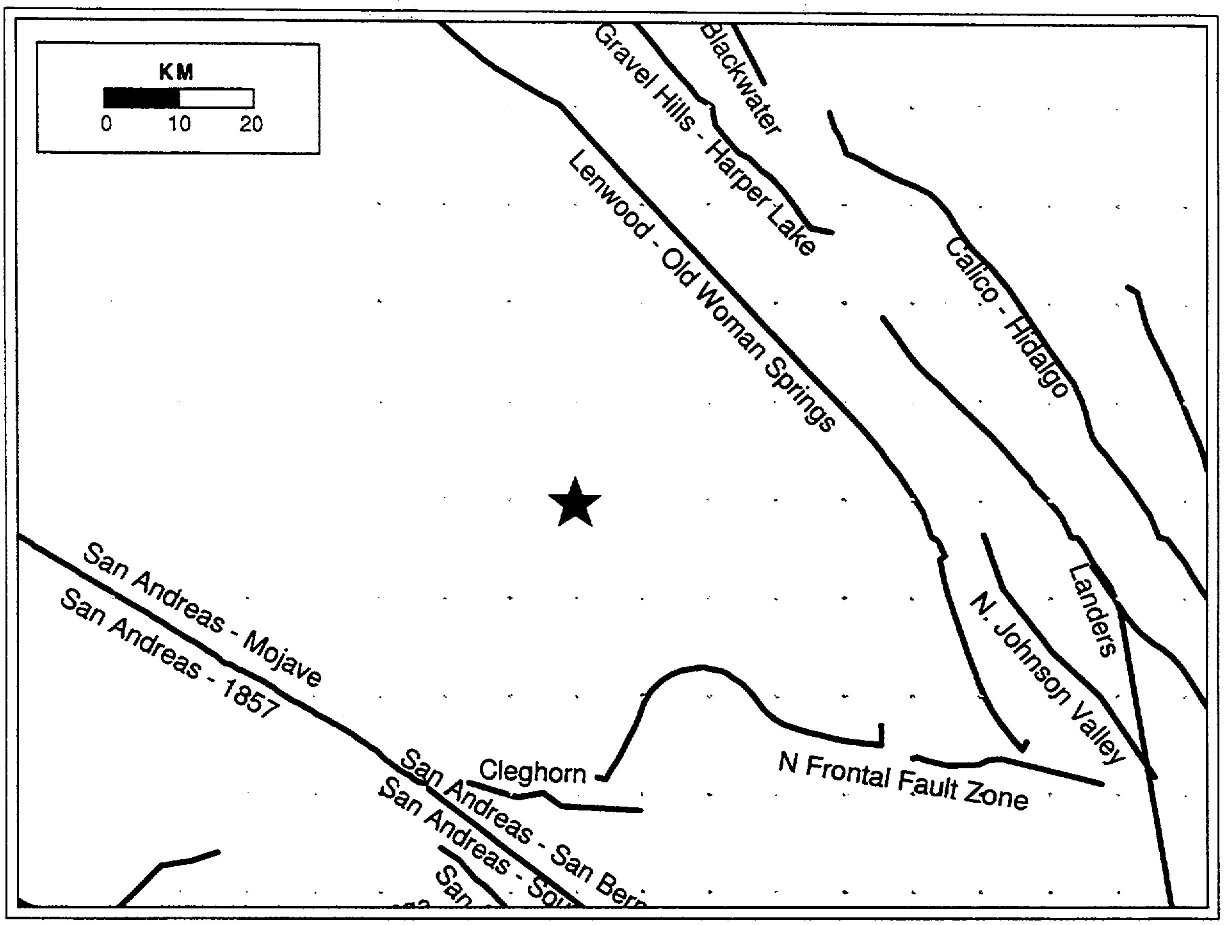

Figure 2-1. Seismic sources used for WUS example site (Mojave Desert), including nearby faults and background seismicity points.

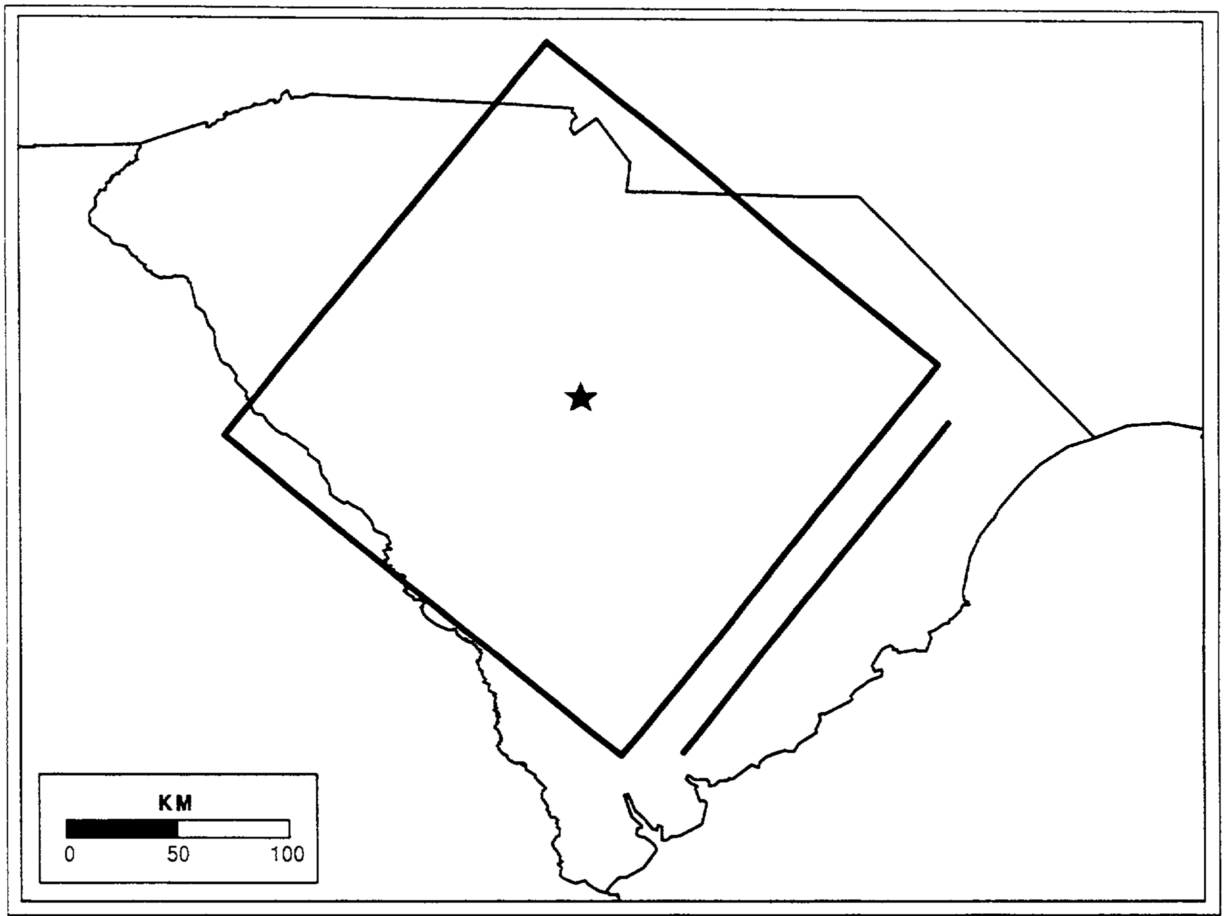

Figure 2-2. Seismic sources used for CEUS example site (Charleston, South Carolina).

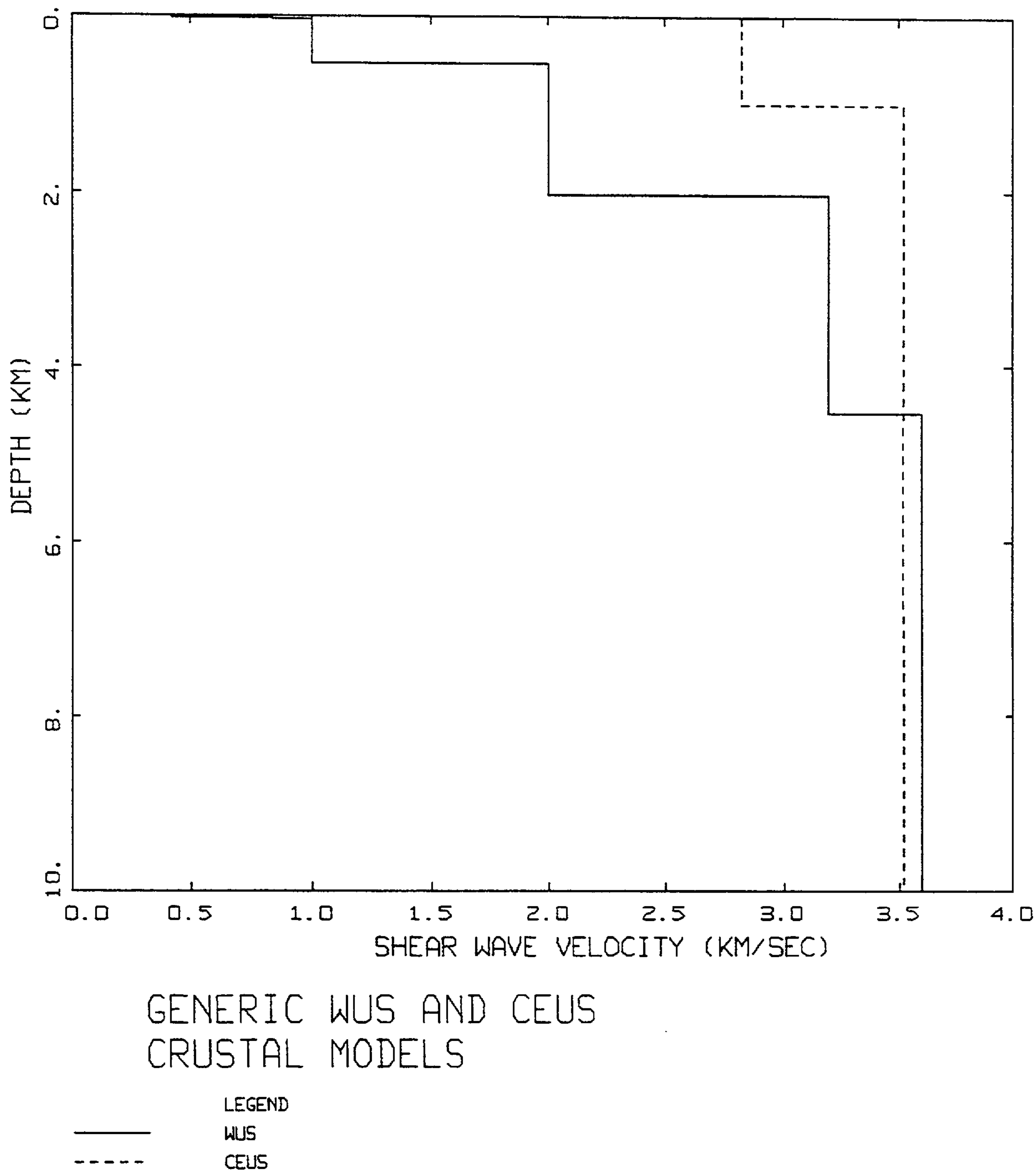

Figure 2-3. Comparison of generic shear-wave velocity profiles for WUS (Los Angeles) and CEUS crustal conditions.

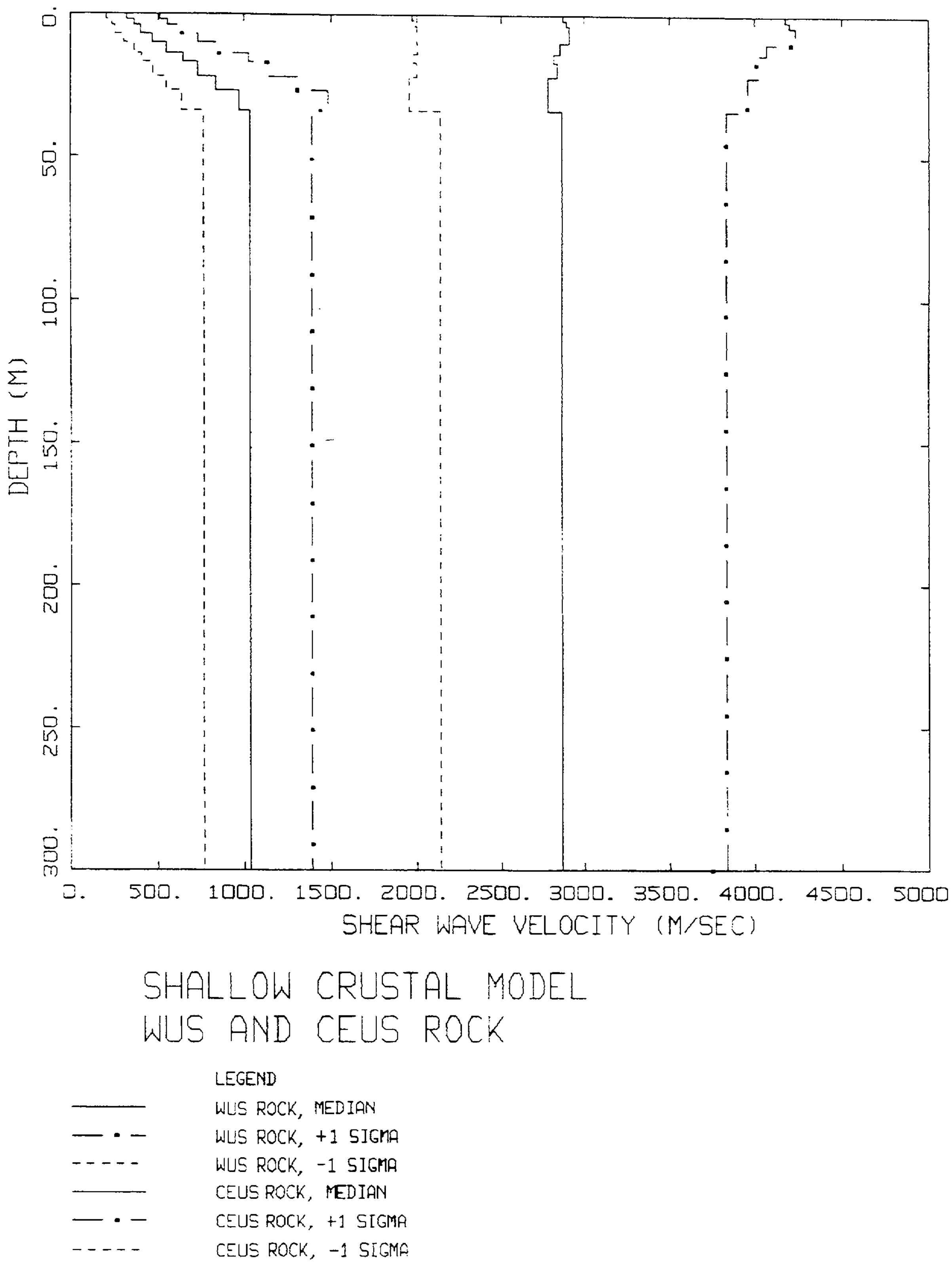

Figure 2-4. Variations in base case shallow crustal velocities. Solid lines are median estimates from a suite of randomly generated profiles (30) using base-case profiles (Figure 2-3) as input. Ranges reflect $\pm$ 1 σ estimates.

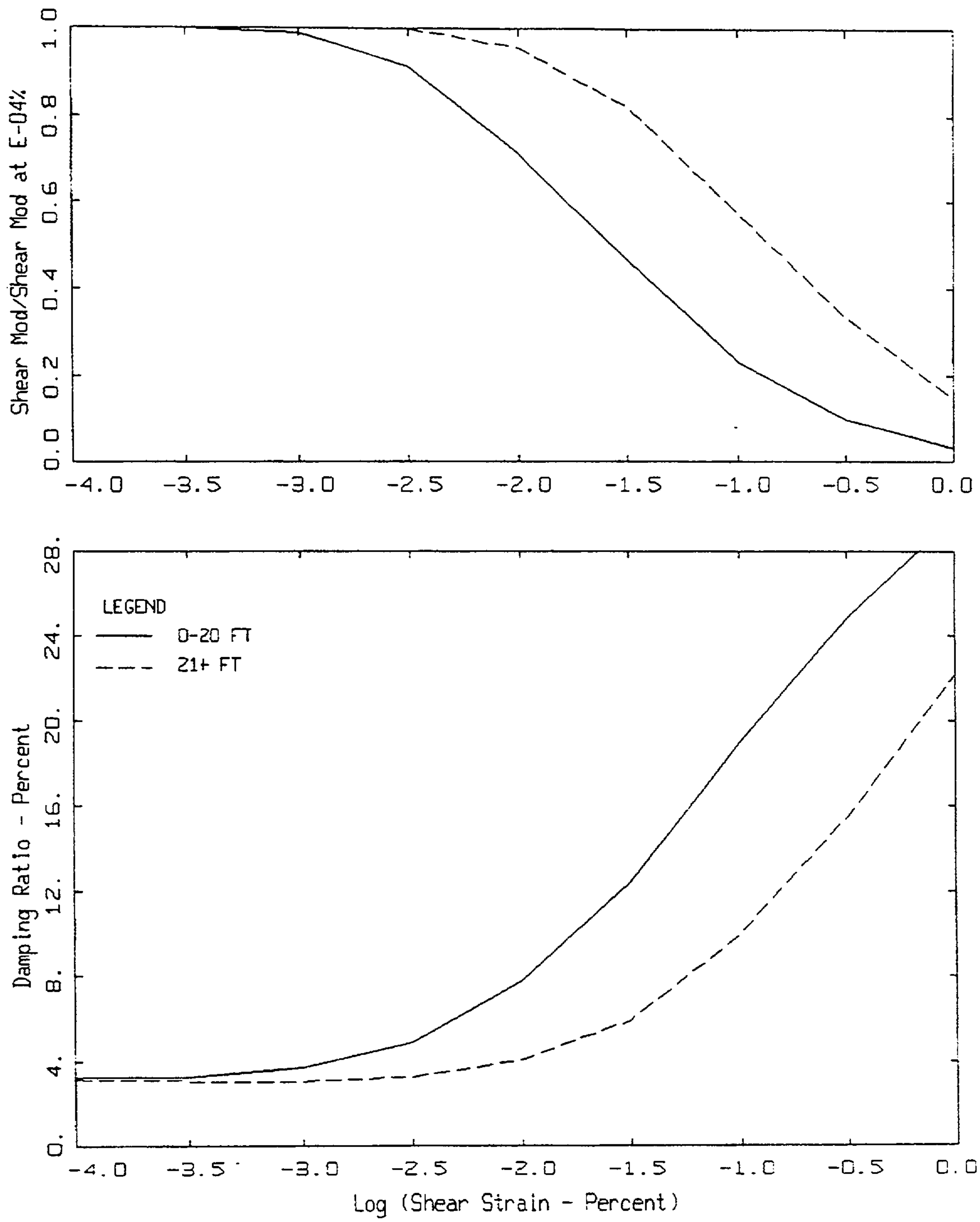

MODULUS REDUCTION AND DAMPING CURVES FOR ROCK

Figure 2-5. Generic G/G_{max} and hysteretic damping curves for soft rock.

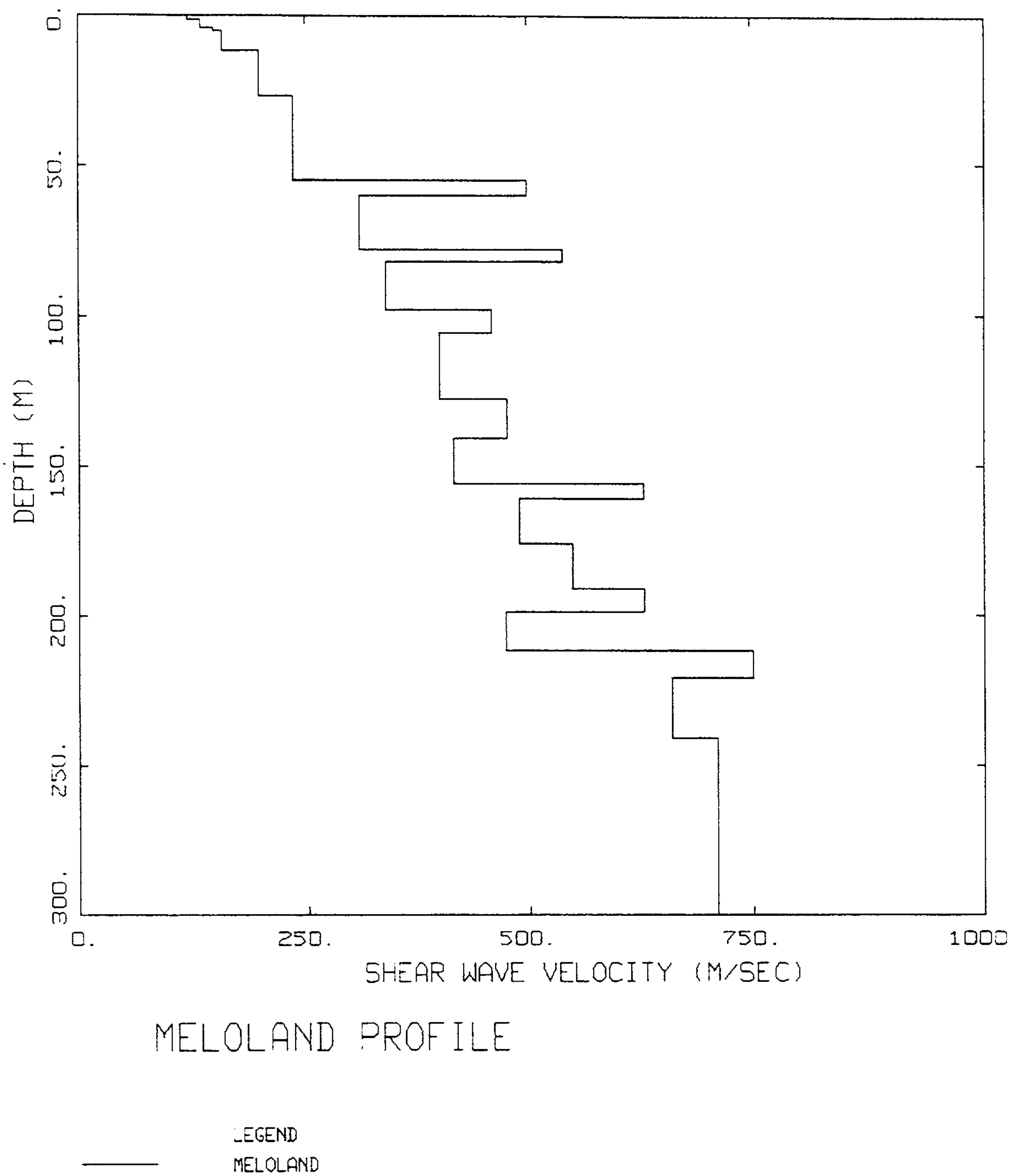

Figure 2-6a. Base case WUS soil shear-wave velocity profile based on suspension logging measurements. Placed on top of Wald and Heaton (1994) crustal model (Table 2-3).

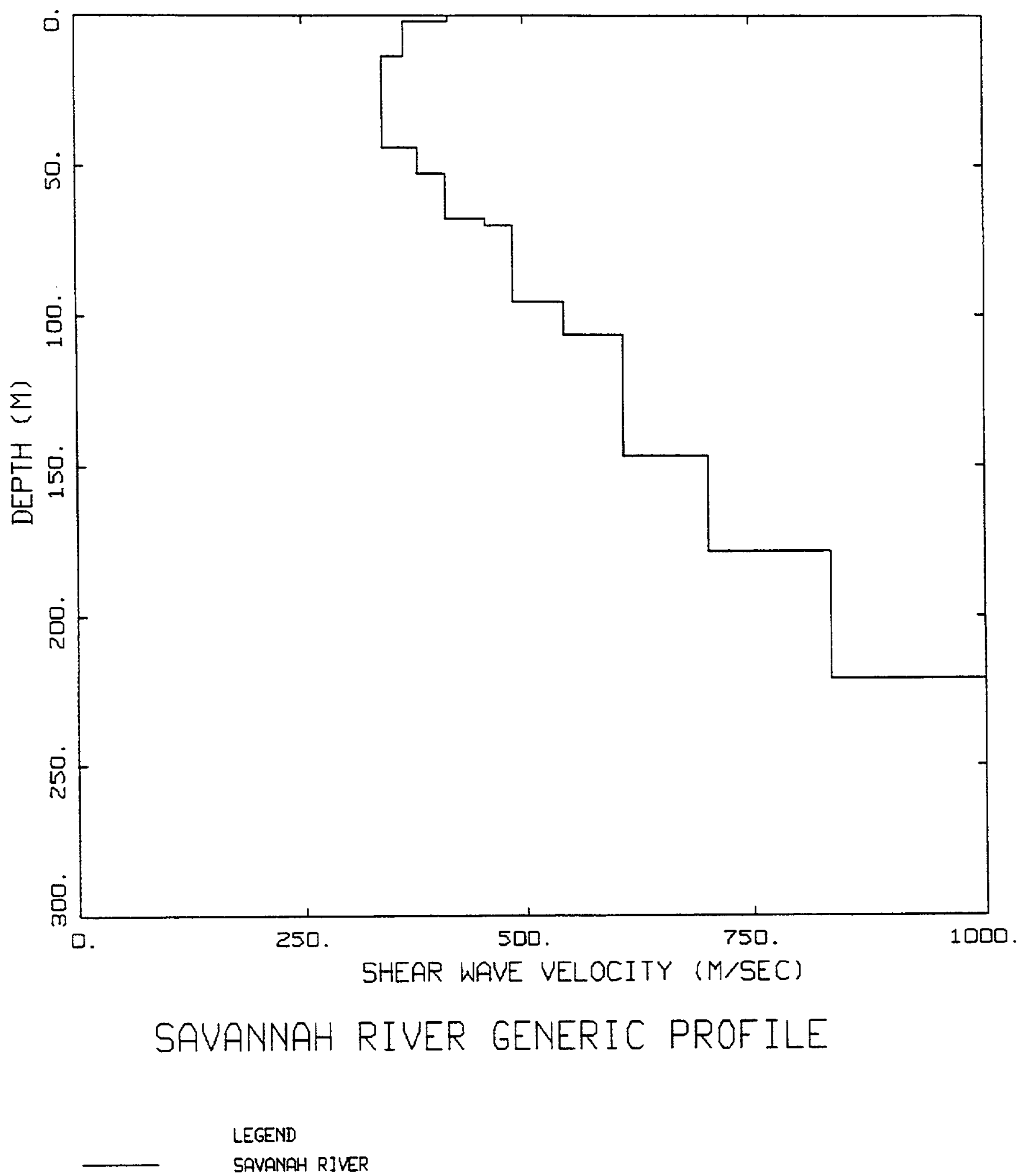

Figure 2-6b. Base case CEUS soil shear-wave velocity profile based on suspension logging measurements. Placed on top of CEUS crustal model (Table 2-3).

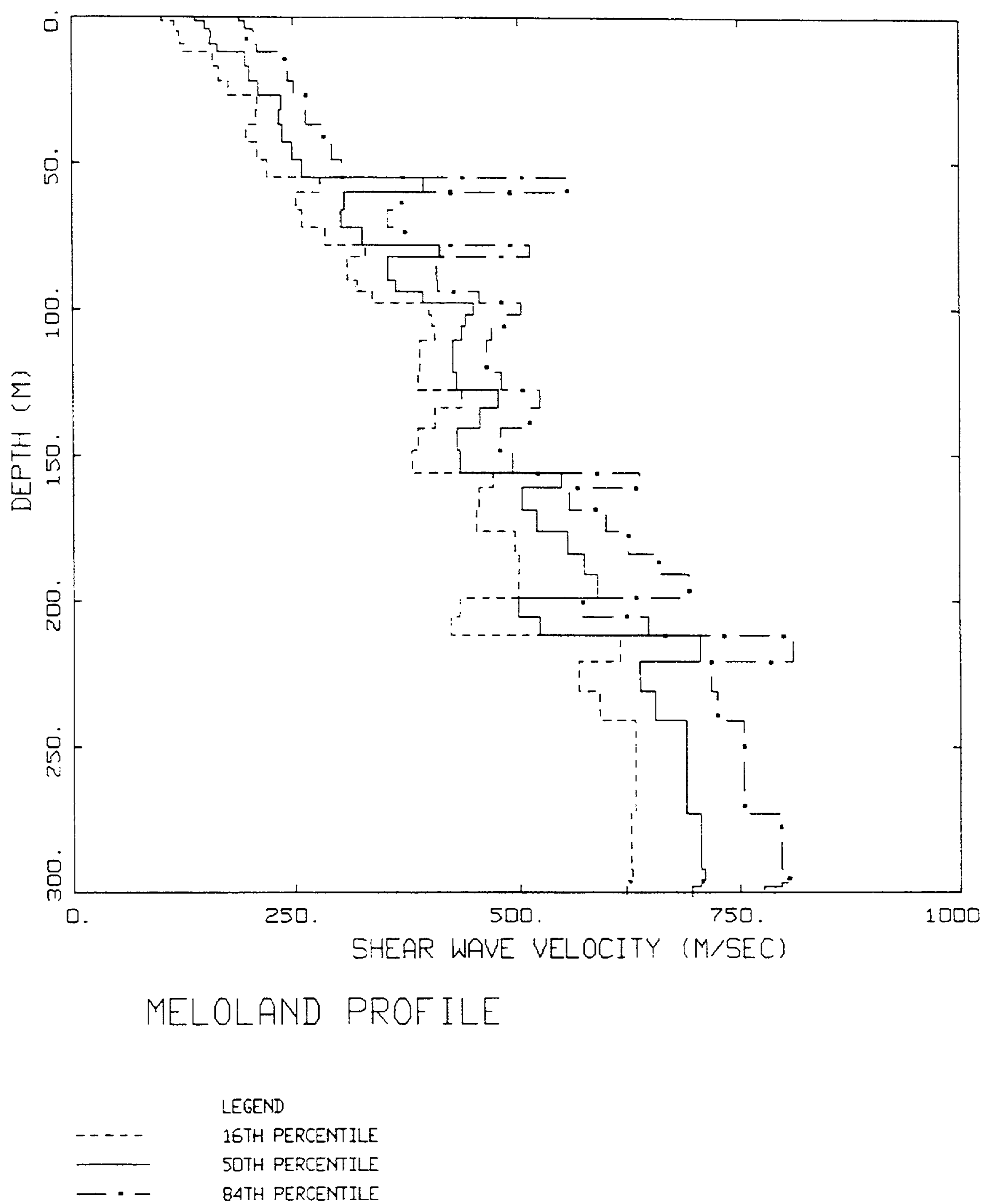

Figure 2-7a. Variation in base case shear-wave velocity for the Meloland profile (Figure 2-6a) based on thirty realizations. Median estimate along with $\pm\sigma$ values.

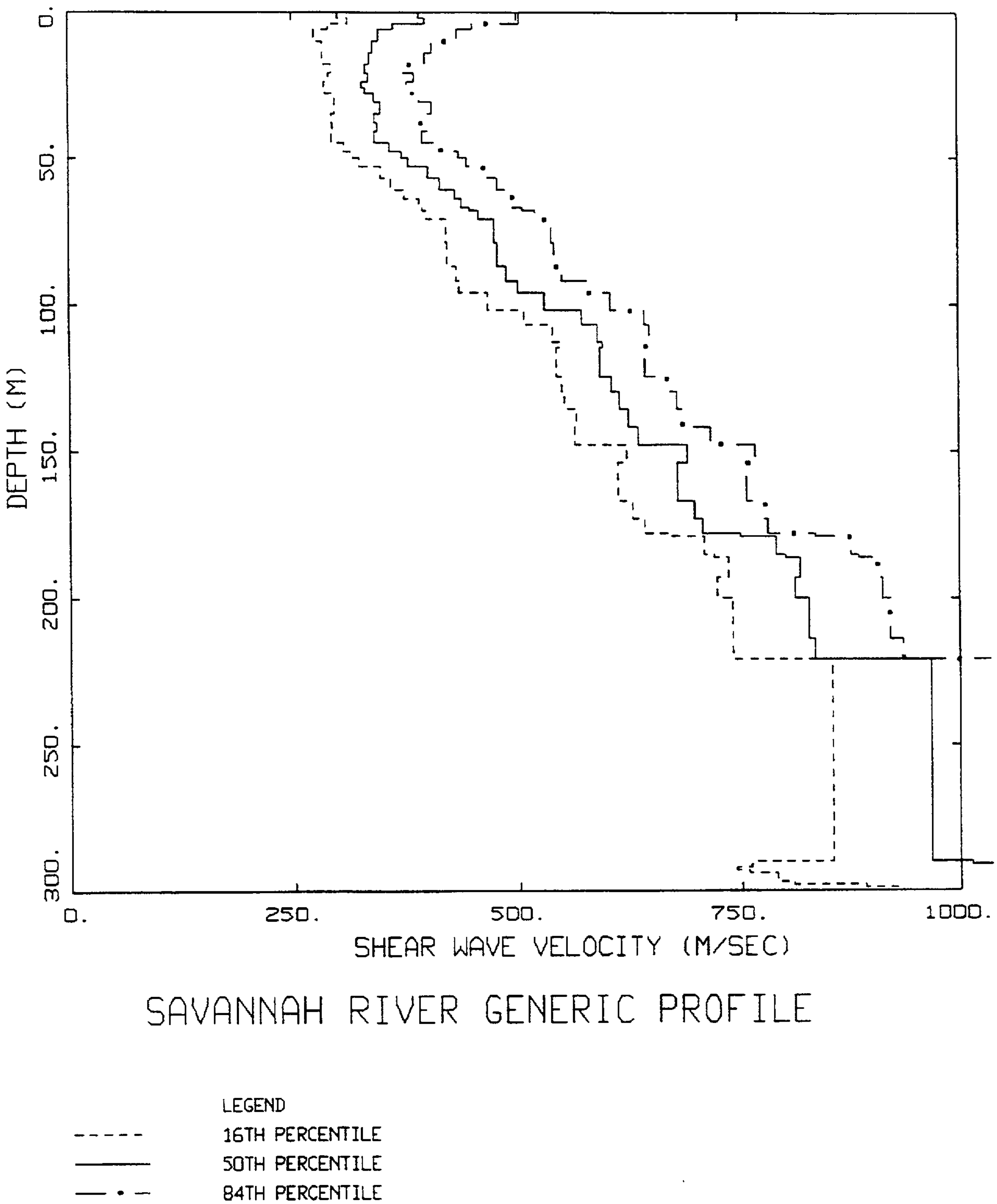

Figure 2-7b. Variation in base case shear-wave velocity for the Savannah River generic profile (Figure 2-6b) based on thirty realizations. Median estimate along with $\pm\sigma$ values.

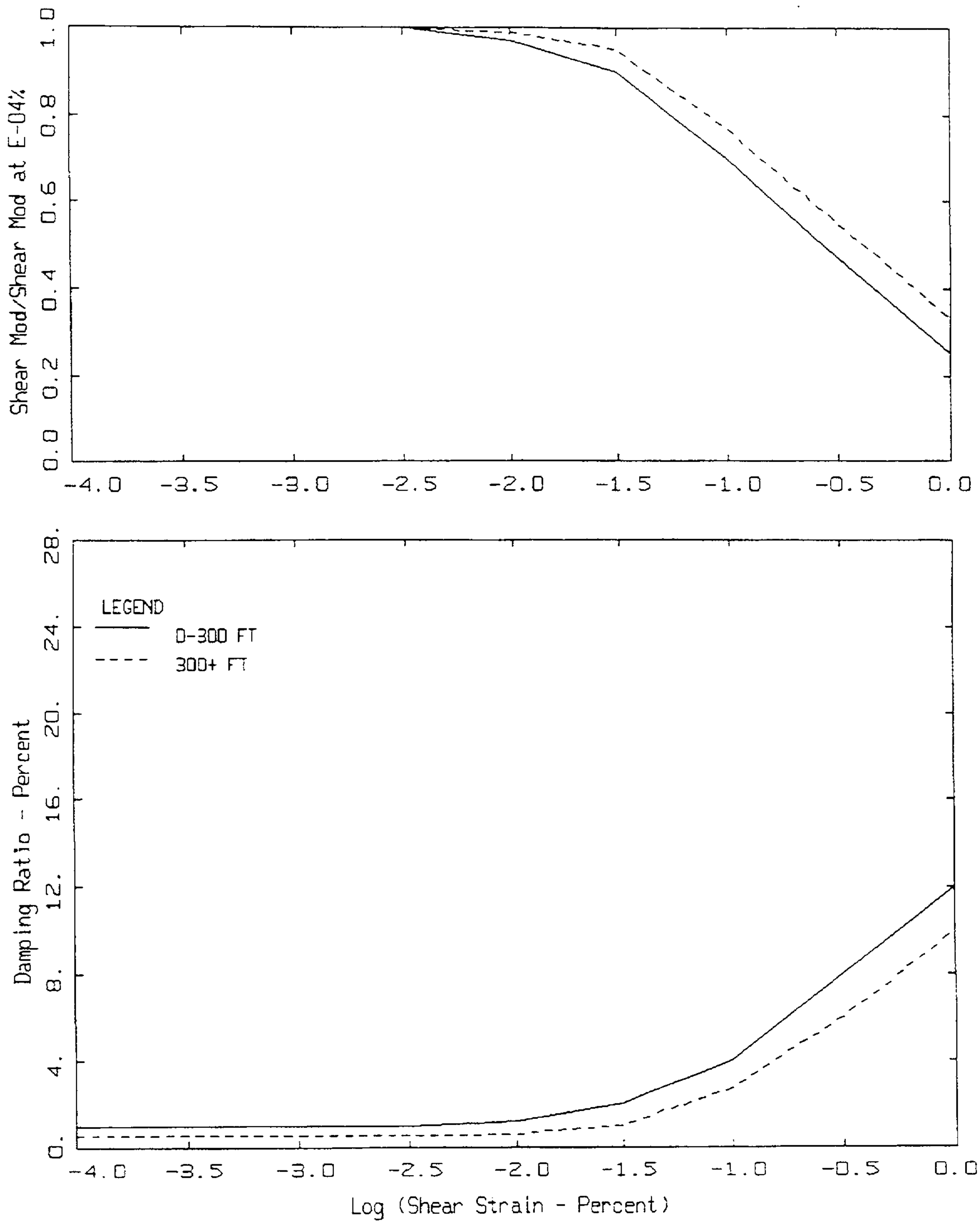

MODULUS REDUCTION AND DAMPING CURVES FOR MELOLAND

Figure 2-8a. Generic G/G_{max} and hysteretic damping curves for Imperial Valley soils. Used for soil site Meloland.

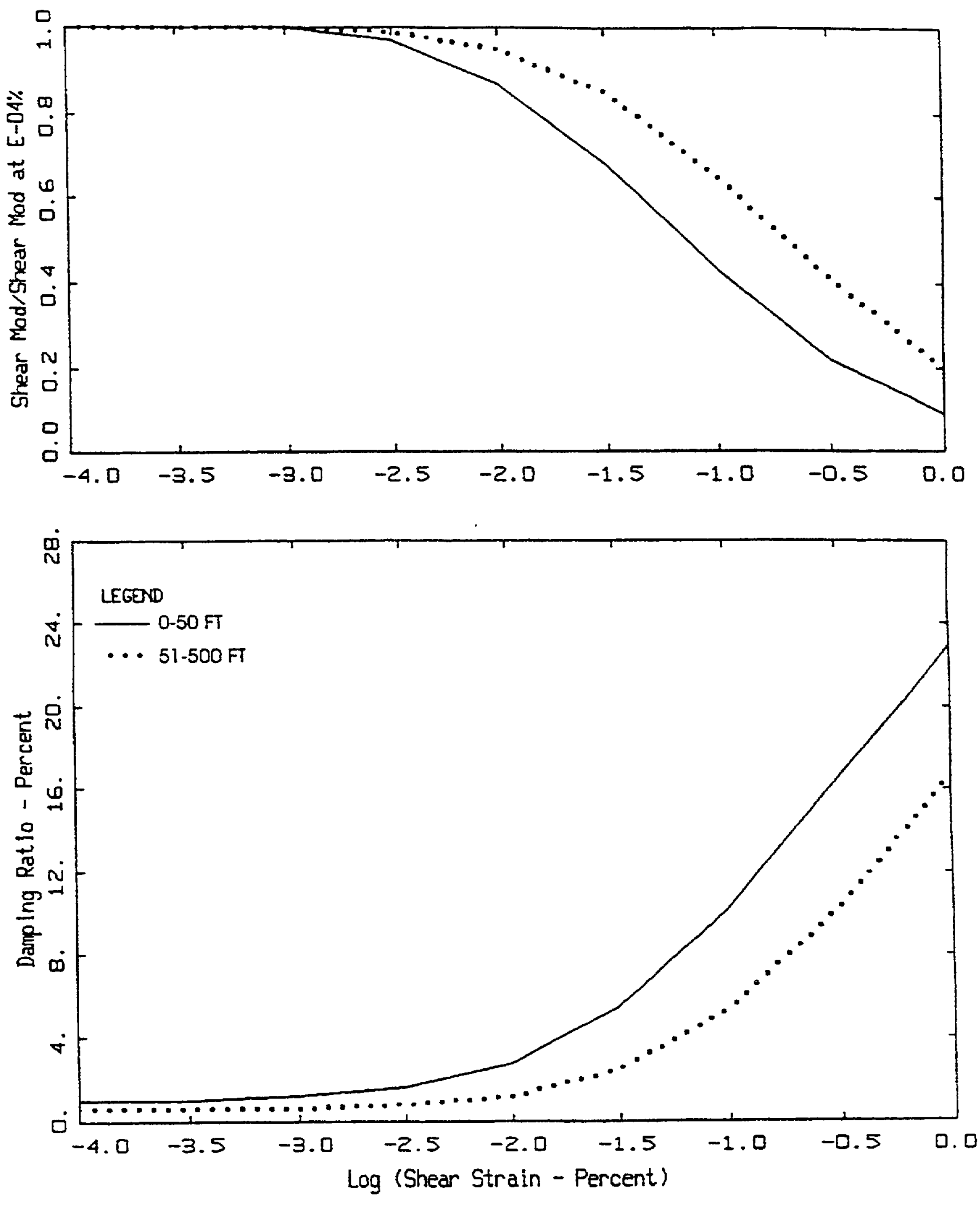

MODULUS REDUCTION AND DAMPING CURVES FOR COHESIONLESS SOILS

Figure 2-8b. Generic G/G_{max} and hysteretic damping curves for Peninsular Range cohesionless soil site conditions (Silva et al., 1997), assumed for Savannah River generic profile.

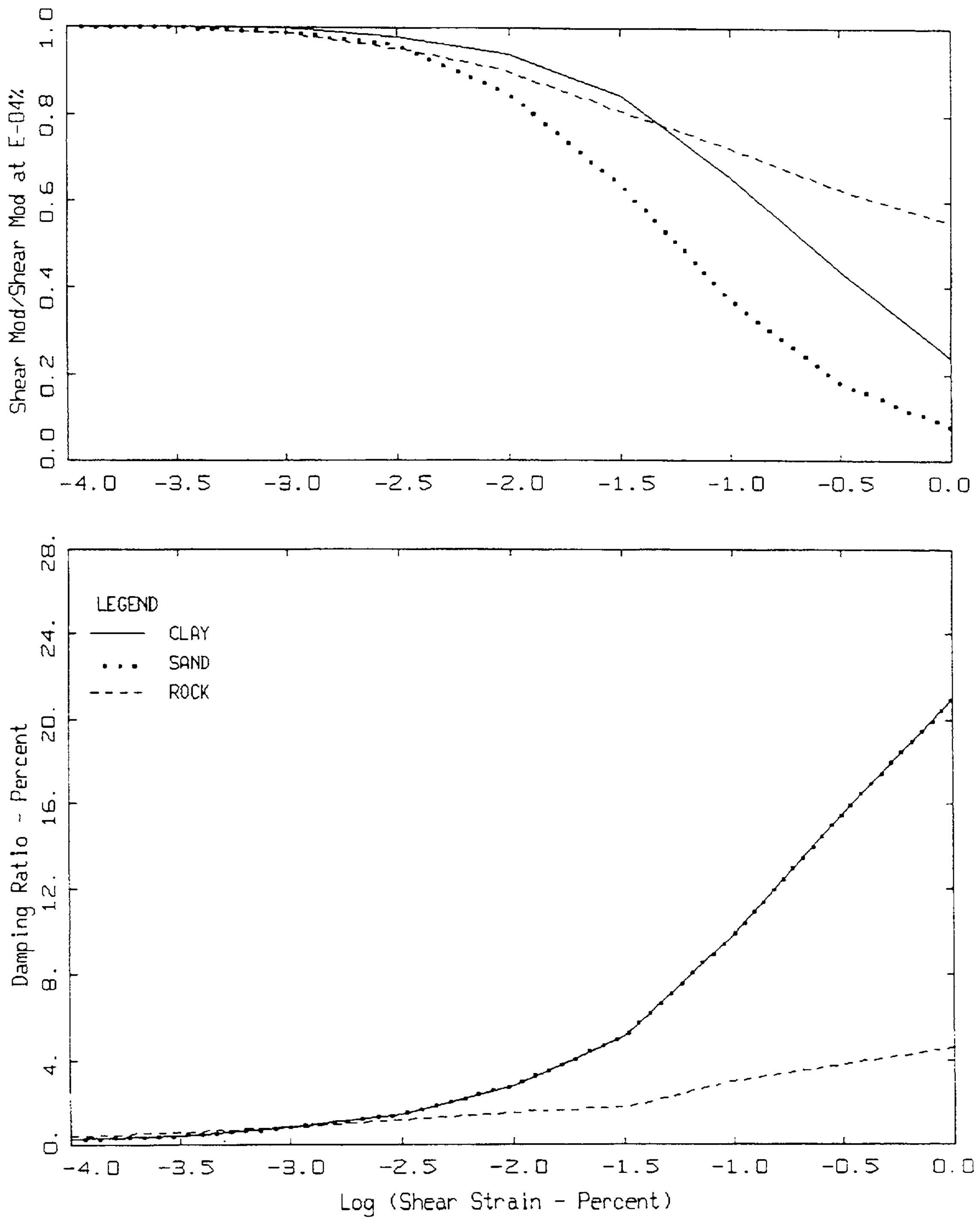

Figure 2-9. Generic G/G_{max} and hysteretic damping curves from SHAKE, 1991.

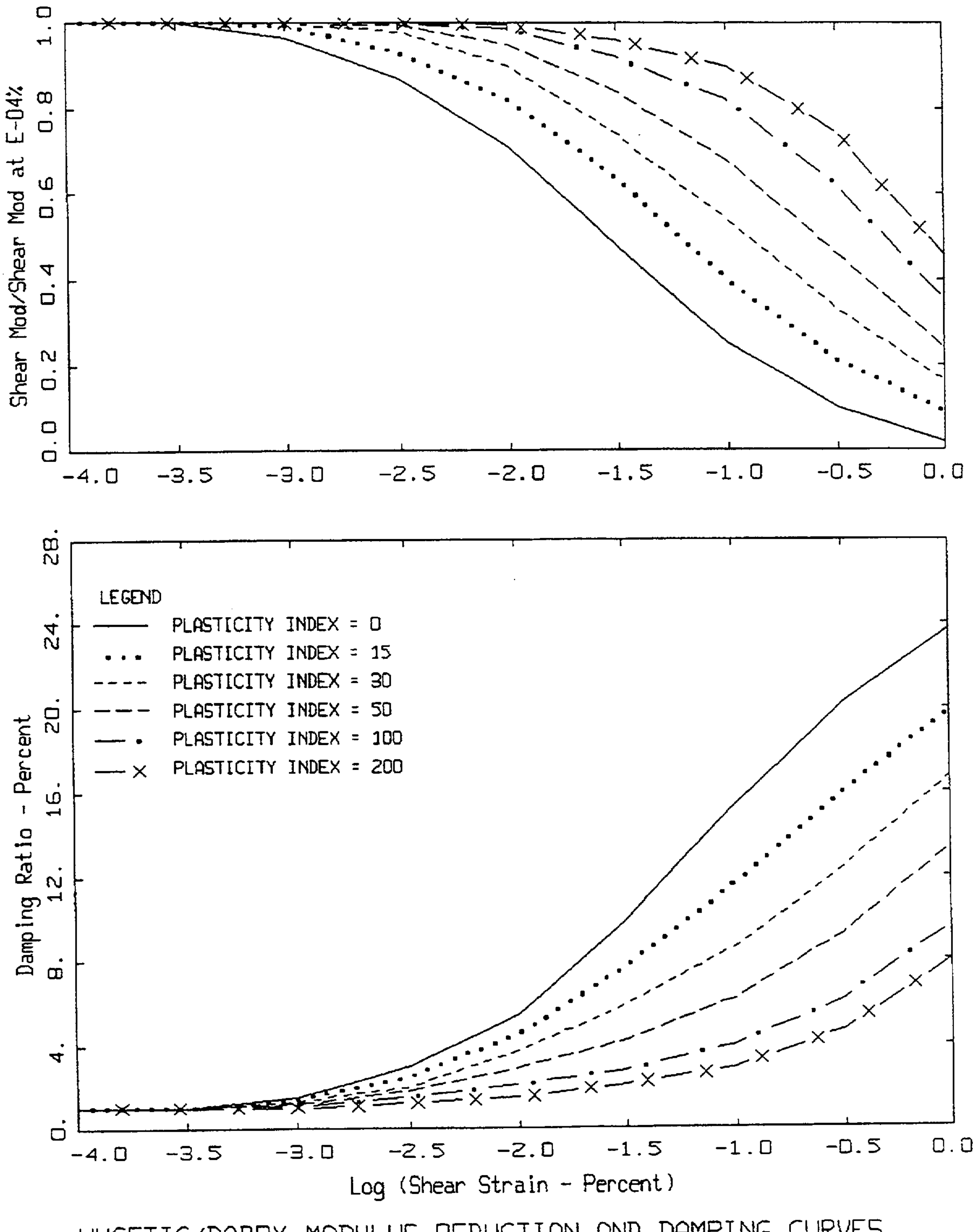

Figure 2-10. Generic G/G_{max} and hysteretic damping curves for cohesive soils (Vucetic and Dobry, 1991).

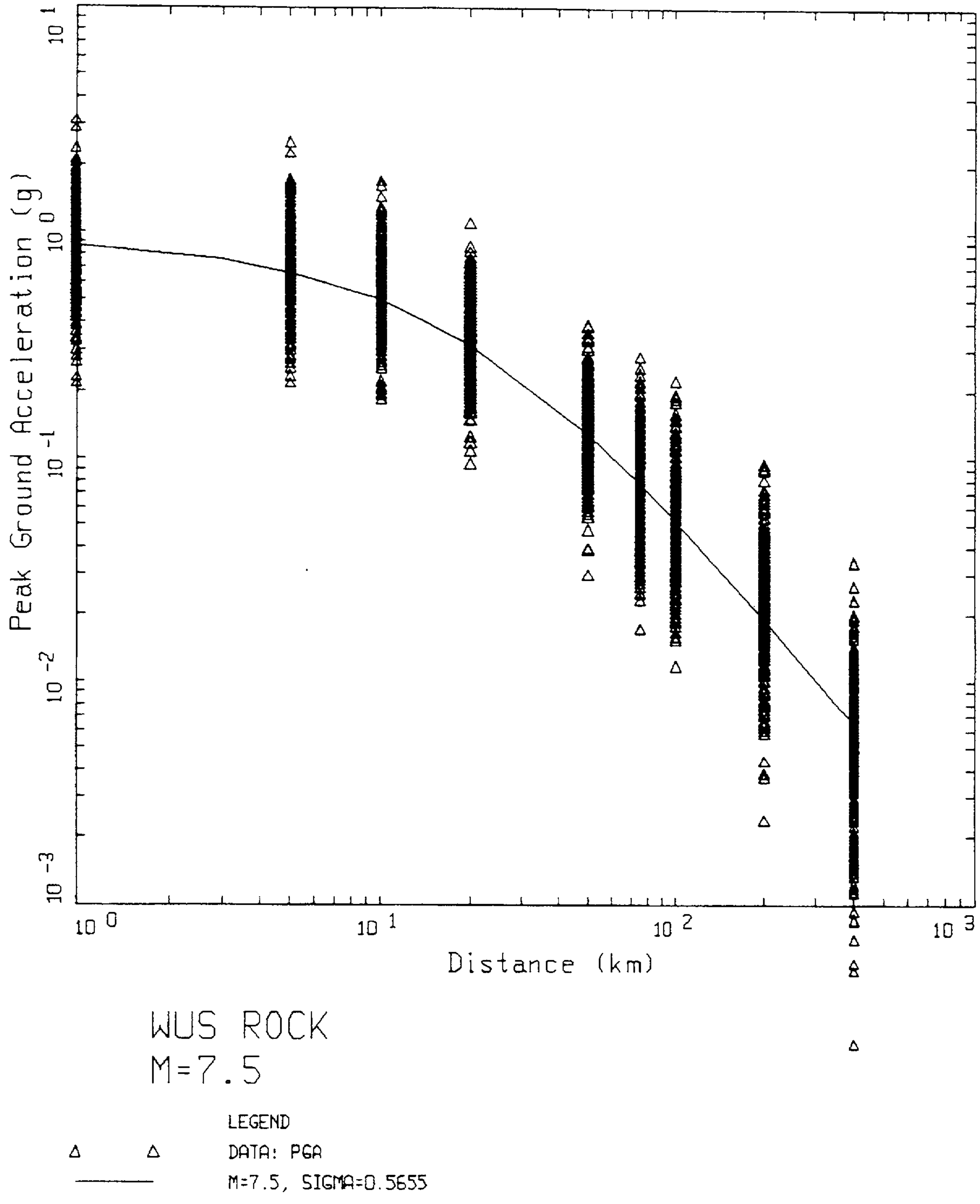

Figure 2-11. Peak acceleration estimates and regression fit at **M** 7.5 for WUS rock site conditions.

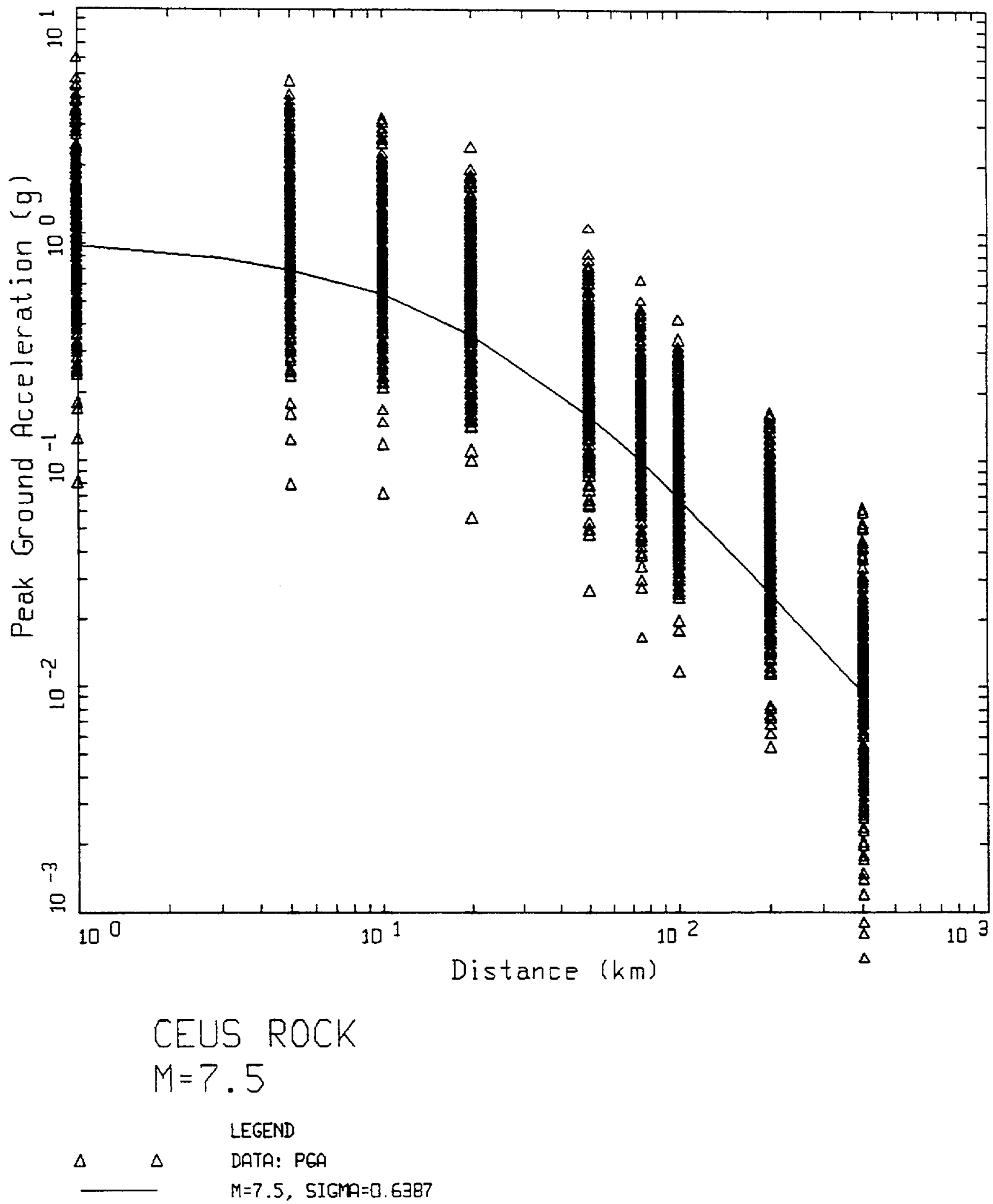

Figure 2-12. Peak acceleration estimates and regression fit at **M** 7.5 for CEUS (1-corner source model) rock site conditions.

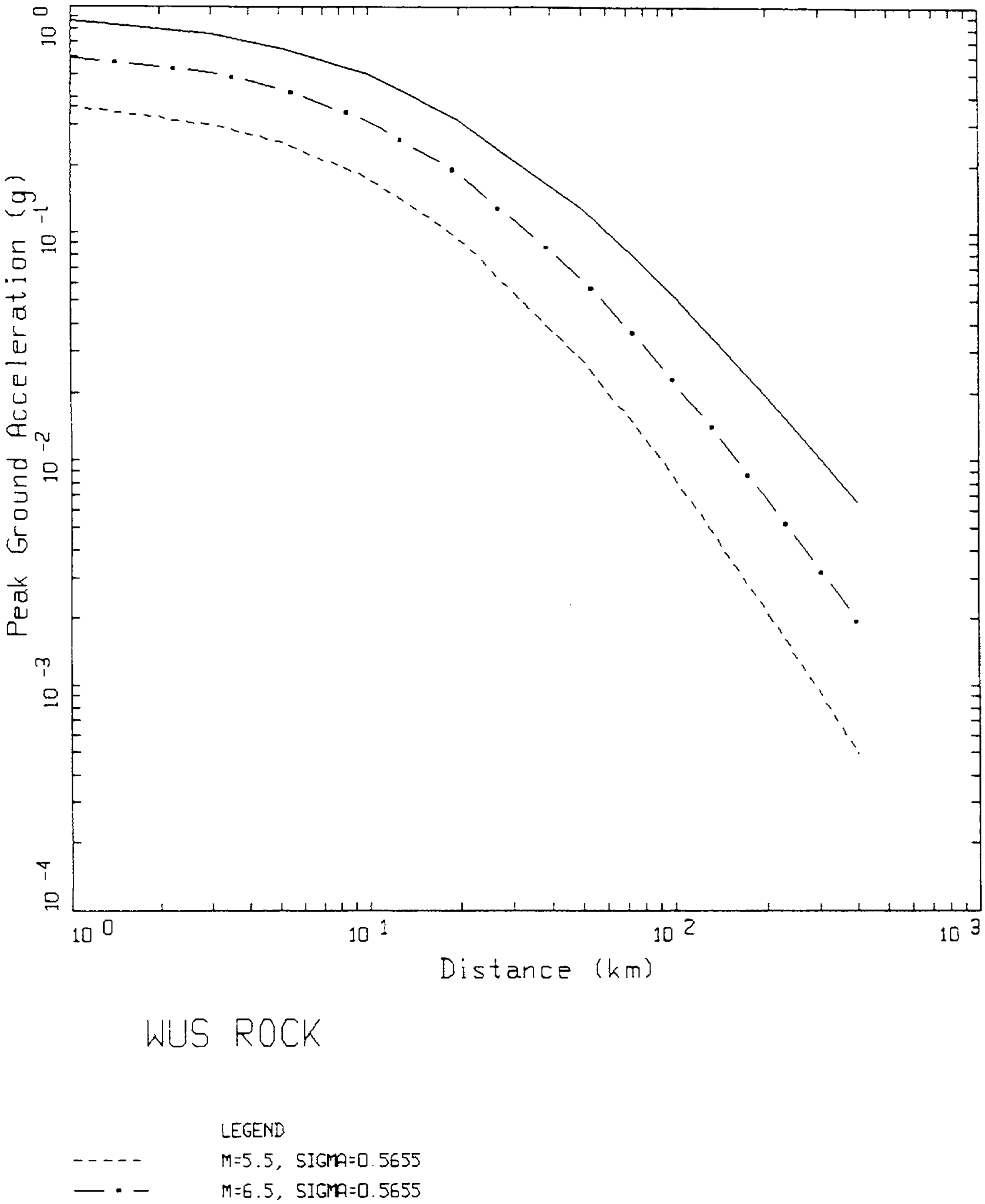

Figure 2-13. Attenuation of median peak horizontal acceleration at **M** 5.5, 6.5, and 7.5 for WUS rock site conditions.

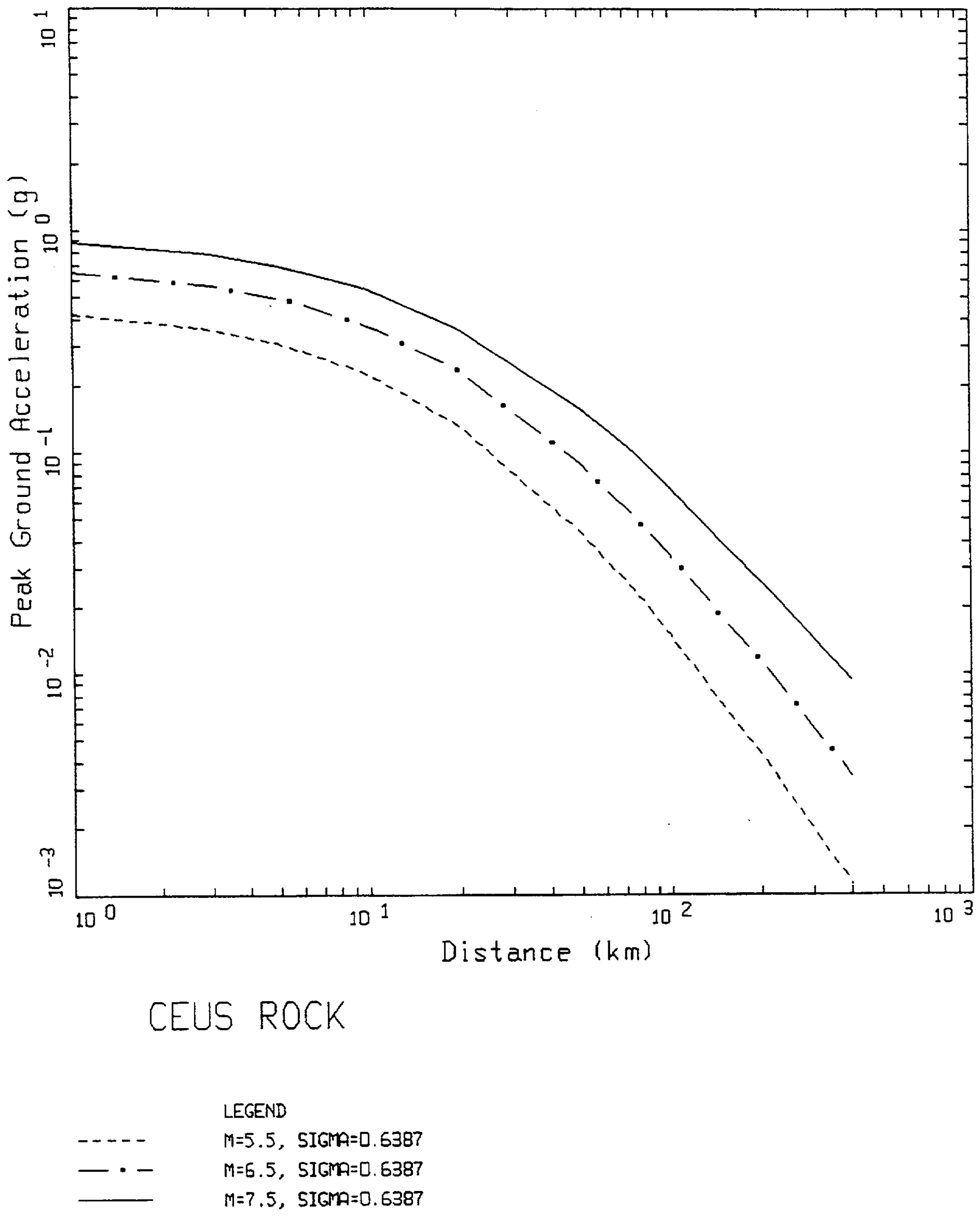

Figure 2-14a. Attenuation of median peak horizontal acceleration at **M** 5.5, 6.5, and 7.5 for CEUS rock site conditions (single-corner source model).

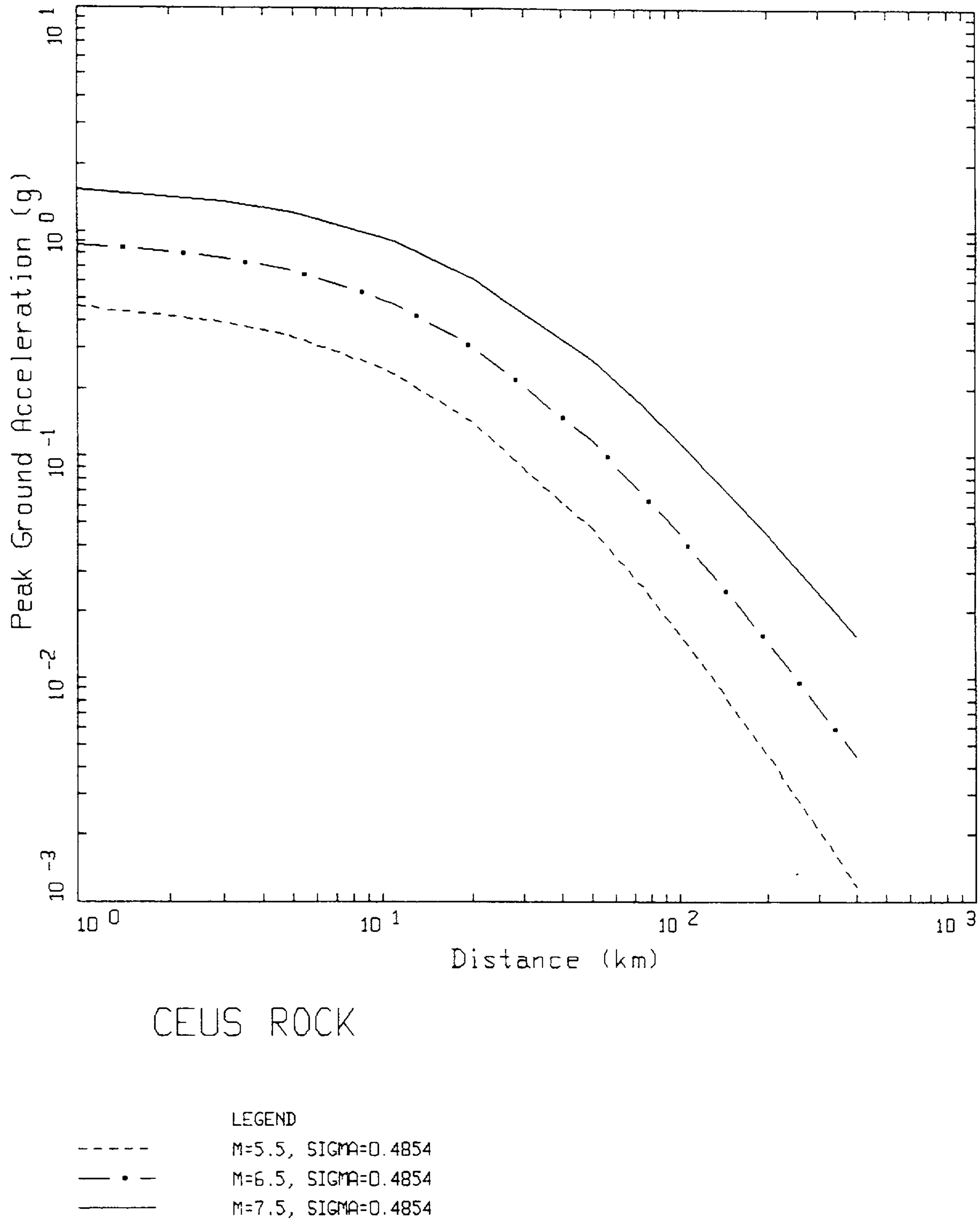

Figure 2-14b. Attenuation of median peak horizontal acceleration at **M** 5.5, 6.5, and 7.5 for CEUS rock site conditions (double corner source model).

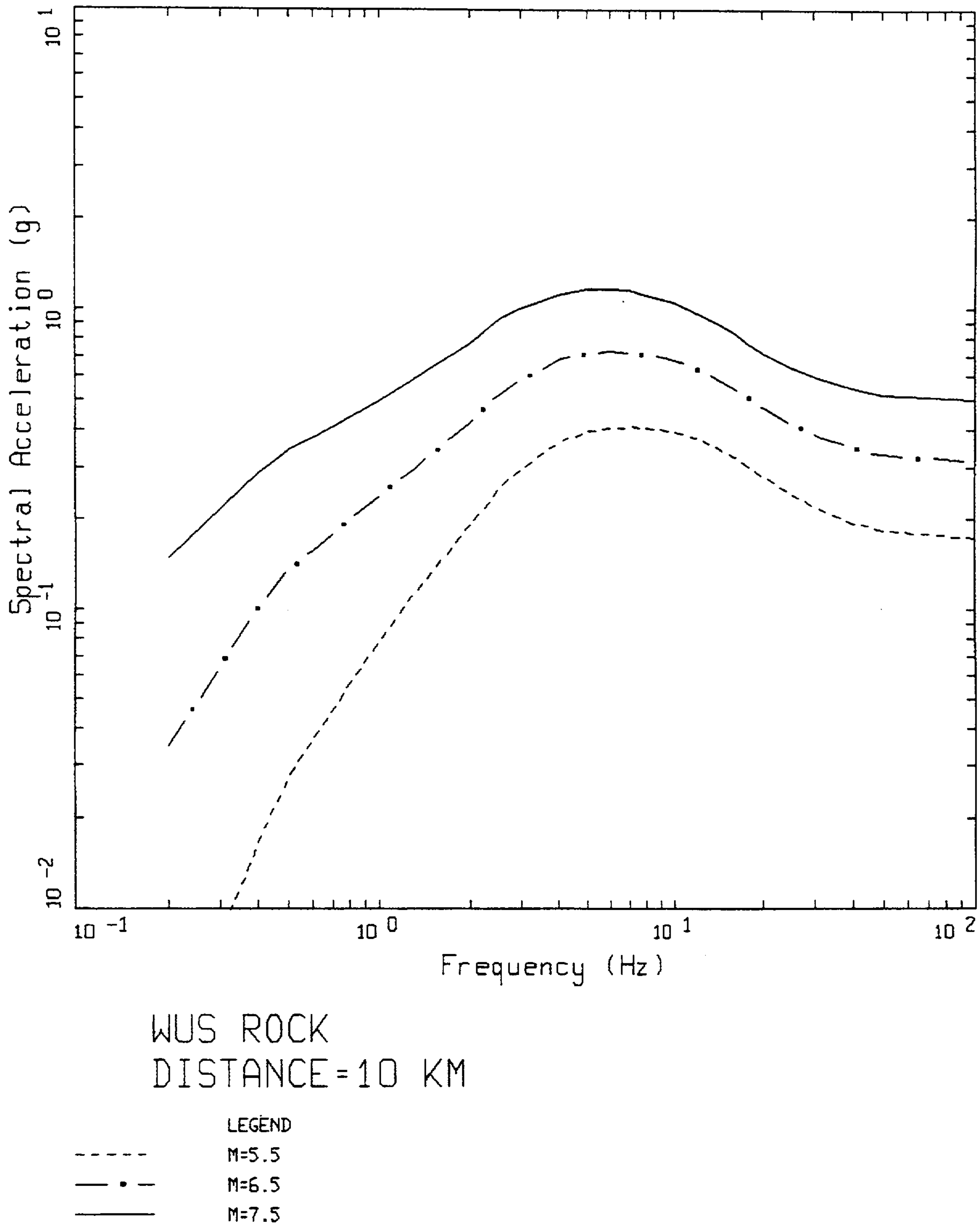

Figure 2-15. Median response spectra (5% damping) at a distance of 10 km for magnitudes **M** 5.5, 6.5, and 7.5: WUS rock site.

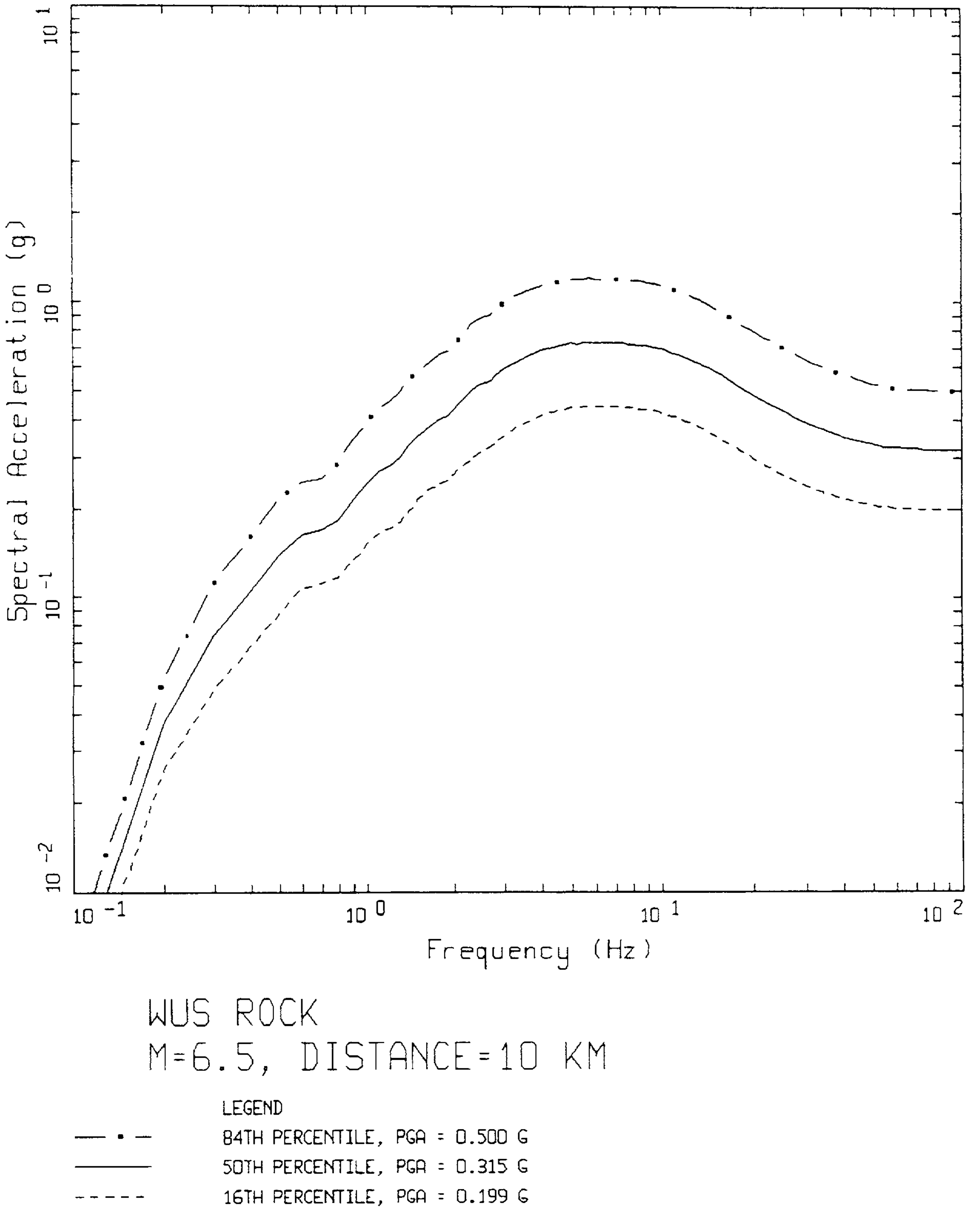

Figure 2-16. Response spectra (5% damping) at a distance of 10 km for **M** 6.5 showing median and ± 1 σ estimates (parametric and regression uncertainty): WUS rock site.

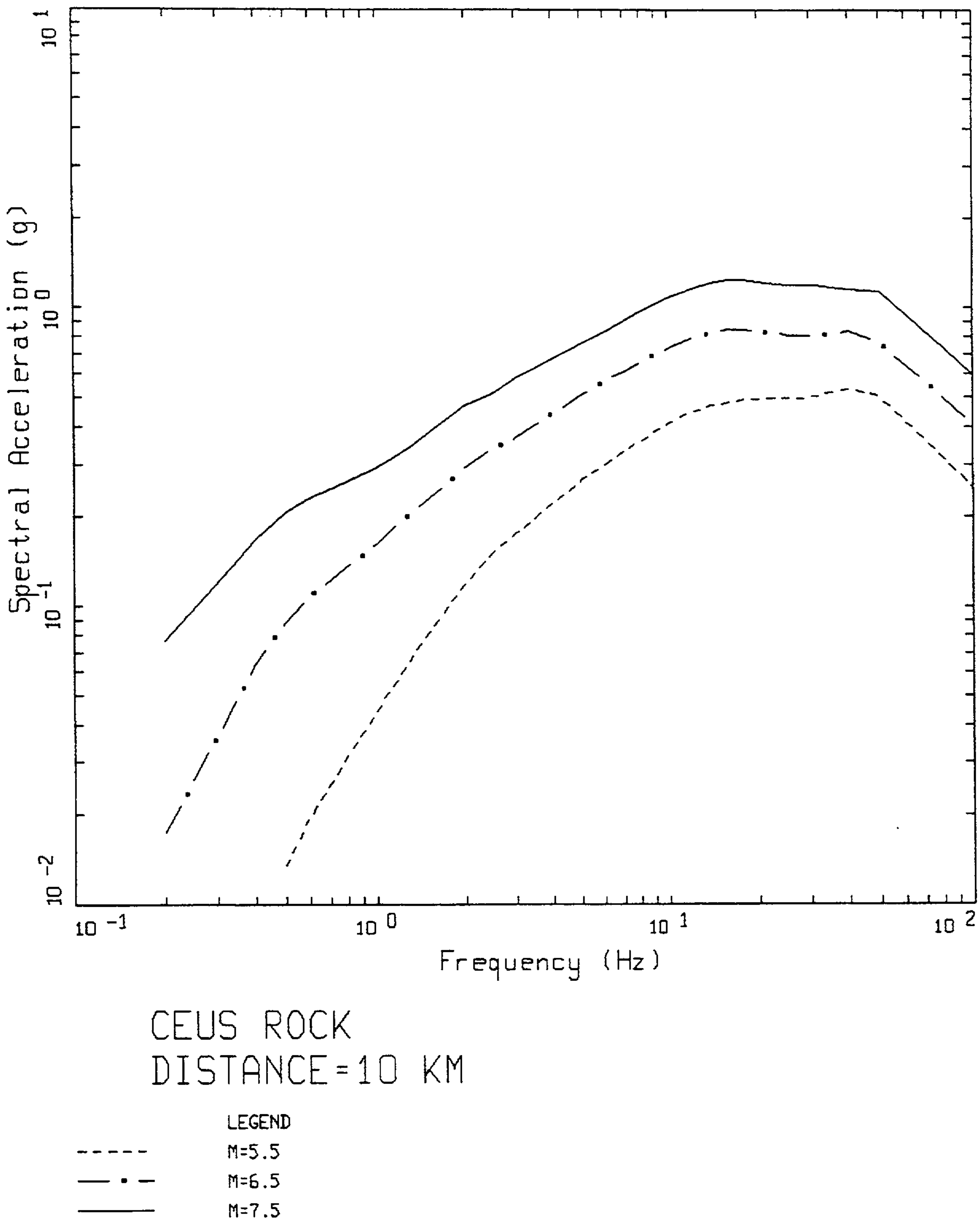

Figure 2-17a. Median response spectra (5% damping) at a distance of 10 km for **M** 5.5, 6.5, and 7.5: CEUS rock site (single-corner source model).

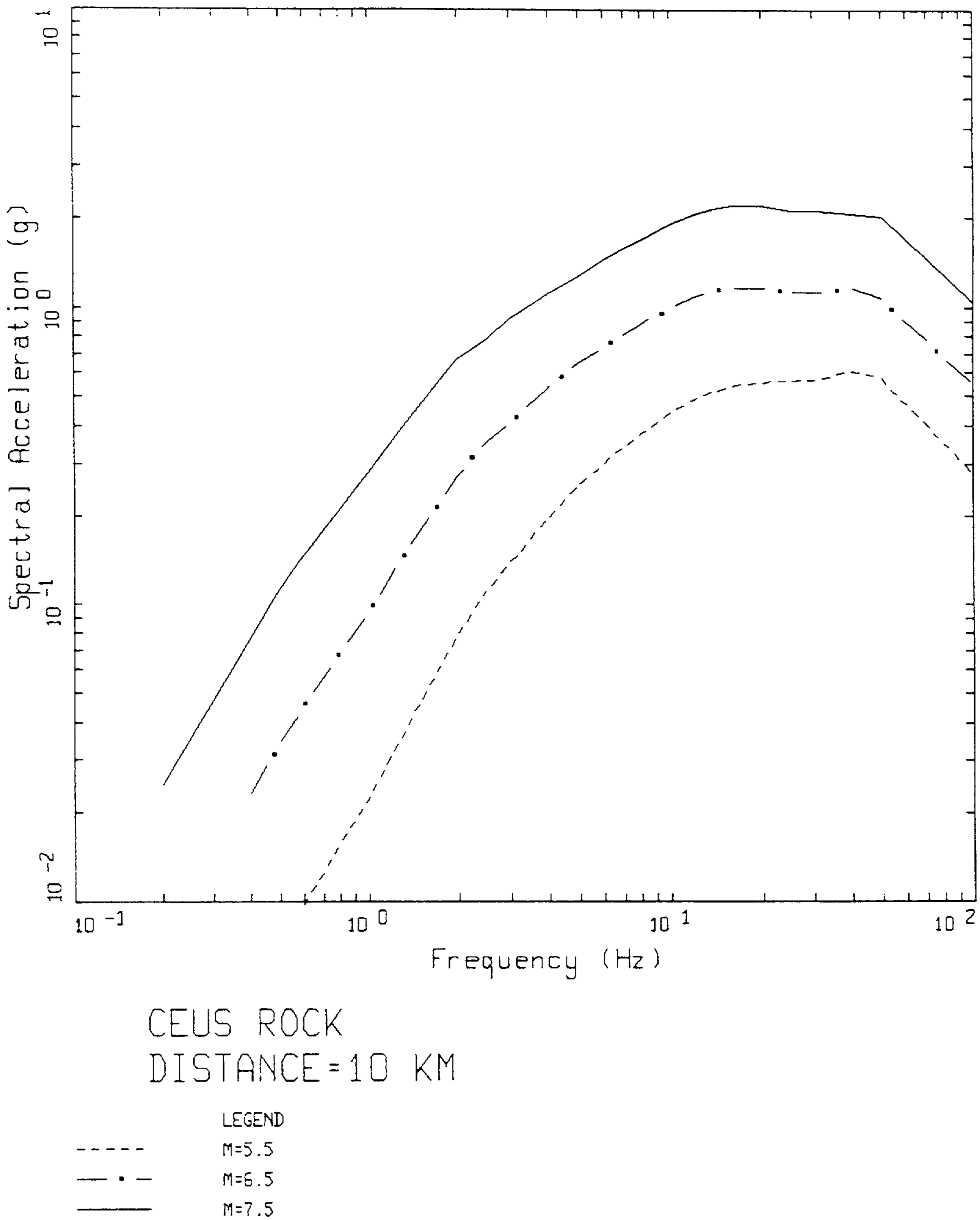

Figure 2-17b. Median response spectra (5% damping) at a distance of 10 km for **M** 5.5, 6.5, and 7.5: CEUS rock site (double-corner source model).

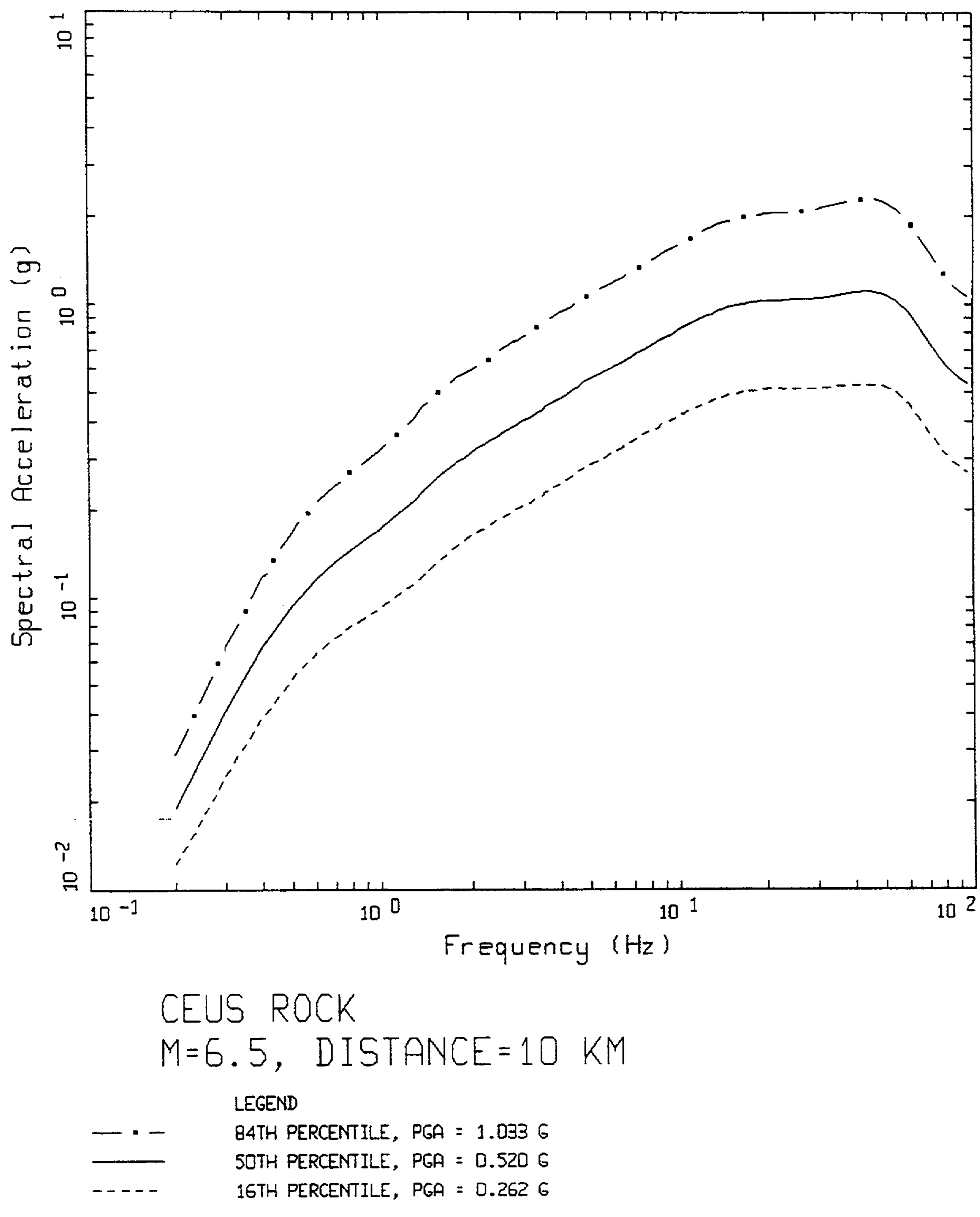

Figure 2-18a. Response spectra (5% damping) at a distance of 10 km for **M** 6.5 showing median and $\pm$ 1 σ estimates (parametric and regression uncertainty): CEUS rock site (single corner source model).

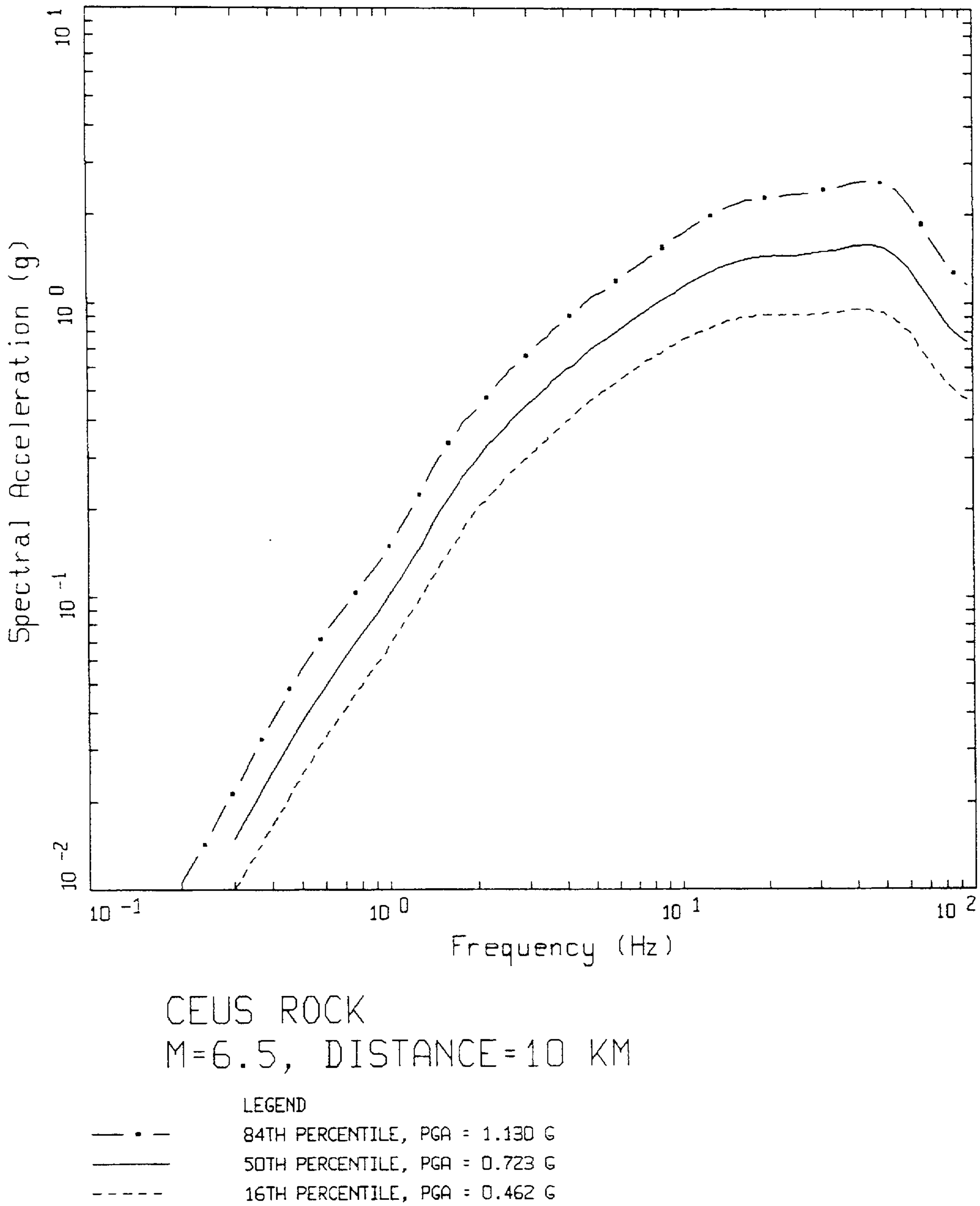

Figure 2-18b. Response spectra (5% damping) at a distance of 10 km for **M** 6.5 showing median and $\pm$ 1 σ estimates (parametric and regression uncertainty): CEUS rock site (double corner source model) variability in stress drop not included.

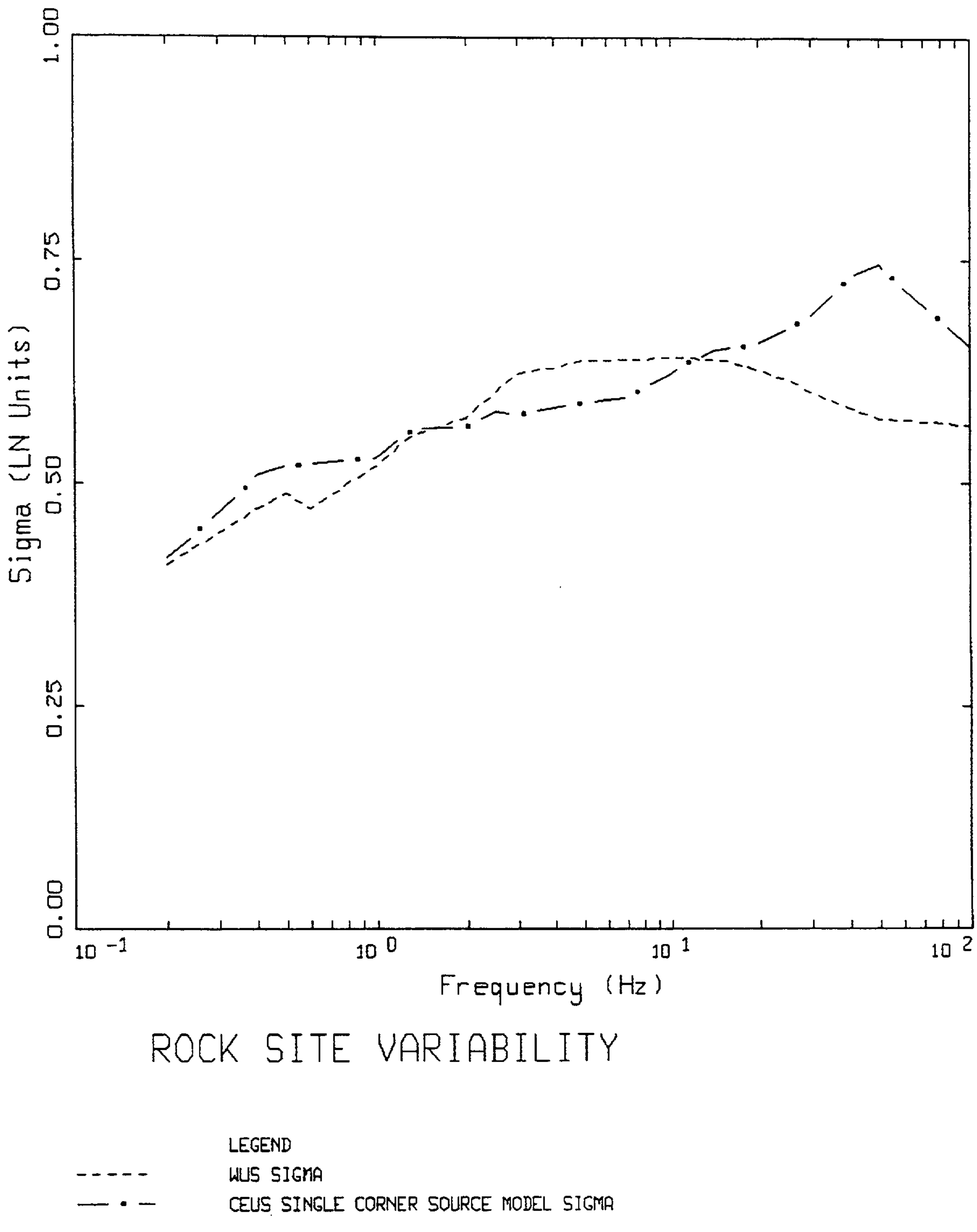

Figure 2-19. Variability in response spectral ordinates at WUS and CEUS rock sites resulting from parametric variability and regression fit over all magnitudes and distances (Tables 2-5 and 2-6).

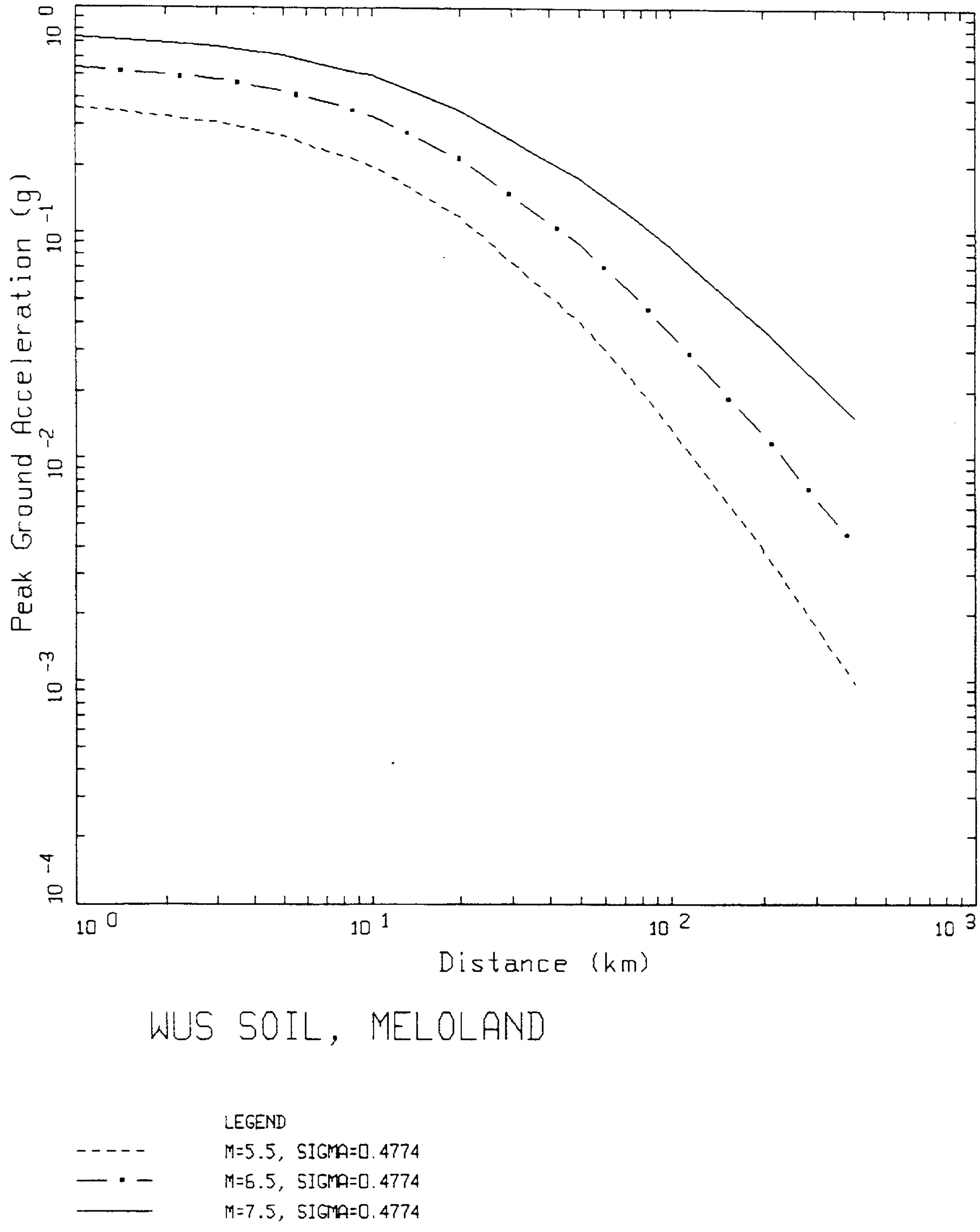

Figure 2-20. Attenuation of median peak horizontal acceleration at **M** 5.5, 6.5, and 7.5 for Meloland profile and WUS conditions.

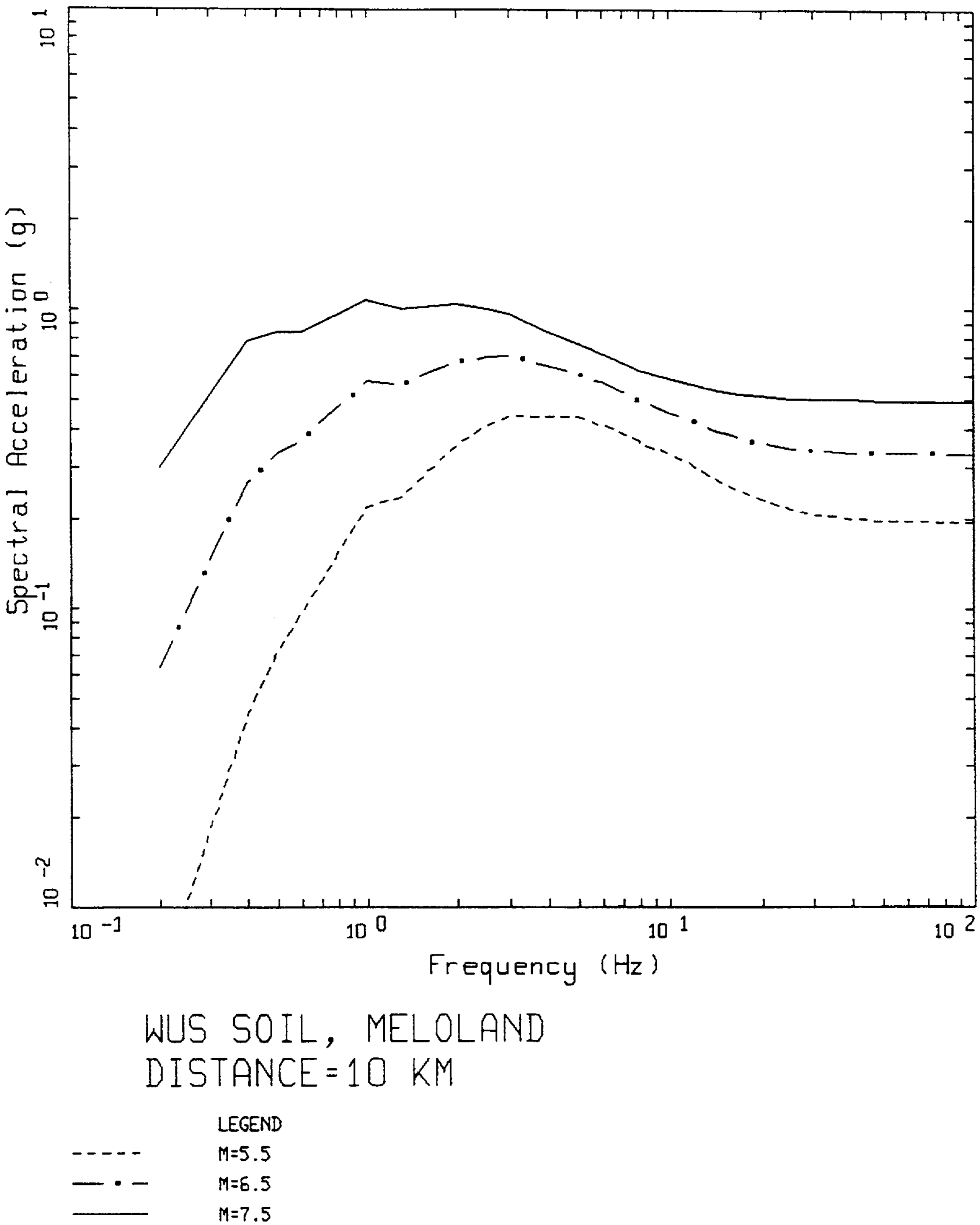

Figure 2-21. Median response spectra (5% damping) at a distance of 10 km for **M** 5.5, 6.5, and 7.5 for Meloland profile and WUS conditions.

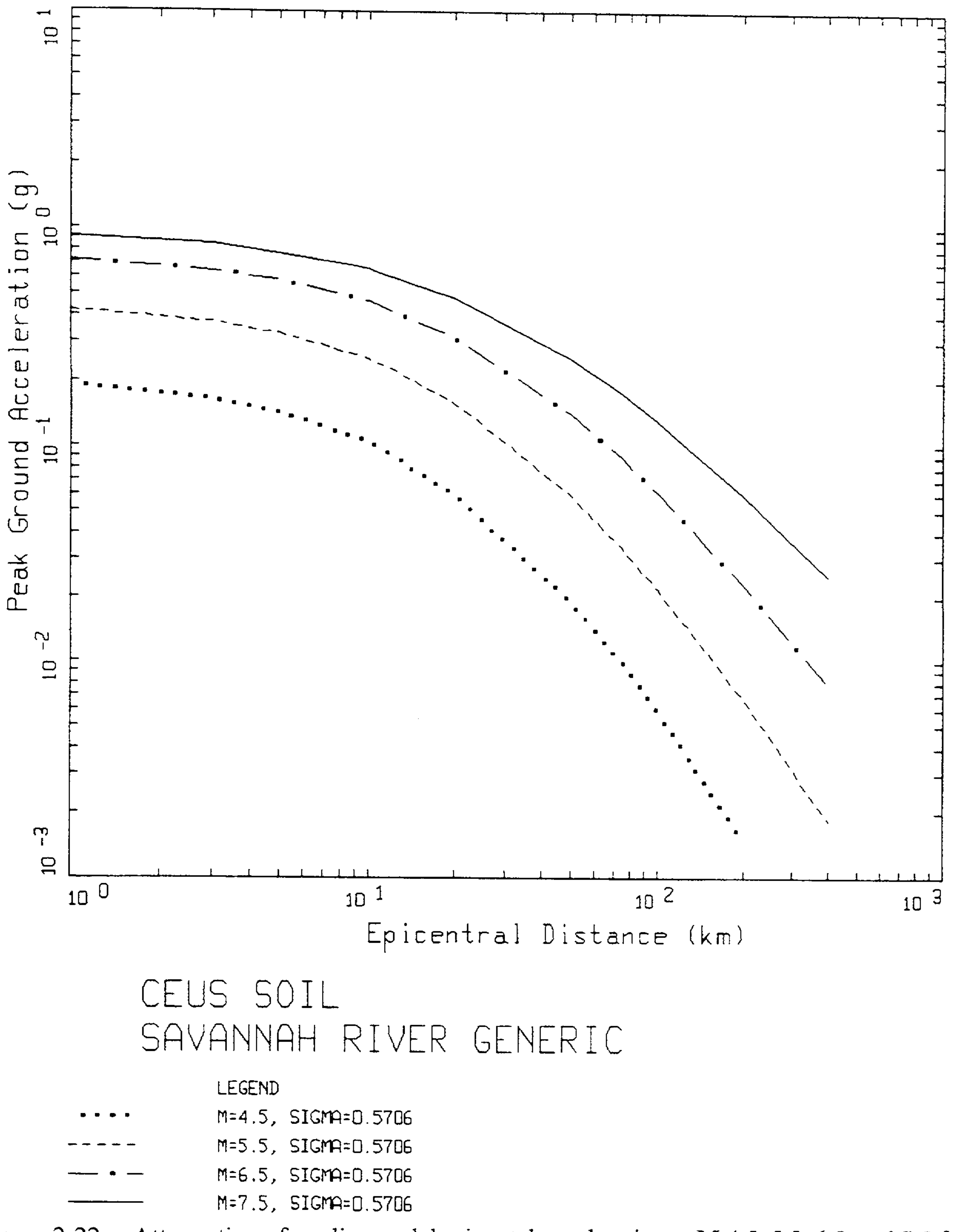

Figure 2-22a. Attenuation of median peak horizontal acceleration at **M** 4.5, 5.5, 6.5, and 7.5 for Savannah River generic profile and CEUS conditions (single-corner source model).

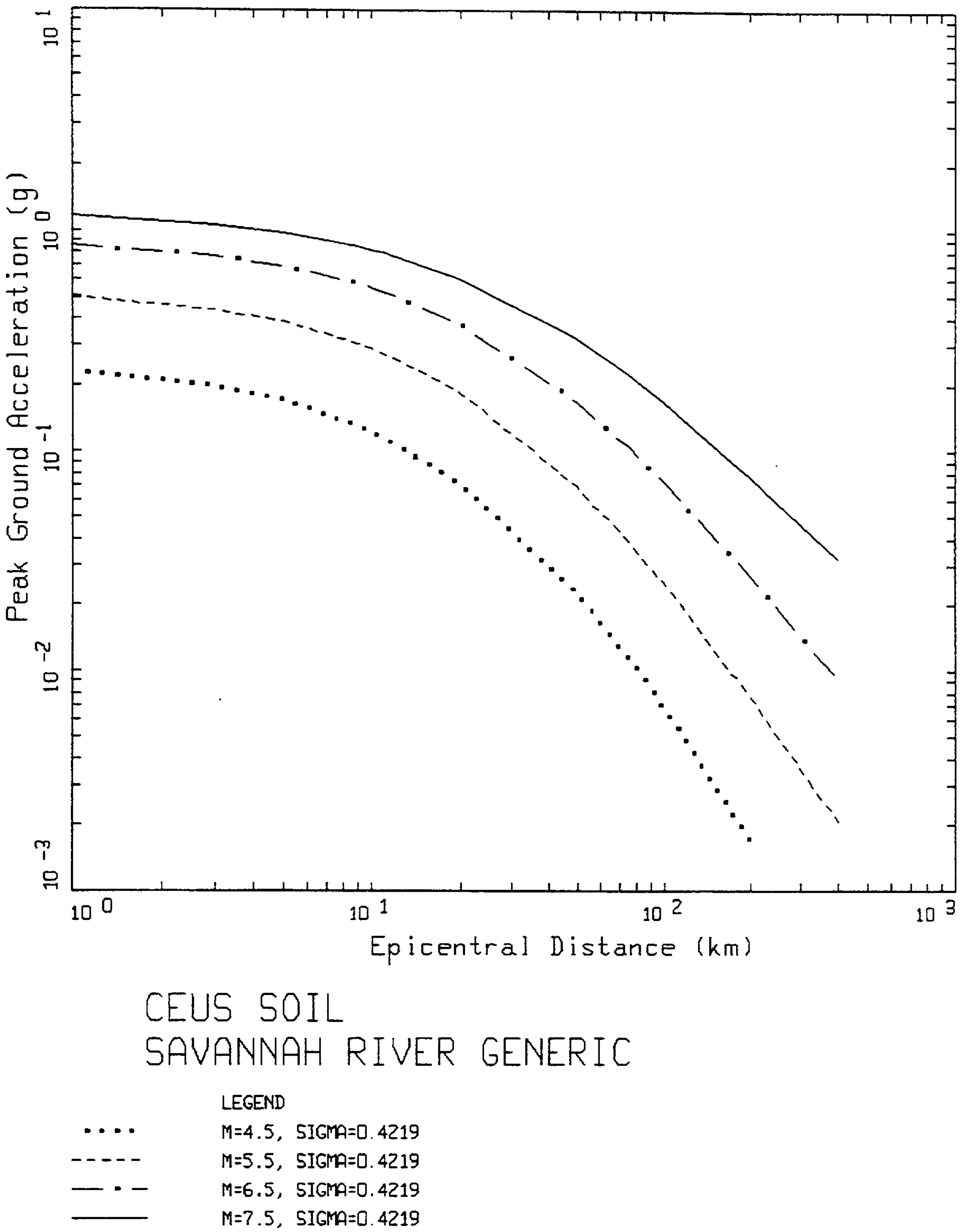

Figure 2-22b. Attenuation of median peak horizontal acceleration at **M** 4.5, 5.5, 6.5, and 7.5 for Savannah River generic profile and CEUS conditions (double-corner source model).

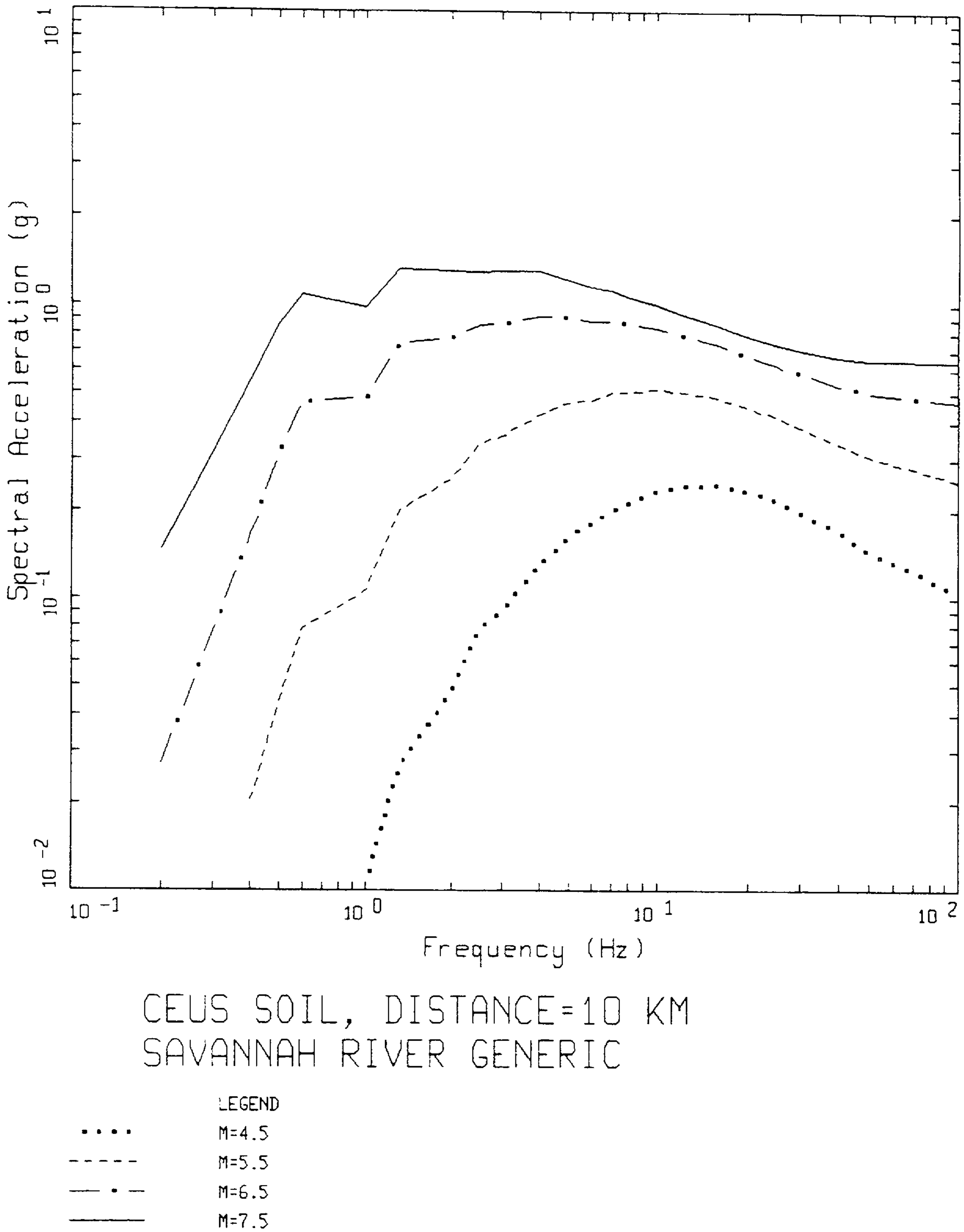

Figure 2-23a. Median response spectra (5% damping) at a distance of 10 km for **M** 4.5, 5.5, 6.5, and 7.5 for Savannah River generic profile and CEUS conditions (single-corner source model).

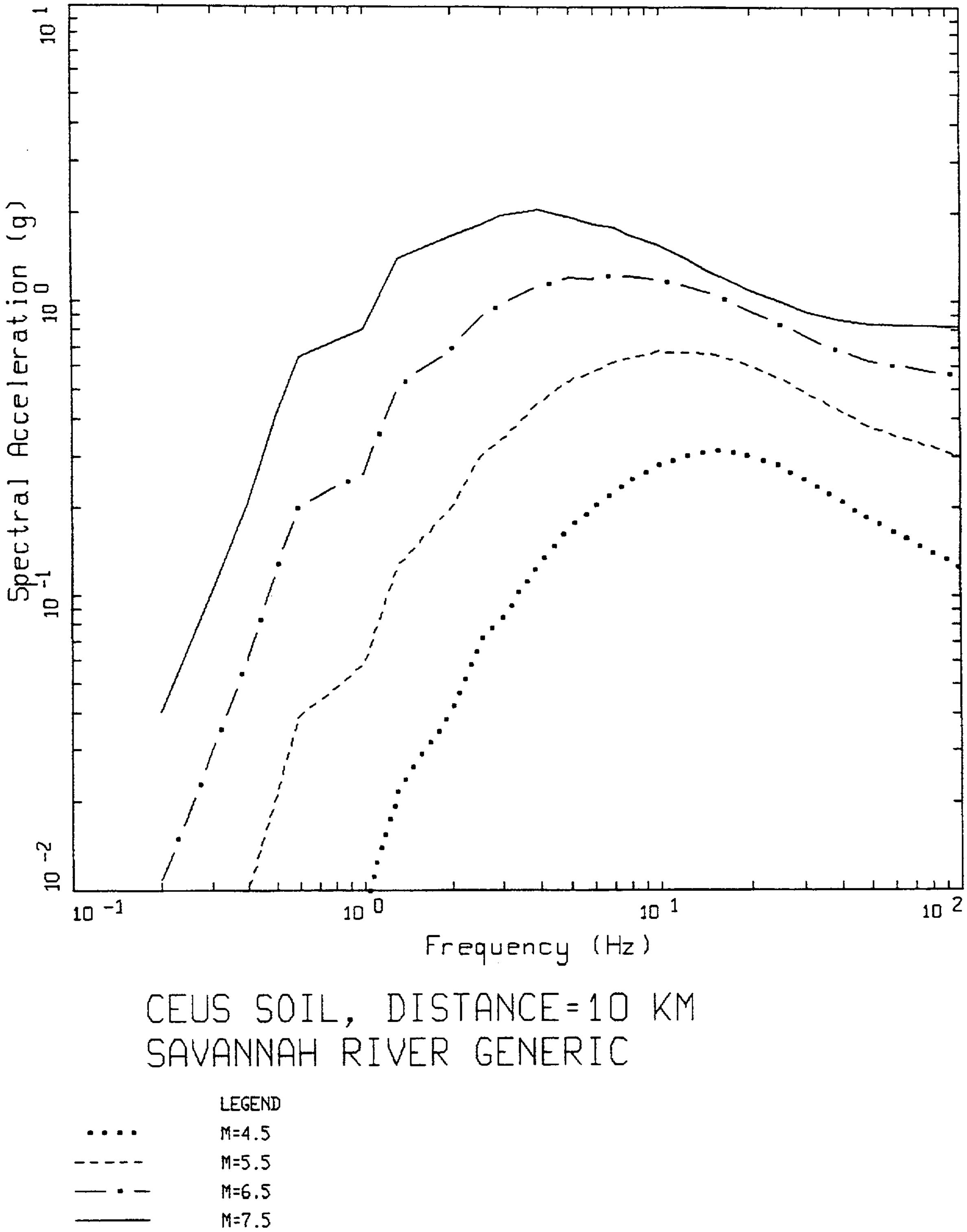

Figure 2-23b. Median response spectra (5% damping) at a distance of 10 km for **M** 4.5, 5.5, 6.5, and 7.5 for Savannah River generic profile and CEUS conditions (double-corner source model).

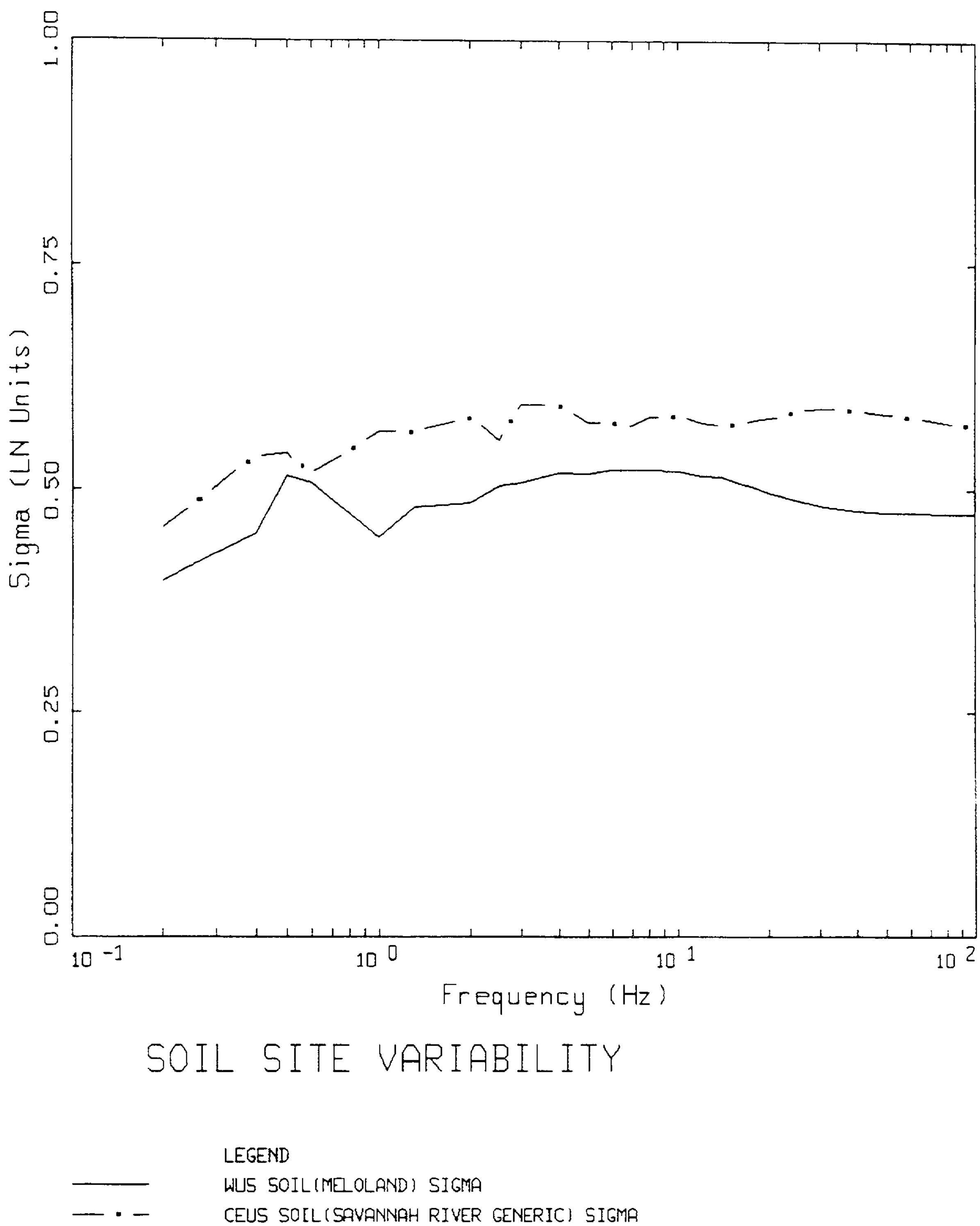

Figure 2-24. Variability in response spectral ordinates for Meloland profile (WUS) and Savannah River generic profile (CEUS) resulting from parametric variability and regression fit over all magnitudes and distances (Tables 2-7 and 2-8).

3.0 SEISMIC HAZARD

3.1 Mojave site

3.1.1 Rock site conditions

A probabilistic seismic hazard analysis (PSHA) was conducted at the Mojave site using the seismic sources and parameters described in Section 2.1 and using the attenuation equation for rock site conditions described in Section 2.3. In all respects the PSHA was typical of the analysis that would be conducted for a critical facility except that epistemic uncertainties in seismicity parameters and attenuation equations were not considered, for simplicity. The application of procedures to develop design spectra and ground motions will be the same whether applied to a single seismic hazard curve or to the mean of a family of seismic hazard curves.

Figure 3-1 shows the seismic hazard in terms of peak ground acceleration (PGA) vs. annual frequency of exceedence. This illustrates that the site is in a location of relative high seismic hazard, with PGA$\simeq$0.32g for a 500-year return period, and PGA$\simeq$0.9g for 10,000-year return period. (Note that PGA results are shown in Figure 3-1 only because they provide a common benchmark for experience.) Seismic hazard curves are documented in Table 3-1 for PGA, 10 Hz, 5 Hz, 2.5 Hz, and 1 Hz. The uniform hazard spectra (UHS) are shown in Figure 3-2 for annual frequencies of exceedence of 1E-3, 1E-4, and 1E-5, and these spectra are documented in Table 3-2.

The Mojave site was chosen because small, close earthquakes dominate the hazard at high frequencies (f> 10 Hz), but large distant events on the San Andreas fault contribute significantly at lower frequencies (1 Hz and less). This is illustrated in Figures 3-3 and 3-4, which show hazard contributions at 10 and 1 Hz, respectively, for the individual sources affecting the site. Particularly in the range of annual frequencies of 1E-3 to 1E-4, the San Andreas Fault has an important effect on 1 Hz hazard. This influence also occurs at lower structural frequencies.

The contribution of sources can be seen by deaggregating the hazard by magnitude, distance, and the attenuation equation ε term. These deaggregations are shown in Figures 3-5 through 3-8 for ground motions at 10 and 1 Hz corresponding to 1E-4 annual frequency of exceedence. The strong contribution of the San Andreas (**M**=7.8 at 30 km) for 1 Hz is apparent. The ε distributions are similar for 10 and 1 Hz; both indicate that ground motion above the median (ε>0) dominate the hazard at the 1E-4 level of motion. Mean ε values are 1.36 and 1.23 for 10 and 1 Hz, respectively.

Magnitudes and distances chosen from deaggregation to represent the range of values contributing to hazard are as follows:

Annual Frequency	**Structural Frequency**	**description**	**M**	**R**	**weight**
1E-4	10 Hz	lower magnitude	5.1	10 km	0.2
"	"	mean magnitude	6.1	14 km	0.6
"	"	upper magnitude	7.8	30 km	0.2
"	1 Hz	lower magnitude	5.4	10 km	0.2
"	"	mean magnitude	6.6	18 km	0.6
"	"	upper magnitude	7.8	30 km	0.2

For each frequency all three magnitudes are used to develop "deaggregation spectra" for Approach 2B (see Section 6.1.2). Only the mean magnitude is used to develop spectra for Approach 2A (Section 6.1.2). The lower and upper magnitude values were selected from the deaggregation results, identifying the magnitude associated with 5% and 95% cumulative probability from the magnitude deaggregation and then selecting the most likely distance associated with this magnitude (from Figures 3-5 and 3-7). The mean magnitude and associated distance (selected as the mean distance) were chosen from deaggregation.

For application of Approach 3 (Section 6.2), we also deaggregated the seismic hazard at 1E-3 and 1E-5 annual frequencies, to select appropriate magnitudes and distances. These are as follows:

Annual Frequency	**Structural Frequency**	**description**	**M**	**R**
1E-3	10 Hz	mean magnitude	6.1	23 km
"	1 Hz	mean magnitude	7.1	28 km
1E-5	10 Hz	mean magnitude	5.9	12 km
"	1 Hz	mean magnitude	6.4	14 km

3.1.2 Soil site conditions

A PSHA was conducted for the Mojave site assuming soil conditions as described in Section 2.1.2. For this analysis the soil attenuation equation was used to compute directly the hazard at the soil surface.

Figure 3-9 illustrates the PGA hazard at the site. By comparison to rock conditions, the soil hazard indicates slightly higher ground motions (0.34g) for the 500-year motion, and somewhat lower ground motions (0.7g) for the 10,000-year motion. This is evidence that the soil is undergoing non-linear response at high levels of input shaking, which is consistent with the deep soil profile and soil parameters chosen for this example (see Section 2.1.2). Table 3-3 documents the seismic hazard curves for soil, for PGA, 10 Hz, 5 Hz, 2.5 Hz, and 1 Hz. Figure 3-10 shows the 1E-3, 1E-4, and 1E-5 UHS for soil conditions, and Table 3-4 indicates the values of UHS for the three annual frequencies. Comparison with the UHS on rock illustrates the larger low-frequency content on soil and the decreased high frequencies.

Figures 3-11 and 3-12 show the contribution to 10 and 1 Hz seismic hazard, respectively, by seismic source. As is the case for the rock site conditions, the San Andreas Fault plays an important role in the seismic hazard at low frequencies, particularly in the range of amplitudes corresponding to 1,000- to 10,000-year return periods.

The deaggregation of seismic hazard by **M**, R, and ε is illustrated in Figures 3-13 through 3-16 for the two natural frequencies and for ground motion amplitudes corresponding to 1E-4 annual exceedence frequency. The contribution of the San Andreas Fault at 1 Hz is clear (Figure 3-15). As for rock conditions, the ε distribution for soil indicates that ground motions above the median ($\varepsilon>0$) dominate the hazard for 1E-4. The mean values are 1.73 and 1.40 for 10 and 1 Hz, respectively.

3.2 Columbia site

3.2.1 Rock site conditions

We conducted a PSHA for the Columbia site using the seismic sources described in Section 2.2 and the rock attenuation equation described in Section 2.3. These consist of a 1-corner and a 2-corner ground motion model, which were weighted equally in order to produce a composite seismic hazard. Note that the use of equal weights here is only for example and is not meant as a recommendation. The weights actually used in seismic hazard calculations must be justified with sound technical arguments and comparisons to data, where relevant. For the same reasons given for the Mojave site, no epistemic uncertainties were included in the Columbia site analysis other than those just mentioned for the attenuation equation.

Figure 3-17 shows the PGA seismic hazard curve for Columbia. The seismic hazard is, of course, much lower than in California, with a 500-year PGA of about 0.05g and a 10^{-4} PGA of 0.27g. Table 3-5 documents seismic hazard levels for PGA and for 10, 5, 2.5, and 1 Hz SA. Figure 3-18 shows the UHS for Columbia for 10^{-3}, 10^{-4}, and 10^{-5} annual frequencies of exceedence, and the mean UHS are documented in Table 3-6.

The Columbia site was chosen because small earthquakes in the local background dominate the high-frequency hazard, and large distant earthquakes from the Charleston fault dominate the low-frequency hazard. These dominances are illustrated in Figures 3-19 and 3-20, which show the contribution by seismic source for 10 Hz and 1 Hz SA, respectively, for the 1-corner model (results for the 2-corner model are similar). In the annual frequency range of 10^{-3} to 10^{-4}, the Charleston fault controls the seismic hazard at 1 Hz and lower frequencies.

Deaggregation of the seismic hazard shows the contribution by **M**, R, and ε. This deaggregation is illustrated for 10^{-4} annual frequency in Figures 3-21 through 3-24. The first of these figures indicates the contribution by **M** and R for 10 Hz, for the 1-corner and 2-corner models where the dominance of small, local earthquakes is evident. Figure 3-22 shows the ε distributions, where generally positive ε values contribution most to the hazard. Figure 3-23 indicates the contribution by **M** and R for 1 Hz, where the large contribution of Charleston-size events (**M**$\simeq$7.8, R$\simeq$130 km) is clear for both ground motion models. The ε distribution from these events also indicates positive values (Figure 3-24).

Values of **M** and R chosen from deaggregation of the hazard at 10^{-4} to represent the range of magnitudes and distances contributing to hazard are as follows:

Annual Frequency	**Structural Frequency**	**description**	**M**	**R**	**weight**
1E-4	10 Hz:	lower magnitude	4.6	10 km	0.22
”	”	mean magnitude	6.0	46 km	0.58
”	”	upper magnitude	7.7	130 km	0.20
”	1 Hz:	lower magnitude	6.0	10 km	0.07
”	”	mean magnitude	7.2	110 km	0.73
”	”	upper magnitude	7.7	130 km	0.20

For each frequency all three magnitudes were used to develop "deaggregation spectra" for Approach 2B (see Section 6.1.2). Only the mean magnitude at each frequency is used to develop spectra according to Approach 2A (Section 6.1.2). The lower and upper magnitudes were selected from the **M** and R deaggregation to represent the contributions of local and Charleston earthquakes, respectively. The weights on the upper magnitudes were calculated to reflect the contribution to the 10^{-4} hazard from the Charleston source, and the weights on the lower magnitudes were calculated to give the correct mean magnitude.

To apply Approach 3 we also deaggregated the seismic hazard at amplitudes corresponding to 10^{-3} and 10^{-5} annual frequencies, to select appropriate magnitudes and distances. These are as follows:

Annual Frequency	**Structural Frequency, Hz**	**description**	**M**	**R**
1E-3	10 Hz	mean magnitude	6.2	73 km
”	1 Hz	mean magnitude	7.1	115 km
1E-5	10 Hz	mean magnitude	5.8	20 km
”	1 Hz	mean magnitude	7.1	90 km

3.2.2 Soil site conditions

We conducted a PSHA for the Columbia site, using the soil conditions described in Section 2.3. For this analysis we used the soil attenuations for the CEUS (Section 2.3.5), consisting of 1- and 2-corner models weighted equally.

Figure 3-25 shows the PGA hazard at the Columbia site for soil conditions. By comparison to the rock hazard curves (Figure 3-17), the soil shows slightly higher amplitudes at 10^{-3} annual frequency

(0.11g vs. 0.08g on rock), about the same amplitudes at 10^{-4} annual frequency (~0.28g on both soil and rock), and lower amplitudes at 10^{-5} annual frequency (0.59g vs. 0.68g on rock). This indicates that the soil is behaving more nonlinearly for the extreme motions (low annual frequencies). Table 3-7 documents the seismic hazard curves for soil for PGA and for 10 Hz, 2.5 Hz, and 1 Hz SA. Figure 3-26 plots the 10^{-3}, 10^{-4}, and 10^{-5} UHS for soil, and Table 3-8 indicates the numerical values of UHS for these annual frequencies. Comparison of these spectra with UHS for rock (Figure 3-18) indicates the larger long period content of the soil motion and the spectral peak around 10 Hz.

Figures 3-27 and 3-28 show the contribution to 10 Hz and 1 Hz hazard, respectively, by source. As for the rock hazard analysis, the local background source dominates at 10 Hz and the Charleston source dominates at 1 Hz for annual frequencies between 10^{-3} and 10^{-5}.

The deaggregation of seismic hazard by **M**, R, and ε at 10 and 1 Hz is illustrated in Figures 3-29 through 3-32, for ground motions corresponding to 10^{-4} annual frequency. The contribution of the Charleston source is clear in both the **M**-R deaggregations and in the ε deaggregations (the Charleston source causes the highest spike in both ε plots). As is the case for rock conditions, ε values for soil are generally greater than zero. Mean values for ε are 1.10 and 1.18 for 10 and 1 Hz, respectively.

Table 3-1
Seismic hazard curves
Mojave site, rock conditions

	Annual frequency of exceedence				
Amplitude, g	**PGA**	**10 Hz**	**5 Hz**	**2.5 Hz**	**1 Hz**
0.05	6.246E-2	1.281E-1	1.359E-1	9.855E-2	4.614E-2
0.1	2.871E-2	7.086E-2	7.388E-2	5.292E-2	1.983E-2
0.2	7.001E-3	3.432E-2	3.661E-2	2.245E-2	4.234E-3
0.3	2.282E-3	1.788E-2	1.983E-2	1.036E-2	1.311E-3
0.4	9.724E-4	9.716E-3	1.115E-2	5.236E-3	5.235E-4
0.5	5.069E-4	5.567E-3	6.567E-3	2.893E-3	2.520E-4
0.6	3.036E-4	3.370E-3	4.058E-3	1.726E-3	1.398E-4
0.7	1.989E-4	2.149E-3	2.625E-3	1.098E-3	8.610E-5
0.8	1.380E-4	1.436E-3	1.770E-3	7.362E-4	5.703E-5
0.9	9.937E-5	1.001E-3	1.239E-3	5.163E-4	3.972E-5
1	7.343E-5	7.242E-4	8.968E-4	3.759E-4	2.866E-5
1.25	3.712E-5	3.674E-4	4.518E-4	1.926E-4	1.401E-5
1.5	2.015E-5	2.135E-4	2.600E-4	1.119E-4	7.488E-6
1.75	1.152E-5	1.355E-4	1.641E-4	7.049E-5	4.246E-6
1.91	8.230E-6	1.045E-4	1.265E-4	5.400E-5	3.025E-6
2	6.857E-6	9.111E-5	1.102E-4	4.685E-5	2.517E-6
2.5	2.679E-6	4.586E-5	5.597E-5	2.295E-5	9.790E-7
3	1.160E-6	2.523E-5	3.127E-5	1.229E-5	4.223E-7
4	2.728E-7	8.946E-6	1.149E-5	4.175E-6	9.812E-8
5	7.986E-8	3.651E-6	4.847E-6	1.650E-6	2.818E-8

Table 3-2
Uniform hazard spectra
Mojave site, rock conditions

Structural frequency, Hz	Spectral amplitudes, g		
	10^{-3} UHS	10^{-4} UHS	10^{-5} UHS
100	3.962E-1	8.980E-1	1.816
50	4.178E-1	9.522E-1	1.929
40	4.494E-1	9.974E-1	2.001
31	4.993E-1	1.120	2.259
25	5.621E-1	1.240	2.481
20	6.432E-1	1.396	2.778
18	6.889E-1	1.503	2.999
16	7.412E-1	1.625	3.240
14	7.968E-1	1.715	3.398
12	8.464E-1	1.831	3.658
10	9.003E-1	1.939	3.878
8	9.427E-1	2.002	4.004
7	9.527E-1	2.054	4.138
6	9.646E-1	2.043	4.083
5	9.651E-1	2.065	4.146
4	9.175E-1	1.969	3.951
3	8.228E-1	1.759	3.523
2.5	7.221E-1	1.557	3.170
2	5.710E-1	1.228	2.500
1.3	4.097E-1	8.644E-1	1.806
1	3.266E-1	6.675E-1	1.379
0.6	2.340E-1	4.529E-1	8.561E-1
0.5	2.191E-1	4.170E-1	7.669E-1
0.4	1.755E-1	3.298E-1	5.879E-1
0.2	8.502E-2	1.499E-1	2.412E-1

Table 3-3
Seismic hazard curves
Mojave site, Meloland profile

	Annual frequency of exceedence				
Amplitude, g	**PGA**	**10 Hz**	**5 Hz**	**2.5 Hz**	**1 Hz**
0.01	3.913E-1	5.622E-1	6.552E-1	6.597E-1	5.163E-1
0.05	8.873E-2	1.589E-1	2.084E-1	1.894E-1	1.192E-1
0.07	6.484E-2	1.151E-1	1.518E-1	1.367E-1	8.675E-2
0.1	4.426E-2	8.086E-2	1.078E-1	9.710E-2	6.372E-2
0.2	1.214E-2	3.283E-2	5.125E-2	4.851E-2	3.282E-2
0.3	3.450E-3	1.344E-2	2.654E-2	2.704E-2	1.665E-2
0.4	1.152E-3	5.538E-3	1.345E-2	1.482E-2	8.445E-3
0.5	4.594E-4	2.396E-3	6.831E-3	8.115E-3	4.485E-3
0.6	2.140E-4	1.111E-3	3.555E-3	4.526E-3	2.503E-3
0.7	1.118E-4	5.542E-4	1.921E-3	2.599E-3	1.459E-3
0.8	6.291E-5	2.959E-4	1.085E-3	1.546E-3	8.838E-4
0.9	3.712E-5	1.672E-4	6.418E-4	9.553E-4	5.547E-4
1	2.260E-5	9.876E-5	3.961E-4	6.137E-4	3.601E-4
1.25	7.136E-6	3.036E-5	1.382E-4	2.369E-4	1.401E-4
1.5	2.465E-6	1.059E-5	5.625E-5	1.083E-4	6.436E-5
1.75	9.140E-7	4.014E-6	2.520E-5	5.508E-5	3.333E-5
2	3.601E-7	1.623E-6	1.205E-5	2.988E-5	1.870E-5
3	1.402E-8	6.954E-8	9.486E-7	3.600E-6	2.738E-6
4	9.571E-10	5.083E-9	1.150E-7	5.949E-7	5.427E-7
5	9.619E-11	5.341E-10	1.855E-8	1.229E-7	1.292E-7

Table 3-4
Uniform hazard spectra
Mojave site, Meloland profile

Structural frequency, Hz	Spectral amplitudes, g 10^{-3} UHS	10^{-4} UHS	10^{-5} UHS
100	4.140E-1	7.183E-1	1.171
50	4.165E-1	7.233E-1	1.179
40	4.192E-1	7.285E-1	1.187
31	4.252E-1	7.402E-1	1.205
25	4.377E-1	7.470E-1	1.198
20	4.599E-1	7.716E-1	1.218
18	4.741E-1	7.965E-1	1.255
16	4.960E-1	8.189E-1	1.272
14	5.247E-1	8.546E-1	1.310
12	5.627E-1	9.231E-1	1.412
10	6.141E-1	9.975E-1	1.514
8	6.607E-1	1.083	1.665
7	7.048E-1	1.157	1.776
6	7.499E-1	1.234	1.901
5	8.148E-1	1.336	2.060
4	8.535E-1	1.450	2.298
3	9.049E-1	1.550	2.492
2.5	8.900E-1	1.528	2.467
2	8.576E-1	1.490	2.434
1.3	7.511E-1	1.348	2.316
1	7.741E-1	1.353	2.282
0.6	5.545E-1	9.735E-1	1.650
0.5	5.248E-1	9.488E-1	1.648
0.4	4.691E-1	8.799E-1	1.592
0.2	1.704E-1	3.232E-1	5.142E-1

Table 3-5
Seismic hazard curves*
Columbia site, rock

	Annual frequency of exceedence for:				
Acceleration, g	**PGA**	**10 Hz**	**5 Hz**	**2.5 Hz**	**1 Hz**
.001	1.284E-2	1.284E-2	1.284E-2	1.258E-2	7.906E-3
.005	1.137E-2	1.234E-2	1.109E-2	7.905E-3	3.033E-3
.01	8.574E-3	1.056E-2	8.220E-3	5.097E-3	1.946E-3
.02	5.304E-3	7.487E-3	5.189E-3	3.008E-3	1.033E-3
.05	2.094E-3	3.674E-3	2.261E-3	1.112E-3	1.933E-4
.1	7.655E-4	1.690E-3	8.752E-4	3.207E-4	2.134E-5
.2	2.035E-4	5.596E-4	2.199E-4	5.298E-5	1.426E-6
.3	8.145E-5	2.439E-4	7.908E-5	1.485E-5	3.196E-7
.4	4.040E-5	1.248E-4	3.540E-5	5.736E-6	1.148E-7
.5	2.288E-5	7.124E-5	1.840E-5	2.728E-6	5.117E-8
.6	1.416E-5	4.407E-5	1.064E-5	1.487E-6	2.582E-8
.7	9.336E-6	2.898E-5	6.656E-6	8.899E-7	1.419E-8
.8	6.456E-6	2.000E-5	4.418E-6	5.688E-7	8.294E-9
.9	4.630E-6	1.433E-5	3.068E-6	3.818E-7	5.092E-9
1	3.418E-6	1.060E-5	2.208E-6	2.661E-7	3.252E-9
1.25	1.762E-6	5.523E-6	1.087E-6	1.215E-7	1.210E-9
1.5	1.002E-6	3.200E-6	5.995E-7	6.251E-8	5.175E-10
2	3.921E-7	1.312E-6	2.256E-7	2.079E-8	1.252E-10

* mean results from 1- and 2-corner models

Table 3-6
Uniform hazard spectra*
Columbia site, rock

Structural Frequency, Hz	Spectral Acceleration, g 1E-3 UHS	1E-4 UHS	1E-5 UHS
100	8.410E-2	2.740E-1	6.824E-1
50	1.777E-1	6.241E-1	1.611
40	1.815E-1	6.282E-1	1.600
31	1.725E-1	5.853E-1	1.467
25	1.687E-1	5.679E-1	1.407
20	1.664E-1	5.516E-1	1.354
18	1.661E-1	5.461E-1	1.330
16	1.643E-1	5.361E-1	1.296
14	1.599E-1	5.173E-1	1.238
12	1.517E-1	4.847E-1	1.146
10	1.390E-1	4.369E-1	1.020
8	1.199E-1	3.728E-1	8.604E-1
7	1.117E-1	3.422E-1	7.829E-1
6	1.024E-1	3.086E-1	6.964E-1
5	9.140E-2	2.733E-1	6.123E-1
4	7.711E-2	2.309E-1	5.079E-1
3	6.180E-2	1.838E-1	3.959E-1
2.5	5.349E-2	1.566E-1	3.381E-1
2	4.309E-2	1.301E-1	2.729E-1
1.3	2.573E-2	8.420E-2	1.676E-1
1	2.036E-2	6.307E-2	1.214E-1
0.6	1.203E-2	4.230E-2	8.431E-2
0.5	1.020E-2	3.566E-2	7.352E-2
0.4	7.111E-3	2.771E-2	2.388E-2
0.2	2.384E-3	1.240E-2	2.388E-2

* mean results from 1- and 2-corner models

Table 3-7
Seismic hazard curves*
Columbia site, Savannah River generic profile

	Annual frequency of exceedence for:				
Acceleration, g	PGA	10 Hz	5 Hz	2.5 Hz	1 Hz
.002	1.276E-2	1.284E-2	1.283E-2	1.279E-2	8.157E-3
.005	1.171E-2	1.271E-2	1.255E-2	1.155E-2	4.855E-3
.01	9.324E-3	1.196E-2	1.115E-2	8.750E-3	3.250E-3
.02	6.259E-3	9.855E-3	8.333E-3	5.785E-3	2.207E-3
.05	2.946E-3	5.881E-3	4.570E-3	3.063E-3	1.110E-3
.07	1.843E-3	4.294E-3	3.293E-3	2.206E-3	6.677E-4
.1	1.208E-3	3.301E-3	2.514E-3	1.664E-3	4.091E-4
.2	2.896E-4	1.400E-3	1.043E-3	6.155E-4	7.165E-5
.3	9.458E-5	6.833E-4	4.985E-4	2.566E-4	1.767E-5
.4	3.849E-5	3.652E-4	2.617E-4	1.183E-4	5.801E-6
.5	1.823E-5	2.098E-4	1.478E-4	5.955E-5	2.402E-6
.6	9.593E-6	1.279E-4	8.862E-5	3.235E-5	1.188E-6
.7	5.444E-6	8.193E-5	5.589E-5	1.878E-5	6.696E-7
.8	3.266E-6	5.459E-5	3.676E-5	1.153E-5	4.138E-7
1	1.325E-6	2.668E-5	1.760E-5	4.990E-6	1.891E-7
1.5	2.146E-7	6.390E-6	4.155E-6	1.049E-6	4.515E-8
2	5.015E-8	2.064E-6	1.367E-6	3.341E-7	1.537E-8

* mean results from 1- and 2-corner models

Table 3-8
Uniform hazard spectra*
Columbia site, Savannah River generic profile

Structural Frequency, Hz	Spectral Acceleration, g		
	1E-3 UHS	1E-4 UHS	1E-5 UHS
100	1.101E-1	2.940E-1	5.930E-1
50	1.415E-1	3.700E-1	7.299E-1
40	1.634E-1	4.217E-1	8.256E-1
31	1.885E-1	4.830E-1	9.475E-1
25	2.087E-1	5.390E-1	1.0567
20	2.221E-1	5.811E-1	1.147
18	2.308E-1	6.065E-1	1.201
16	2.382E-1	6.258E-1	1.240
14	2.389E-1	6.360E-1	1.274
12	2.428E-1	6.469E-1	1.292
10	2.419E-1	6.540E-1	1.321
8	2.306E-1	6.280E-1	1.282
7	2.250E-1	6.170E-1	1.255
6	2.129E-1	5.891E-1	1.196
5	2.046E-1	5.747E-1	1.172
4	1.825E-1	5.328E-1	1.104
3	1.483E-1	4.516E-1	9.365E-1
2.5	1.456E-1	4.224E-1	8.309E-1
2	1.089E-1	3.345E-1	6.802E-1
1.3	9.595E-2	3.063E-1	6.036E-1
1	5.435E-2	1.790E-1	3.475E-1
0.6	5.226E-2	1.848E-1	3.511E-1
0.5	2.875E-2	1.190E-1	2.379E-1
0.4	1.648E-2	7.465E-2	1.485E-1
0.2	3.390E-3	2.179E-2	4.559E-2

* mean results from 1- and 2-corner models

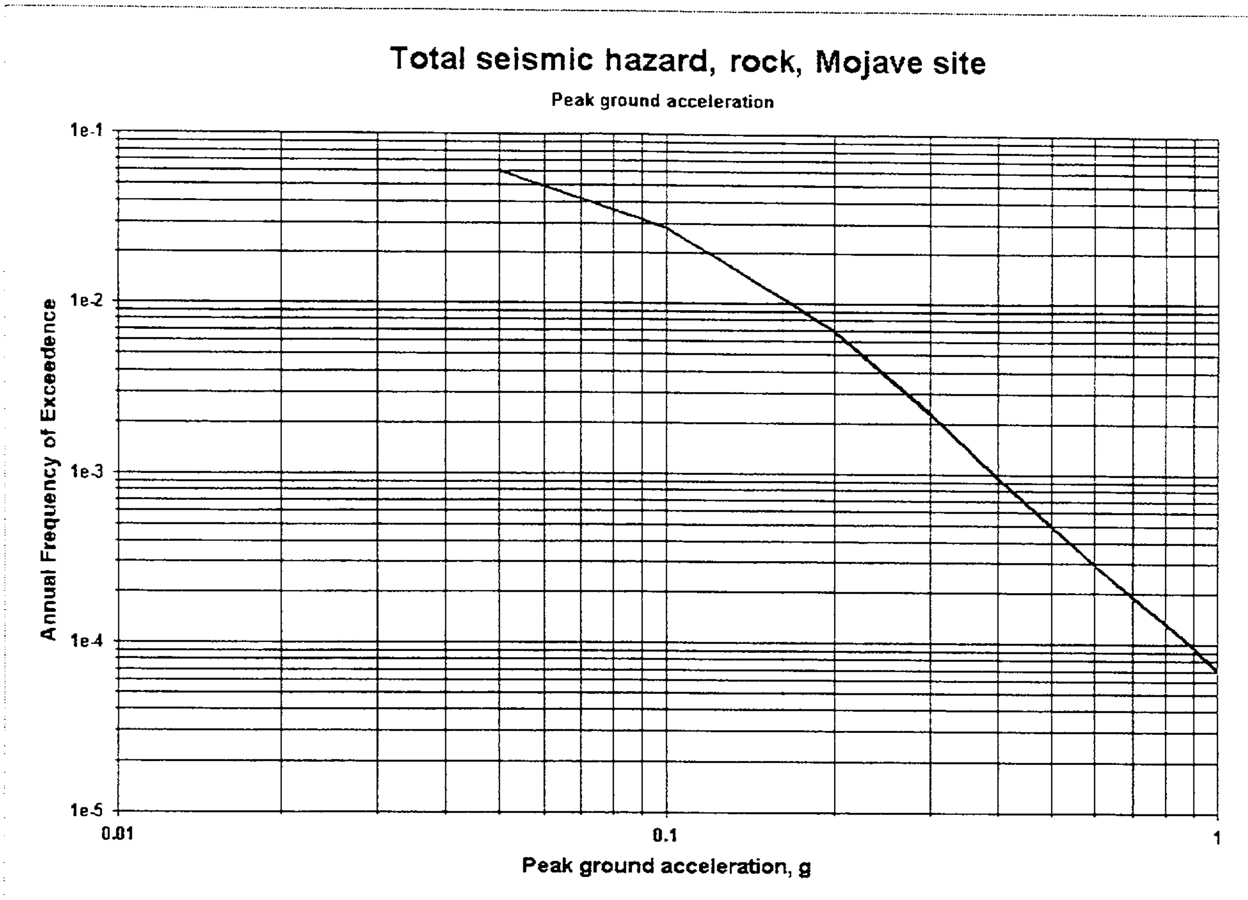

Figure 3-1. PGA seismic hazard curve for Mojave site, rock conditions.

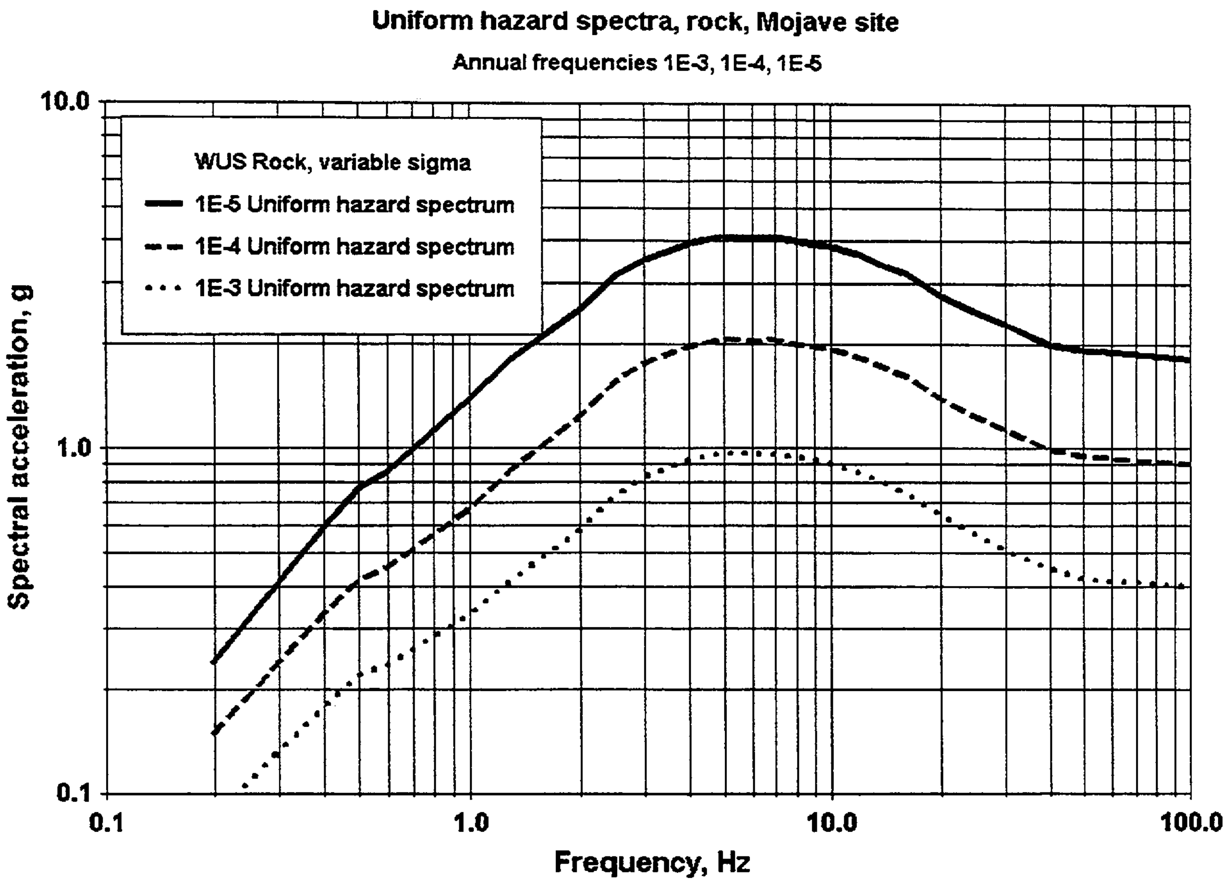

Figure 3-2. UHS for Mojave site, rock conditions.

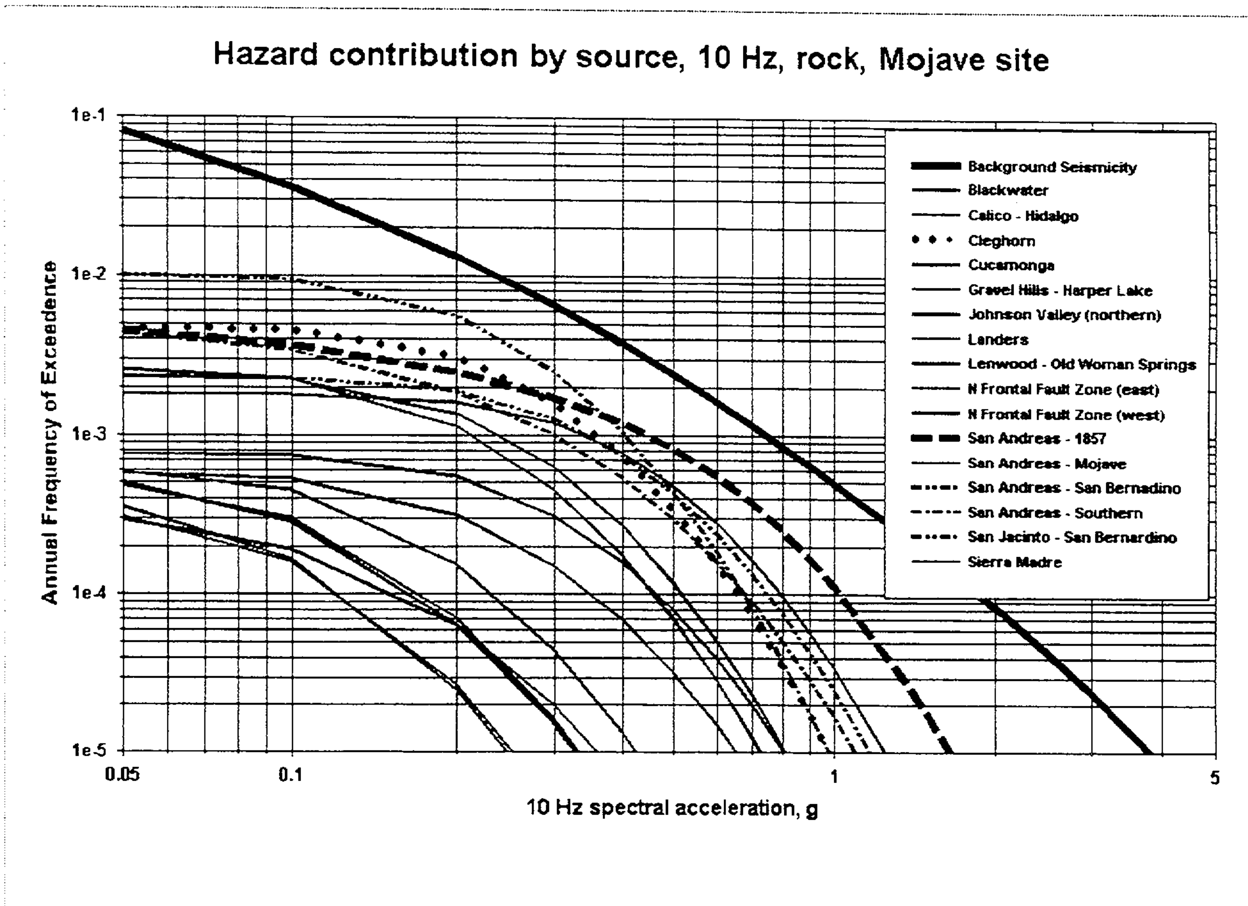

Figure 3-3. Contribution to 10 Hz spectral acceleration hazard by source for Mojave site, rock conditions.

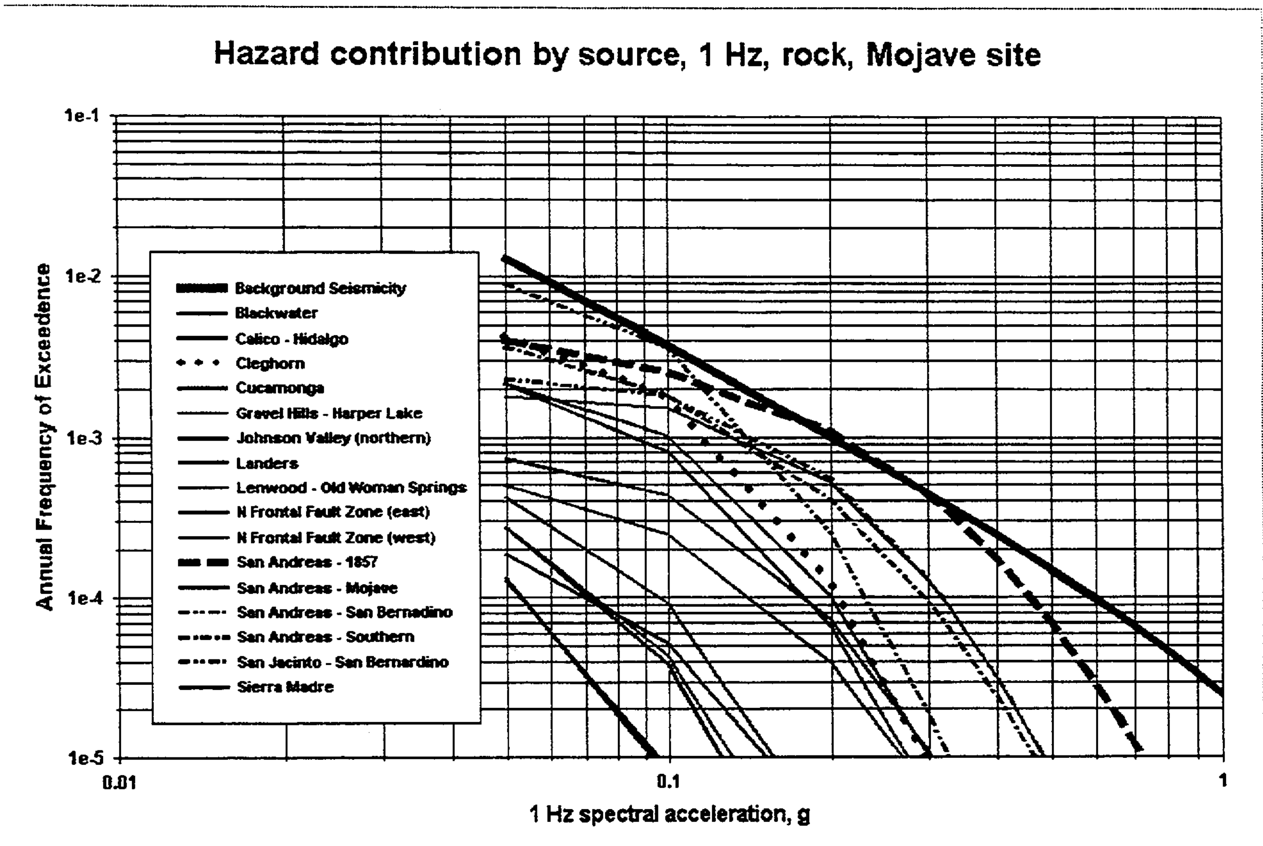

Figure 3-4. Contribution to 1 Hz spectral acceleration hazard for Mojave site, rock conditions.

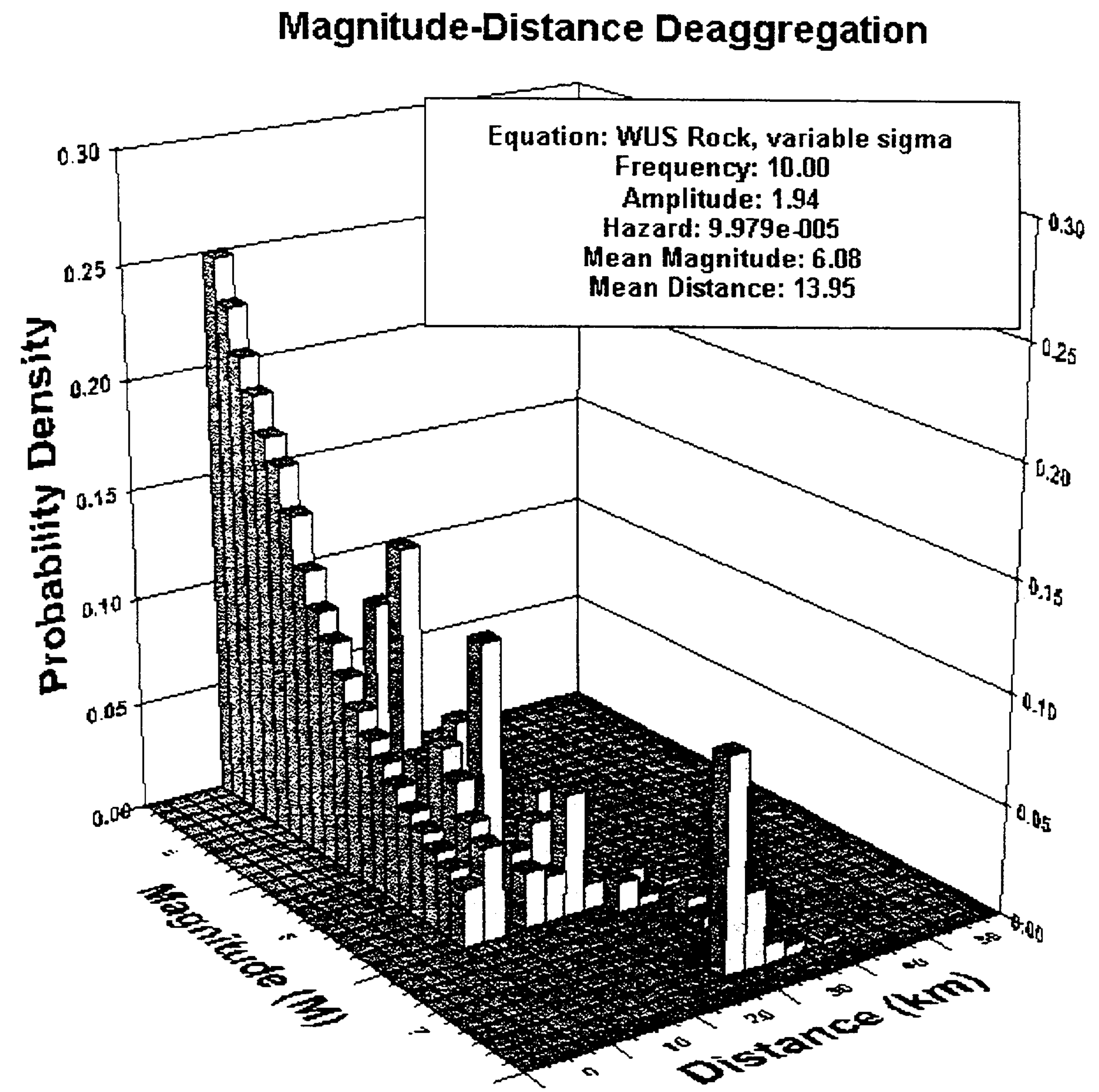

Figure 3-5. Magnitude and distance deaggregation of 10^{-4} hazard at 10 Hz for Mojave site, rock conditions.

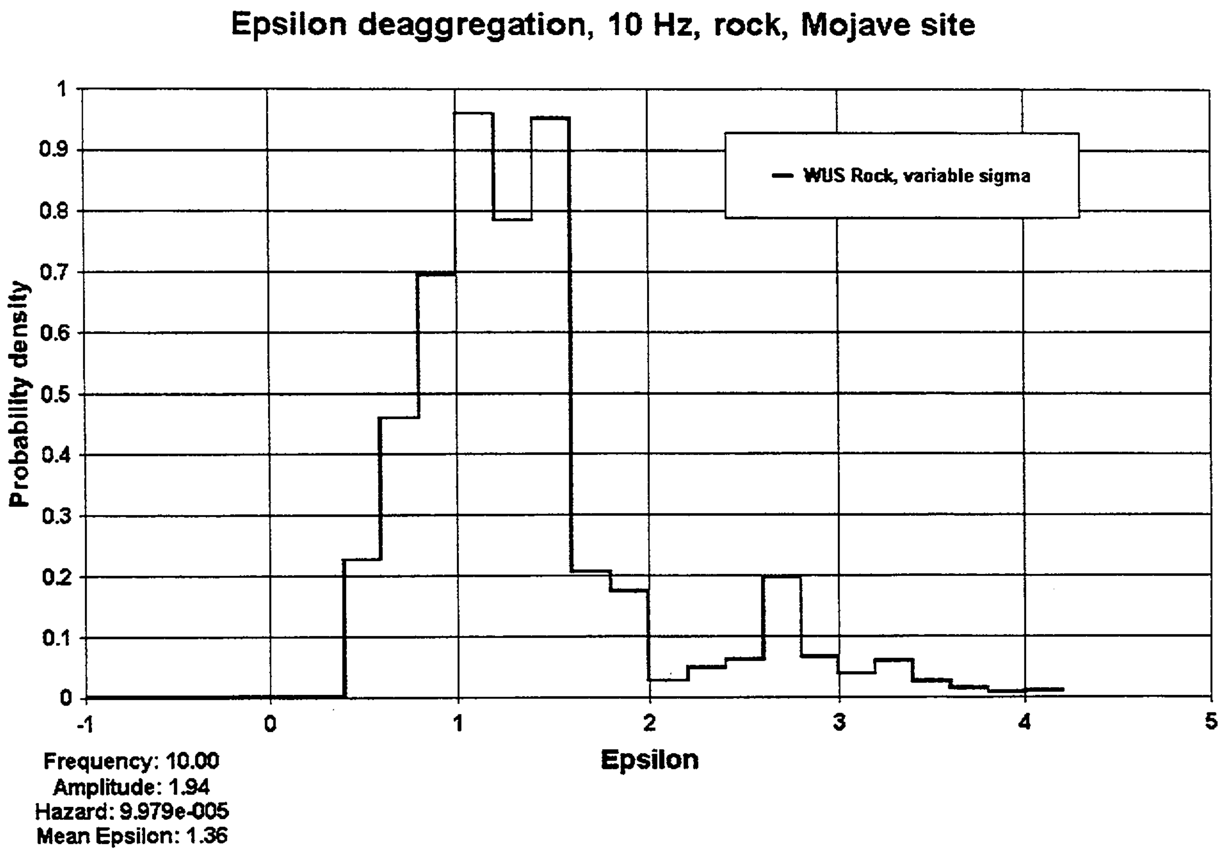

Figure 3-6. Epsilon deaggregation of 10^{-4} hazard at 10 Hz for Mojave site, rock conditions.

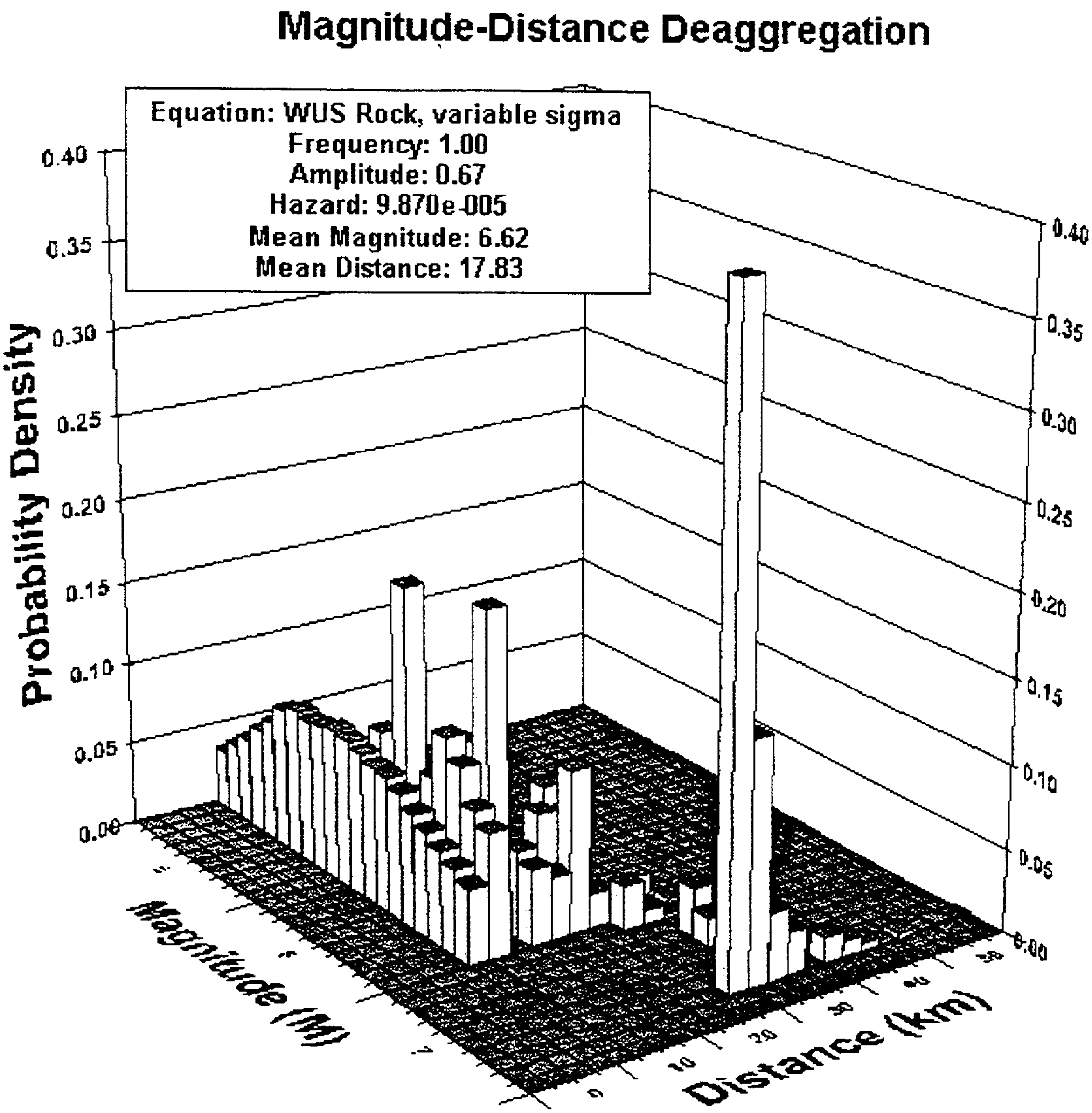

Figure 3-7. Magnitude and distance deaggregation of 10^{-4} hazard at 1 Hz for Mojave site, rock conditions.

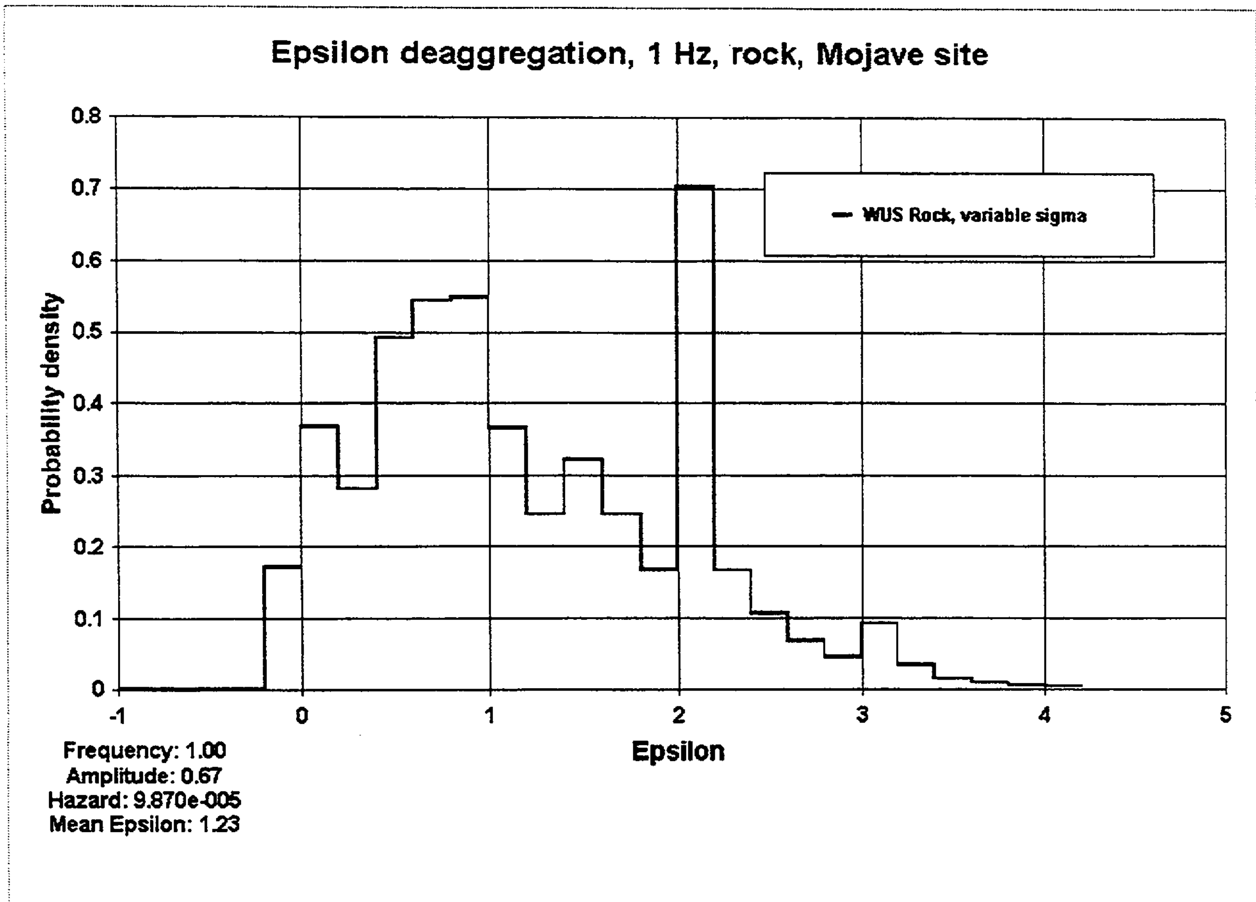

Figure 3-8. Epsilon deaggregation of 10^{-4} hazard at 1 Hz for Mojave site, rock conditions.

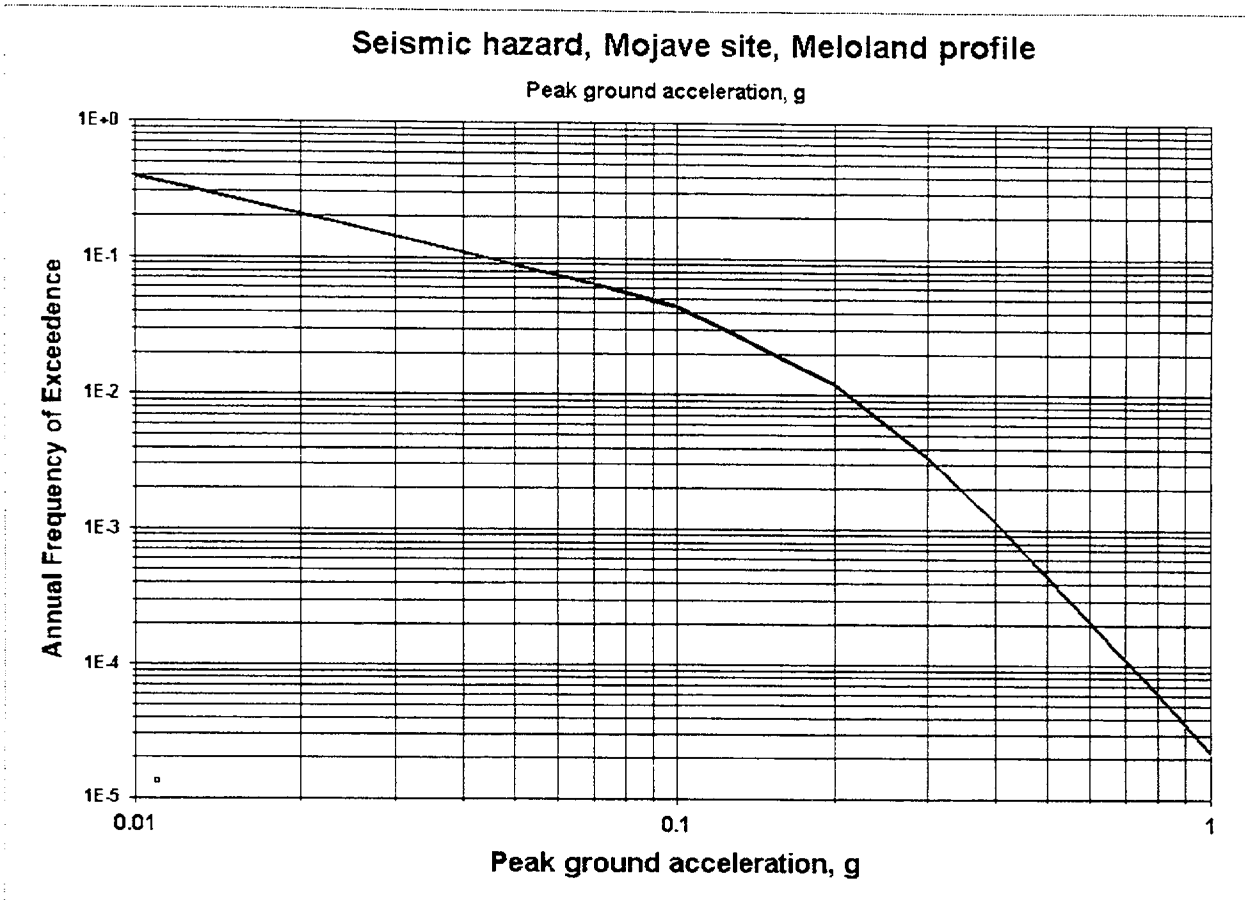

Figure 3-9. PGA seismic hazard curve for Mojave site, soil conditions.

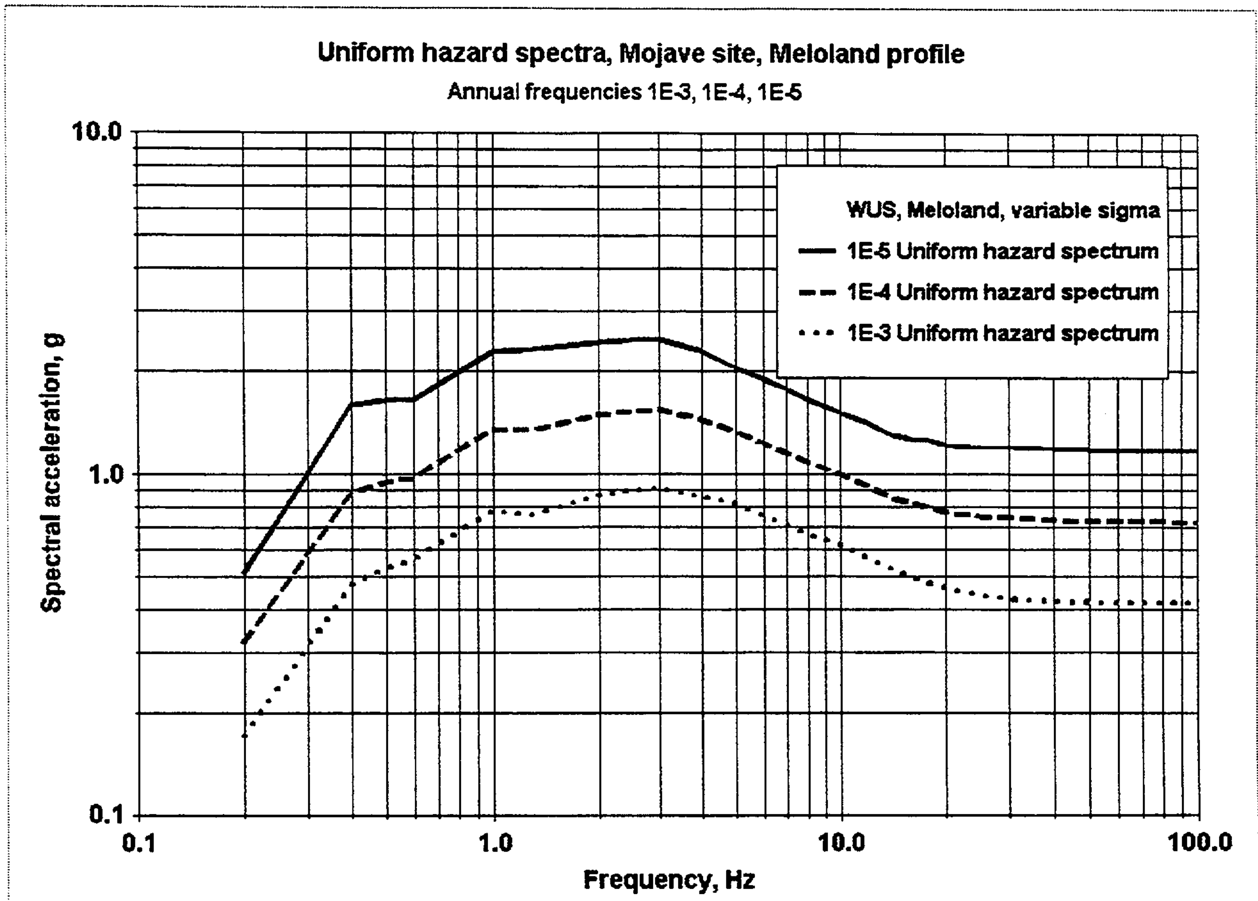

Figure 3-10. UHS for Mojave site, soil conditions.

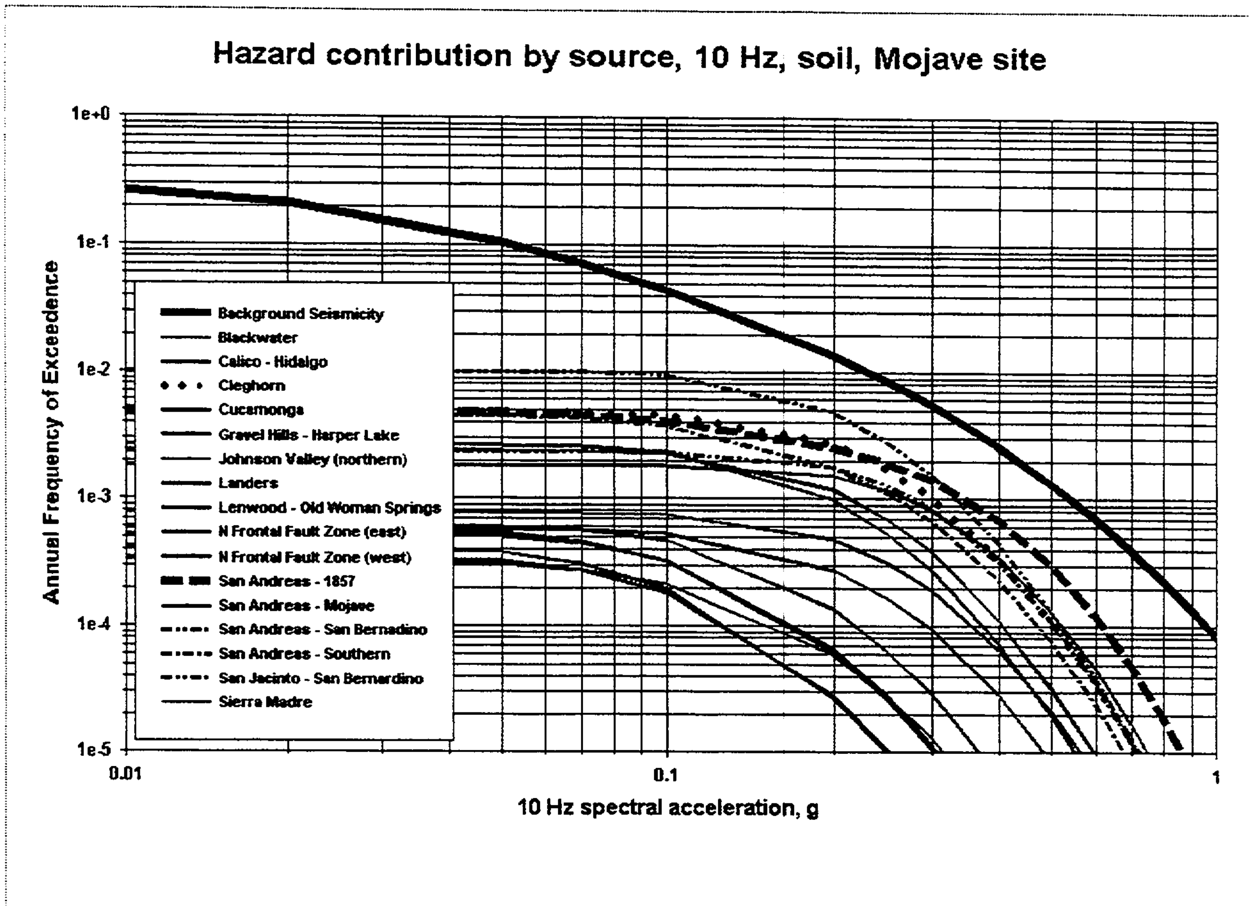

Figure 3-11. Contribution to 10 Hz spectral acceleration hazard by source for Mojave site, soil conditions.

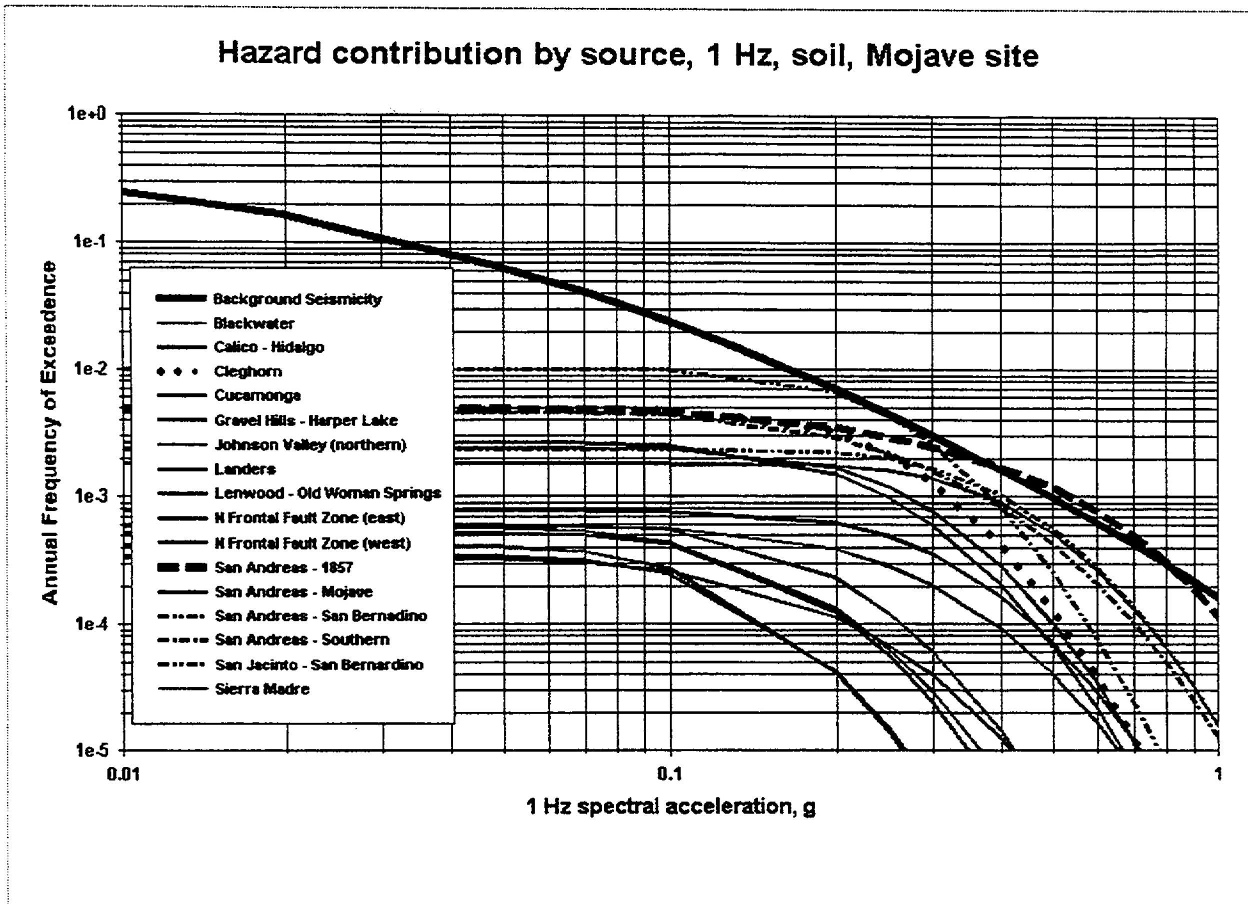

Figure 3-12. Contribution to 1 Hz spectral acceleration hazard for Mojave site, soil conditions.

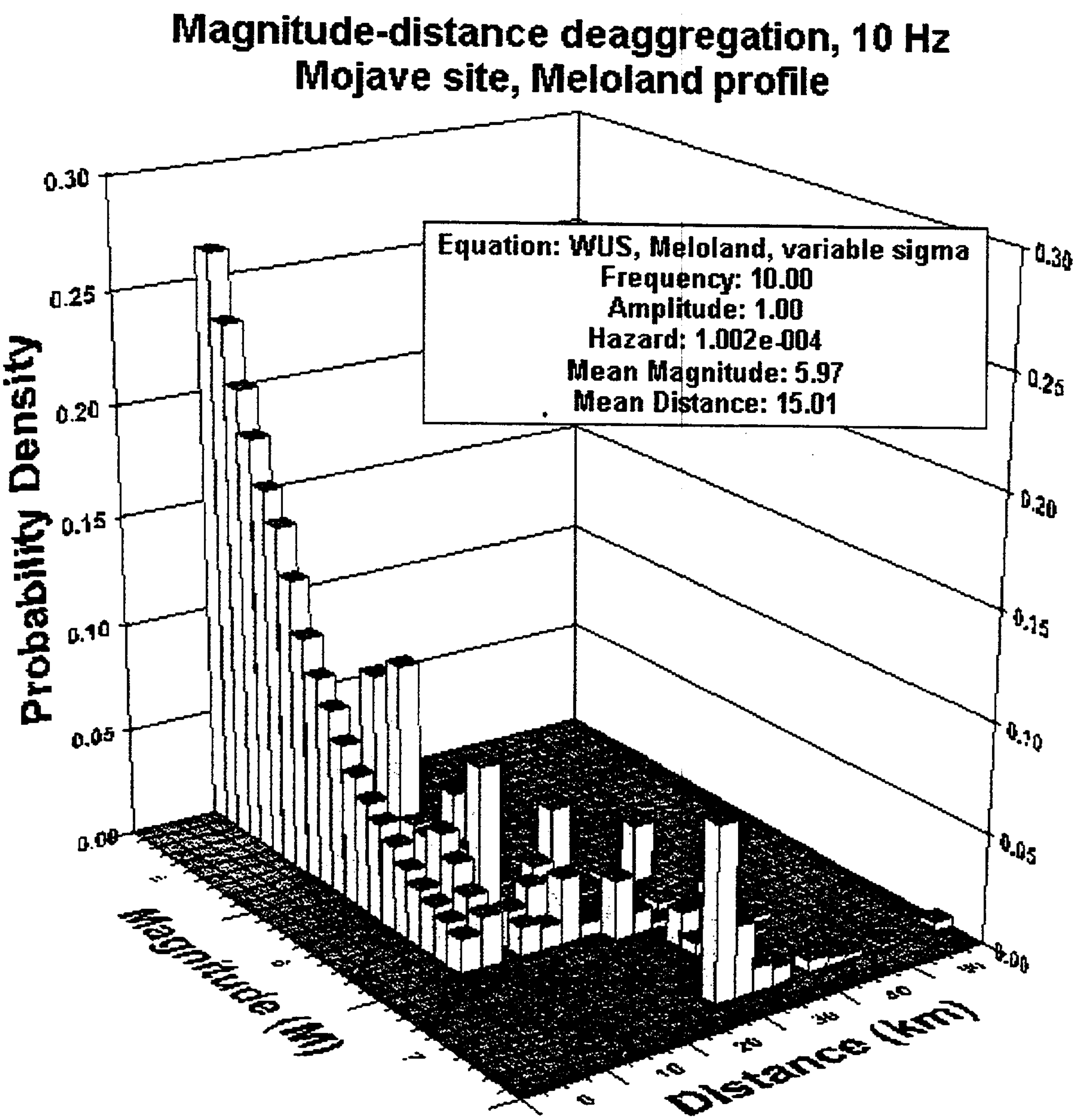

Figure 3-13. Magnitude and distance deaggregation of 10^{-4} hazard at 10 Hz for Mojave site, soil conditions.

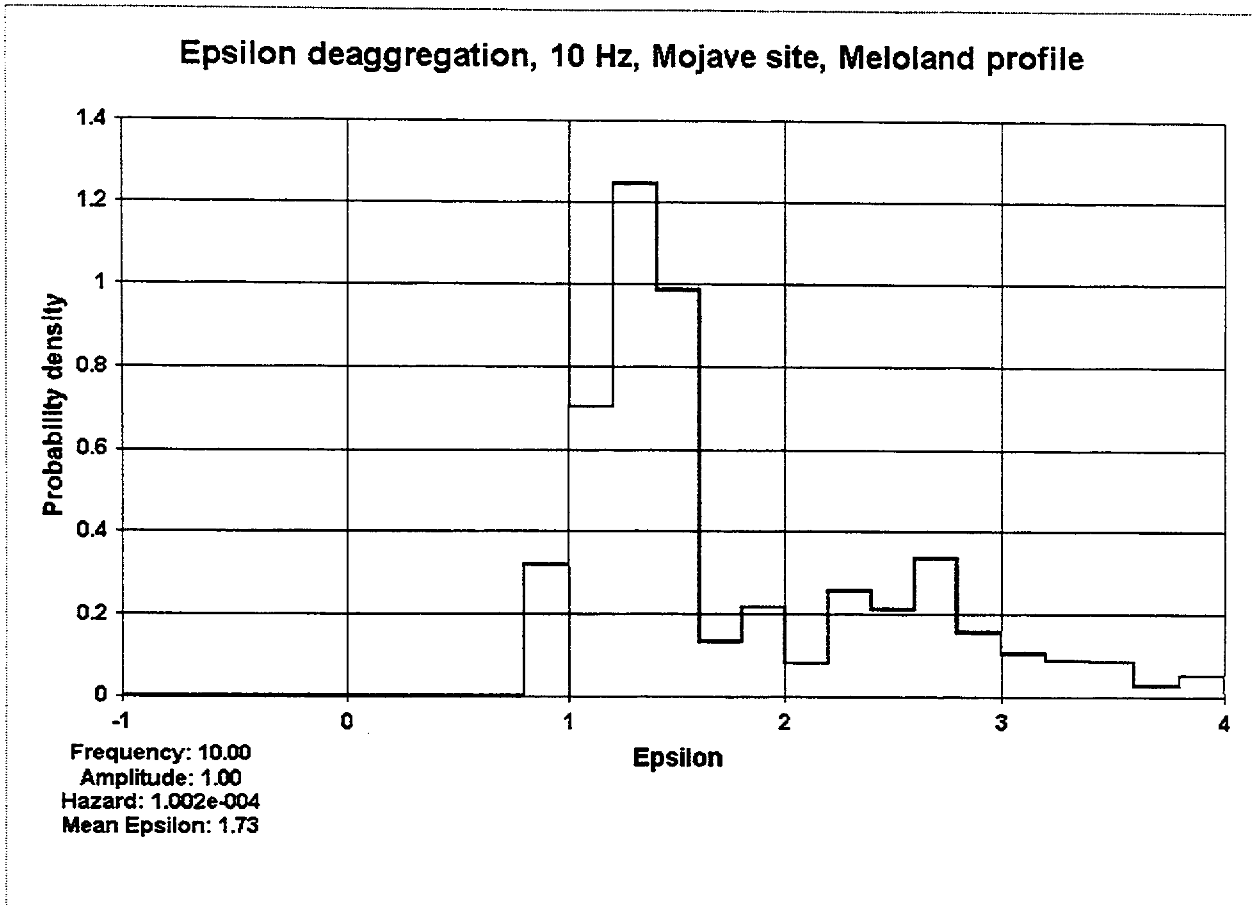

Figure 3-14. Epsilon deaggregation of 10^{-4} hazard at 10 Hz for Mojave site, soil conditions.

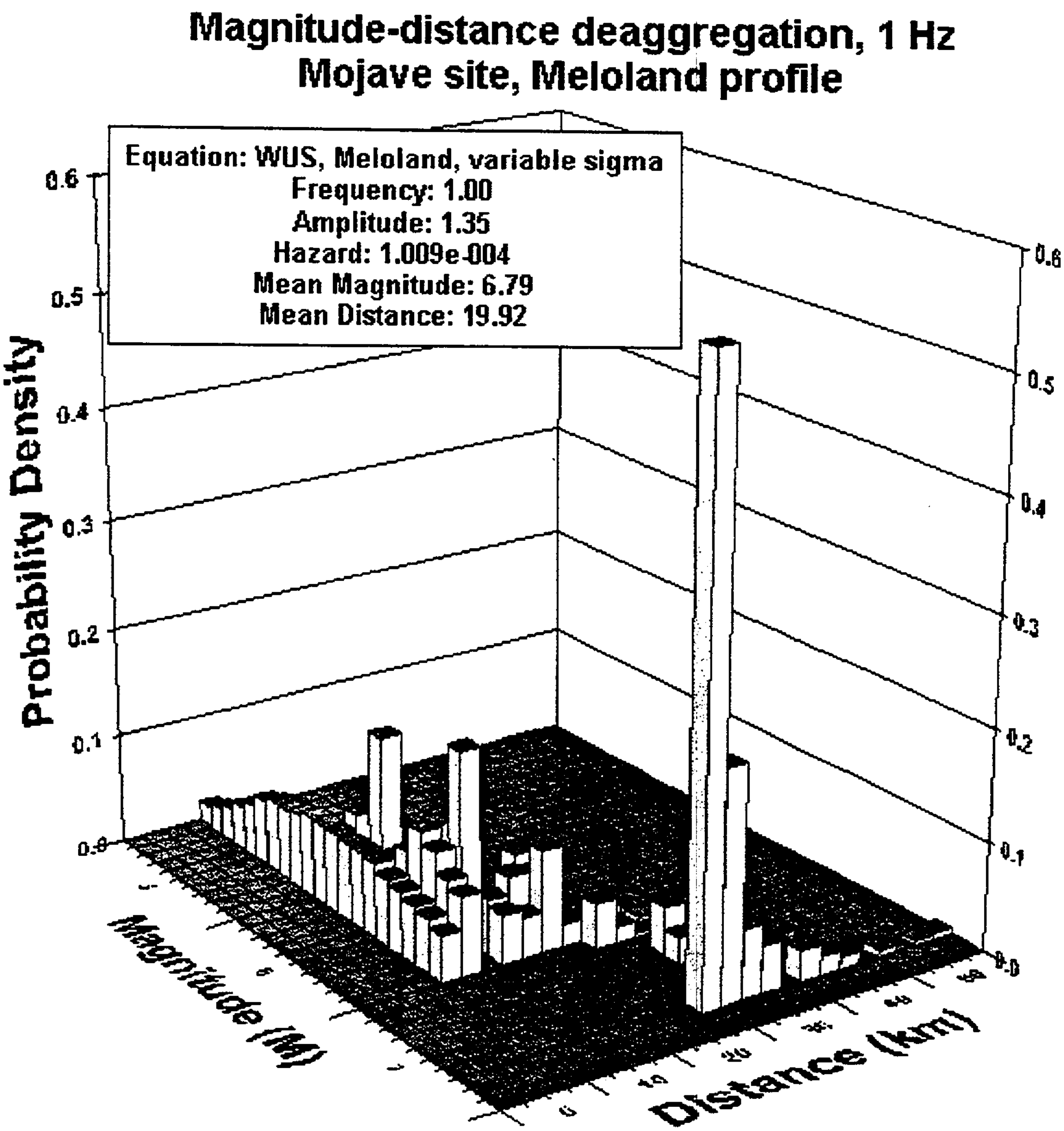

Figure 3-15. Magnitude and distance deaggregation of 10^{-4} hazard at 1 Hz for Mojave site, soil conditions.

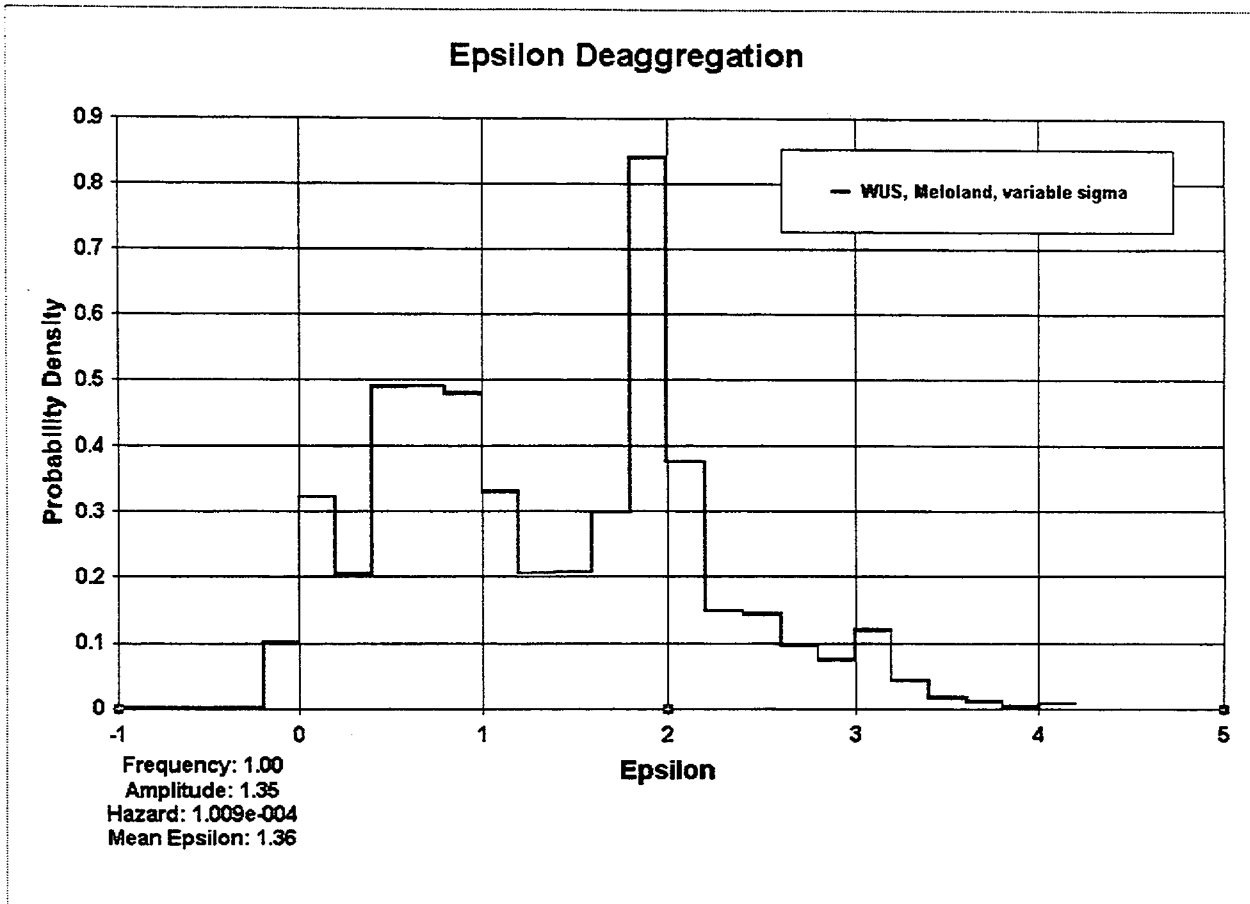

Figure 3-16. Epsilon deaggregation of 10^{-4} hazard at 1 Hz for Mojave site, soil conditions.

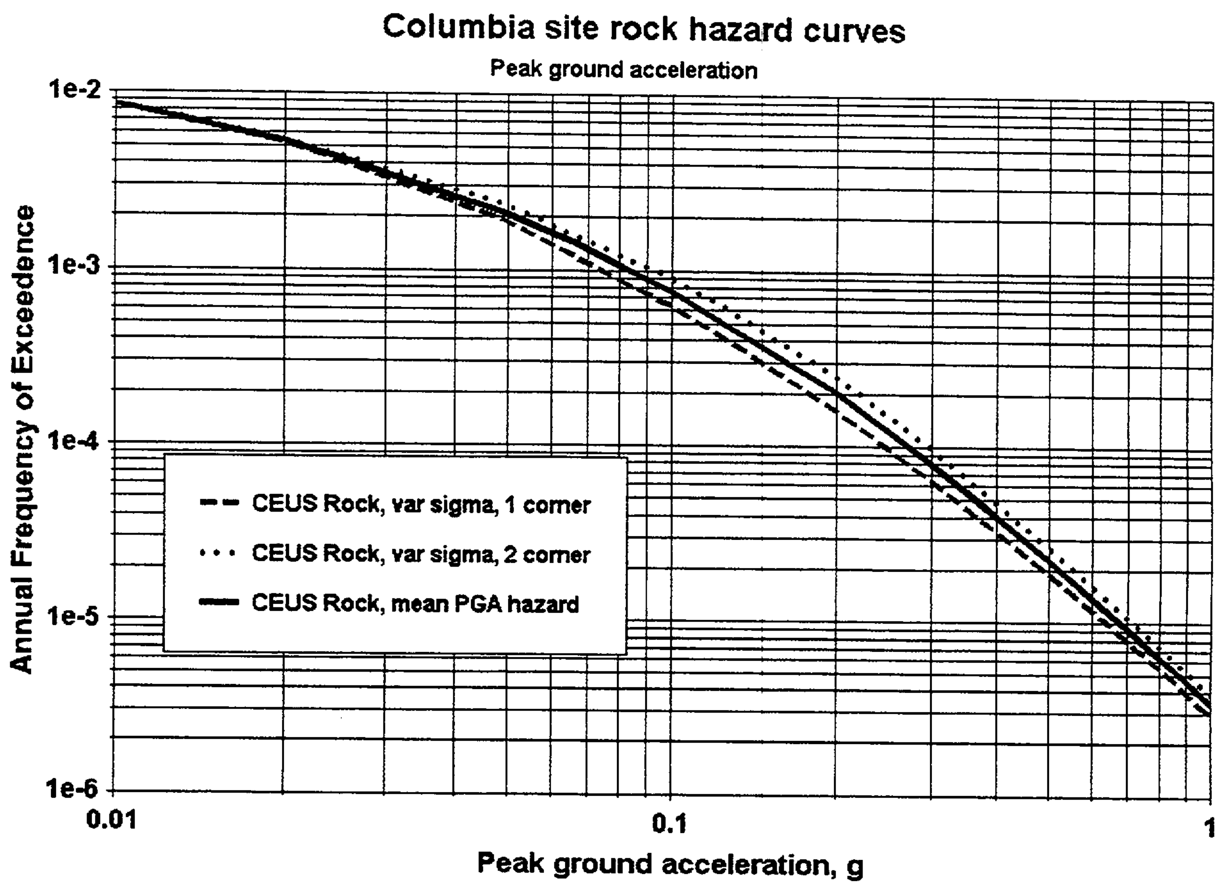

Figure 3-17. PGA seismic hazard, Columbia site, rock.

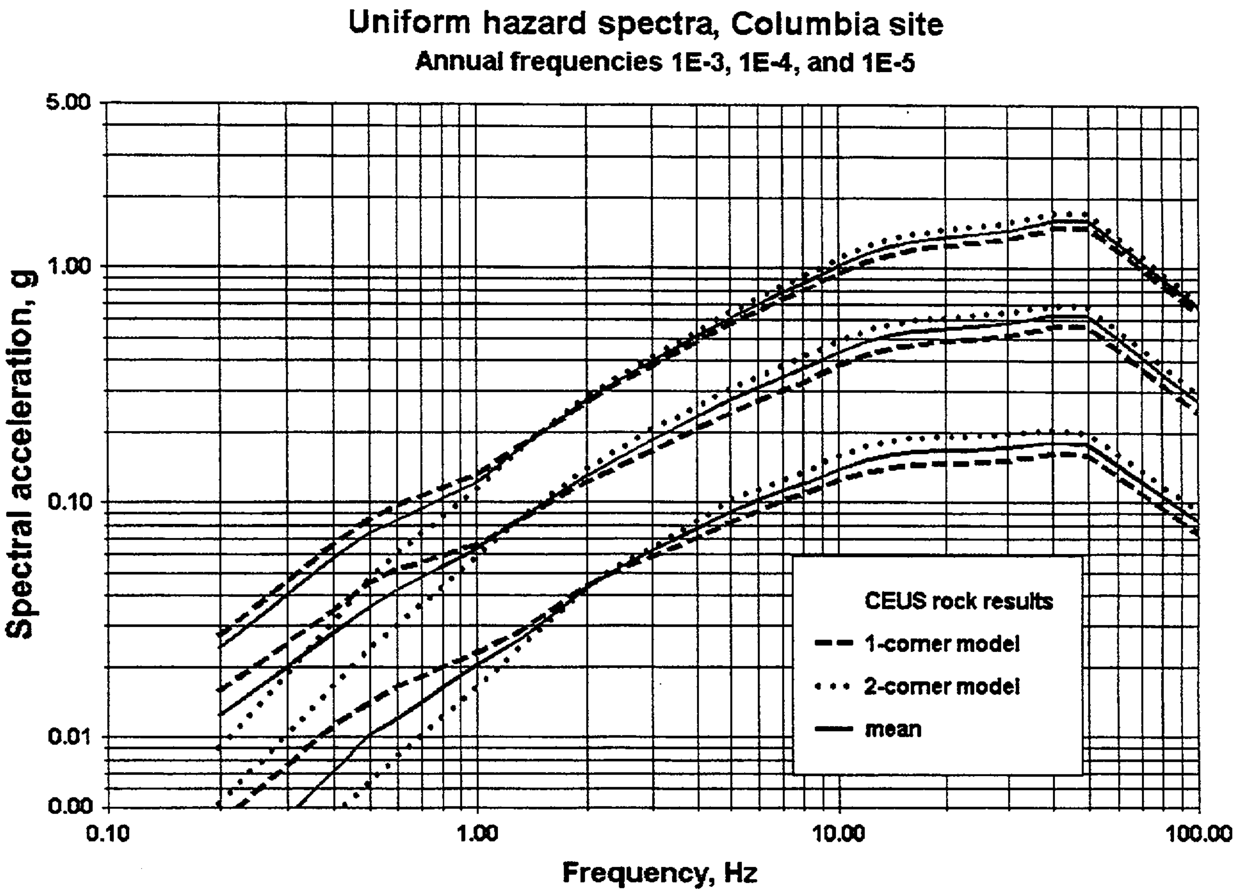

Figure 3-18. UHS for Columbia site, rock: 10^{-5} (top three curves), 10^{-4} (middle three curves), 10^{-3} (bottom three curves).

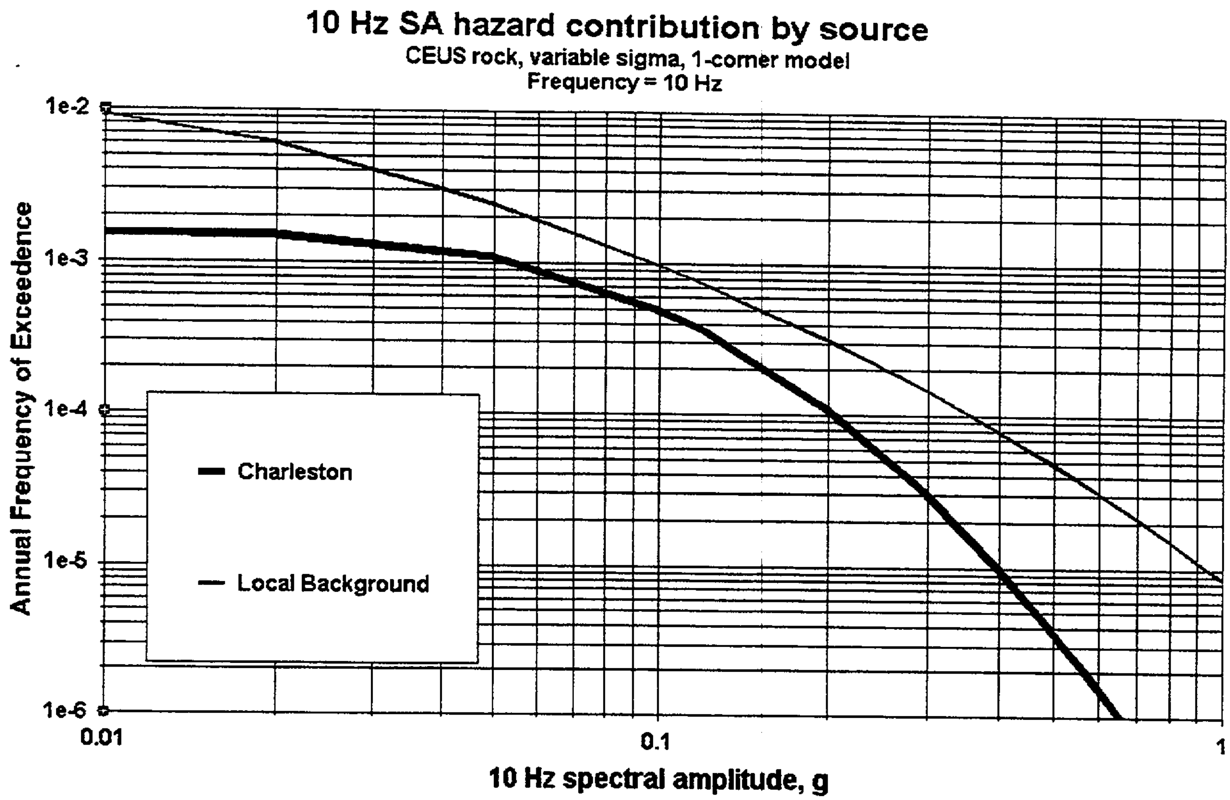

Figure 3-19. Contribution to 10 Hz hazard by source for Columbia site, rock, 1-corner model.

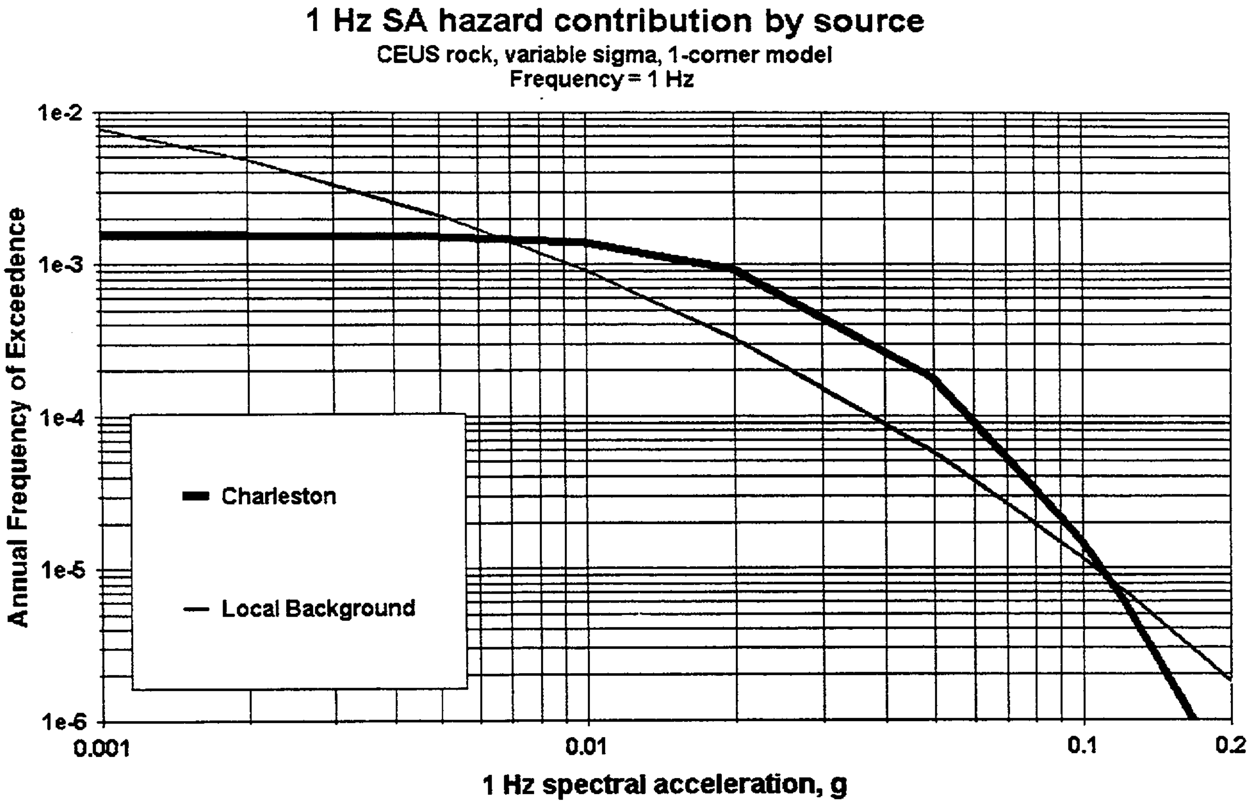

Figure 3-20. Contribution to 1 Hz hazard by source for Columbia site, rock, 1-corner model.

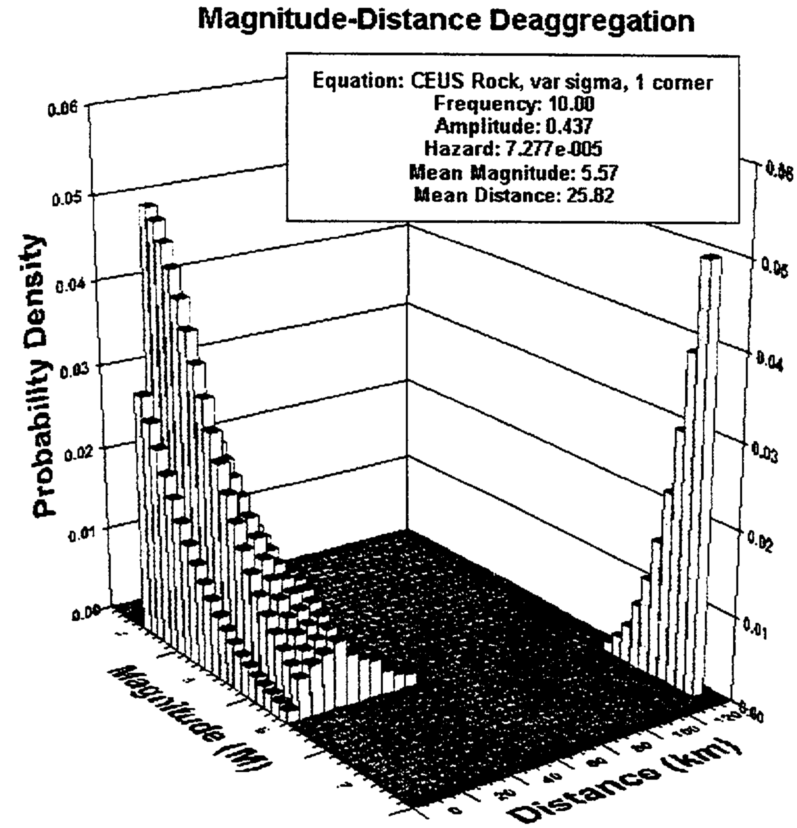

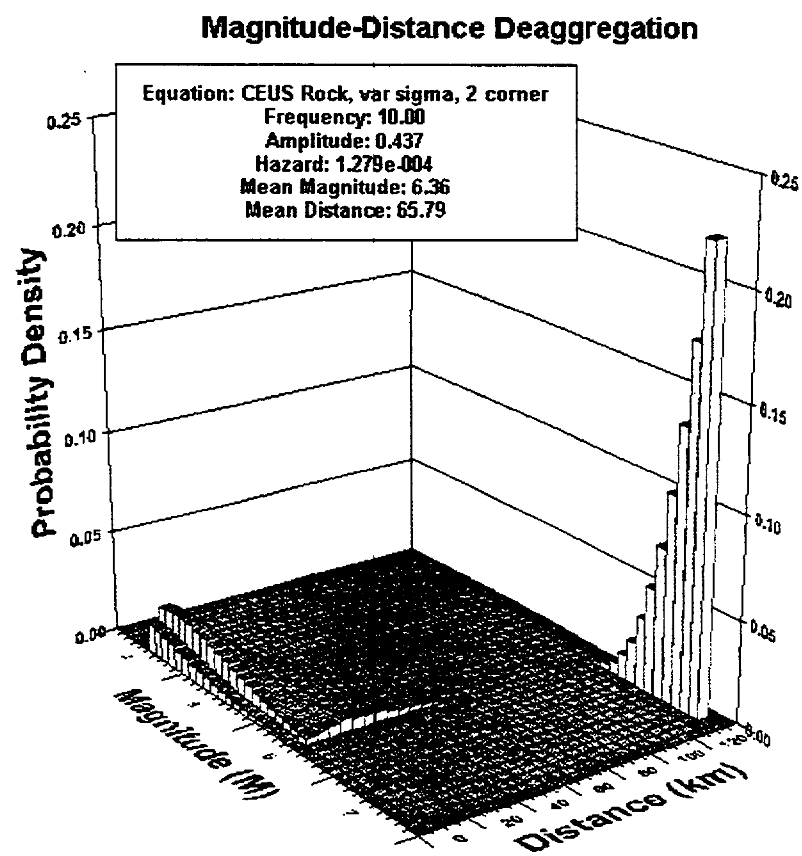

Figure 3-21. 1E-4 10 Hz **M**-R deaggregation for Columbia site, rock, 1-corner model (top) and 2-corner model (bottom).

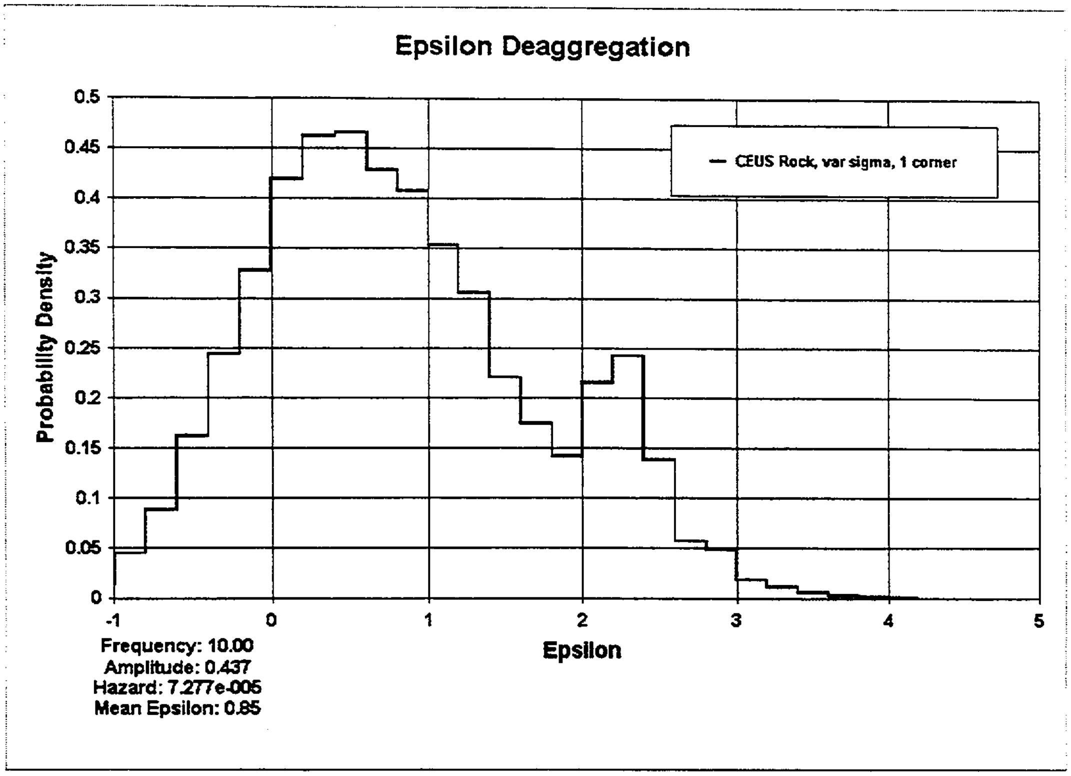

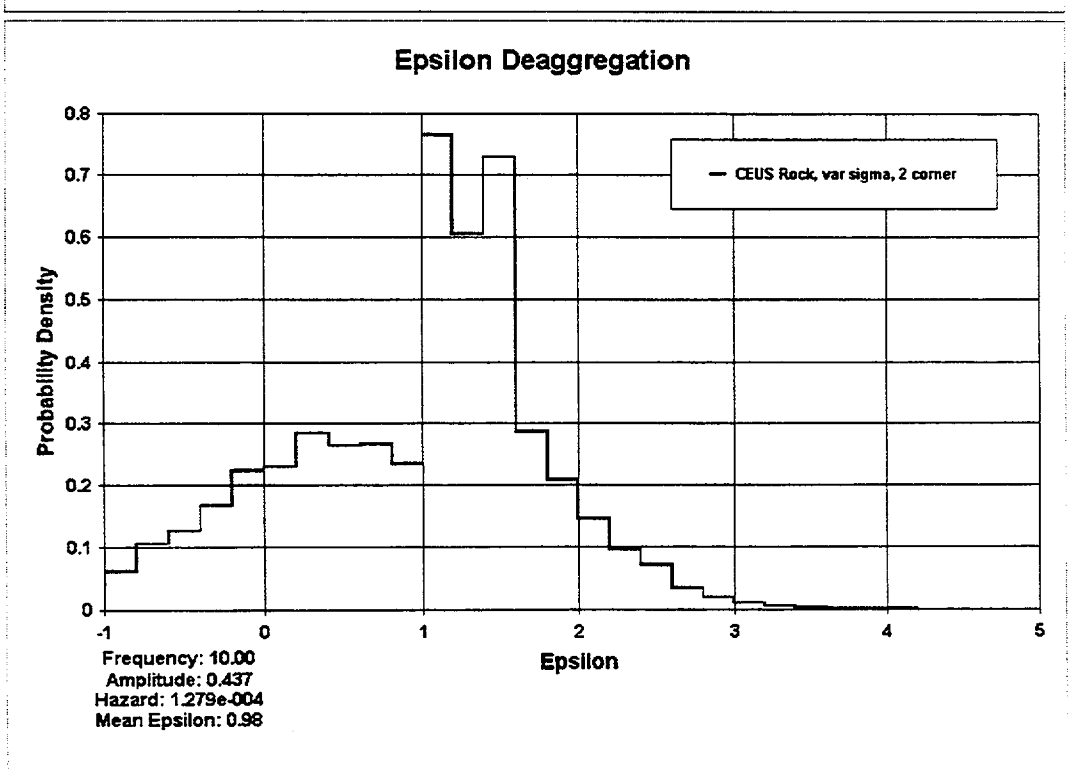

Figure 3-22. 1E-4, 10 Hz, ε deaggregation for Columbia site, rock, 1-corner model (top) and 2-corner model (bottom).

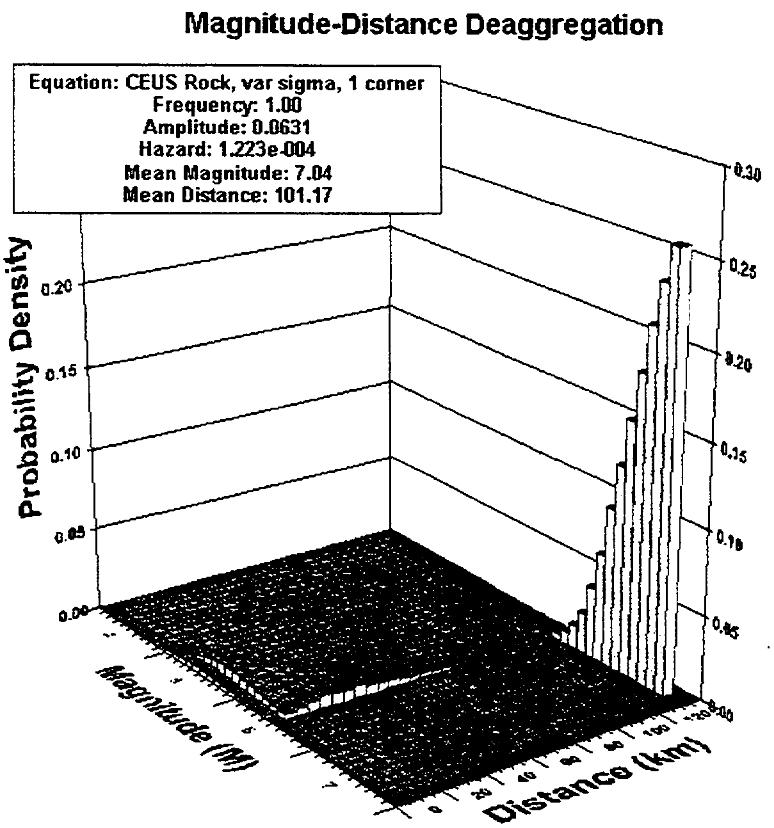

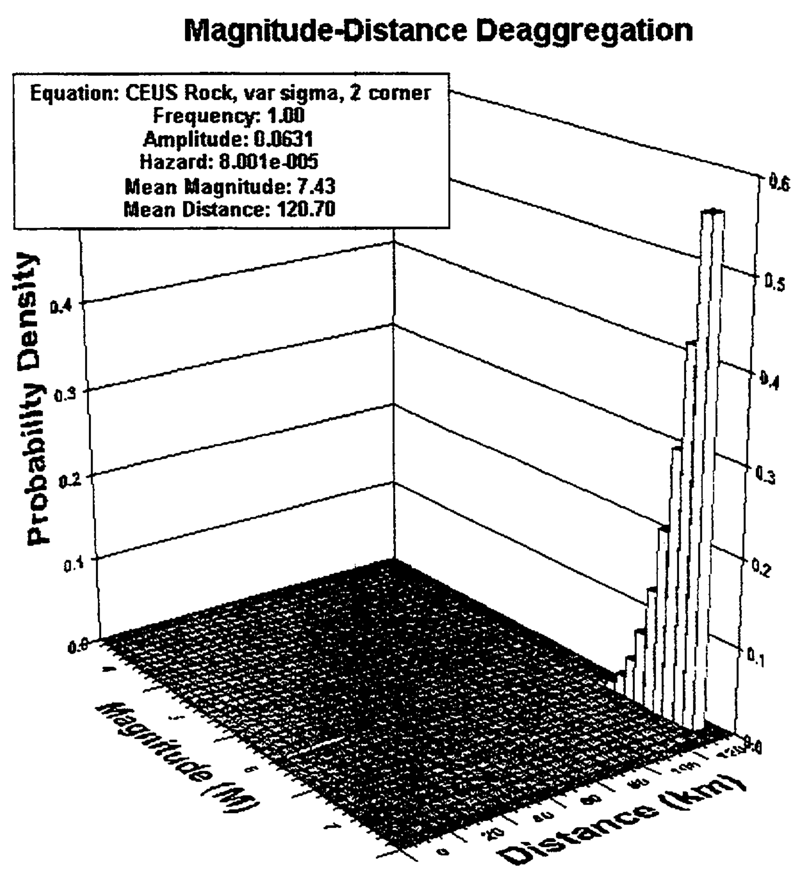

Figure 3-23. 1E-4, 1 Hz, M-R deaggregation for Columbia site, rock, 1-corner model (top) and 2-corner model (bottom).

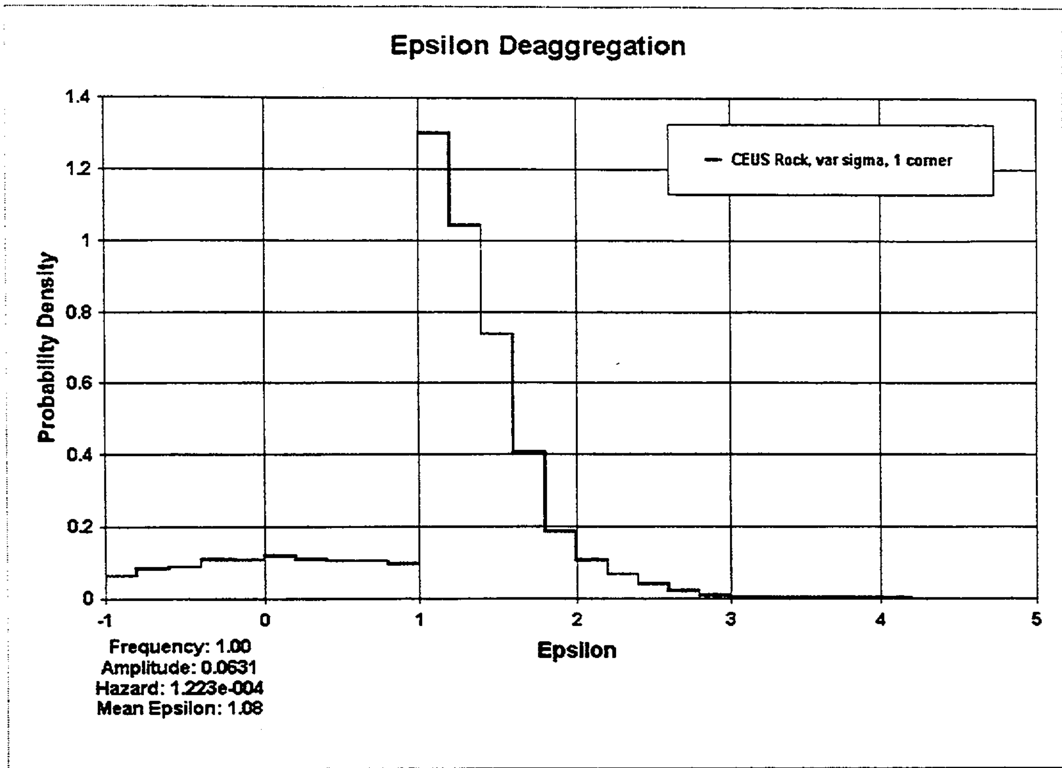

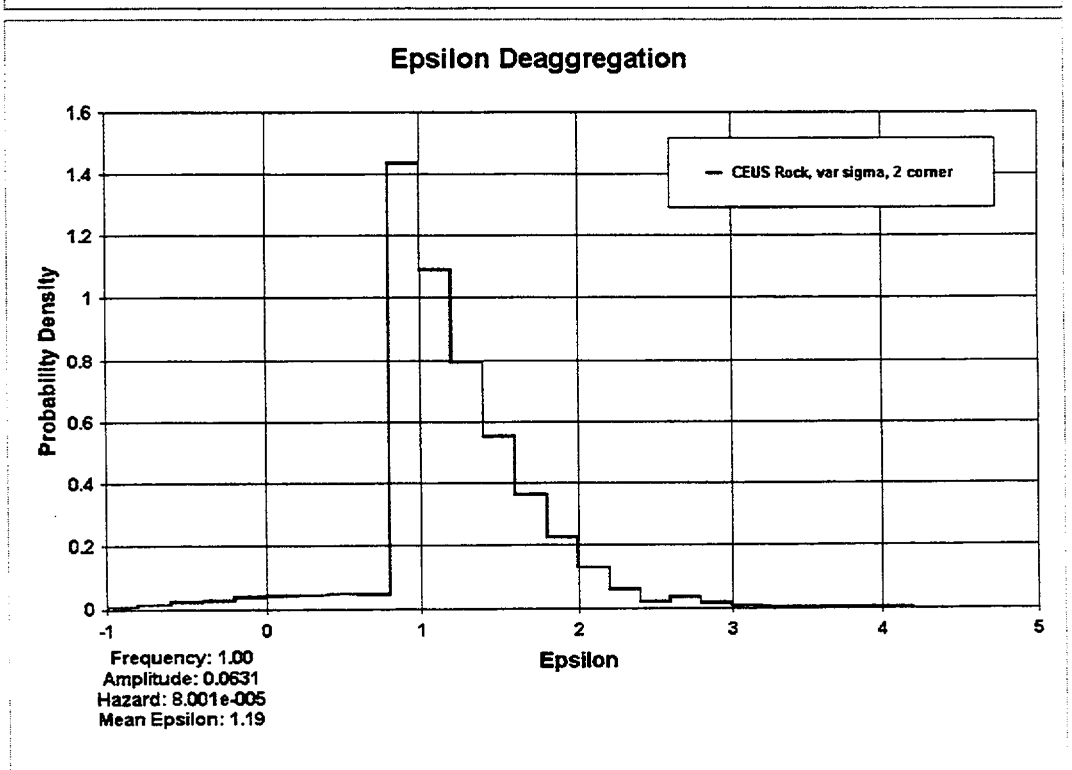

Figure 3-24. 1E-4, 1 Hz, ε deaggregation, Columbia site, rock, 1-corner model (top) and 2-corner model (bottom).

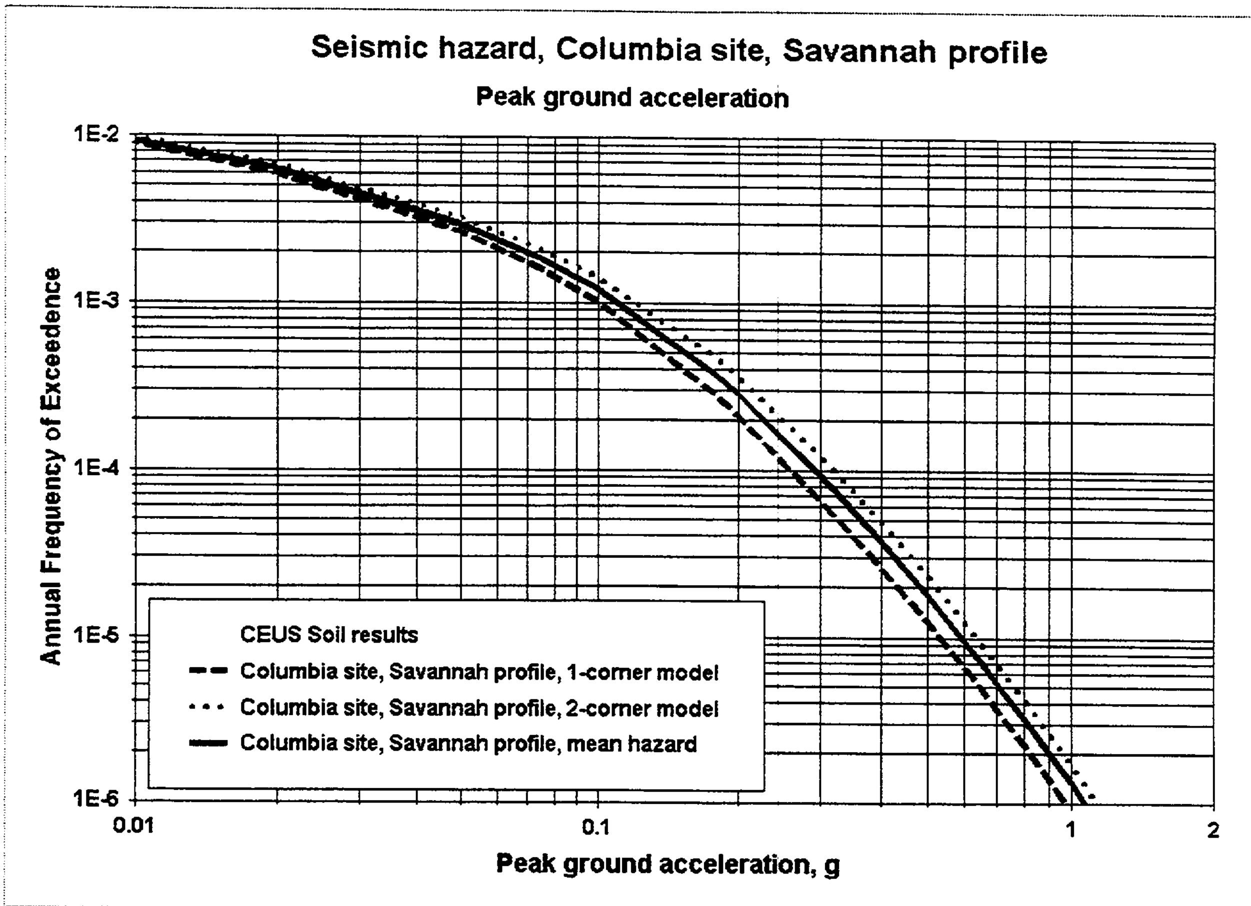

Figure 3-25. PGA seismic hazard, Columbia site, Savannah profile.

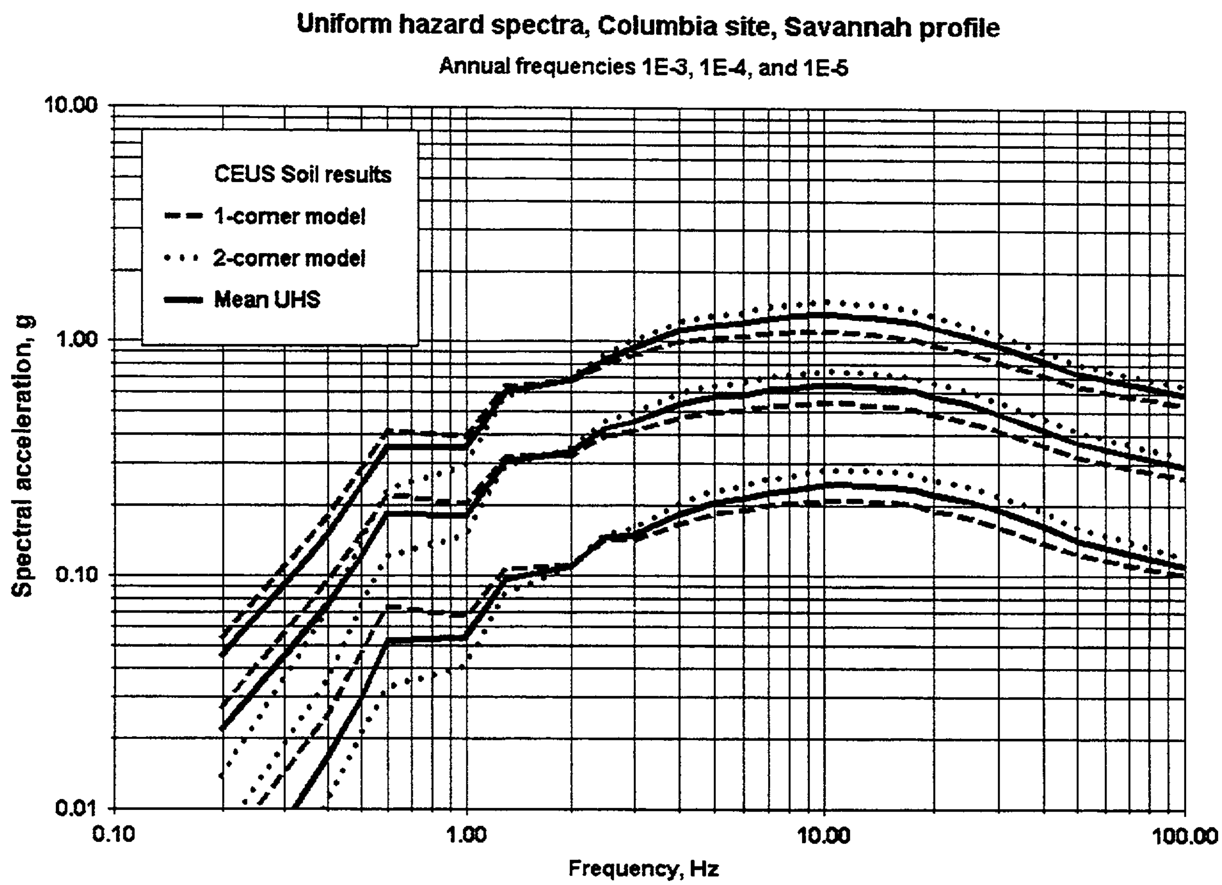

Figure 3-26. UHS for Columbia site, Savannah profile: 10^{-5} (top three curves), 10^{-4} (middle three curves), and 10^{-3} (bottom three curves).

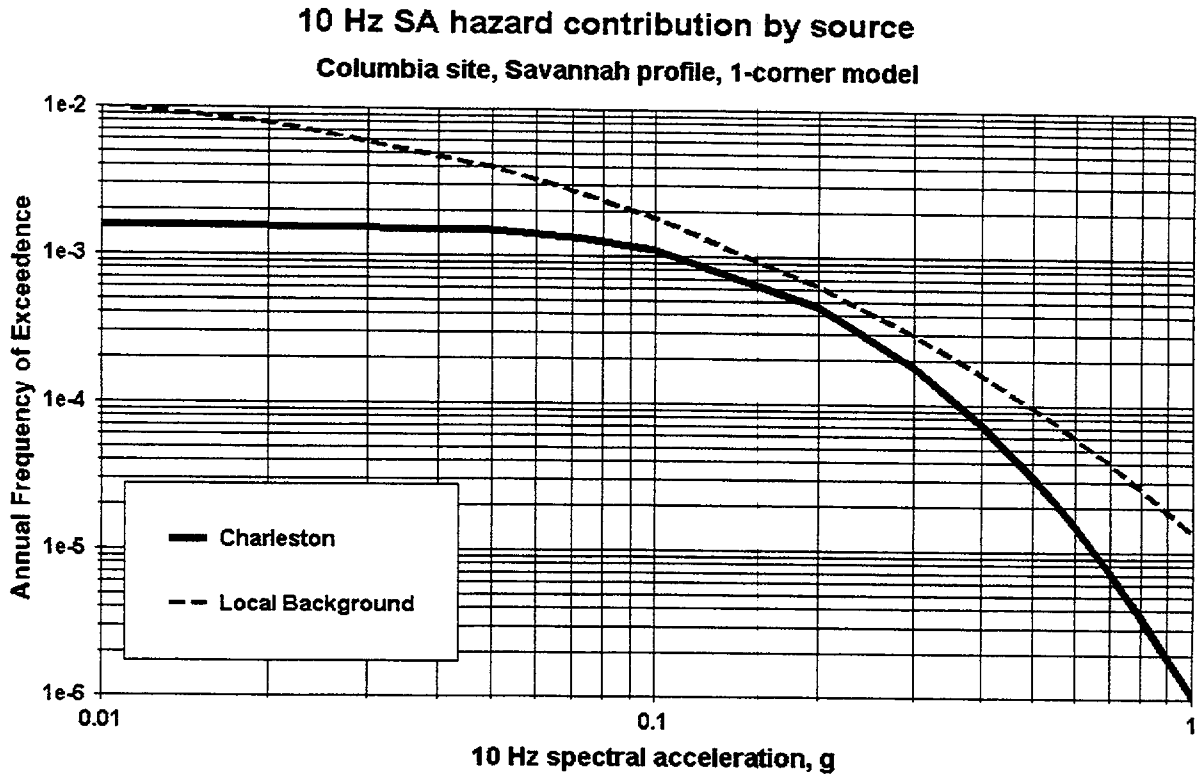

Figure 3-27. Contribution to 10 Hz hazard by source for Columbia site, Savannah profile, rock, 1-corner model.

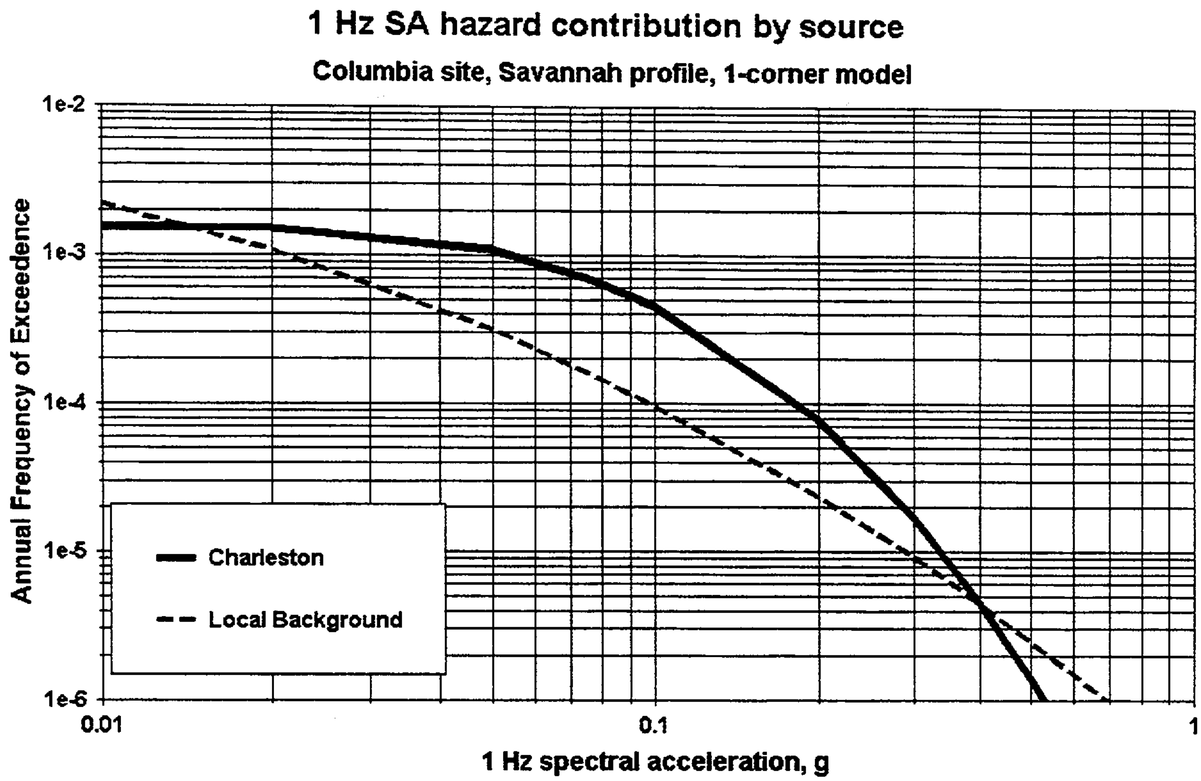

Figure 3-28. Contribution to 1Hz hazard by source for Columbia site, Savannah profile, rock, 1-corner model.

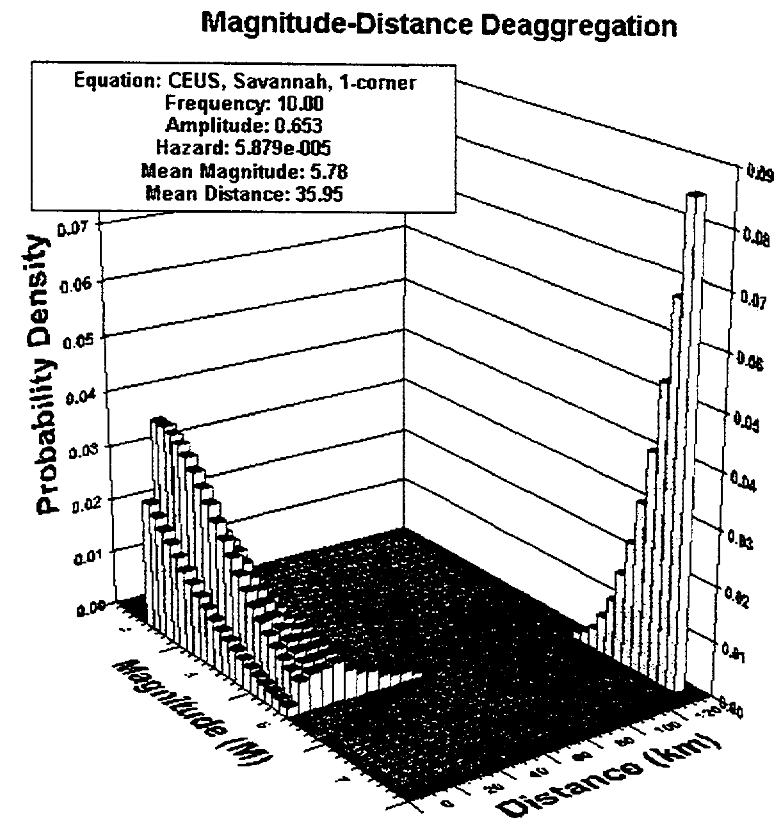

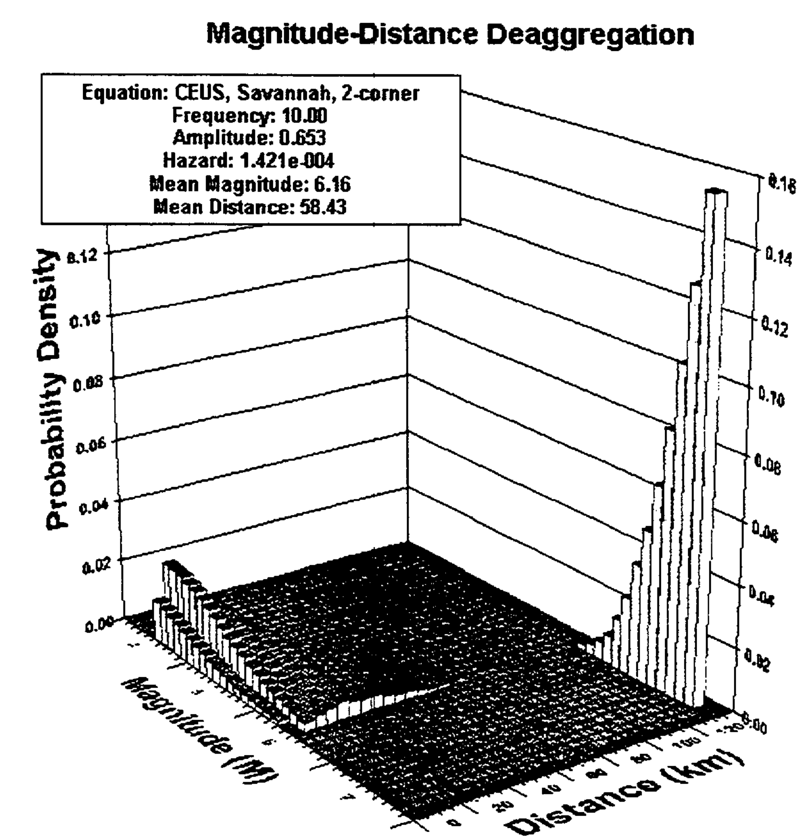

Figure 3-29. 1E-4 10 Hz **M**-R deaggregation for Columbia site, Savannah profile, 1-corner model (top) and 2-corner model (bottom).

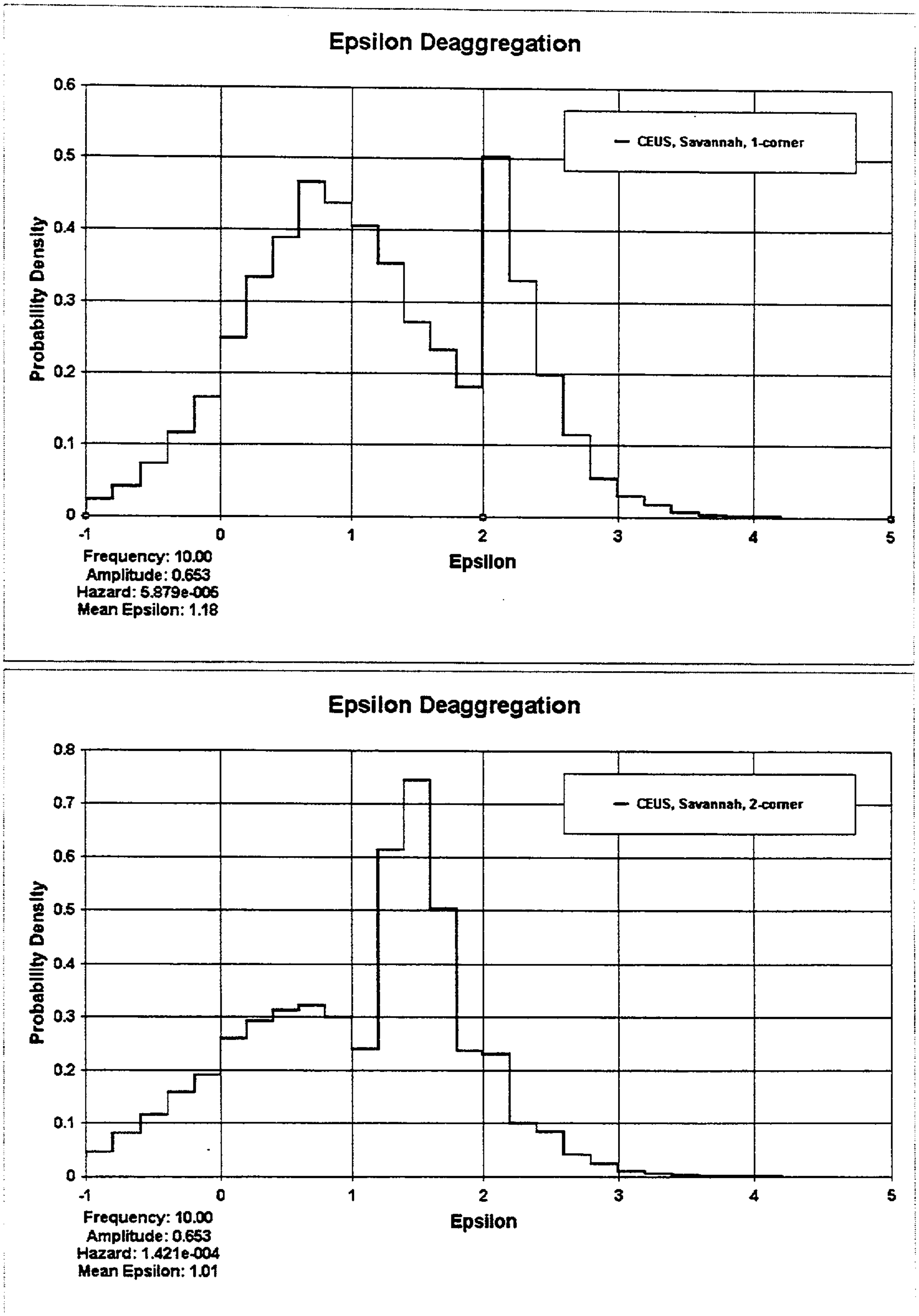

Figure 3-30. 1E-4, 10 Hz ε deaggregation for Columbia site, Savannah profile, 1-corner model (top) and 2-corner model (bottom).

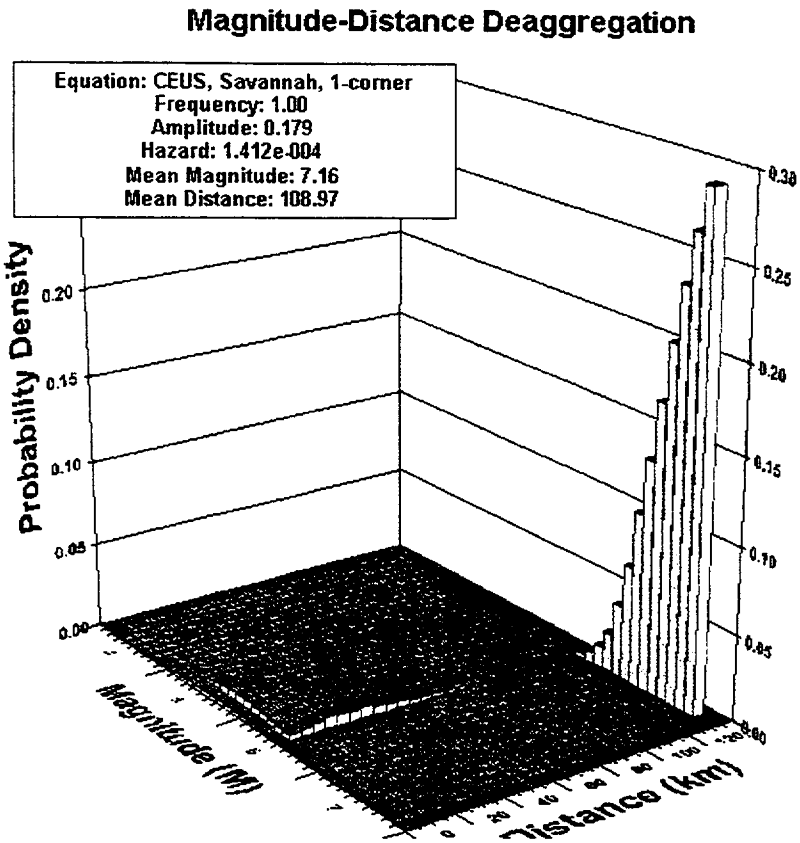

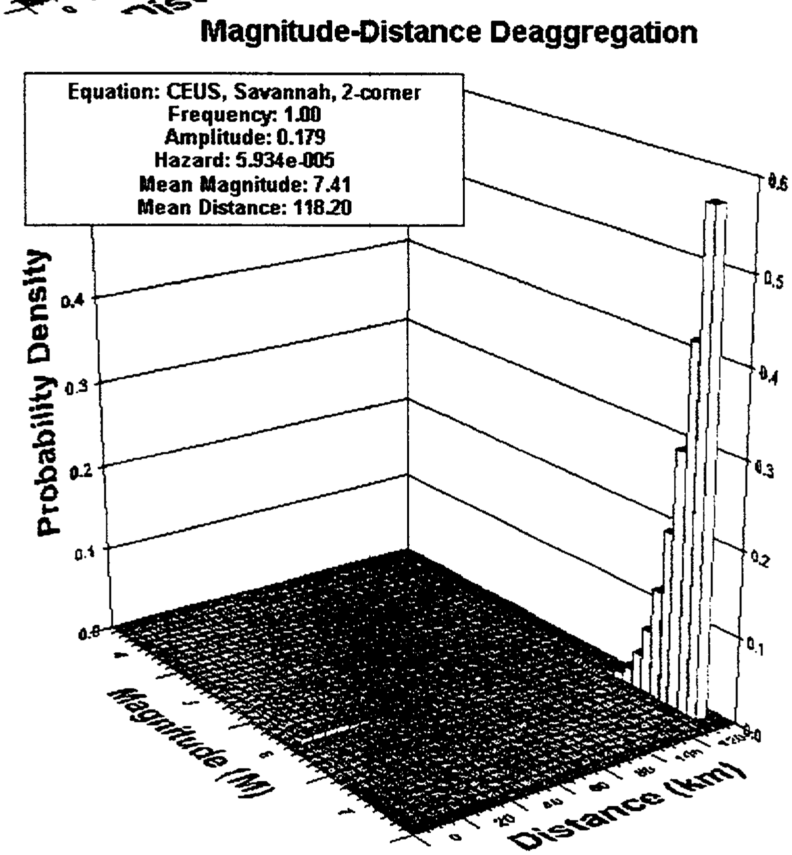

Figure 3-31. 1E-4 **M**-R deaggregation for Columbia site, Savannah profile, 1-corner model (top) and 2-corner model (bottom).

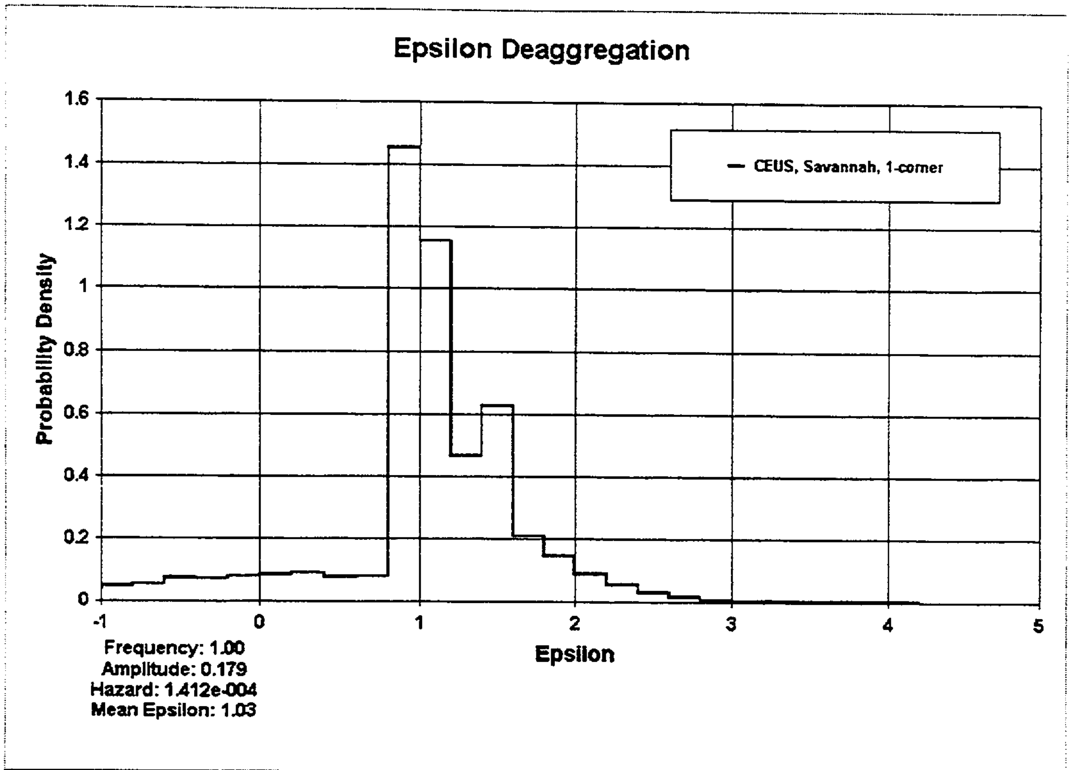

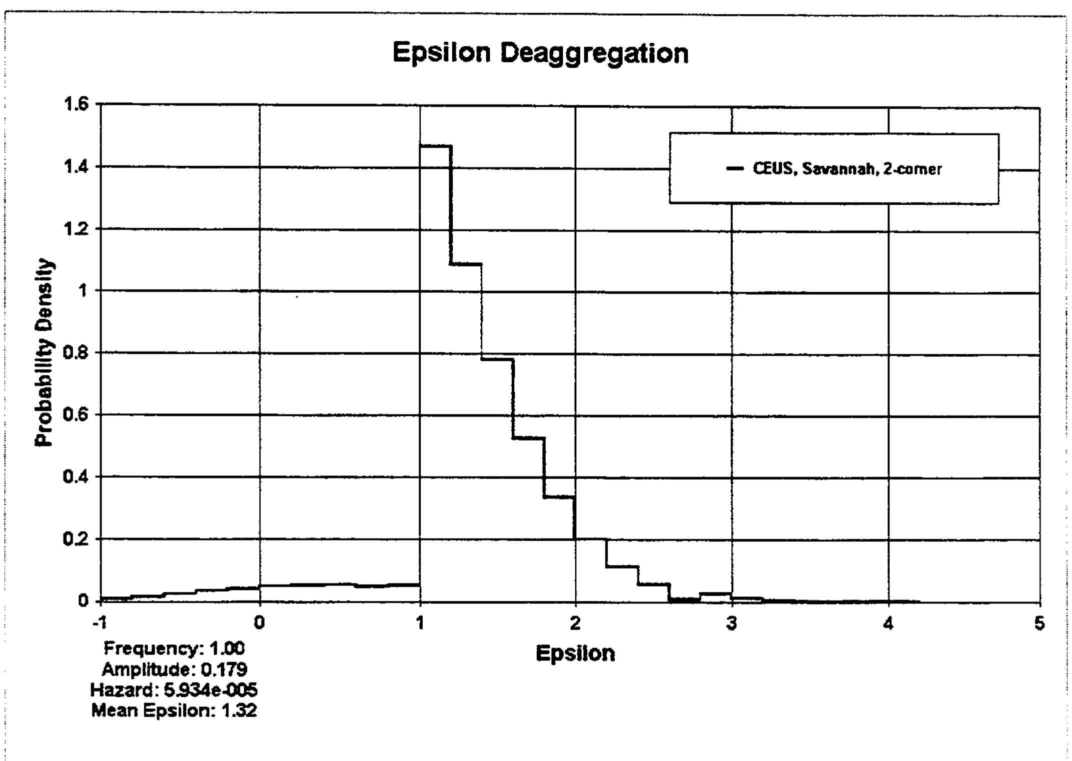

Figure 3-32. 1E-4, 1Hz ε deaggregation for Columbia site, Savannah profile, 1-corner model (top) and 2-corner (bottom).

4.0 UNIFORM RELIABILITY SPECTRA, ROCK

4.1 Mojave site

4.1.1 Derivation of uniform reliability spectrum (URS)

As discussed in McGuire et al., (2001), the uniform reliability spectrum (URS) is a spectrum derived from the UHS that accounts for differences in hazard levels, slopes of hazard curves for different structural periods, and the seismic ruggedness of components (and the uncertainty in that ruggedness) from site to site. By its nature, of course, the URS is a general spectrum that "corrects" the UHS for seismic hazard levels, slopes of hazard curves, and generic component response, but it corrects different sites in appropriate ways to achieve an approximate uniform reliability of seismic components across sites and structural periods.

The URS is derived from the UHS by multiplying the amplitude at each structural frequency by a scale factor SF:

$$URS = UHS \text{ X } SF \tag{4-1}$$

where, for this example,

$$SF = \max\{0.7, 0.35\, A_R^{1.2}\} \tag{4-2}$$

The basis for this scale factor is described in Section 7.3 of McGuire et al., (2001). The procedure to obtain other scale factors is described in Section 9.1.

Table 4-1 documents the 10^{-4} and 10^{-5} UHS from the rock hazard analysis at the Mojave site. These are the same UHS described in Section 3. In addition, Table 4-1 shows the values of A_R and K_H calculated from these UHS. Recall that A_R is the ratio of 10^{-5} to 10^{-4} ground motion at each frequency, and K_H is the negative logarithmic slope between 10^{-4} and 10^{-5}. The 10^{-4} URS value for each frequency is shown in the last column of Table 4-1, calculated using equation (4-1).

The Mojave site lies in an area of high seismic hazard, and as a result the hazard curves are dropping steeply at 10^{-4} annual frequency. As described in Section 7.3 of McGuire et al., (2001), if the A_R value at any frequency is less than 2.4, the URS will be less than the UHS. This is the case for the Mojave site. Because the seismic hazard curves are falling off steeply above the 10^{-4} UHS amplitudes, there is relatively low probability of ground motions say twice the 10^{-4} UHS, so the design spectrum can be reduced from the UHS somewhat. Note that from equation (4-2), the UHS is never decreased by more than 30%.

We assume for this example that the URS will be based on the UHS at 10^{-4} annual frequency of exceedence. Figure 4-1 compares the UHS and URS spectra for the Mojave site. The URS is typically 18% - 20% below the UHS. This URS is the spectrum to which seismic structures, equipment, and components would be designed.

4.1.2 Derivation of scaled spectra

Deaggregation of the rock seismic hazard was described in Section 3.1. At the 10^{-4} hazard level, the mean magnitude and associated distances are:

10 Hz: **M** = 6.1, R = 14 km,
1 Hz: **M** = 6.6, R = 18 km.

Using these magnitudes and distances, spectral amplitudes were calculated from the rock attenuation equations described in Section 2.3, and were scaled to the UHS at 10 and 1 Hz, as appropriate. That is, the **M**=6.1 spectrum was scaled to the 10 Hz UHS amplitude, and the **M**=6.6 spectrum was scaled to the 1 Hz UHS amplitude.

The above magnitudes and distances were also used to develop scaled spectra using equation (4-8) of McGuire et al., (2001). These are the recommended spectral shapes developed from the strong motion database of this project. The same magnitudes and distances were used, and the spectra also were scaled to the 10 Hz and 1 Hz UHS.

Figure 4-2 shows the UHS and these four scaled design spectra. Because the two mean magnitudes differ by only 0.5 units, the spectral shapes are similar. Also, the spectra derived from the attenuation equations are similar to those derived from the recommended spectral shapes. The purpose of this comparison is a consistency check, to ensure that the shape of the UHS is consistent with spectra from individual events representing both the high- and low-frequency motion. The values of the scaled design spectra are shown in Table 4-2.

Figure 4-3 shows the 10^{-4} URS and spectra scaled from the attenuation equations to the 10 Hz and 1 Hz URS amplitudes. These individual spectra represent an alternative design criterion to the broad-banded URS. For the spectra in Figure 4-3, there is not much advantage in designing to the individual spectra, so the designer would likely opt to use the broad-banded URS. As discussed above, this results from the 10 Hz and 1 Hz dominant magnitudes differing by only 0.5 magnitude units. The values for the spectra scaled to the URS are given in Table 4-3.

4.1.3 Vertical motions

WUS rock site vertical motions corresponding to the horizontal rock URS were estimated by applying the recommended WUS empirical V/H ratios (McGuire et al., 2001) to the URS. For the WUS, these ratios were developed from empirical WUS rock attenuation relations. For the CEUS they were based on model predictions using inclined P-SV waves (Silva, 1997; McGuire et al., 2001). Both WUS and CEUS V/H ratios were based on expected horizontal component peak acceleration values, equal to the UHS value at 100 Hz. The dependency of V/H ratios on expected horizontal component peak acceleration captures the general trends in V/H ratios with magnitude and distance in a manner that is unambiguous in the context of probabilistic seismic hazard analyses. The ratios are shown in Figure 4-4a for WUS rock site conditions and Figure 4-4b for CEUS rock site conditions. These V/H ratios were developed and presented in Section 4 of McGuire et al. (2001). For the WUS, the ratios are applied to the horizontal rock URS because the ratios are based on horizontal and vertical motions recorded at soft rock sites (McGuire et al., 2001). Figure 4-5 shows the horizontal and vertical rock URS for the Mojave site.

4.2 Columbia Site

4.2.1 Derivation of URS

The URS for the Columbia site was derived in a parallel manner to the URS for the Mojave site. For the Columbia site, the average hazard from the two ground motion models was used to establish the ratio A_R of amplitudes at annual frequencies of 10^{-4} and 10^{-5}. These values of A_R for each structural frequency were then used with equations (4-1) and (4-2) to calculate the URS. Table 4-4 documents the values of A_R and the URS at each frequency.

Figure 4-6 shows the UHS and URS for the Columbia site for rock conditions. For frequencies below 15 Hz, the hazard curves are steep ($K_H > 2.63$), so the UHS is decreased to obtain the URS. At higher frequencies the hazard curves are shallow ($K_H < 2.63$), so the UHS is increased to obtain the URS.

This characteristic, that the high frequency hazard curves are shallower than the low frequency hazard curves, results from the specific sources and their characteristics that we have assumed to affect the Columbia site. Often all frequencies will have a shallow slope in the CEUS, and the calculated URS will exceed the UHS at all frequencies. For an example, see Section 7.3.2 and Figure 7.12 of McGuire et al., 2001.

4.2.2 Derivation of scaled spectra

Deaggregation of rock hazard for the Columbia site was described in Section 3.2. At the 10^{-4} hazard level the mean magnitudes and associated distances are:

10 Hz:	**M** = 6.0, R = 46 km
1 Hz:	**M** = 7.2, R = 110 km

These magnitudes and distances, and the CEUS rock attenuation equations, were used to estimate one spectrum scaled to the 10 Hz UHS, and a second spectrum scaled to the 1 Hz UHS. These spectra were the average of spectra calculated from the two ground motion models. In addition, two spectra were derived from the recommended spectral shapes from this project, using equation (4-9) of McGuire et al., (2001). The procedure was the same as described above for the Mojave site. Figure 4-7 shows the UHS and the two scaled spectra. For the Columbia site the two magnitudes differ by 1.2 units, so the spectral shapes differ markedly.

In general, however, the UHS at high frequencies is consistent with the 10 Hz scaled spectra, and the UHS at low frequencies is consistent with the 1 Hz scaled spectra. This illustrates the purpose of the comparison, to determine the consistency of the UHS shape with several scaled spectra. The spectral values are documented in Table 4-5.

Figure 4-8 shows a comparison of the 10^{-4} URS with spectra calculated from the CEUS rock attenuation equations (weighting the 1- and 2-corner models equally, as was done in the PSHA). Here the 1.2 magnitude unit difference in dominant magnitudes between 10 and 1 Hz leads to a significant difference across the entire frequency band. If the designer were concerned about a structure with both high-frequency and long-period response, he might elect to use one spectrum for low frequencies and the other at high frequencies. Values of the spectra scaled to the URS are documented in Table 4-6.

Figure 4-8 shows that there is a mismatch between the URS at high frequencies ($f > 20$ Hz) and the spectrum scaled to 10 Hz. This results from the scale factor at high frequencies being > 1.0 (see Table 4-4). To avoid scaling the 10 Hz spectrum up to achieve a match at these high frequencies, the designer could add a third spectrum scaled to 30 or 50 Hz that would replicate the URS for design purposes and not impact frequencies below 10 Hz.

4.2.3 Vertical motions

For the CEUS, V/H ratios were developed based on model predictions using inclined P-SV waves (Silva, 1997; McGuire et al., 2001). The resulting ratios are summarized in Figure 4-4b, and are a function of horizontal component peak acceleration (equal to the UHS at 100 Hz). Figure 4-9 illustrates the resulting CEUS rock vertical URS, compared to the corresponding horizontal URS. This vertical URS was produced with the 0.2 to 0.5g hard rock V/H ratio (Figure 4-4b). The V/H ratios were developed and presented in Section 4 of McGuire et al., (2001).

REFERENCE

McGuire, R.K., W.J. Silva, and C. Costantino (2001). "Technical Basis for Revision of Regulatory Guidance on Design Ground Motions: Hazard and Risk-consistent Ground Motion Spectra Guidelines," US Nuclear Reg. Comm., Rept NUREG/CR-6728, October.

Table 4-1
Slope parameters for rock hazard curves
Mojave site

Structural Frequency, Hz	10^{-4} UHS, g	10^{-5} UHS, g	A_R	K_H	SF	10^{-4} URS, g
100	8.98E-1	1.82	2.02	3.27	8.14E-1	7.31E-1
50	9.52E-1	1.93	2.03	3.26	8.17E-1	7.78E-1
40	9.97E-1	2.00	2.01	3.31	8.07E-1	8.05E-1
31	1.12	2.26	2.02	3.28	8.12E-1	9.10E-1
25	1.24	2.48	2.00	3.32	8.04E-1	9.98E-1
20	1.40	2.78	1.99	3.35	7.99E-1	1.12
18	1.50	3.00	2.00	3.33	8.02E-1	1.21
16	1.63	3.24	1.99	3.34	8.01E-1	1.30
14	1.72	3.40	1.98	3.37	7.95E-1	1.36
12	1.83	3.66	2.00	3.33	8.03E-1	1.47
10	1.94	3.88	2.00	3.32	8.04E-1	1.56
8	2.00	4.00	2.00	3.32	8.04E-1	1.61
7	2.05	4.16	2.02	3.27	8.15E-1	1.67
6	2.04	4.09	2.00	3.31	8.06E-1	1.65
5	2.07	4.16	2.02	3.28	8.12E-1	1.68
4	1.97	3.95	2.01	3.31	8.07E-1	1.59
3	1.76	3.52	2.00	3.32	8.05E-1	1.42
2.5	1.56	3.17	2.04	3.24	8.21E-1	1.28
2	1.23	2.50	2.04	3.24	8.21E-1	1.01
1.3	8.64E-1	1.81	2.09	3.12	8.47E-1	7.32E-1
1	6.67E-1	1.38	2.07	3.17	8.36E-1	5.58E-1
.6	4.53E-1	8.56E-1	1.89	3.62	7.51E-1	3.40E-1
.5	4.17E-1	7.67E-1	1.84	3.78	7.27E-1	3.03E-1
.4	3.30E-1	5.88E-1	1.78	3.98	7.00E-1	2.31E-1
.2	1.50E-1	2.41E-1	1.61	4.84	7.00E-1	1.05E-1

Table 4-2
Spectra scaled to 10^{-4} UHS
Mojave site, rock conditions

Structural frequency, Hz	10 Hz scaled spectrum from attenuation eq.	1 Hz scaled spectrum from attenuation eq.	10 Hz scaled spectrum from spectral shapes	1 Hz scaled spectrum from spectral shapes
100	8.578E-1	8.127E-1	1.002	9.513E-1
50	9.022E-1	8.470E-1	1.035	9.722E-1
40	9.592E-1	9.019E-1	1.070	9.973E-1
31	1.053	9.784E-1	1.138	1.050
25	1.176	1.087	1.226	1.121
20	1.345	1.241	1.355	1.230
18	1.441	1.324	1.430	1.294
16	1.556	1.427	1.522	1.376
14	1.688	1.560	1.638	1.481
12	1.820	1.684	1.778	1.613
10	1.940	1.805	1.940	1.774
8	2.016	1.898	2.101	1.955
7	2.029	1.913	2.161	2.038
6	2.030	1.932	2.186	2.100
5	1.993	1.907	2.146	2.113
4	1.851	1.793	2.000	2.037
3	1.573	1.564	1.696	1.811
2.5	1.370	1.394	1.471	1.620
2	1.074	1.127	1.193	1.366
1.3	7.124E-1	8.068E-1	7.285E-1	9.003E-1
1	5.522E-1	6.670E-1	5.148E-1	6.670E-1
.6	3.258E-1	4.610E-1	2.398E-1	3.418E-1
.5	2.701E-1	4.075E-1	1.776E-1	2.623E-1
.4	1.911E-1	3.200E-1	1.205E-1	1.861E-1
.2	5.253E-2	1.223E-1	3.057E-2	5.489E-2

Table 4-3
Spectra scaled to 10^{-4} URS
Mojave site, rock conditions

Structural Frequency, Hz	**URS, g**	**10 Hz spectrum scaled from atten. eq.**	**1 Hz spectrum scaled from atten. eq.**
100	7.31E-1	6.898E-1	7.041E-1
50	7.78E-1	7.254E-1	7.339E-1
40	8.05E-1	7.713E-1	7.827E-1
31	9.10E-1	8.467E-1	8.501E-1
25	9.98E-1	9.460E-1	9.466E-1
20	1.12	1.082	1.082
18	1.21	1.159	1.155
16	1.30	1.251	1.243
14	1.36	1.358	1.359
12	1.47	1.464	1.467
10	1.56	1.560	1.571
8	1.61	1.621	1.650
7	1.67	1.632	1.661
6	1.65	1.633	1.676
5	1.68	1.602	1.652
4	1.59	1.488	1.550
3	1.42	1.265	1.346
2.5	1.28	1.102	1.196
2	1.01	8.640E-1	9.610E-1
1.3	7.32E-1	5.729E-1	6.809E-1
1	5.58E-1	4.440E-1	5.580E-1
.6	3.40E-1	2.620E-1	3.787E-1
.5	3.03E-1	2.172E-1	3.314E-1
.4	2.31E-1	1.537E-1	2.563E-1
.2	1.05E-1	4.224E-2	9.260E-2

Table 4-4
Slope parameters for rock hazard curves
Columbia site

Structural Frequency, Hz	10^{-4} UHS, g	10^{-5} UHS, g	A_R	K_H	SF	10^{-4} URS, g
100	2.74E-1	6.82E-1	2.49	2.52	1.05	2.87E-1
50	6.24E-1	1.61	2.58	2.43	1.09	6.81E-1
40	6.28E-1	1.60	2.55	2.46	1.07	6.75E-1
31	5.85E-1	1.47	2.51	2.51	1.05	6.17E-1
25	5.68E-1	1.41	2.48	2.54	1.04	5.90E-1
20	5.52E-1	1.35	2.45	2.56	1.03	5.67E-1
18	5.46E-1	1.33	2.44	2.59	1.02	5.56E-1
16	5.36E-1	1.30	2.42	2.61	1.01	5.41E-1
14	5.17E-1	1.24	2.39	2.64	9.97E-1	5.16E-1
12	4.85E-1	1.15	2.36	2.68	9.82E-1	4.76E-1
10	4.38E-1	1.02	2.33	2.72	9.66E-1	4.23E-1
8	3.72E-1	8.60E-1	2.31	2.75	9.57E-1	3.56E-1
7	3.42E-1	7.83E-1	2.29	2.78	9.46E-1	3.23E-1
6	3.09E-1	6.96E-1	2.26	2.83	9.30E-1	2.87E-1
5	2.73E-1	6.12E-1	2.24	2.85	9.21E-1	2.52E-1
4	2.31E-1	5.08E-1	2.20	2.92	9.01E-1	2.08E-1
3	1.84E-1	3.96E-1	2.15	3.00	8.79E-1	1.62E-1
2.5	1.57E-1	3.38E-1	2.16	2.99	8.81E-1	1.38E-1
2	1.30E-1	2.73E-1	2.10	3.11	8.52E-1	1.11E-1
1.3	8.39E-2	1.68E-1	2.00	3.33	8.03E-1	6.74E-2
1	6.32E-2	1.21E-1	1.92	3.53	7.66E-1	4.84E-2
.6	4.23E-2	8.41E-2	1.99	3.35	7.98E-1	3.38E-2
.5	3.57E-2	7.32E-2	2.05	3.20	8.29E-1	2.96E-2
.4	2.77E-2	5.77E-2	2.08	3.14	8.44E-1	2.34E-2
.2	1.24E-2	2.39E-2	1.93	3.51	7.69E-1	9.53E-3

Table 4-5
Spectra scaled to 10^{-4} UHS
Columbia site, rock conditions

Structural frequency, Hz	10 Hz scaled spectrum from atten. eq.	1 Hz scaled spectrum from atten. eq.	10 Hz. scaled spectrum from spectral shapes	1 Hz scaled spectrum from spectral shapes
100	2.548E-1	1.500E-1	2.790E-1	1.660E-1
50	4.987E-1	2.672E-1	5.647E-1	3.379E-1
40	5.392E-1	2.831E-1	6.136E-1	3.687E-1
31	5.119E-1	2.911E-1	6.274E-1	3.793E-1
25	5.120E-1	2.977E-1	6.177E-1	3.770E-1
20	5.188E-1	3.112E-1	5.919E-1	3.674E-1
18	5.196E-1	3.182E-1	5.747E-1	3.609E-1
16	5.164E-1	3.214E-1	5.520E-1	3.520E-1
14	5.044E-1	3.192E-1	5.226E-1	3.404E-1
12	4.786E-1	3.100E-1	4.851E-1	3.250E-1
10	4.380E-1	2.911E-1	4.380E-1	3.050E-1
8	3.840E-1	2.646E-1	3.804E-1	2.789E-1
7	3.532E-1	2.488E-1	3.473E-1	2.630E-1
6	3.172E-1	2.318E-1	3.114E-1	2.447E-1
5	2.827E-1	2.125E-1	2.725E-1	2.237E-1
4	2.351E-1	1.878E-1	2.299E-1	1.989E-1
3	1.818E-1	1.577E-1	1.814E-1	1.687E-1
2.5	1.601E-1	1.413E-1	1.534E-1	1.504E-1
2	1.260E-1	1.232E-1	1.214E-1	1.283E-1
1.3	7.374E-2	8.172E-2	7.064E-2	8.614E-2
1	5.178E-2	6.320E-2	4.866E-2	6.320E-2
.6	2.730E-2	4.259E-2	2.240E-2	3.177E-2
.5	2.060E-2	3.642E-2	1.673E-2	2.464E-2
.4	1.358E-2	2.842E-2	1.157E-2	1.801E-2
.2	2.944E-3	1.169E-2	3.251E-3	6.545E-3

Table 4-6
Spectra scaled to 10^{-4} URS
Columbia site, rock conditions

Structural frequency, Hz	10 Hz scaled spectrum from attenuation equation	1 Hz scaled spectrum from attenuation equation
100	2.346E-1	1.187E-1
50	4.554E-1	2.140E-1
40	4.951E-1	2.263E-1
31	4.762E-1	2.325E-1
25	4.753E-1	2.370E-1
20	4.819E-1	2.466E-1
18	4.849E-1	2.515E-1
16	4.847E-1	2.538E-1
14	4.782E-1	2.522E-1
12	4.570E-1	2.442E-1
10	4.230E-1	2.290E-1
8	3.680E-1	2.068E-1
7	3.417E-1	1.941E-1
6	3.086E-1	1.808E-1
5	2.783E-1	1.656E-1
4	2.344E-1	1.460E-1
3	1.810E-1	1.218E-1
2.5	1.617E-1	1.090E-1
2	1.298E-1	9.481E-2
1.3	7.901E-2	6.276E-2
1	5.703E-2	4.840E-2
0.6	3.137E-2	3.233E-2
0.5	2.426E-2	2.761E-2
0.4	1.619E-2	2.145E-2
0.2	3.724E-3	8.716E-3

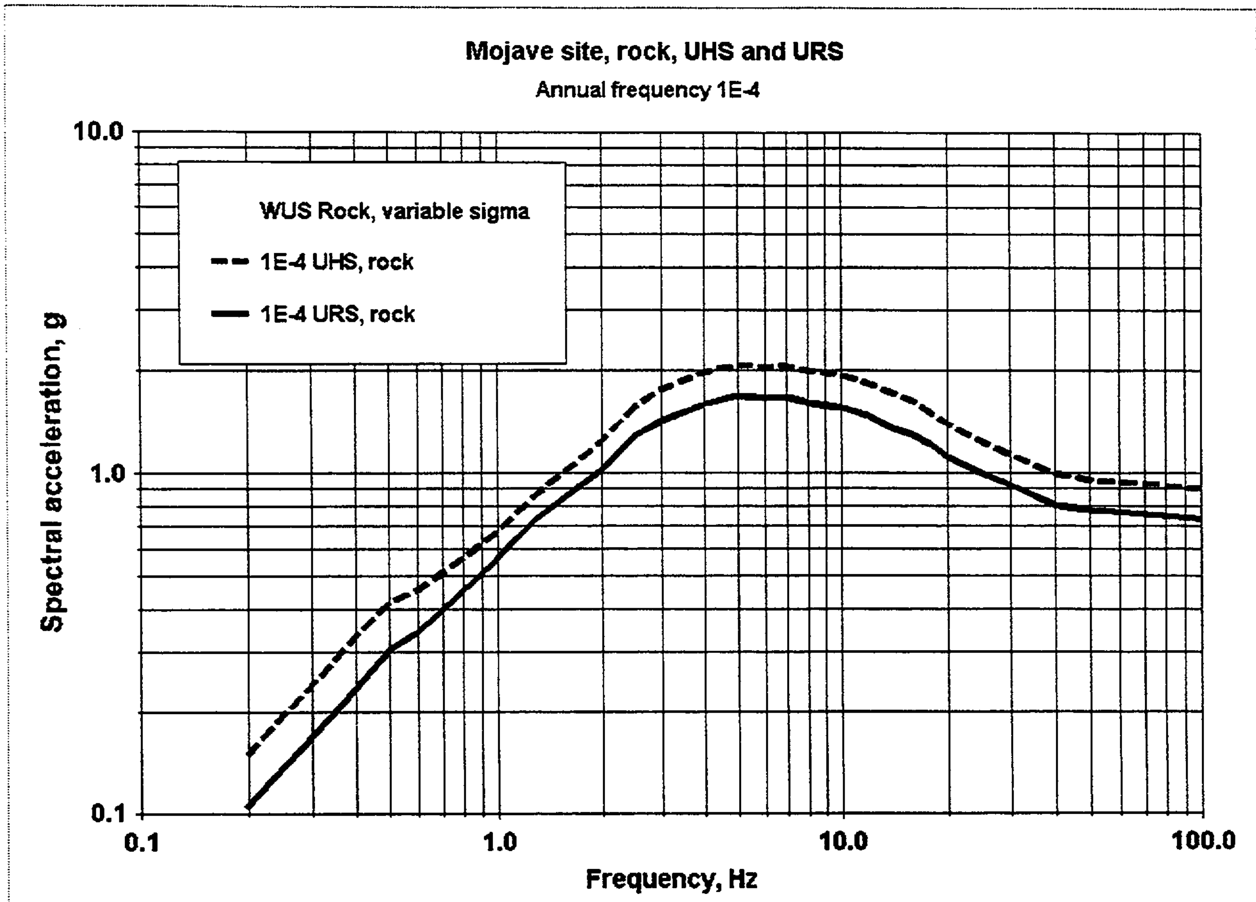

Figure 4-1. 10^{-4} UHS and URS for Mojave site, rock conditions.

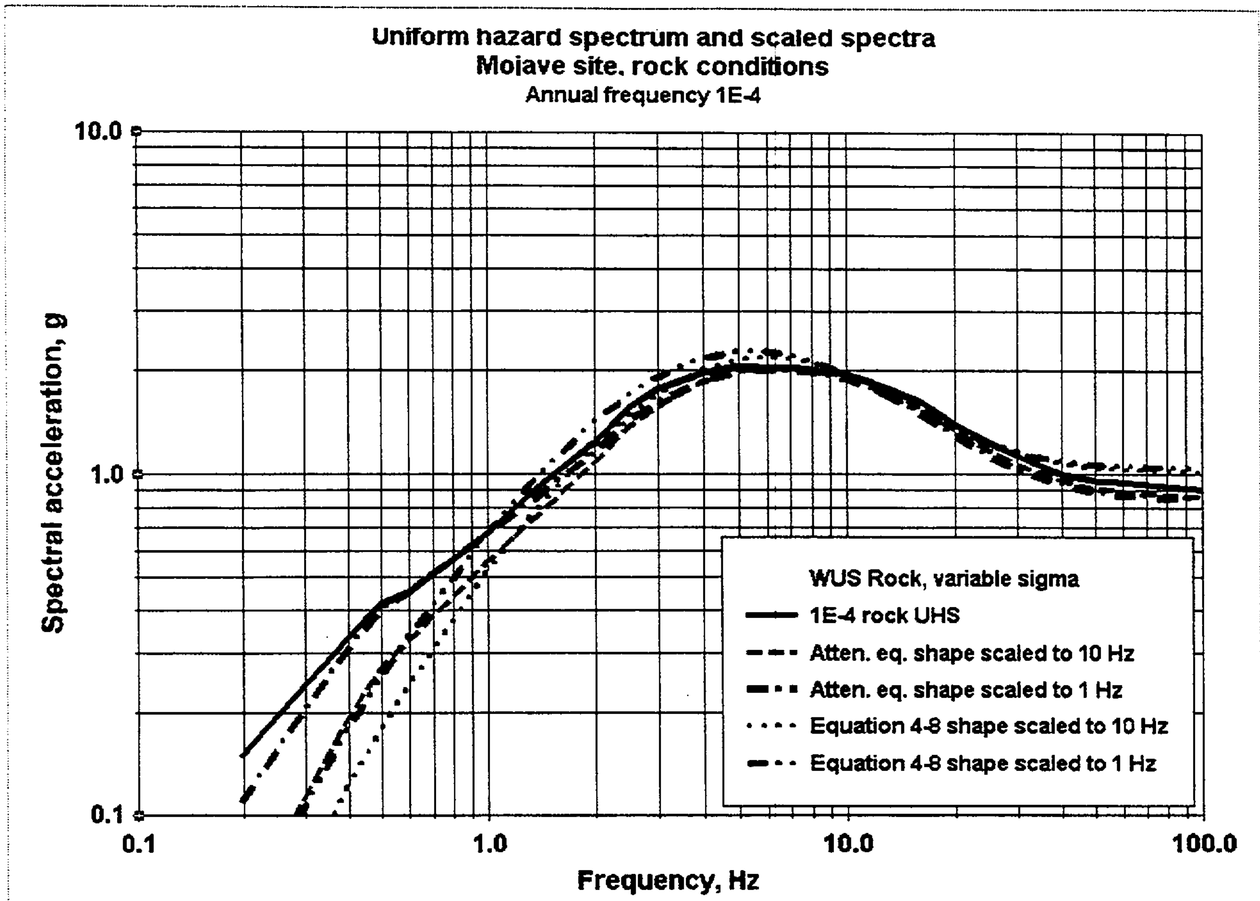

Figure 4-2. 10^{-4} UHS and scaled spectra at Mojave site, rock conditions, from attenuation equations and from recommended spectral shapes (labeled "Equation 4-8").

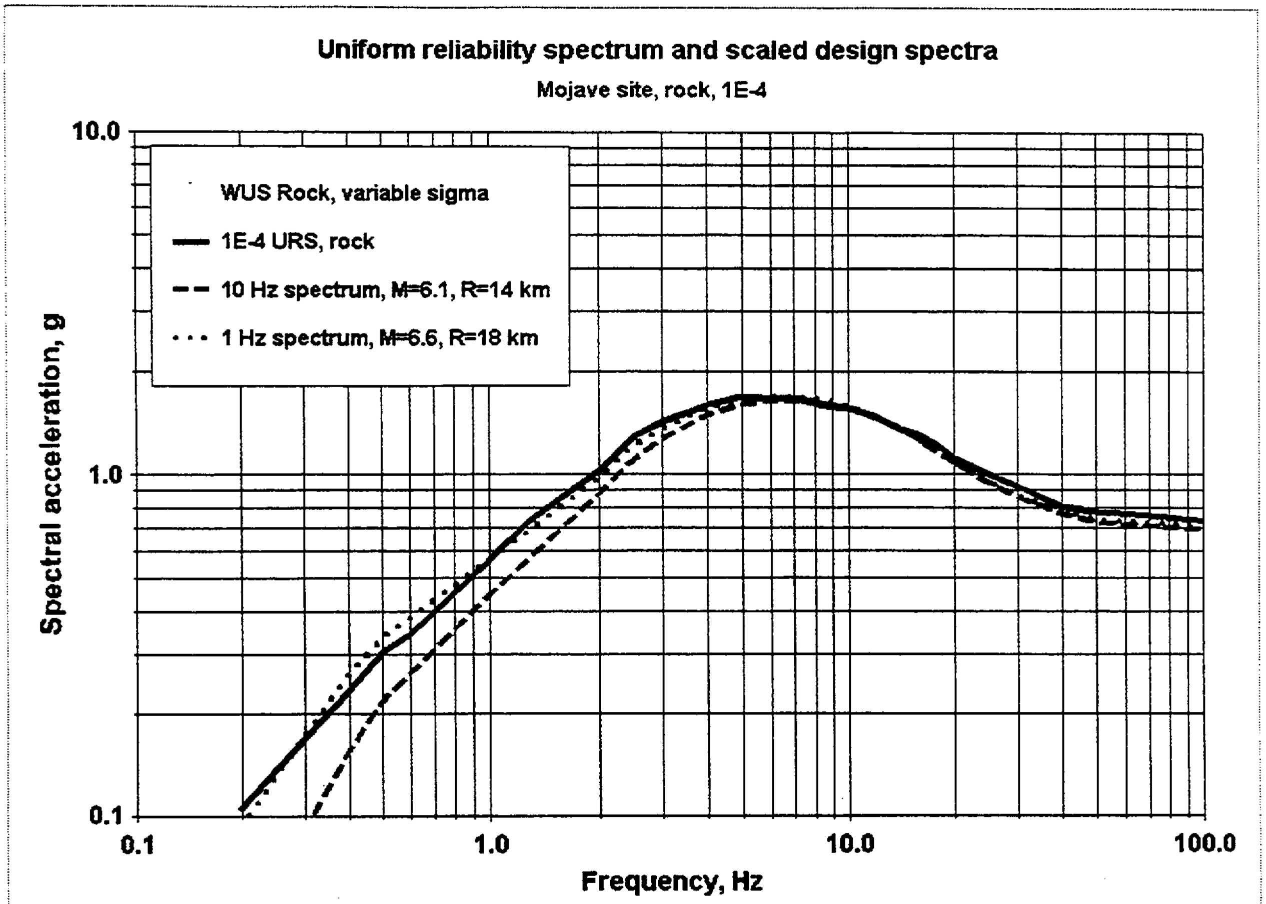

Figure 4-3. 10^{-4} URS and scaled spectra at Mojave site, rock conditions.

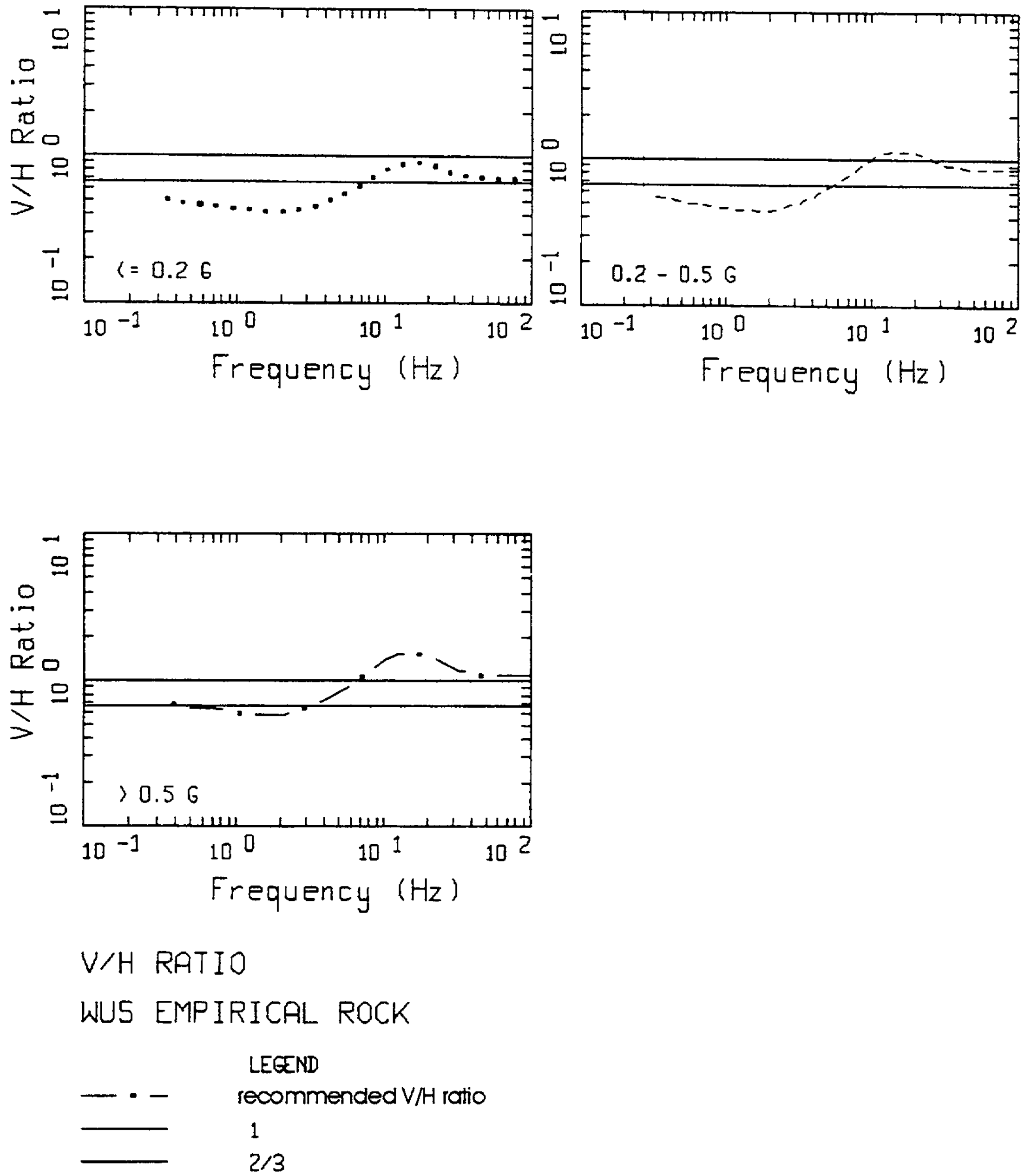

Figure 4-4a. Recommended V/H ratios (for 5% damping) for WUS soft rock site conditions for ranges in expected horizontal component peak accelerations (McGuire et al., 2001)

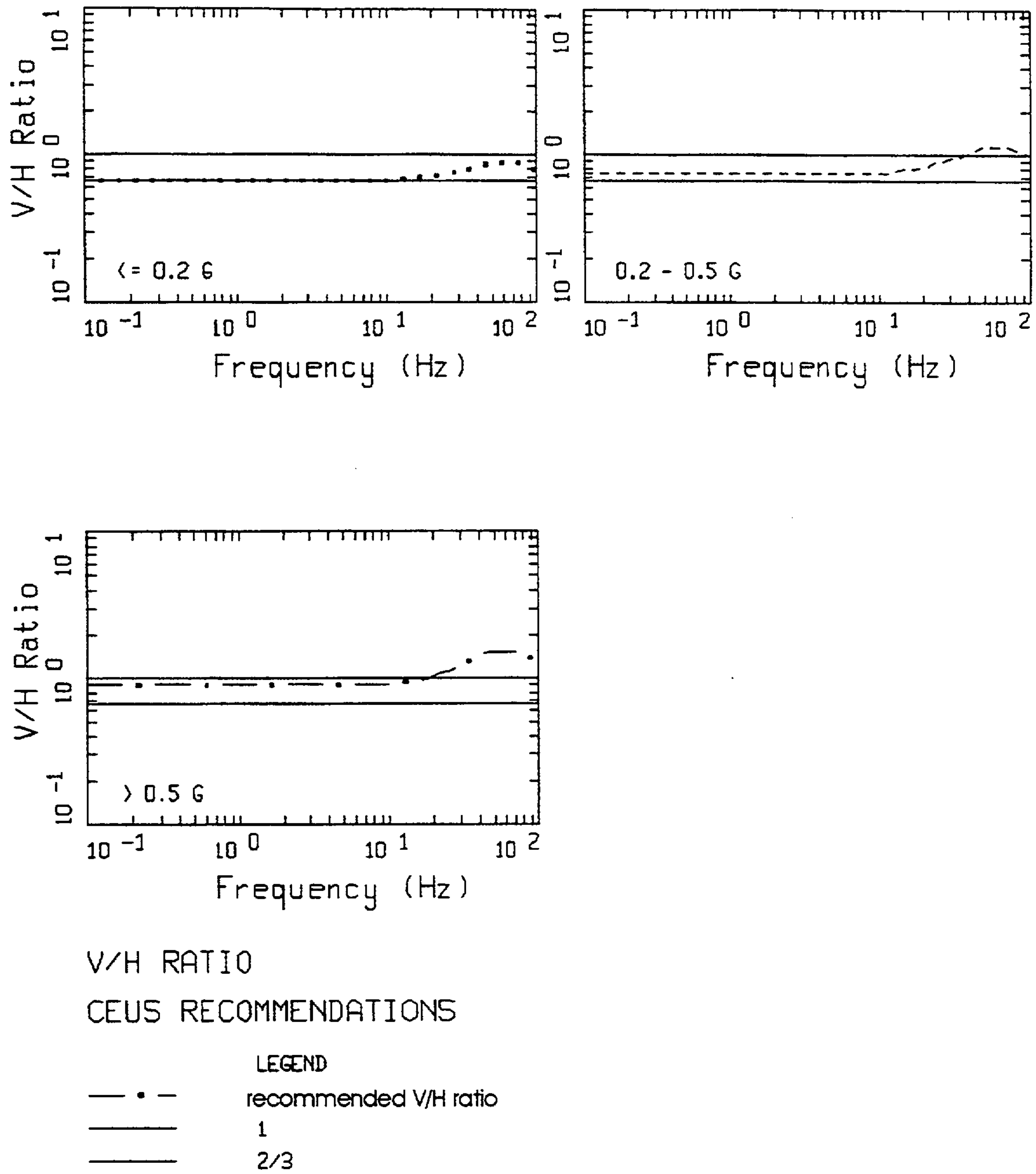

Figure 4-4b. Recommended V/H ratios (for 5% damping) for CEUS hard rock site conditions for ranges in horizontal component peak accelerations.

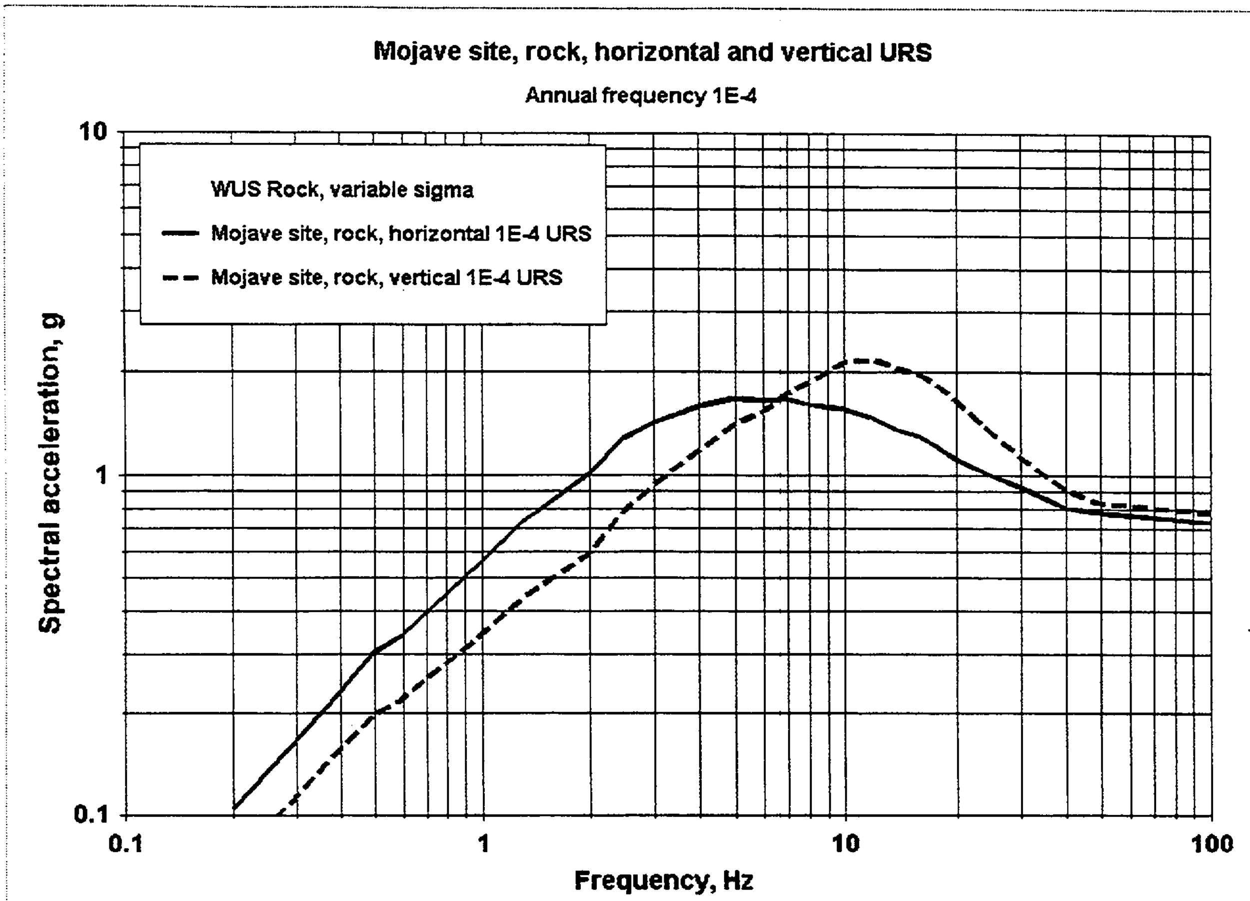

Figure 4-5. WUS rock horizontal 10^{-4} URS and corresponding vertical URS.

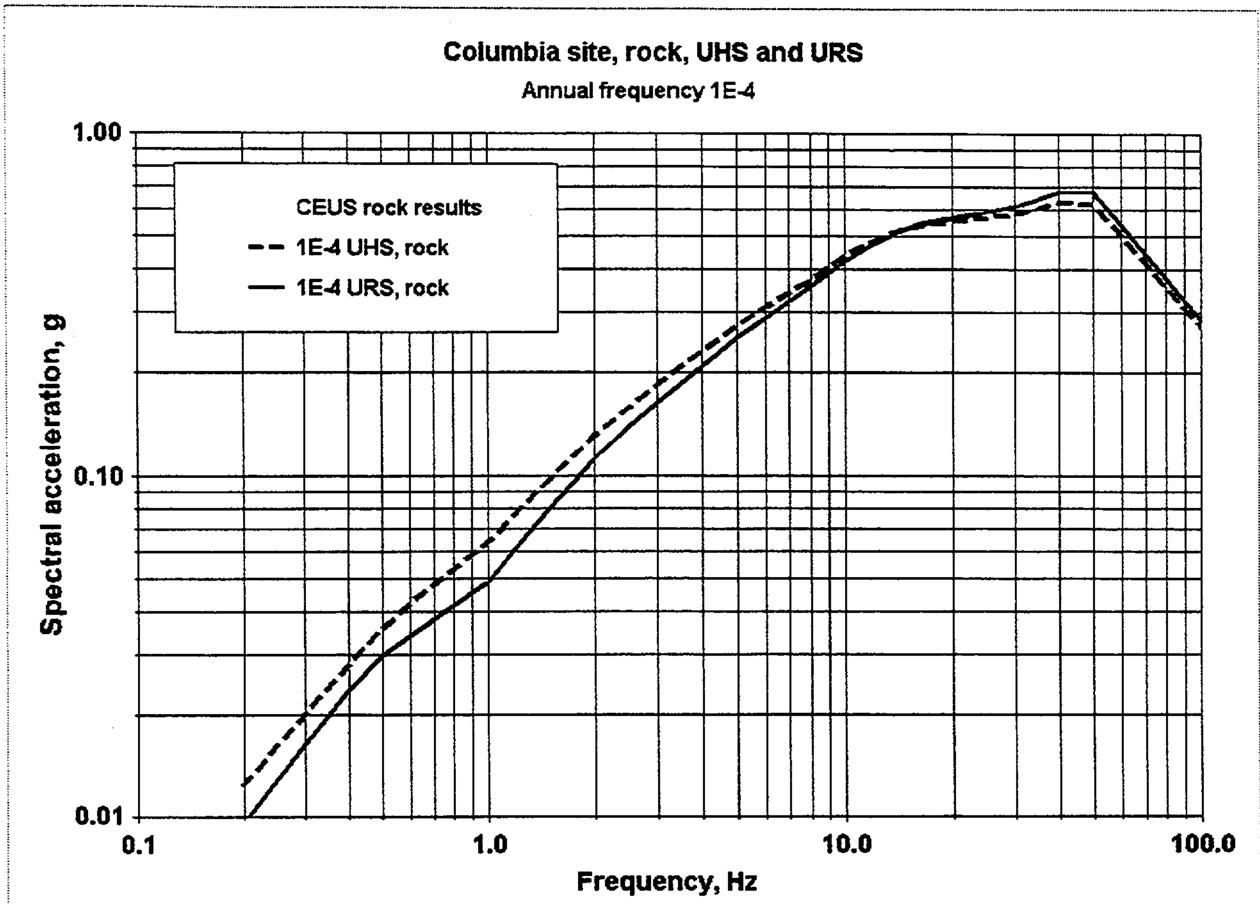

Figure 4-6. 10^{-4} UHS and URS for Columbia site, rock conditions.

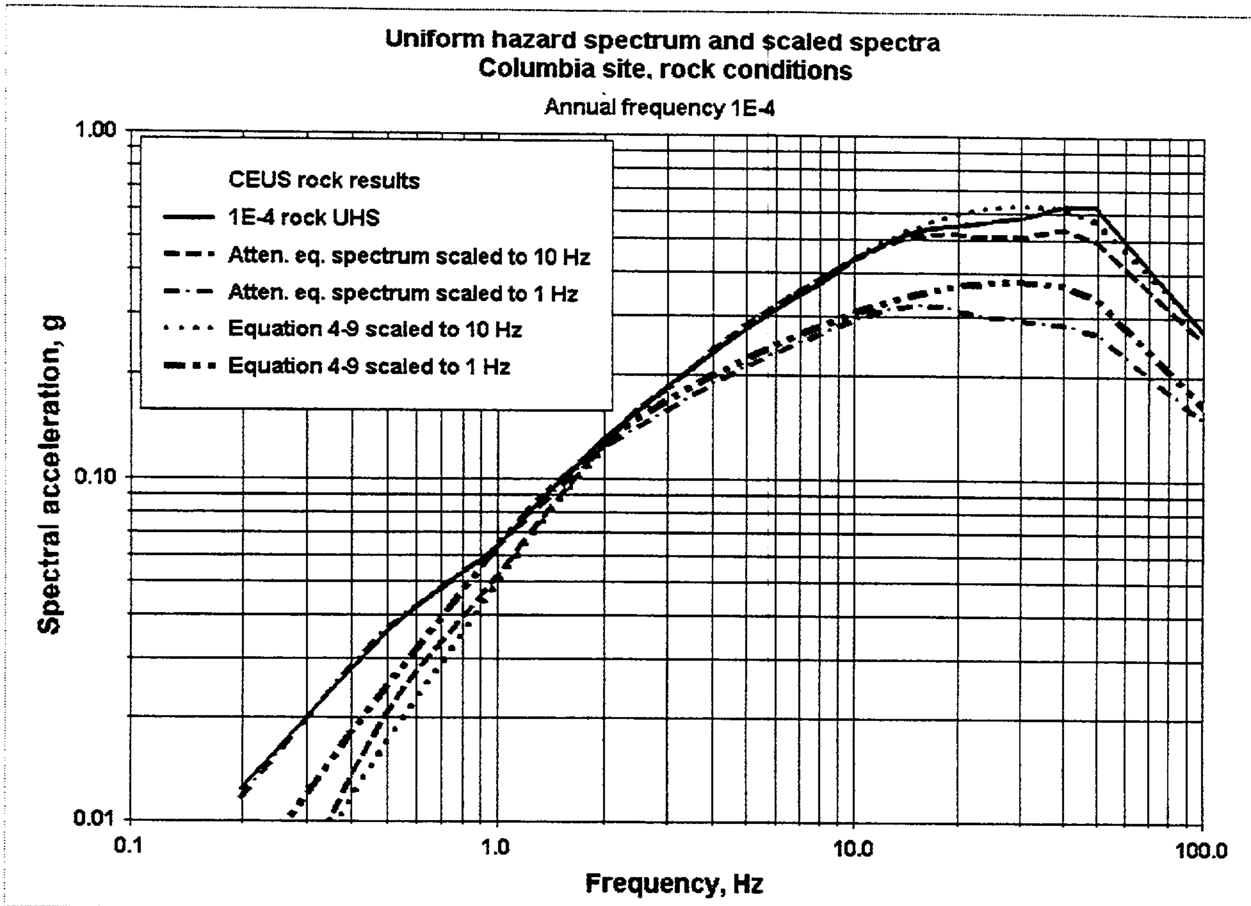

Figure 4-7. 10^{-4} UHS and scaled spectra at Columbia site, rock conditions, from attenuation equations and from recommended spectral shapes (labeled "Equation 4-8").

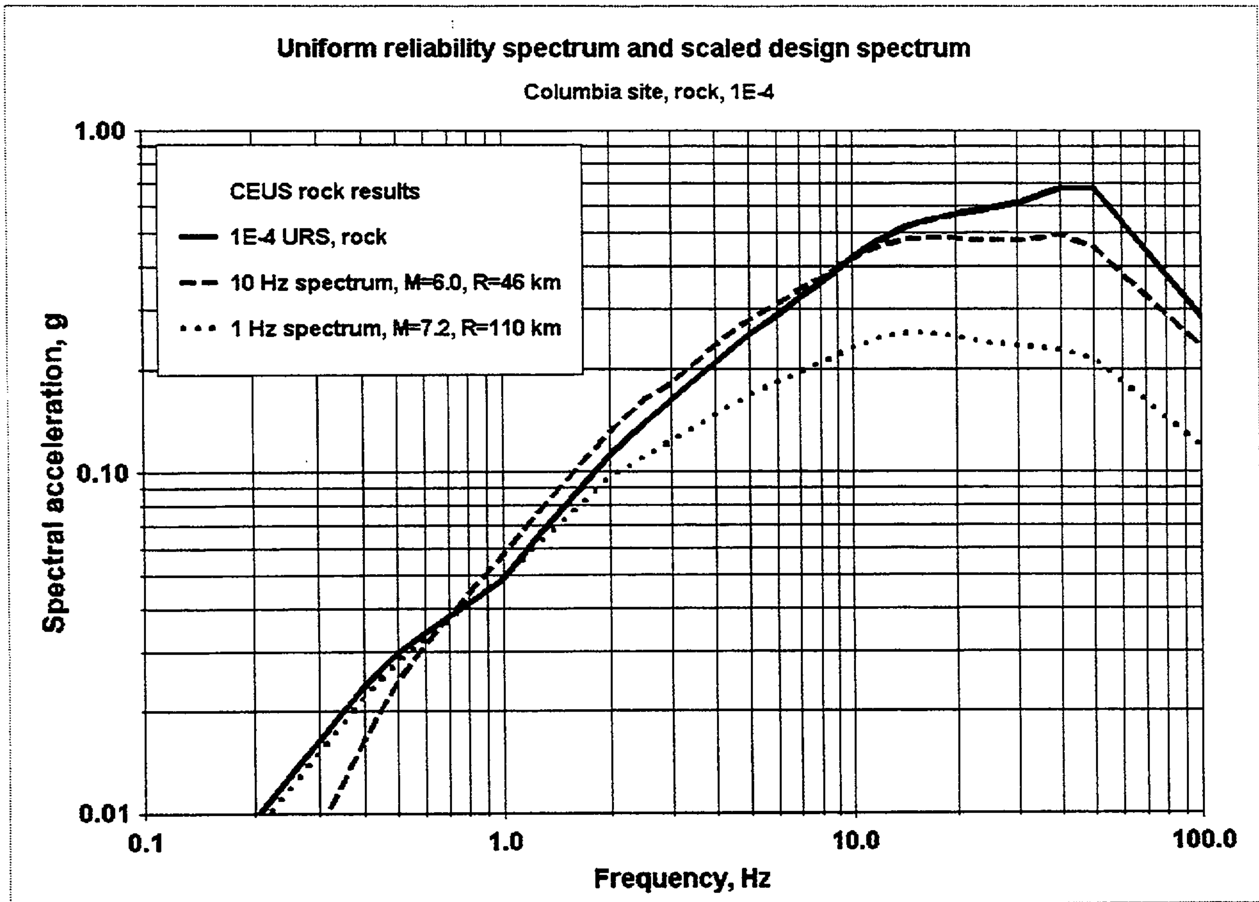

Figure 4-8. 10^{-4} URS and scaled spectra for 10 Hz and 1 Hz, Columbia site, rock conditions.

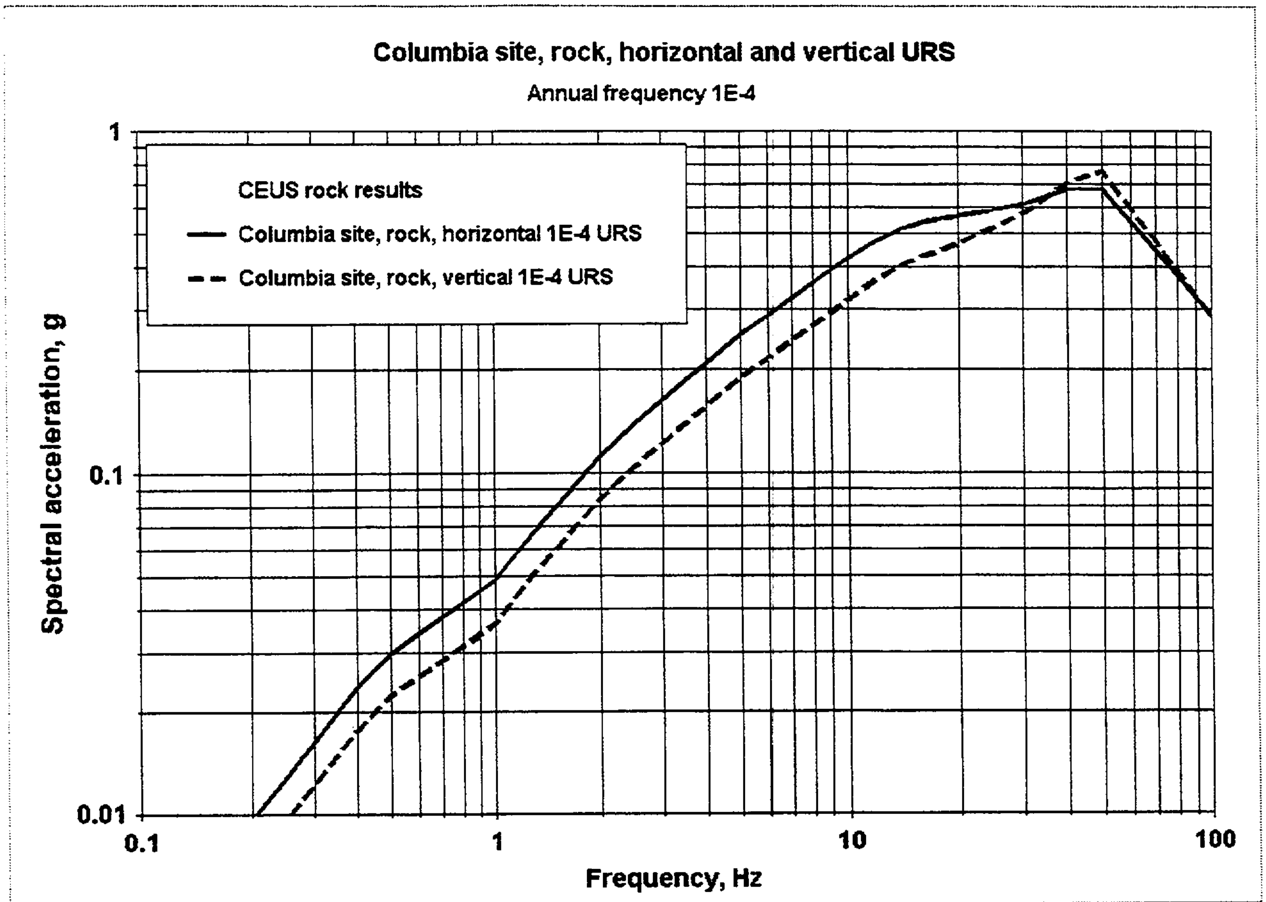

Figure 4-9. CEUS rock horizontal 10^{-4} URS and corresponding vertical URS.

5.0 GENERATING ARTIFICIAL TIME HISTORIES FOR WUS ROCK SITES

Control motions for the site response analyses using Approaches 1, 2A, and 2B (Section 6.1) are represented with Fourier amplitude spectra, because the equivalent-linear random vibration technique (RVT) is used (Schneider et al., 1993; Silva et al., 1997; McGuire et al., 2001). In general, development of a Fourier amplitude spectrum and associated response spectrum that are consistent with a specified target response spectrum results in a close match. Examples are shown in Section 6.4 for the WUS rock UHS and in McGuire et al. (2001). Time histories are generated for comparisons of equivalent-linear results with fully nonlinear site response analyses. Since control motion time histories are generally used in conventional equivalent-linear (SHAKE-type) analyses, the time history spectral matching is presented here in detail.

5.1 Spectral matching methodology

Spectral matching to the target spectra was conducted using the procedure described in Silva and Lee (1987). In this procedure, acceleration time histories are produced by combining a Fourier amplitude spectrum (which is generated by matching the target spectrum) with a phase spectrum from an observed strong ground motion recording. This approach has been used extensively for NRC, DOE, and other federal agencies in developing appropriate time histories for seismic design.

To avoid any tendency of the spectral matching process to develop gaps or low points in the time history power spectrum, this matching process begins with a smooth Fourier amplitude spectrum based on the Brune source model. Initial RVT-based matches are used to produce a smooth response spectrum that is close to the target. Subsequent matching is done by combining the Fourier phase spectrum from the recording with the smooth Fourier amplitude spectrum resulting from the RVT matching and computing the response spectrum from the resulting time history. The time history response spectrum is then used for final matching, resulting in a time history (acceleration, velocity, and displacement) that resembles the original recording in time domain characteristics, and that possesses realistic frequency-to-frequency variability in response and power spectra. Additionally, a baseline correction is included by high-pass filtering the acceleration record at 0.1 Hz. The result is a synthetic time history that closely matches the target spectrum and that possess realistic integrations to velocity and displacement.

The two most important criteria in selecting the phase spectrum from a recorded earthquake for the matching are that the seismic moment (or **M**) and the source-to-site distance should be comparable. These criteria produce synthetic records with appropriate durations and timing of the major phase arrivals so that the distribution of energy with time in the synthetic record is realistic. The time histories are intended to approximate expected durations and therefore to be appropriate for nonlinear analyses.

This project has recommended a duration criterion based on target spectra deaggregation magnitude, distance, and site condition (rock or soil), and has documented recorded motions in a time history database (McGuire et al., 2001). The time history database is segmented into **M**, *R*, and site condition bins (Table 5-1) so that appropriate input records for generating artificial motions can be appropriately selected. Statistics on PGA, PGV, PGD, PGV/PGA, and PGA•PGD/PGV^2 are shown in Table 5-2. Table 5-3 shows the duration guidelines for the corresponding record bins. The durations represent the 5 to 75% cumulative Arias Intensity, a duration measure considered significant in nonlinear analyses of nuclear facility structures (Kennedy et al., 1985; McGuire et al., 2001). The listed duration ranges are meant to reflect guidelines rather than strict criteria (McGuire et al., 2001).

5.2 Mojave Site

For the Mojave site, the deaggregation magnitudes (target spectra) and distances are listed in Table 5-4 along with the applicable duration guidelines from Table 5-3. The time histories selected from the WUS rock motion bins for inputs to the spectral matching are listed in Table 5-4 with their associated durations, both prior and subsequent to the matching process. The resulting spectra, their targets, spectral matches, and time histories are plotted in Figures 5-1 through 5-16 for the UHS horizontal and vertical components, for the 1 Hz low, moderate, and high magnitudes (designated ML, MM, and MH, respectively), and for the 10 Hz low, moderate, and high magnitudes. Note that all of these spectra are for rock motions at the base of the soil column, rather than at the rock surface, so the spectra are different from the rock surface spectra shown in Section 3.

The spectra were computed and matched at 298 points from 0.1 Hz to 100 Hz (peak acceleration) following the guidelines in McGuire et al., (2001). The associated matching criteria, no points exceeding 30% above the target nor more than 20 points below the target (with none more than 10% below) have not been applied here. In this case, the motions are used as control motions for site response analyses so mean based time histories, with respect to the target spectra, are desired. Applying the matching criteria (McGuire et al., 2001) necessarily results in spectra that are biased high with respect to target spectra, an undesirable feature in site response analyses. An examination of the spectral matches shows the fits to be quite good overall, mean-based, and with no spectral ordinates falling significantly below the targets over the important frequency range 0.3 Hz to 25 Hz. For example, in the mean based fit to the rock UHS (Figure 5-1) from 0.2 Hz to 100 Hz, 130 out of 268 points are below the target with about 100 less than 5% below and only 3 points are more than 10% under the target. The lowest point is only about 15% below the target and the maximum exceedence is about 15% (about 3 points). The remaining mean based fits show similar distributions around the targets.

REFERENCES

Kennedy, R.P., Kincaid, R.H., and Short, S.A. (1985). "Engineering characterization of ground motion, Task II: Effects of ground motion characteristics on structural response considering localized structural nonlinearities and soil-structure interaction effects." Prepared for U.S. Nuclear Regulatory Commission. NUREG/CR-3805, vol. 2.

McGuire, R.K., W.J. Silva, and C. Costantino (2001). "Technical Basis for Revision of Regulatory Guidance on Design Ground Motions: Hazard- and Risk-consistent Ground Motion Spectra Guidelines," U.S. Nuclear Reg. Comm., Rept NUREG/CR-6728, October.

Schneider, J.F., W.J. Silva, and C.L. Stark (1993). "Ground motion model for the 1989 M 6.9 Loma Prieta earthquake including effects of source, path and site." *Earthquake Spectra*, 9(2), 251-287.

Silva, W.J. and Lee, K. (1987). "*WES RASCAL code for synthesizing earthquake ground motions.*" State-of-the-Art for Assessing Earthquake Hazards in the United States, Report 24, U.S. Army Engineers Waterways Experiment Station, Miscellaneous Paper S-73-1.

Silva, W.J., N. Abrahamson, G. Toro, C. Costantino (1997). "Description and validation of the stochastic ground motion model." Report to Brookhaven National Laboratory, Associated Universities, Inc. Upton, New York, Contract 770573.

Table 5-1a
WUS Time History Bins

M, site conditions	$\overline{M}$	*R* (km)	$\overline{R}$ (km)	Number of Sets
5 - 6, rock	5.50	0 - 50	17.29	15
	6.00	50 - 100	64.88	15
5 - 6, soil	5.77	0 - 50	16.97	15
	5.77	50 - 100	63.81	15
6 - 7, rock	6.53	0 - 10	6.00	15
	6.39	10 - 50	31.29	30
	6.38	50 - 100	66.12	15
	6.66	100 - 200	89.03*	15
6 - 7, soil	6.51	0 - 10	6.65	15
	6.41	10 - 50	27.83	15
	6.57	50 - 100	67.10	15
	6.64	100 - 200	131.53	15
7+, rock	7.34	0 - 10	4.95	15
	7.38	10 - 50	31.48	15
	7.49	50 - 100	80.56	15
	7.49	100 - 200	134.85	15
7+, soil	7.47	0 - 10	4.62	15
	7.47	10 - 50	29.81	15
	7.53	50 - 100	67.84	15
	7.44	100 - 200	133.50	15

*Supplemented with records from 50 to 100 km bin which had durations within 30% of the 100 to 200 km bin minimum.

Table 5-1b
CEUS Time History Bins*

M, site conditions	$\overline{M}$	R (km)	$\overline{R}$ (km)	Number of Sets
5 - 6, rock	5.50	0 - 50	17.29	15
	5.85	50 - 100	78.34	15
5 - 6, soil	5.69	0 - 50	18.81	15
	5.38	50 - 100	72.30	15
6 - 7, rock	6.51	0 - 10	6.55	15
	6.32	10 - 50	28.58	15
	6.35	50 - 100	66.47	15
	6.66	100 - 200	89.03	15
6 - 7, soil	6.51	0 - 10	6.65	15
	6.34	10 - 50	29.04	15
	6.50	50 - 100	66.49	15
	6.64	100 - 200	131.53	15
7+, rock	7.34	0 - 10	4.95	15
	7.38	10 - 50	31.43	15
	7.49	50 - 100	80.56	15
	7.49	100 - 200	134.85	15
7+, soil	7.47	0 - 10	5.72	15
	7.47	10 - 50	29.81	15
	7.53	50 - 100	67.84	15
	7.44	100 - 200	133.50	15

*Supplemented with WUS to CEUS scaled records (McGuire et al., 2001; Section 3)

Table 5-2
WUS Statistical Shape Bins

Magnitude Bins (**M**) Range	Bin Center
5 - 6	5.5
6 - 7	6.5
7+	7.5

Distance Bin (km)	$\overline{M}$	$\overline{R}$ (km)	Number of Spectra	PGA**(g), σ_{ln}	PGV**(cm/sec), σ_{ln}	PGD**(cm), σ_{ln}	$\frac{PGV^*}{PGA}$ ($\frac{cm/sec}{g}$), σ_{ln}	$\frac{PGA \cdot PGD^*}{PGV^2}$, σ_{ln}
0 - 10, rock	5.54	7.91	30	0.18, 0.91	8.14, 1.14	0.80, 1.60	44.50, 0.58	2.17, 0.28
	6.53	5.75	32	0.44, 0.76	32.65, 0.93	6.22, 1.26	73.51, 0.40	2.54, 0.42
	7.51	4.99	27	0.45, 0.62	60.41, 0.49	38.47, 0.86	135.42, 0.50	4.61, 0.55
0 - 10, soil	5.76	7.80	24	0.26, 0.65	18.57, 0.56	3.11, 0.46	70.72, 0.33	2.32, 0.35
	6.46	6.00	77	0.38, 0.43	46.88, 0.59	14.79, 0.89	122.00, 0.44	2.54, 0.41
	7.50	5.77	42	0.27, 0.52	51.81, 0.31	43.08, 0.36	194.11, 0.44	4.20, 0.42
10 - 50, rock	5.57	21.80	180	0.11, 0.87	5.08, 0.85	0.54, 1.04	46.96, 0.37	2.24, 0.38
	6.43	30.28	238	0.13, 0.73	8.81, 0.76	1.96, 1.01	70.41, 0.49	3.09, 0.54
	7.52	34.57	64	0.12, 0.87	15.31, 0.84	9.11, 1.15	126.39, 0.59	4.62, 0.59
10-50, soil	5.69	21.82	378	0.11, 0.73	6.63, 0.77	0.87, 0.94	59.88, 0.34	2.16, 0.33
	6.35	28.27	542	0.14, 0.63	10.77, 0.74	2.25, 1.04	78.78, 0.41	2.57, 0.41

**Median values

Table 5-2 (cont.)
WUS Statistical Shape Bins

Magnitude Bins (M)	
Range	Bin Center
5 - 6	5.5
6 - 7	6.5
7+	7.5

Distance Bin (km)	$\overline{M}$	$\overline{R}$ (km)	Number of Spectra	PGA**(g), σ_{ln}	PGV**(cm/sec), σ_{ln}	PGD**(cm), σ_{ln}	$\frac{PGV^*}{PGA}(\frac{cm/sec}{g})$, σ_{ln}	$\frac{PGA \cdot PGD^*}{PGV^2}$, σ_{ln}
10 - 50, soil	7.53	32.27	169	0.12, 0.59	24.04, 0.70	16.39, 0.86	207.08, 0.51	3.23, 0.50
50 - 100, rock	5.91	64.27	34	0.05, 0.40	2.22, 0.53	0.21, 0.83	41.16, 0.43	2.24, 0.57
	6.51	76.29	132	0.06, 0.48	8.62, 0.63	7.55, 0.88	152.29, 0.45	5.64, 0.48
	7.58	81.46	10	0.06, 0.52	5.16, 0.87	2.64, 1.17	80.63, 0.45	6.23, 0.50
50 - 100, soil	5.80	67.22	42	0.06, 0.80	3.12, 0.78	0.38, 0.92	53.20, 0.23	2.28, 0.49
	6.49	67.34	158	0.07, 0.67	6.23, 0.78	1.26, 0.99	88.00, 0.42	2.26, 0.44
	7.59	73.86	196	0.07, 0.49	13.42, 0.43	10.75, 0.56	203.68, 0.37	3.86, 0.45
100 - 200, rock	5.40	107.80	2	0.02, -----	1.16, ----	0.10, ----	49.72, -----	1.74, ---
	6.64	114.57	14	0.02, 0.86	2.03, 0.38	1.09, 0.68	132.54, 0.59	3.98, 0.27
	7.53	134.32	52	0.03, 0.60	5.97, 0.64	4.61, 0.96	214.91, 0.37	3.52, 0.37
100-200, soil	6.00	105.00	2	0.03, ----	1.50, ----	0.11, ----	42.92, ----	1.74, ----
	6.64	132.97	28	0.03, 0.78	3.05, 0.58	0.89, 0.97	98.24, 0.53	2.90, 0.42
	7.50	128.34	206	0.04, 0.55	9.95, 0.55	6.78, 0.70	224.81, 0.31	2.97, 0.41

Table 5-2 (cont.)
WUS Statistical Shape Bins

Magnitude Bins (M)	
Range	Bin Center
5 - 6	5.5
6 - 7	6.5
7+	7.5

Distance Bin (km)	$\overline{M}$	$\overline{R}$ (km)	Number of Spectra	PGA**(g), σ_{ln}	PGV**(cm/sec), σ_{ln}	PGD**(cm), σ_{ln}	$\frac{PGV^*}{PGA}(\frac{cm/\sec}{g})$, σ_{ln}	$\frac{PGA \cdot PGD^*}{PGV^2}$, σ_{ln}
0 - 50, rock	5.57	19.91	208	0.12, 0.89	5.39, 0.91	0.57, 1.14	46.73, 0.40	2.22, 0.37
	6.44	27.39	270	0.15, 0.84	10.27, 0.89	2.24, 1.10	70.77, 0.48	3.02, 0.53
	7.52	25.92	89	0.18, 1.00	22.81, 0.98	14.16, 1.27	129.78, 0.56	4.69, 0.57
0 - 50, soil	5.69	21.10	398	0.12, 0.75	7.02, 0.79	0.93, 0.97	60.48, 0.34	2.16, 0.33
	6.37	25.50	619	0.16, 0.70	12.93, 0.87	2.85, 1.20	83.17, 0.44	2.57, 0.41
	7.52	27.02	211	0.14, 0.66	27.99, 0.71	19.85, 0.87	204.45, 0.50	3.40, 0.49

Table 5-3
Magnitude and Distance Bins and Duration Criteria

M	*R* (km)	Duration (sec)**	
		Rock	Soil
5.5 (5 - 6)	0 - 50*	1.1 - 3.6*	1.6 - 4.8*
	50 - 100	3.6 - 8.2	2.9 - 6.4
6.5 (6 - 7)	0 - 10	2.6 - 5.8	3.1 - 7.0
	10 - 50	3.1 - 7.0	3.6 - 8.2
	50 - 100	5.1 - 11.6	5.7 - 12.8
	100 - 200	8.1 - 18.3	8.7 - 19.5
	200 - 400***		
7.5 (7+)	0 - 10	6.1 - 13.8	6.6 - 15.0
	10 - 50	6.6 - 14.9	7.2 - 16.1
	50 - 100	8.7 - 19.5	12.2 - 27.5
	100 - 200	11.7 - 26.3	16.2 - 36.5
	200 - 400***		

*For the **M** 5.5 bin, there were too few records in the 0-10 km, so distance bins 0-10 and 10-50 were combined into one 0-50 km bin

**5% - 75% total cumulative Arias Intensity

***CEUS only

Table 5-4
Rock Motion Durations (Annual Probability of Exceedence 10^{-4})

UHS	**Magnitude**	**Distance (km)**	**Durations (5 to 75%) (sec)**		
			Input	**Match**	**Target**
1 Hz	ML: 5.4	10	2.843	4.944	1.1 - 3.6
	MM: 6.6	18	5.643	8.400	3.1 - 7.0
	MH: 7.8	30	15.85	18.98	6.6 - 14.9
10 Hz	ML: 5.1	10	2.843	4.749	1.1 - 3.6
	MM: 6.1	14	5.678	7.715	3.1 - 7.0
	MH: 7.8	30	15.85	19.05	6.6 - 14.9

RECORDS SELECTED

Target **M**	Earthquake	**M**	Site	Distance (km)	Site Condition
5.1, 5.4	Coalinga*	5.2	C-OLP, 270	11.9	rock
6.1	Morgan Hill	6.2	Gilroy 1, 320	16.2	rock
6.6	Loma Prieta	6.9	UCSC, 000	18.1	rock
7.8	Chi Chi	7.5	TCUO78; EW, Z	7.5	rock

* Coalinga aftershock on July 9, 1983.

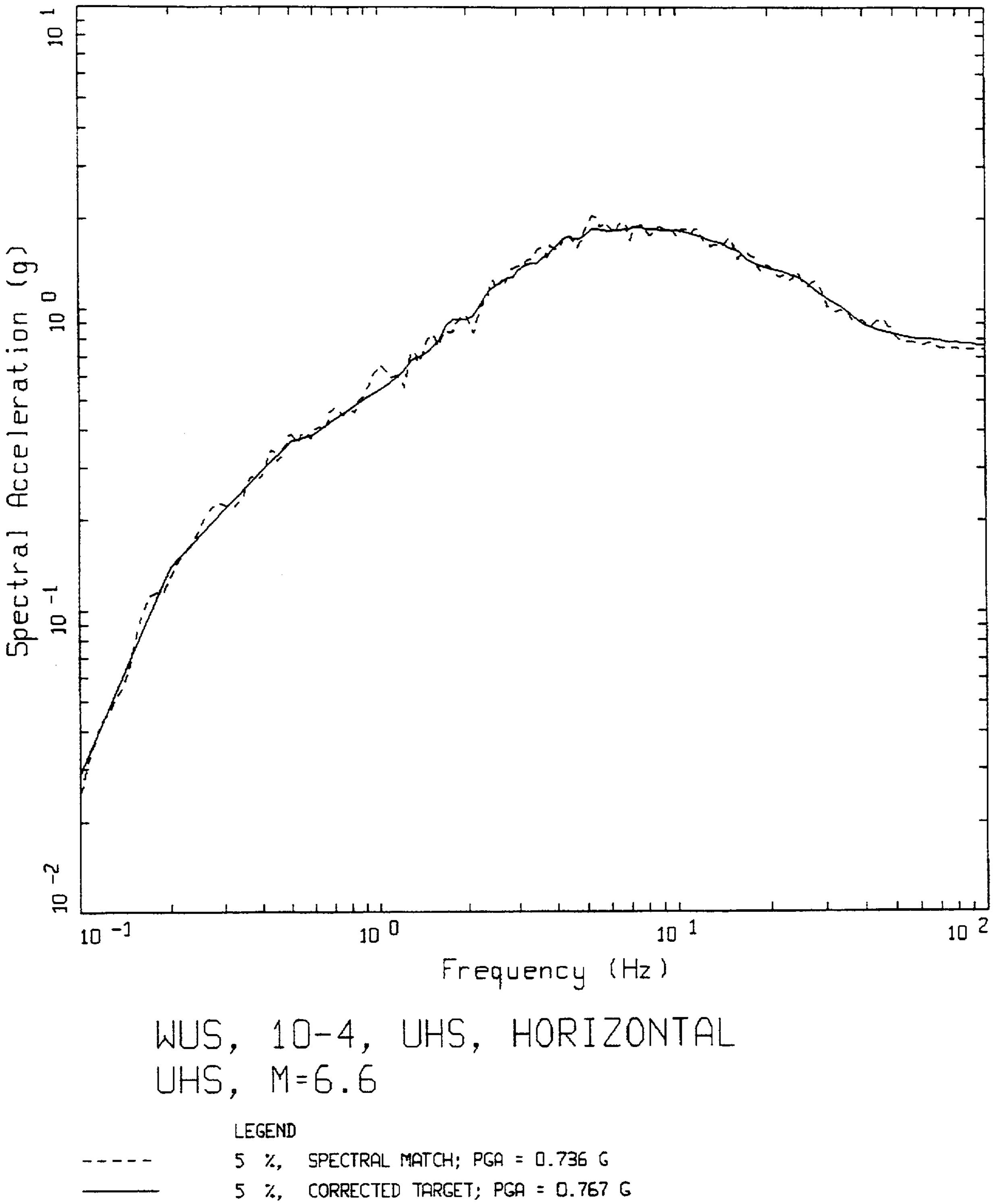

Figure 5-1. Spectral match to corrected (base of soil) rock horizontal 1E-4 UHS, Mojave site.

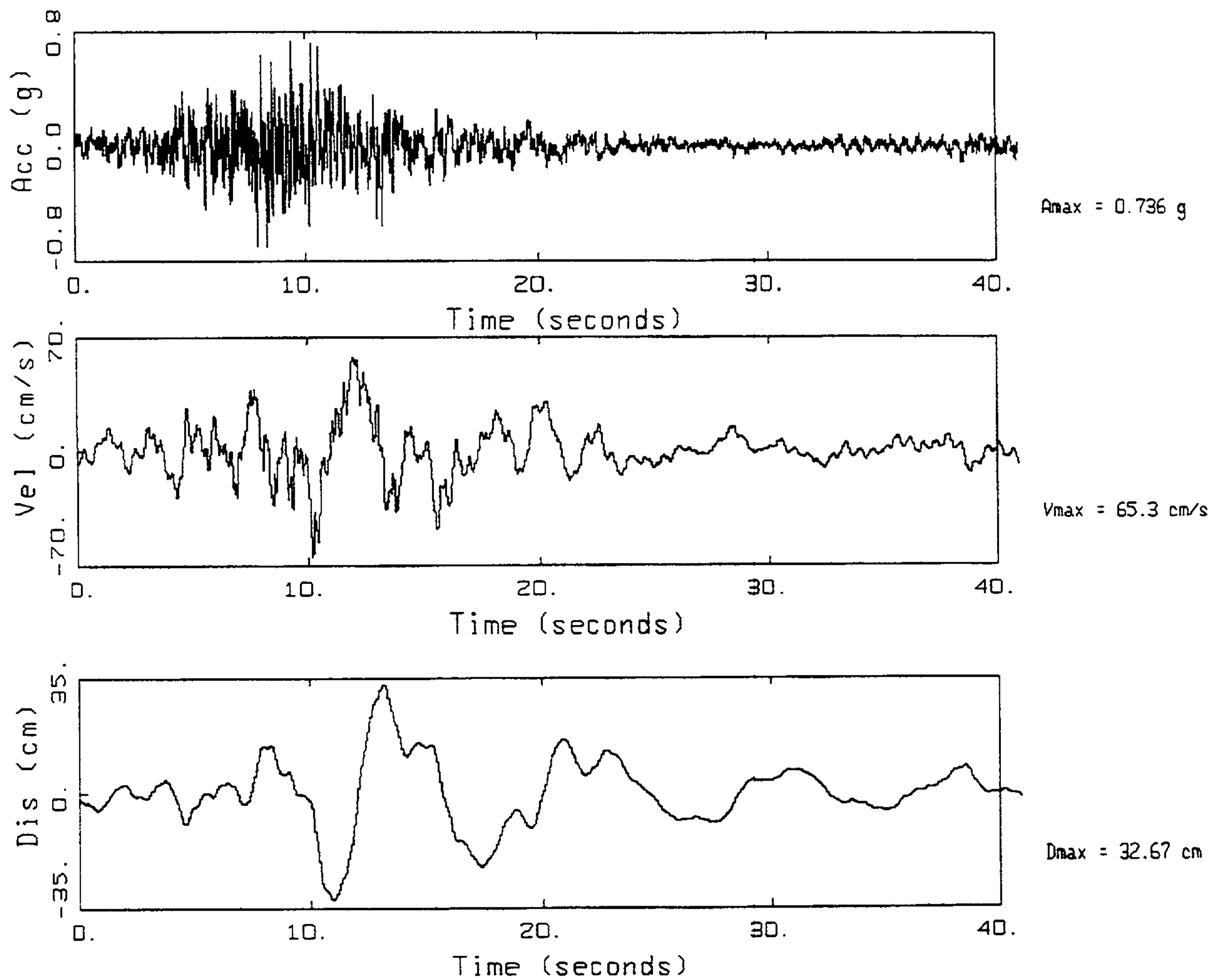

Figure 5-2. Acceleration, velocity, and displacement time histories corresponding to the corrected (base of soil) rock horizontal UHS spectral match, Mojave site.

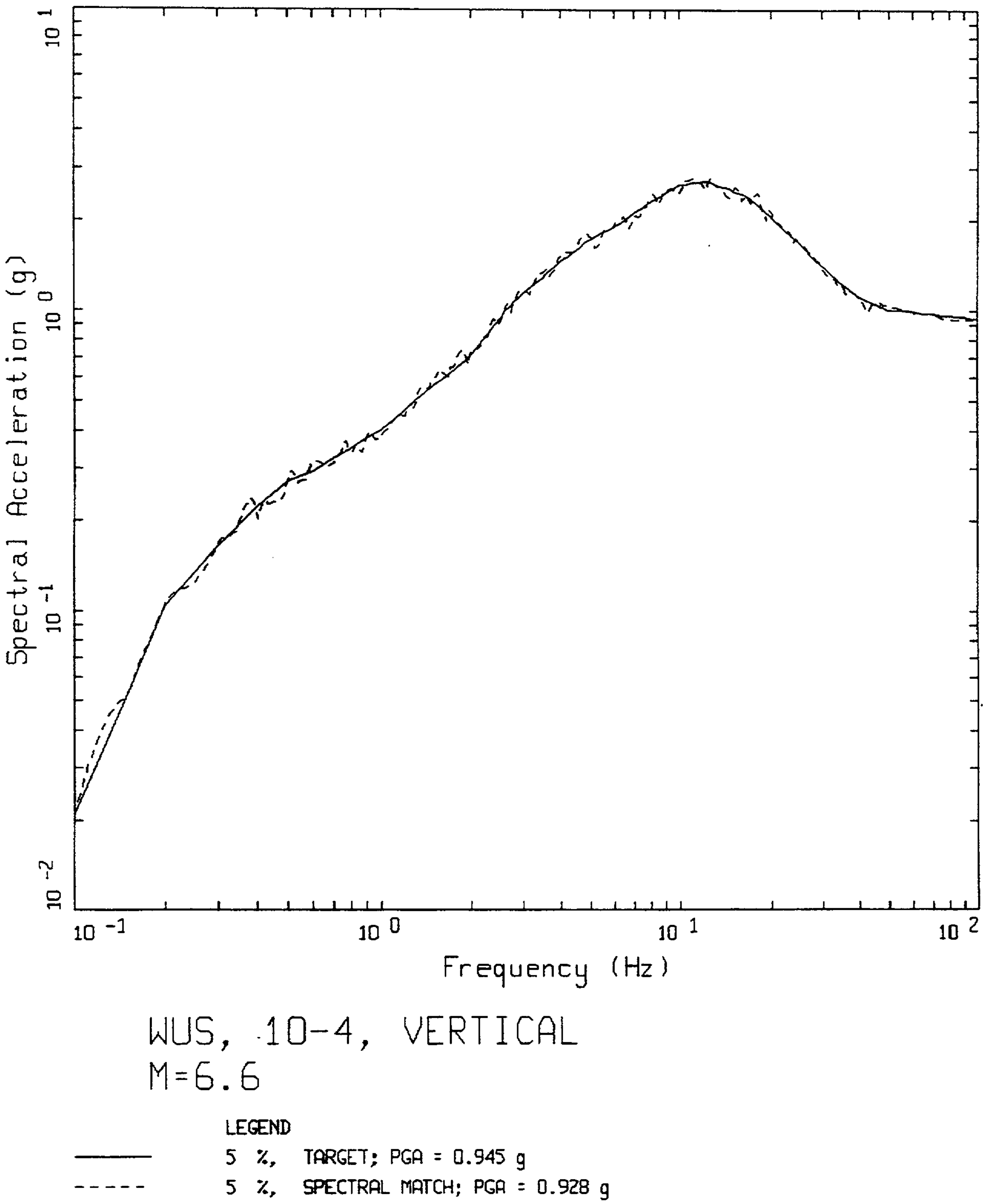

Figure 5-3. Spectral match to rock vertical component 1E-4 spectrum, at base of soil for Mojave site.

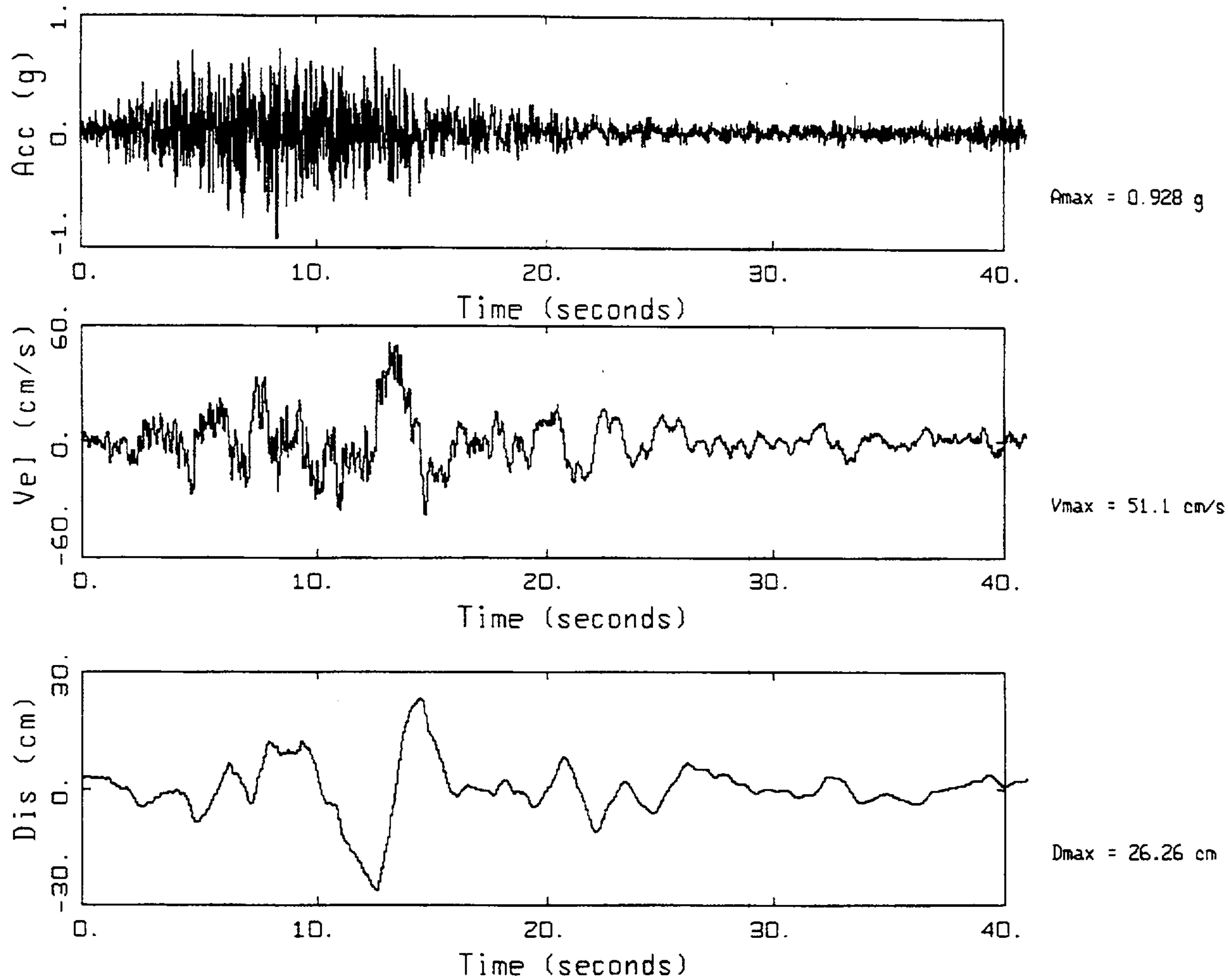

Figure 5-4. Acceleration, velocity, and displacement time histories corresponding to the rock vertical component spectral match at base of soil for Mojave site.

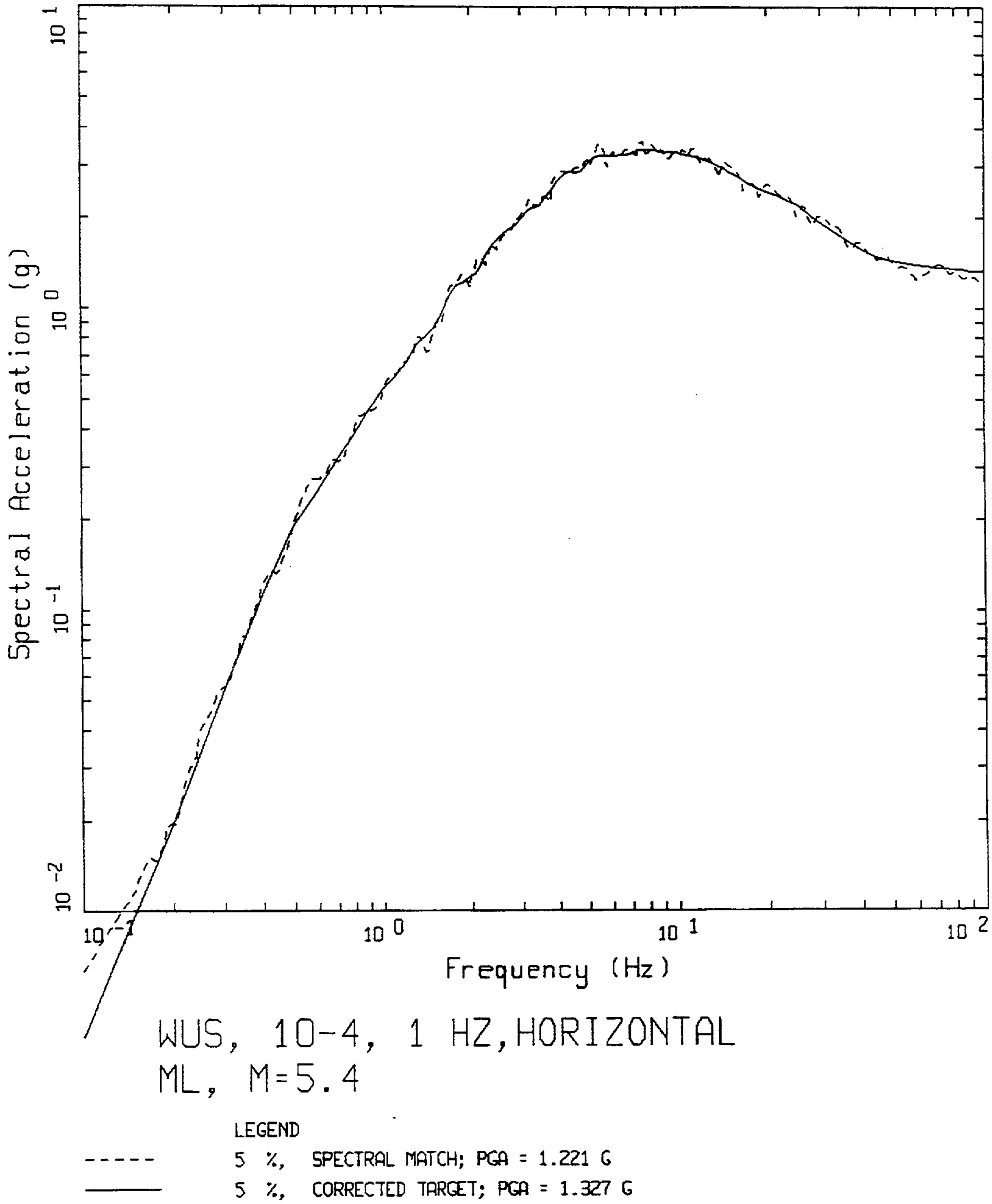

Figure 5-5. Spectral match to corrected (base of soil) 1 Hz rock 1E-4 spectrum: ML.

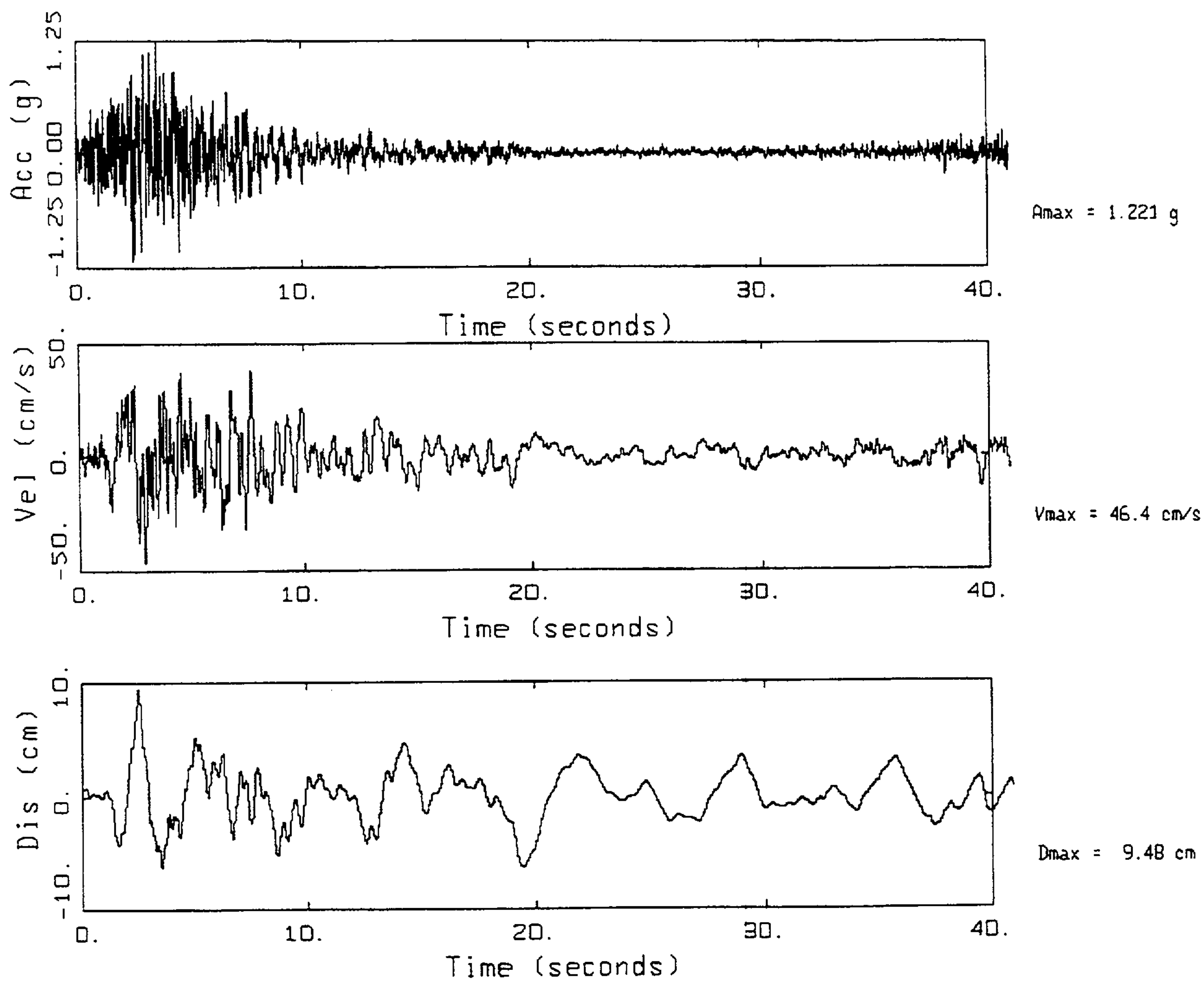

Figure 5-6. Acceleration, velocity, and displacement time histories corresponding to the corrected (base of soil) 1 Hz rock spectral match: ML.

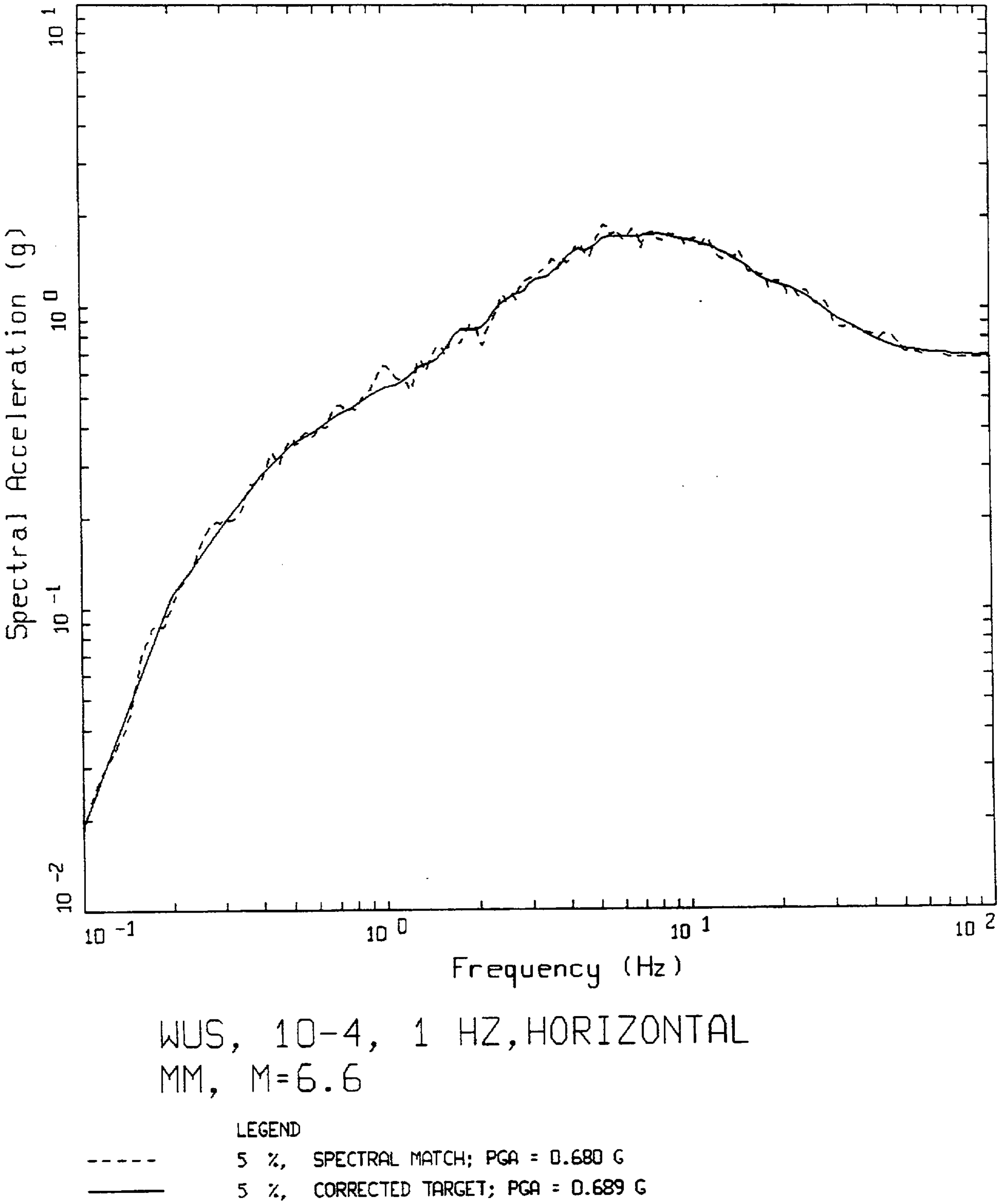

Figure 5-7. Spectral match to corrected (base of soil) 1 Hz rock 1E-4 spectrum: MM.

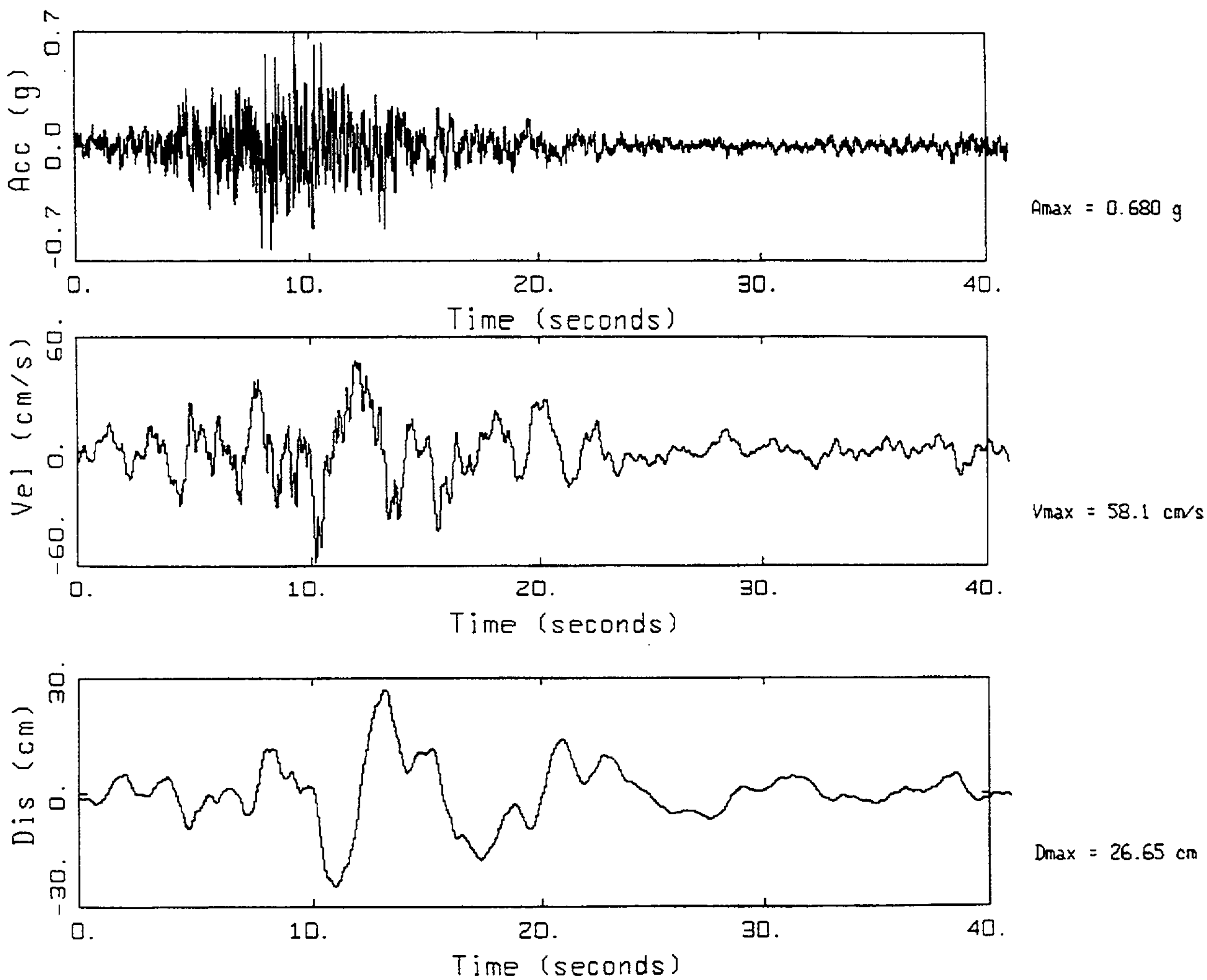

Figure 5-8. Acceleration, velocity, and displacement time histories corresponding to the corrected (base of soil) 1 Hz rock spectral match: MM.

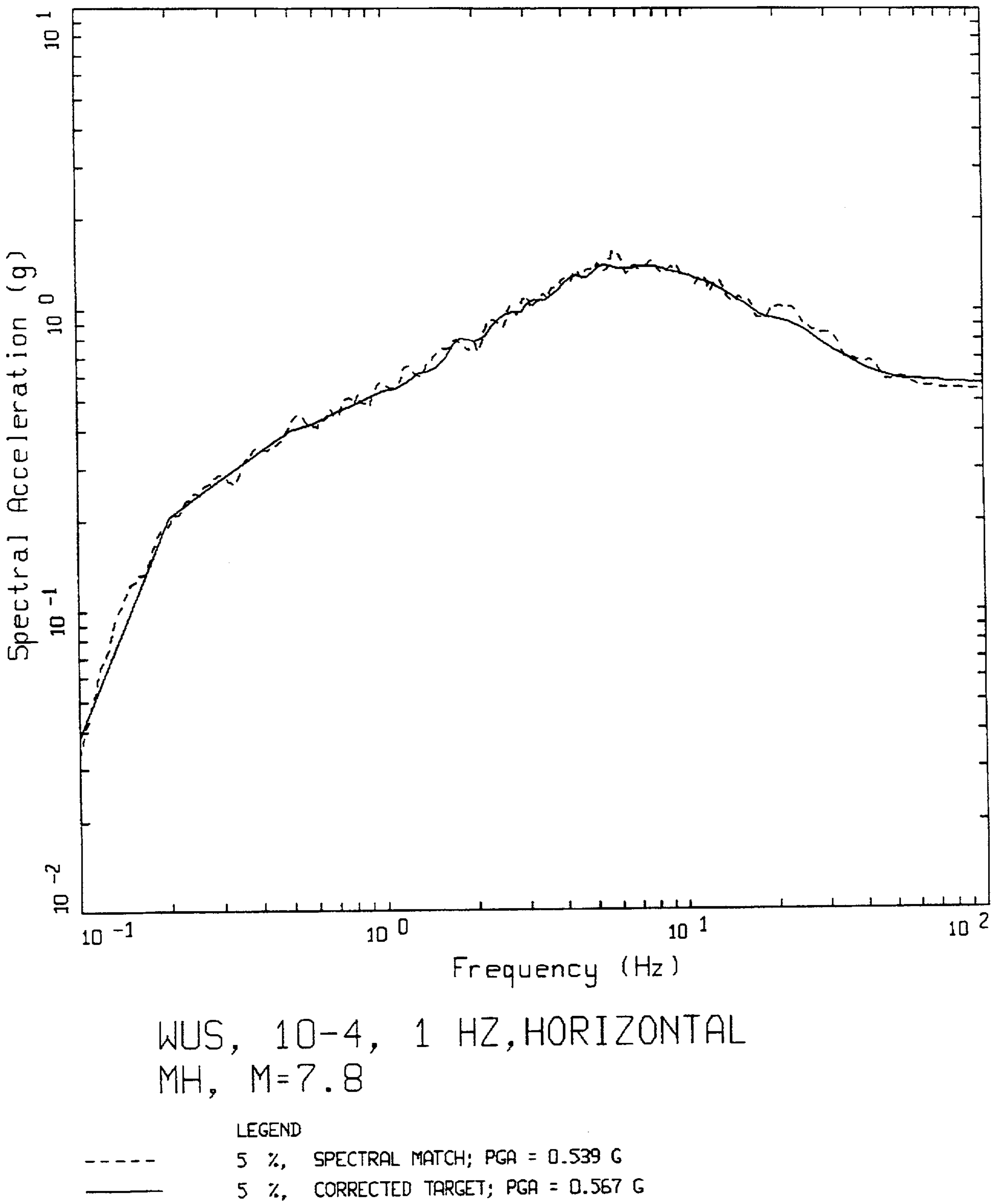

Figure 5-9. Spectral match to corrected (base of soil) 1 Hz rock 1E-4 spectrum: MH.

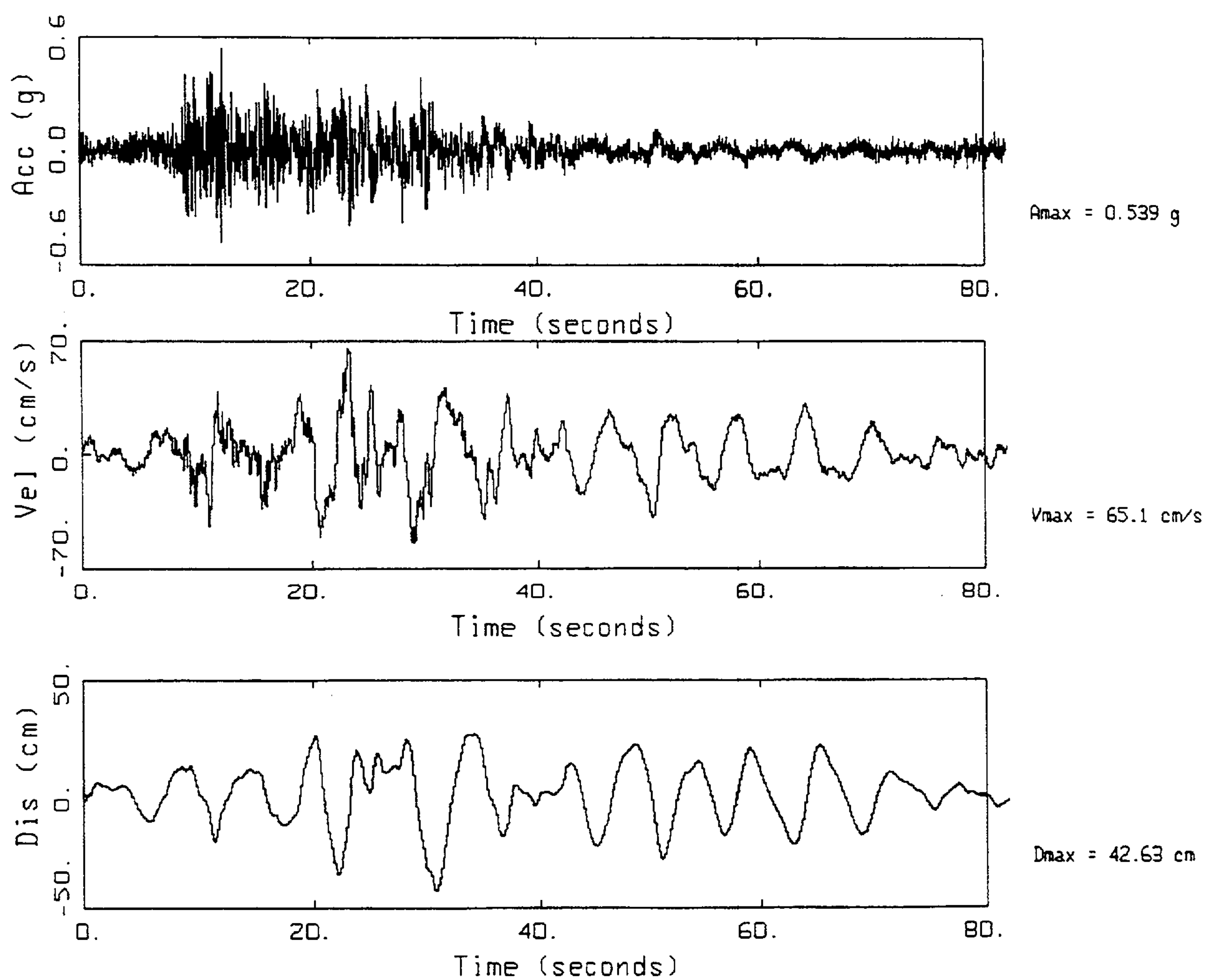

Figure 5-10. Acceleration, velocity, and displacement time histories corresponding to the corrected (base of soil) 1 Hz rock spectral match: MH.

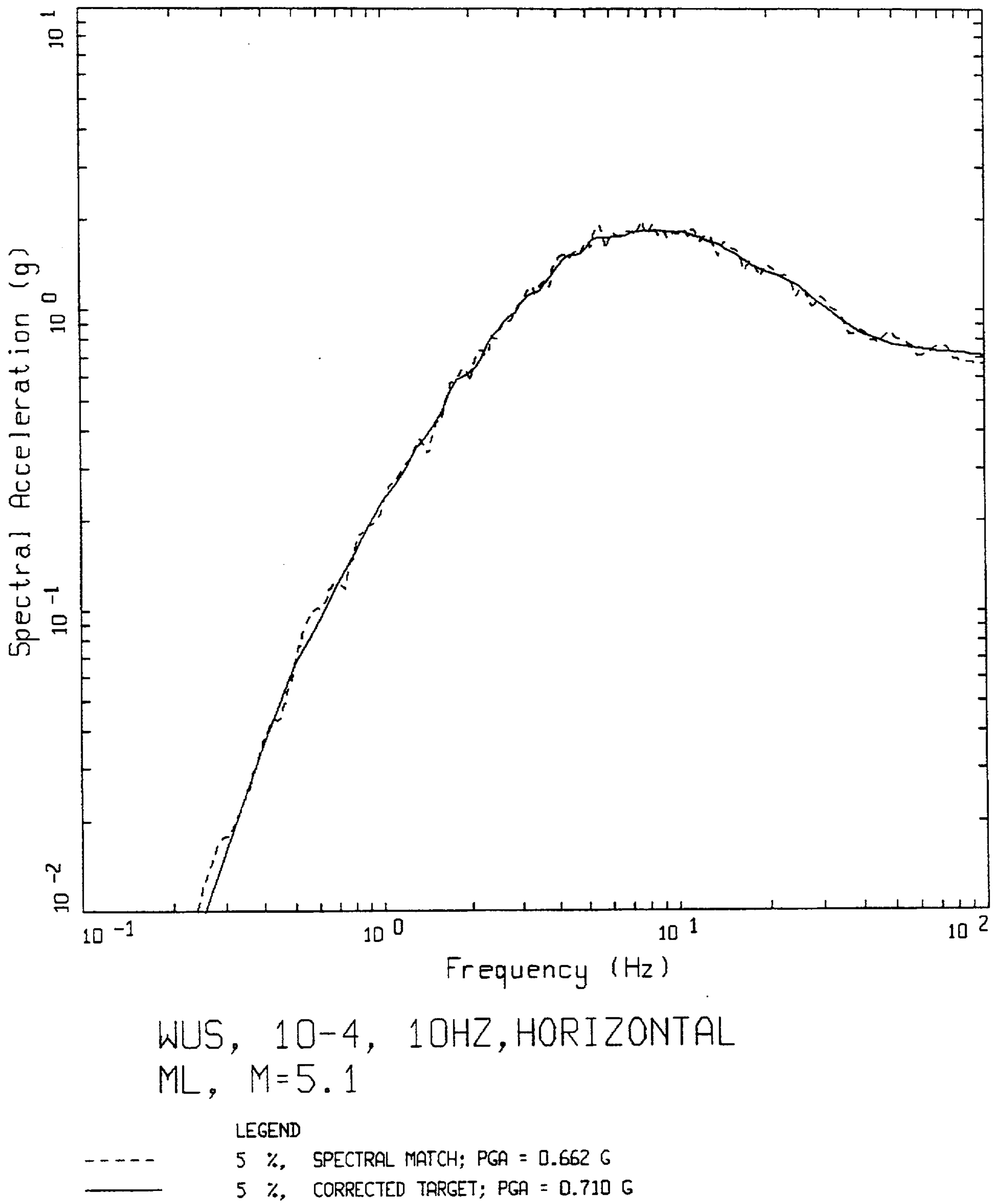

Figure 5-11. Spectral match to corrected (base of soil) 10 Hz rock 1E-4 spectrum: ML.

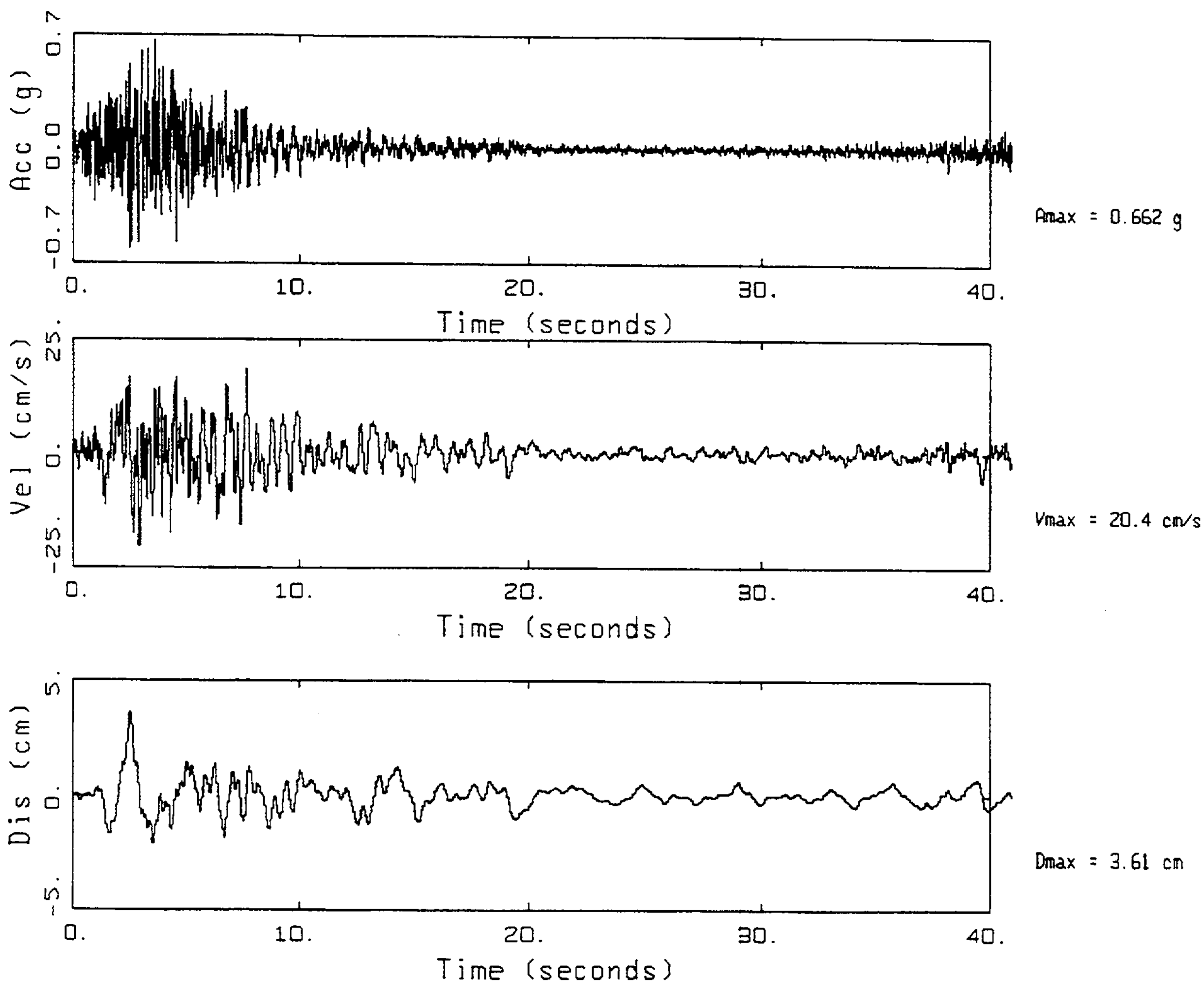

Figure 5-12. Acceleration, velocity, and displacement time histories corresponding to the corrected (base of soil) 10 Hz rock spectral match: ML.

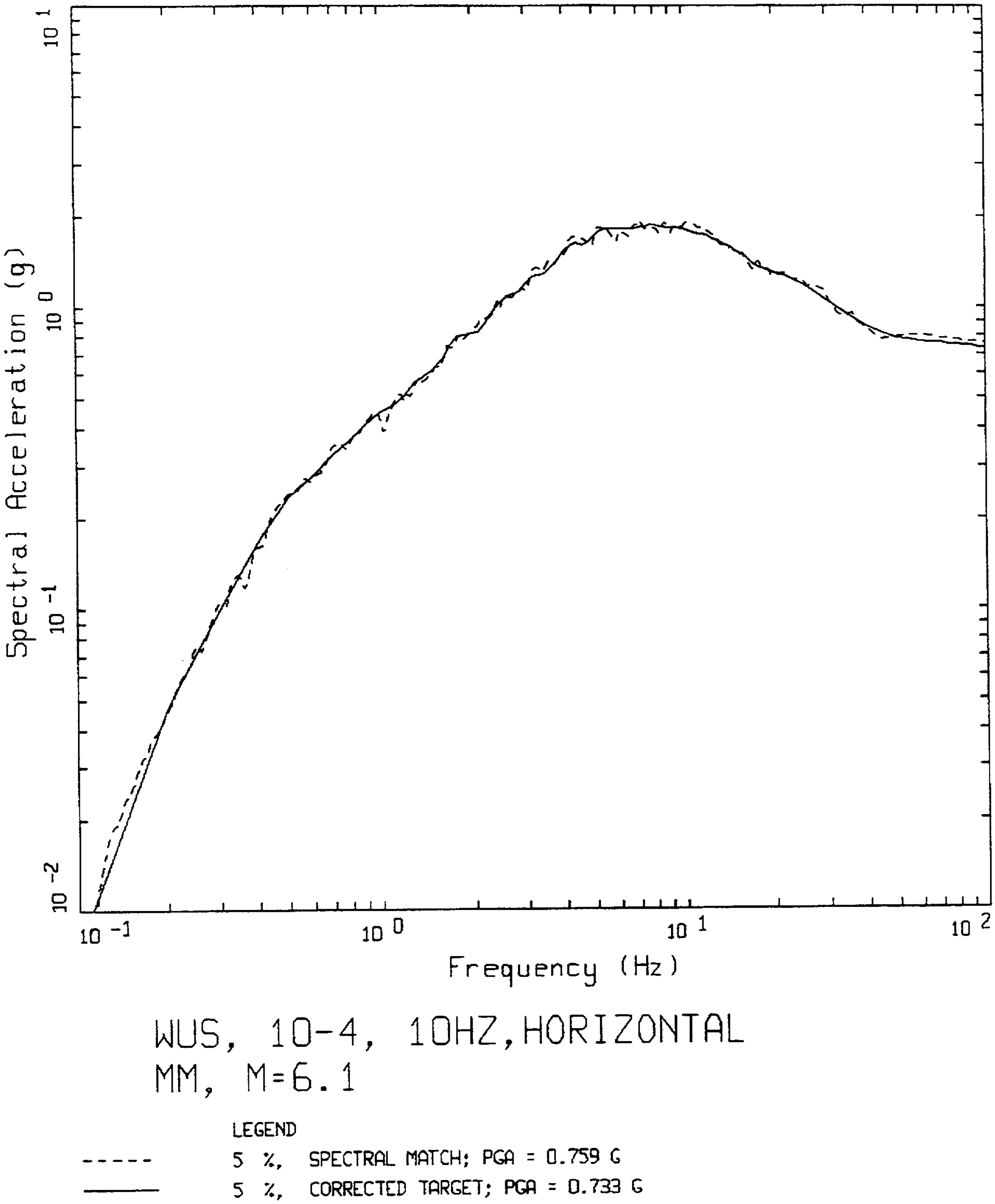

Figure 5-13. Spectral match to corrected (base of soil) 10 Hz rock 1E-4 spectrum: MM.

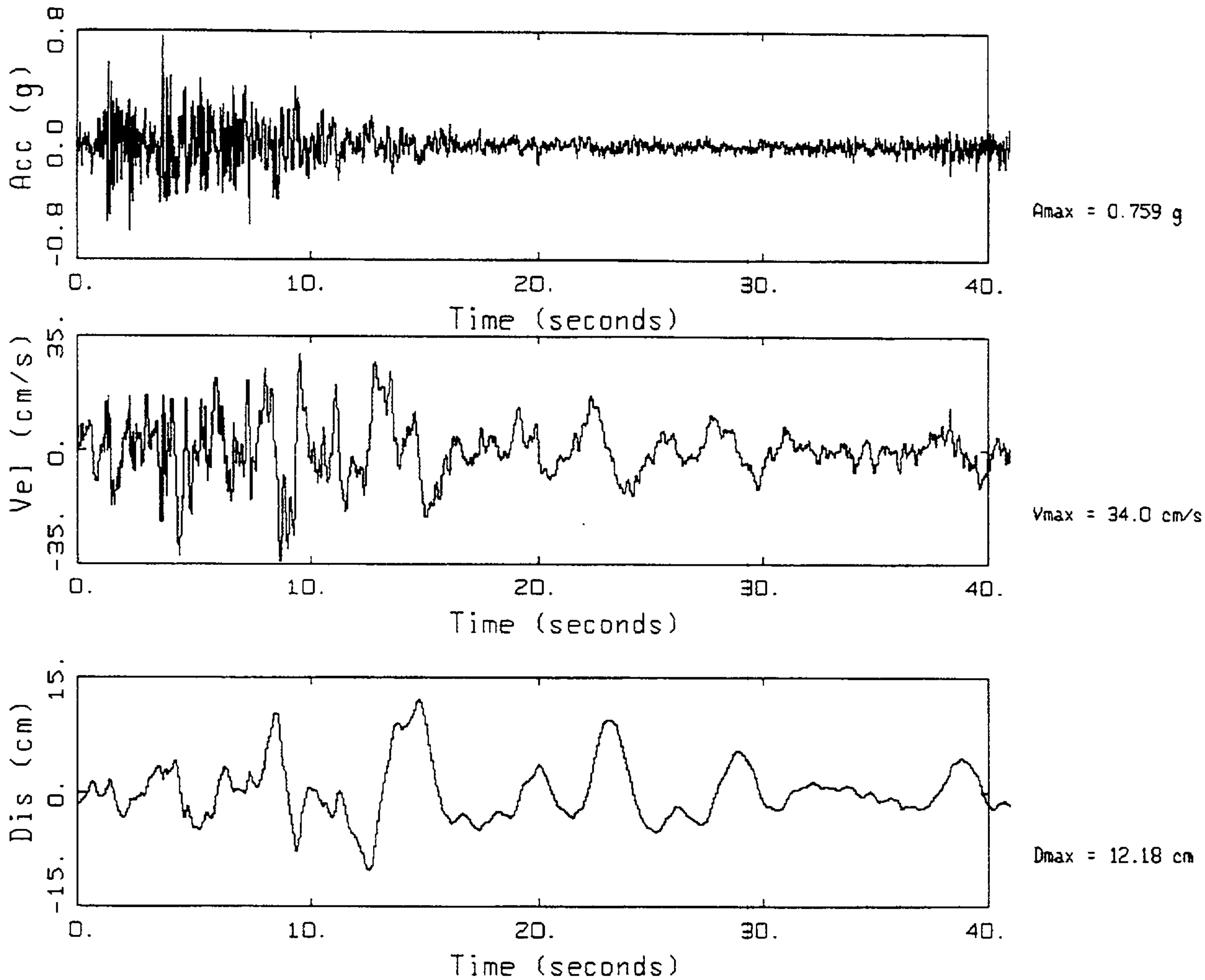

Figure 5-14. Acceleration, velocity, and displacement time histories corresponding to the corrected (base of soil) 10 Hz rock spectral match: MM.

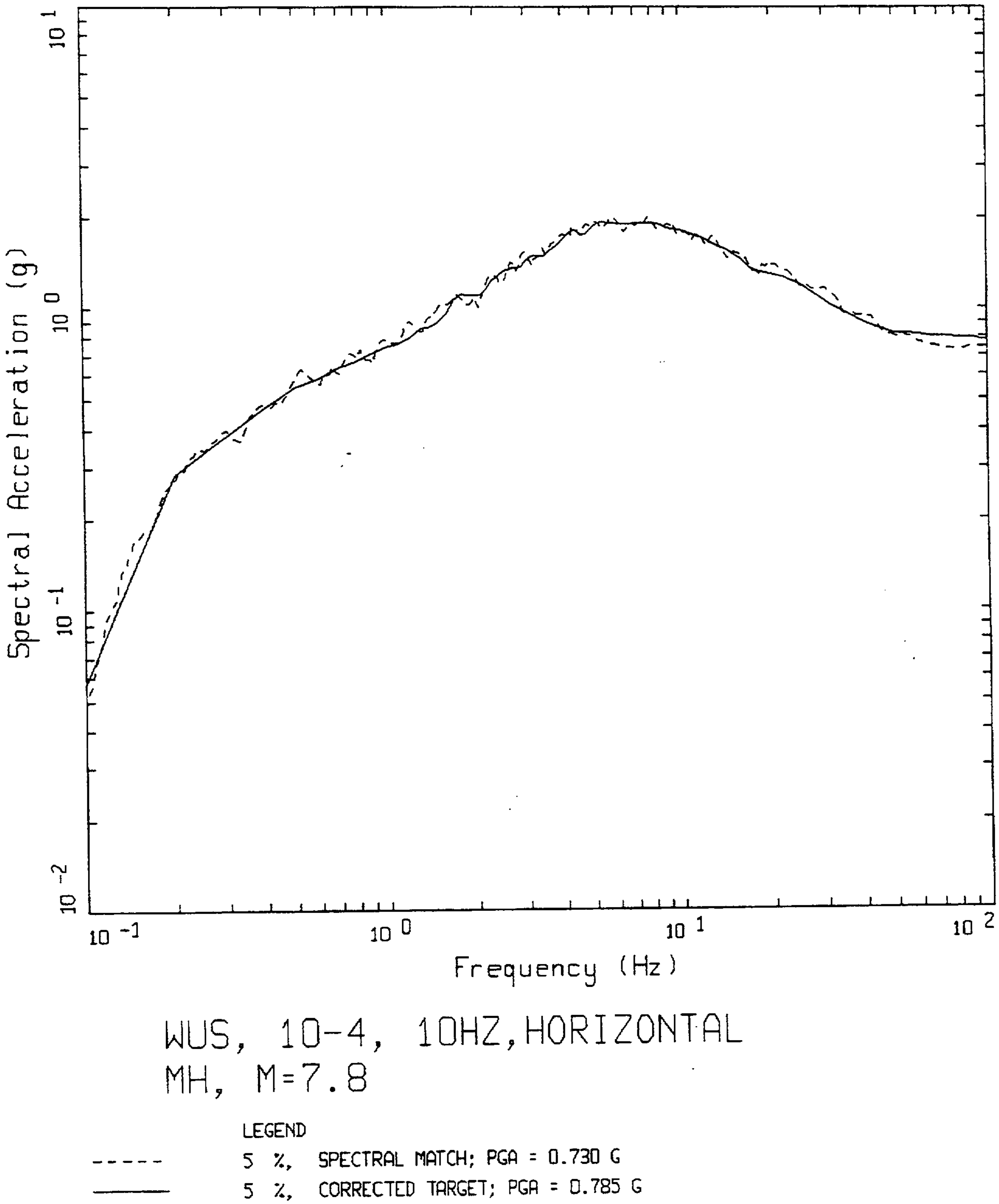

Figure 5-15. Spectral match to corrected (base of soil) 10 Hz rock 1E-4 spectrum: MH.

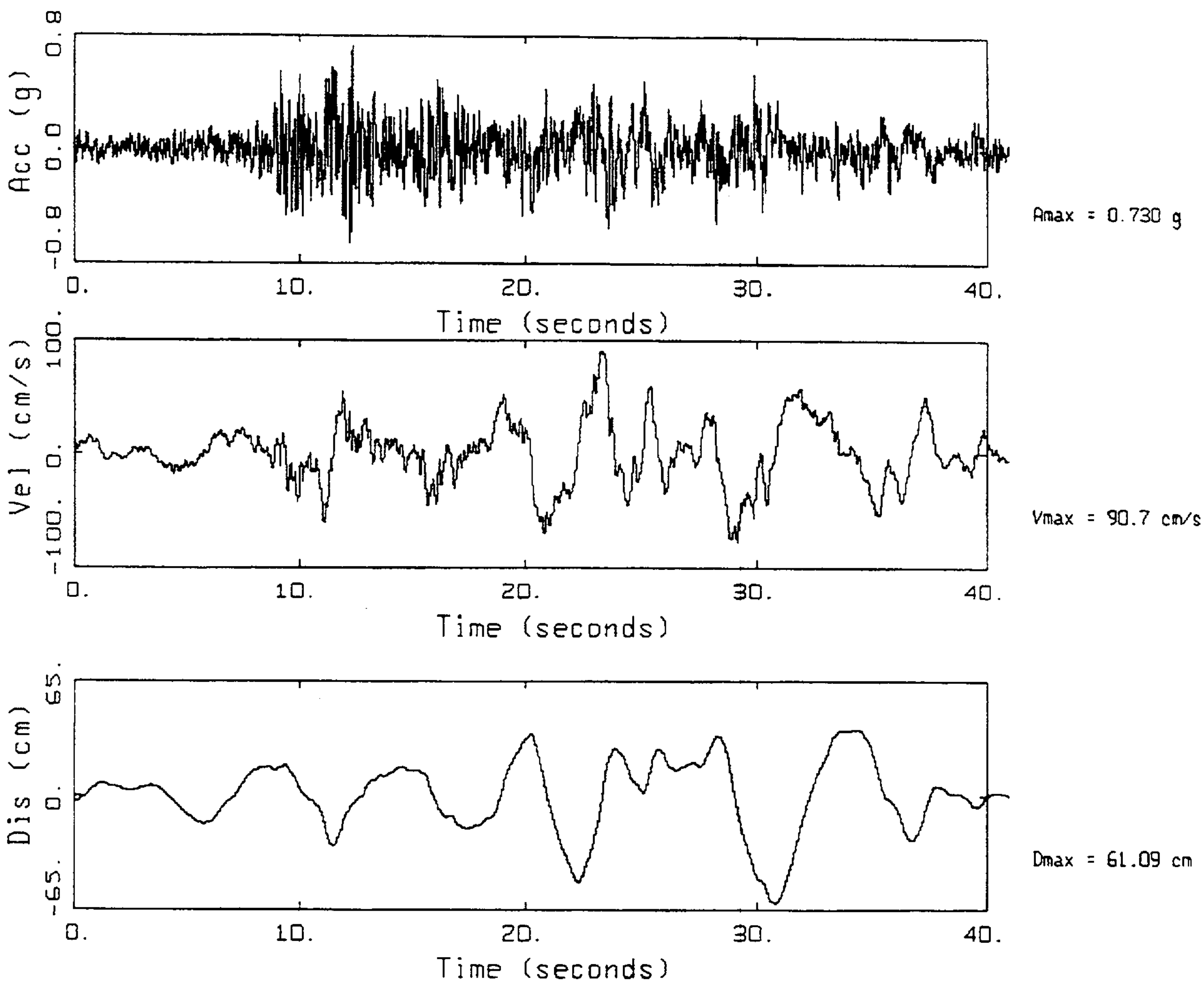

Figure 5-16. Acceleration, velocity, and displacement time histories corresponding to the corrected (base of soil) 10 Hz rock spectral match: MH.